Preparation and characterisation of soluble CLIC1 and liposomes

Roslin Jane Adamson

A dissertation submitted to the Faculty of Science, University of the Witwatersrand, Johannesburg, in fulfillment of the requirements for the degree of Master of Science.

Johannesburg, 2009

Declaration

I declare that this dissertation is my own, unaided work. It is being submitted for the degree of Master of Science in the University of the Witwatersrand, Johannesburg. It has not been submitted for any other degree or examination at any other University.

Roslin Jane Adamson

_____ day of_____, 2009

Abstract

CLIC1 is an intracellular membrane protein that has the intriguing property of being able to exist in both soluble and integral membrane forms. It is unknown how CLIC1 converts from a soluble to a membrane-inserted conformation, but it has been proposed that the transition involves the unfolding of certain regions of the protein followed by refolding into a membrane-competent form. This study characterised the structure and stability of reduced, soluble CLIC1 at the pH values it would encounter in both bulk cytosol and at the membrane surface. Additionally, the preparation and properties of a model membrane system were characterised. At pH 7.0 CLIC1 is more stable and follows a cooperative two-state unfolding transition with a $\Delta G_{(H2O)}$ of 10.3 kcal/mol and *m*-value of 2.3 kcal/mol M^{-1} urea. At pH 5.5 the CLIC1 native structure is looser and more flexible with lower secondary structural content, is less stable, and unfolds via a stable intermediate with exposed hydrophobic surfaces. The $\Delta G_{(H2O)}$ and *m*-values for formation and unfolding of this species are well into the dimeric range, and data from the local probe, Trp35, indicate that the intermediate may be oligomeric. The existence of the intermediate species at low pH and under mild denaturing conditions suggests a mechanism whereby CLIC1 may form channels *in vivo*. Anionic large unilamellar vesicles prepared with a 4:1:1 molar ratio of phosphatidylethanolamine, phosphatidylserine and cholesterol, respectively, were stable up to approximately 50 °C and were highly reproducibly and homogenously sized at ~200 nm diameter. Basal leakage of encapsulated chloride-sensitive fluorescent dye at room temperature was modest for two to three days, and was minimal for up to seven days at 4 °C. These vesicles should prove to be an ideal membrane system for the study of membrane-inserted CLIC1 and with encapsulation of a chloride-sensitive dye may provide the means for a viable functional assay for CLIC1 channel activity.

This work is dedicated to:

My Dad and Mom,
without whom none of this would have been possible

To Karen, who stood by me throughout

And to my siblings, Graeme, Jocelyn and Pears

Acknowledgements

I acknowledge my supervisor, Professor Heini Dirr, and thank him for the guidance and support he provided. I also acknowledge Dr Jonathan Burke and Dr Yasien Sayed for their patience with my endless questions. I thank my colleagues in the Protein Structure-Function Research Unit for the stimulating discussions and the many laughs. Special thanks are due to Dr Sylvia Fanucchi, who always had time to listen, to discuss, question, ponder and speculate on the many mysteries of CLIC1 and other aspects of my project. Grateful thanks are extended to Caroline Lalkhin of the Electron Microscope Unit of the University of the Witwatersrand for her generous help with the transmission electron microscope, and to Philip Tshabalala for his expert printing of the electron microscope images.

I acknowledge the University of the Witwatersrand, the Mellon Postgraduate Foundation, the NRF, CSIR and DAAD for funding.

Table of Contents

List of Figures

List of Tables

Abbreviations

A_{260}	absorbance at 260 nm
A_{280}	absorbance at 280 nm
Å	Ångström
AKAPs	A-kinase anchoring proteins
amp	ampicillin
amp^r	ampicillin resistance
ANS	8-anilino-1-naphthalene sulphonic acid
ATP	adenosine triphosphate
AU	absorbance units; arbitrary units
AUFS	absorbance units full scale
BLM	bilayer lipid membrane
bp	base pairs
CaCC	calcium-activated chloride channels
CD	circular dichroism
CDC	cholesterol-dependent cytolysin
CFTR	cystic fibrosis transmembrane conductance regulator
CHAPSO	3-[(3-cholamidopropyl)dimethylammonio]-2-hydroxyl-1-propanesulfonate
CLC	chloride channel

CLIC	chloride intracellular channel
C_m	the denaturant concentration at the midpoint of the unfolding curve
CMC	critical micellar concentration
C_{mExp}	experimentally derived C_m value
C_{mPred}	predicted C_m value
D	diffusion coefficient
Da	Daltons
DDAO	dodecyldimethyl-*N*-amineoxide
D_H	hydrodynamic diameter
DEAE	diethylaminoethyl
ΔASA	change in (solvent) accessible surface area
ΔG	the change in Gibbs free energy
$\Delta G_{(H2O)}$	change in Gibbs free energy of unfolding in the absence of denaturant
dH_2O	distilled water
DHPC	dihexanoylphosphatidylcholine
DI water	deionised water (18.2 MΩ)
DLS	dynamic light scattering
DMPC	dimyristoylphosphatidylcholine

DNA	deoxyribonucleic acid
DNase	deoxyribonuclease
ds	double-stranded
DT	diphtheria toxin
DTT	dithiothreitol
E_{222}	ellipticity at 222 nm
EDTA	ethylenediaminetetra-acetic acid
endA deficient	endonuclease deficient
ε	molar extinction coefficient; dielectric constant
ER	endoplasmic reticulum
eV	electron volts
Ex.280	excitation at 280 nm
Ex.295	excitation at 295 nm
ExPASy	Expert Protein Analysis System
F_0	fluorescence intensity in the absence of quencher
F	fluorescence intensity in the presence of quencher
F341	fluorescence emission intensity at 341 nm
F342	fluorescence emission intensity at 342 nm
F345	fluorescence emission intensity at 345 nm

F348	fluorescence emission intensity at 348 nm
F460	fluorescence emission intensity at 460 nm
Far-UV CD	far-ultraviolet circular dichroism
GABA	gamma-aminobutyric acid
GPCR	G-protein coupled receptor
GSH	reduced glutathione
GSSG	oxidised glutathione
GST	glutathione *S*-transferase
GUVs	giant unilamellar vesicles
H3R	histamine H3 receptor
HDXMS	hydrogen deuterium exchange mass spectrometry
hGST O1-1	human Omega class glutathione *S*-transferase
HT voltage	the voltage applied to the circular dichroism photomultiplier tube
I	intermediate species
IAA-94	indanyloxyacetic acid 94
IPTG	isopropyl-1-thio-β-D-galactopyranoside
K_{SV}	Stern-Volmer quenching constant
K_d	dissociation constant
K_{eq}	equilibrium constant

ℓ	litre
LB	Luria-Bertani
λ_{max}	fluorescence emission wavelength maximum
LUVETs	large unilamellar vesicles prepared by extrusion
LUVs	large unilamellar vesicles
MAP	mitogen-activated protein
µℓ	microlitre
µM	micromolar
mdeg	millidegrees
mℓ	millilitre
MLVs	multilamellar vesicles
mM	millimolar
M	molar
MQAE	*N*-(6-methoxyquinolyl) acetoethyl ester, also called *N*-(ethoxycarbonylmethyl)-6-methoxyquinolinium bromide
mRNA	messenger ribonucleic acid
mtorr	millitorr
mV	millivolts
m-value	the dependence of the free energy of unfolding on denaturant concentration

MWCO	molecular weight cut-off
N	native
NATA	N-acetyl-tryptophanamide
NCC27	nuclear chloride channel 27
NEM	*N*-ethylmaleimide
NMR	nuclear magnetic resonance spectroscopy
OD	optical density
ORF	open reading frame
P	phosphorus
PA	phosphatidic acid
PAGE	polyacrylamide gel electrophoresis
PC	phosphatidylcholine
PDB	Protein Data Bank
PDI	polydispersity index
PE	phosphatidylethanolamine
PE:PS:chol	a lipid mixture composed of L-α-phosphatidylethanolamine from *Glycine max* (soybean), L-α-phosphatidylserine from *Glycine max* (soybean) and cholesterol
PFT	pore-forming toxin
p*I*	isoelectric point

PI	phosphatidylinositol
PMT	photomultiplier tube
PS	phosphatidylserine
PTM	putative transmembrane region
Q	quencher
recA deficient	recombination deficient
RMSD	root mean square distance
RNA	ribonucleic acid
RNase	ribonuclease
rpm	revolutions per minute
S300HR column	Sephacryl™ 300 High Resolution size exclusion column
SASA	solvent accessible surface area
SDS	sodium dodecyl sulphate
SEC-HPLC	size exclusion high performance liquid chromatography
*Sj*GST	*Schistosoma japonicum* glutathione *S*-transferase
SUVs	small unilamellar vesicles
TEMED	*N*, *N*, *N*’, *N*’-tetramethylethylenediamine
[Θ]	mean residual ellipticity
TM	transmembrane

TNF	tumour necrosis factor
U	unfolded
UV	ultraviolet
V	volts
wtCLIC1	wild-type CLIC1
YT	yeast tryptone

Standard one- and three-letter amino acid codes have been used throughout.

CHAPTER 1. INTRODUCTION

1.1. Biological membranes

Biological membranes are essential to life. They form specialised, permeable barriers between cells and their environments, and between organellar contents and the cytoplasmic environment, allowing passage of water and certain solutes and blocking the passage of other solutes. Contrary to early models of biological membranes as simple sac-like structures functioning only to enclose the contents of the cell, biomembranes are composed of hundreds, if not thousands of different species of lipid molecule that form a highly complex matrix for the basic functions of respiration, photosynthesis, transport, motility and signal transduction (Lee, 2005; Hunte and Richers, 2008). Within their *milieu* exist up to 30 % of the proteins encoded by the genome of a typical organism (Wallin and von Heijne, 1998; Krogh *et al.*, 2001). This exciting, liminal environment is the subject of intense research, not least because of the multiple challenges its complexity presents to the researcher.

1.1.1. Membrane structure and properties

1.1.1.1. Structure

The defining factor within the cellular environment is its aqueous nature. Without water, life as we know it simply would not exist. The unique physical properties of water and its broad solvent power for ions and other polar substances allow for a multiplicity of different functional environments within the cell and its compartments. However, the *lack* of solvent power of water for non-polar substances is as important and unique a property, since without this property, the cell and its compartments could not exist. Biomembranes are composed mostly of amphipathic molecules made up of a strongly hydrophilic head group attached via a glycerol or ceramide molecule to, usually, two long hydrocarbon chains (Quinn, 1976; Tanford, 1980). The head groups are phosphate (phospholipids) or carbohydrate (glycolipids) esters. The amphipathic nature of phospholipids and

glycolipids gives rise to the common structure of biomembranes in aqueous solution: the bilayer lipid membrane (BLM), whereby the hydrocarbon tails of the phospho- or glyco-lipids line up to face each other with the polar head groups exposed to the aqueous solution (Figure 1.1). This structure comes about due to the hydrophobic effect. The attraction of water molecules for each other is much stronger than the attraction of water for hydrocarbon molecules or of hydrocarbon molecules for each other, and thus it is thermodynamically favourable for water to exclude hydrocarbon-water contacts (Tanford, 1980).

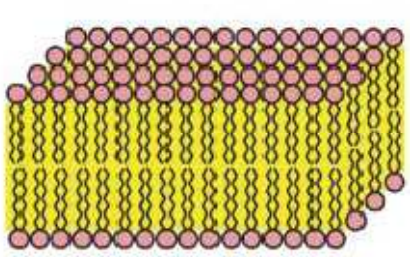

Figure 1.1. Schematic diagram of a typical bilayer lipid membrane.
Structure of a typical bilayer lipid membrane in aqueous solvent. The hydrophilic head groups (pink) are arranged to face the polar solvent, while the hydrophobic fatty acyl chains (yellow) are buried to exclude the polar solvent. (Image from Lee, 2005).

The major components of mammalian biological membranes, depending on cell type and organism, are phosphatidylcholine (PC) (10-60 %), phosphatidyl-ethanolamine (PE) (20-30 %), phosphatidylserine (PS) (~10 %), sphingomyelin (5-20 %), phosphatidylinositol (PI) (5-10 %), glycolipids (10-25 %), phosphatidic acid (PA) (~1.5 %) and cholesterol (20-30 %) (reviewed in Quinn, 1976; Tanford, 1980). The structures of phospholipids will be the focus of this discussion. Generic structures of PC, PE, PS, PI, PA and cholesterol are shown in Figure 1.2. PS, PI and PA are negatively charged at physiological pH. These negative charges act to attract protons to the membrane surface, rendering the pH at the surface of the membrane and extending 5-15 Å out from the surface up to 2 pH units lower than the pH in bulk cytosol (Vaz *et al.*, 1978; Prats *et al.*, 1986; McLaughlin, 1989; Menestrina *et al.*, 1989; van der Goot *et al.*, 1991; Kraayenhof *et al.*, 1993; Bortoleto and Ward, 1999; Murray *et al.*, 1999). This fact has

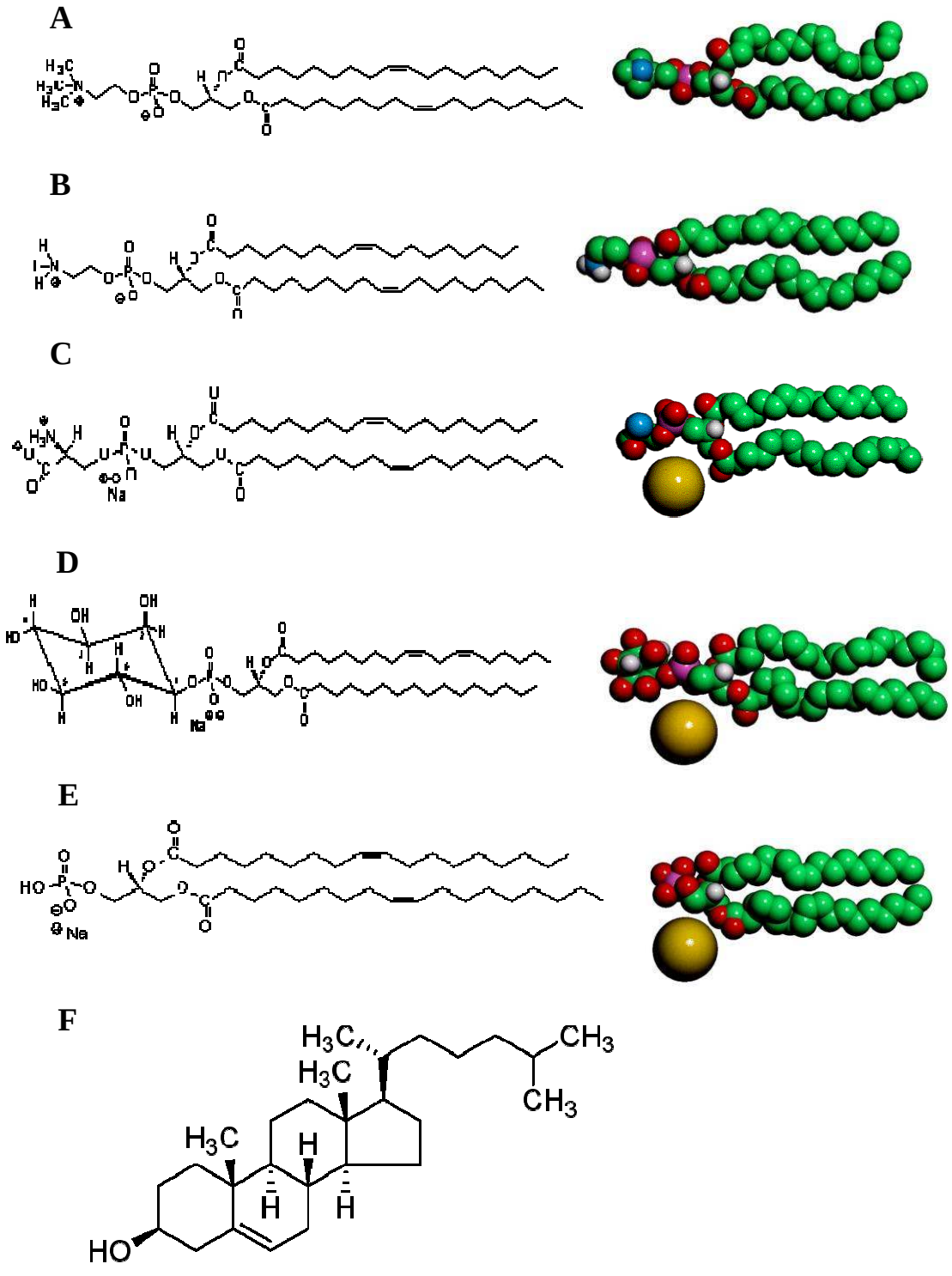

Figure 1.2. Structures of common phospholipids and cholesterol.

Stick and space-filling structures of common phospholipids and cholesterol. (**A**) phosphatidylcholine, (**B**) phosphatidylethanolamine, (**C**) phosphatidylserine (sodium salt), (**D**) phosphatidylinositol (sodium salt), (**E**) phosphatidic acid (sodium salt), (**F**) cholesterol. Carbon atoms are green, oxygen: red, nitrogen: blue, phosphorus: purple, hydrogen: white. Sodium ions are shown in gold.

important consequences for soluble to membrane-bound and integral membrane proteins, and shall be dealt with in Sections 1.1.2. and 1.2. The distribution of phospholipids across the membrane is asymmetric, with the extracellular leaflet of typical eukaryotic plasma membranes being made up mainly of PC and sphingomyelin, while the intracellular leaflet is composed predominantly of PE and PS (Bretscher, 1972; Zachowski, 1993). This distribution is functionally significant, for example, for apoptosis, which is preceded by a translocation of PS to the extracellular leaflet (Balasubramanian and Schroit, 2003).

Phosphatidylcholine and phosphatidylserine are based on the PE structure. In PC, the nitrogen is triply methylated. In PS, the ethanolamine is carboxylated. Generally speaking, saturated fatty acids are esterified to carbon 1 of the *sn*-glycerol 3-phosphate, and unsaturated fatty acids to carbon 2 (Kyte, 1995), although fully saturated and fully unsaturated molecules can be synthesised. Saturated fatty acids usually exist in the all-*trans* conformation, but *gauche* conformations may be introduced with low energetic cost (about 1 kcal/mol^{-1}), resulting in a kink in the chain (Kyte, 1995). The carbon-carbon double bonds in unsaturated fatty acids are almost all in the *cis* conformation, giving a permanent kink to the chain at the double bond. Double bonds are never spaced immediately next to each other, since this would result in a rigid, planar structure forming, and they appear after carbon 8 in the chain (Kyte, 1995), meaning that the chains closer to the head groups are more restricted in their movements than those toward the centre of the bilayer. The existence of double bonds and *gauche* conformations in the fatty acyl chains results in gaps and spaces between the chains and decreases the packing efficiency of the phospholipids. In biological membranes these gaps are often filled by cholesterol, a rigid, planar steroid which is an important precursor to vitamin D_3 and the steroid hormones. Cholesterol is marginally amphiphilic by virtue of its single OH group.

The length of the hydrocarbon chains in biological membranes is of the order of 16-20 carbons. This gives an average thickness of the hydrophobic domain of a membrane of about 30 Å, which means about 21 residues in a typical protein

helix, untilted, would be required to span the hydrophobic portion of the membrane (Lee, 2003).

The mobility of the hydrocarbon chains is temperature-dependent. Below the gel to liquid crystalline phase transition temperature (T_m), bilayers are in an ordered gel phase. Above this temperature, rotational freedom around the carbon bonds of the acyl chains increases and they take on a disordered liquid state (Figure 1.3). In this state, the area of the phospholipid head groups and fatty acid tails increases (Träuble and Eibl, 1974). However, liquid ordered states have been observed, for example, in mixtures of PC, cholesterol and sphingomyelin, where preferential association between cholesterol and sphingomyelin cause the formation of liquid ordered states referred to as rafts (London, 2002). Non-bilayer phases are also possible, but less common. Saturated fatty acids have higher phase transition temperatures than unsaturated fatty acids, which are usually in the liquid phase at room temperature. This has implications for the insertion of membrane proteins. If packing is too tight due to the membrane being in the gel phase or too-ordered a liquid ordered phase, proteins will be unable to insert. Thus the proportion of saturated to unsaturated fatty acids within a membrane is very important. It should be noted, though, that in the absence of large temperature fluctuations in physiological systems, changes in the fluidity of membrane structure can and do occur. Gross changes in bilayer structure can be brought about by rather small changes in ionic environment. The presence of divalent cations increases the T_m of negatively charged membranes by charge neutralisation, in accordance with Gouy-Chapman theory, and monovalent cations lower the T_m (Träuble and Eibl, 1974). These are critical features, for example, in nerve excitation and signal transduction, where cation-induced structural changes in biomembranes are essential for function (Träuble and Eibl, 1974). The fluidity of BLMs gave rise to the "fluid-mosaic" model of membrane structure (Singer and Nicolson, 1972). This model basically depicts membrane proteins as floating in a fluid solvent created by the lipid bilayer. This model is now regarded as an oversimplification, since regions of restricted motion of both proteins and lipids exist in practically all membranes.

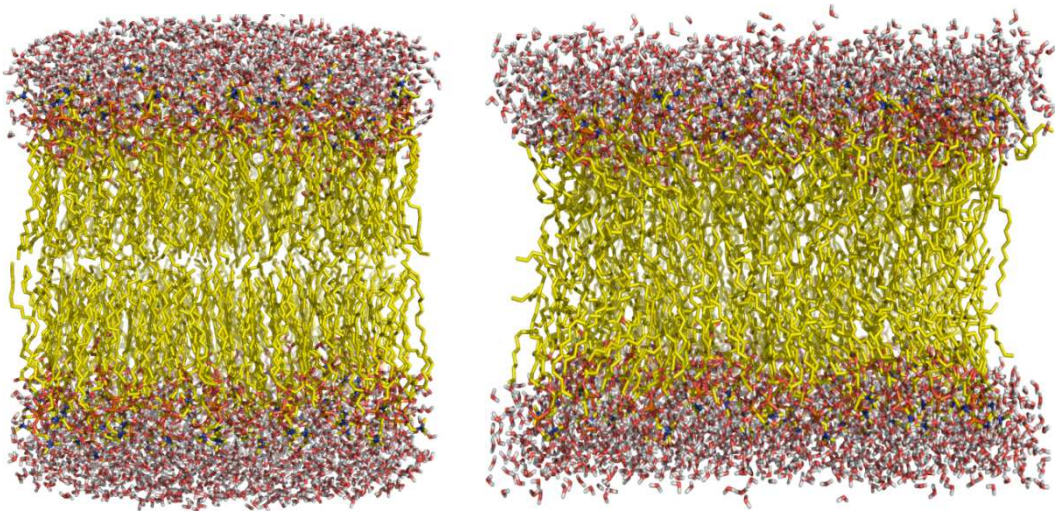

Figure 1.3. Gel and liquid crystalline phases of bilayer lipid membranes.
Ordered gel (left) and disordered liquid crystalline (right) phases of bilayer lipid membranes. In the liquid phase hydrocarbon chains have much greater freedom of movement and are less tightly packed. PDB codes GEL.pdb and FLUID.pdb from Heller *et al.*, 1993; modelled using PyMOL™ v. 0.99 (DeLano Scientific, 2006).

1.1.1.2. Electrostatic properties

The total electric potential profile of a bilayer lipid membrane is made up of the transmembrane potential, the surface potential and internal potentials (Honig *et al.*, 1986). The transmembrane potential is the electric potential difference between the bulk aqueous phases on either side of the membrane. It arises because of the separation of charges across the membrane, and generally ranges from 10 mV to 100 mV in biological systems (Honig *et al.*, 1986). The cytoplasmic side of the membrane is invariably more negative than the extracellular side, due to relative salt ion concentrations, the dominant species being K^+, Na^+ and Cl^- (Honig *et al.*, 1986). It has also recently been found to be due partially to the asymmetric distribution of phospholipids across the membrane (Gurtovenko and Vattulainen, 2008). The surface potential is the electrostatic potential at the interface of the membrane and the aqueous phase relative to that in bulk solution. It is almost always negative, since it arises from the net charge on the membrane surface, which is mainly derived from negatively charged lipids,

particularly PS in biomembranes. Up to 10-20 % of the membrane surface area is composed of negatively charged lipids (Honig *et al.*, 1986; Vance and Steenbergen, 2005). The negative surface potential accounts for the lowered pH at the surface of the membrane, as discussed above. The surface potential is related to surface charge density by the Gouy-Chapman-Stern model, which accounts for differences in ion concentrations at the surface *vs.* in bulk solution and the consequent electrical double layer formed at the membrane surface (Stern, 1924). With a negative surface potential, the surface concentration of anions will be depleted, and that of cations will be increased. Internal potentials stem from dipoles or charges in the low dielectric hydrocarbon interior of the membrane (Honig *et al.*, 1986). Two such potentials are the membrane dipole potential and adsorption potentials. A dipole potential of several hundred mV, inside positive, arises from the structural arrangement of polar molecules at the membrane-water interface. This intramembrane potential can be substantially modified by surface charge asymmetry and adsorbed amphiphiles or proteins. Any protein spanning the membrane will be exposed to a powerful electrical field, which may have implications for structure and/or function (Honig *et al.*, 1986).

The dielectric constant of water is 80 at 20 °C, and oils and aliphatic hydrocarbons have dielectric constants from 2-5, generally accepted as being around 2 within the interior of membranes (Honig *et al.*, 1986). Dielectric constants in the range 10-30 exist for the interfacial region between bulk water and lipid hydrocarbons (reviewed in Honig *et al.*, 1986). The regions of differing dielectric constants have important consequences for the translocation of charged ionic species across membranes. The free energy of transfer of charged bodies between regions of differing dielectric constants is given by the Born expression:

$$W_B = \frac{q^2}{2r}\left(\frac{1}{\varepsilon_1} - \frac{1}{\varepsilon_2}\right) \qquad \textbf{Equation 1-1}$$

where q is the charge on the ion, r is the radius of the ion, and ε_2 and ε_1 are the dielectric constants of the regions from and to which the charged body is moving, respectively (Born, 1920). The unfavourable Born electrostatic energy is the

primary barrier in translocation of charged molecules from the aqueous to the lipid phases, even for so-called hydrophobic ions.

1.1.1.3. Permeability

The Born electrostatic energy barrier is, in fact, large enough to virtually exclude most small ions from the lipid phase of membranes. Typical translocation rates for small physiological ions are in the region of 10^{-8} cm s^{-1} to 10^{-12} cm s^{-1} (Mimms *et al*., 1981; Honig *et al.*, 1986; Paula *et al*., 1998), with rates for Cl^- generally being faster than Na^+ and K^+ (Papahadjopoulos and Watkins, 1967). In contrast, rates for water range between 10^{-4} cm s^{-1} and 10^{-3} cm s^{-1} (Carruthers and Melchior, 1983; Mathai *et al.*, 2008), rendering BLMs substantially permeable to water. Translocation rates are highly dependent upon the lipid phase (and thus temperature) and amount of cholesterol (Carruthers and Melchior, 1983), the permeant size, polarity and partition coefficient, the bilayer thickness, lipid type, and area per lipid molecule (Mathai *et al*., 2008). BLMs exhibit a sharp increase in permeability at and above their transition temperatures (Blok *et al*., 1976; Xiang and Anderson, 1997). The rate-limiting step to water permeability appears to be the interfacial region between the bulk aqueous phase and the bilayer lipid interior, and is strongly correlated with the area per lipid molecule (Xiang and Anderson, 1997; Mathai *et al*., 2008). With a higher water than solute permeability, biological membranes and liposomes, which display similar osmotic properties to biological membranes (Bangham *et al.*, 1967; Mui *et al.*, 1993), are acutely sensitive to osmotic gradients. Physiologically, this fact may be important for mechanosensitive ion channels (Miyamoto *et al.*, 1988; Morris, 1990). When working with liposomes, needless to say, great care must be taken with osmotic components of intra- and extravesicular buffers.

1.1.1.4. Nuclear/organellar membranes

The membranes surrounding the various intracellular organelles have their own idiosyncratic lipid compositions, which are not the same as that of the plasma membrane. While Golgi, mitochondrial, lysosomal and plasma membranes of

liver cells contain 35-50 % PC, nuclear and rough endoplasmic reticulum (ER) membranes are composed of more than 60 % PC (reviewed in Quinn, 1980). Inner and outer mitochondrial and nuclear membranes are made up of close to 25 % PE, while plasma, rough ER, Golgi and lysosomal membranes contain only 18 %. The outer mitochondrial membrane contains up to 5 % more PI than the other types of membranes mentioned, including the inner mitochondrial membrane; but the plasma membrane contains 9 % PS vs. 1-2 % for mitochondrial membranes. Cardiolipin makes up 17 % of the inner mitochondrial membranes, but is not present in nuclear membranes, and is only found in very low to trace amounts in other types of membranes. Nuclear membranes contain only about 3 % sphingomyelin, but lysosomal membranes contain 33 % sphingomyelin. Plasma membranes contain by far the highest proportion of cholesterol, as well as, incidentally, most of the cellular glycolipids (Quinn, 1980). Nuclear and mitochondrial membrane composition does not vary considerably across tissues and across vertebrate species; rough and smooth ER membranes differ across organs within the same species, although they are often similar in the same organ in different species. It is clear that the phospholipid compositions of cellular and subcellular membranes are highly specific and must be functionally significant. Typical mammalian nuclear membrane lipid compositions are shown in Table 1. The fatty acid composition of nuclear membrane phospholipids is fairly unique, as determined by Khandwala and Kasper (1971). The major saturated fatty acids were found to be palmitate (C16:0) and stearate (C18:0), the latter comprising almost half the fatty acids of PS and PI fractions. Arachidonate (20:4) made up 35 % of the fatty acids of the PS and PI fractions. Oleate (C18:1), linoleate (C18:2) and dodecahexanoate (C22:6) made significant contributions to the nuclear membrane unsaturated fatty acid complement. Almost 50 % of the PC and PE fatty acids were unsaturated, and the highest degree of saturation was found in sphingomyelin. These results were confirmed by Baumrucker and Keenan (1973).

The nuclear membrane is made up of two bilayer membranes up to 7.5 nm thick and separated by a gap of about 40-70 nm (Quinn, 1980). The outer membrane is

Table 1. Nuclear membrane phospholipid composition.

Phospholipid/lipid	Rat liver nuclear membrane[a]		Rat liver nuclear membrane[b]	Pig liver nuclear membranes[c]	Rat liver nuclear membrane[c]	Rat nuclear membrane[d]	Hen erythrocyte nuclear membranes[e]	Bovine mammary gland nuclear membranes[f]
	µg lipid/mg protein	% of TPL*	% of total P (lipid P per µg of total P = 0.64 ± 0.02)	Percent of total lipid P	% of TPL	% of TPL	% of total lipid P	% of TPL
Lysophosphatidylcholine	9.66 ± 1.88	6.29	1.4 ± 0.4	< 1.0	1.2 ± 0.5	n/i	n/i	3.9
Sphingomyelin	13.21 ± 2.30	8.60	2.5 ± 0.3	2.4 ± 0.4	3.2 ± 1.2	3.95 ± 1.03	13.0 ± 1.5	5.1
Phosphatidylcholine	68.11 ± 3.17	44.38	61.8 ± 1.0	58.2 ± 2.4	61.4 ± 1.5	60.61 ± 3.19	53.0 ± 2.1	51.7
Phosphatidylserine	13.52 ± 0.05	8.78	13.9 ± 0.2 (PS + PI)	4.4 ± 0.6	3.6 ± 1.0	1.75 ± 0.22	n/i	4.7
Phosphatidylinositol	23.51 ± 0.09	15.32	n/i	8.9 ± 0.9	8.6 ± 0.8	10.14 ± 3.75	7.1 ± 1.0	10.3
Phosphatidyl-ethanolamine	13.12 ± 1.55	8.54	18.3 ± 1.0	25.9 ± 1.8	22.7 ± 1.4	23.52 ± 0.65	26.0 ± 1.5	19.6
Dimethylphosphatidyl-ethanolamine	5.07 ± 0.10	3.30	n/i	n/i	n/i	n/i	n/i	n/i
Phosphatidylglycerol	4.37 ± 0.98	2.85	n/i	n/i	n/i	n/i	n/i	1.5
Diphosphatidylglycerol	2.91 ± 0.14	1.89	n/i	n/i	n/i	n/i	n/i	n/i
Phosphatidic acid	n/i		1.4 ± 0.3 (incl. cardiolipin)	< 1.0	< 1.0	n/i	n/i	n/i
Molar ratio cholesterol to phospholipid	n/i		n/i	0.104	0.104	n/i	0.42 ± 0.04	16.4 % total neutral lipids

* Total phospholipids. [a] Neitcheva and Peeva (1995). [b] Khandwala and Kasper (1971). [c] Kleinig (1970). [d] Albi *et al*. (1997). [e] Kleinig *et al.* (1971). [f] Baumrucker and Keenan (1973). P: phosphorus. n/i: no information.

continuous with the rough ER, and the two have similar phospholipid complements. The inner and outer nuclear membranes anastomose at regular intervals to form nuclear pore complexes about 80 nm in diameter (Quinn, 1980), through which most cytosolic-nuclear trafficking occurs.

1.1.1.5. Model membrane systems

One of the primary hurdles in the study of membrane proteins is the provision *in vitro* of an appropriate environment to satisfy the complex structural requirements of molecules that normally reside within a fluid *milieu* enriched with an intricate array of amphiphilic and hydrophobic lipids. A number of model membrane systems have been developed in order to study the structures and functions of membrane proteins. The major systems in use are micelles, bicelles, planar lipid bilayers, lipid monolayers and liposomes. Micelles are small, roughly spherical structures formed from the self-association of detergent monomers above a critical concentration threshold called the critical micellar concentration (CMC) (Garavito and Ferguson-Miller, 2001). The size and shape of micelles depends on the size, type and stereochemistry of the detergent monomer and the solvent environment (Wennerström and Lindman, 1979; Mitchell *et al.*, 1983). A number of different detergents can be used for micelle formation, the main categories of which are: a) ionic detergents; b) non-ionic detergents; and c) zwitterionic detergents (Seddon *et al.*, 2004). Ionic detergents have a head group with either a net cationic of anionic charge attached to a hydrophobic hydrocarbon chain (as in SDS) or steroidal backbone (as in bile acid salts such as sodium cholate). Ionic detergents can be relatively denaturing. Non-ionic detergents such as Triton® X-100 are mild and relatively non-denaturing. They contain uncharged hydrophilic head groups with hydrophobic tails. Zwitterionic detergents such as dodecyldimethyl-*N*-amineoxide (DDAO) combine the properties of ionic and non-ionic detergents. The advantage of using micelle-forming detergents as model membrane systems is that the detergents can both solubilise membrane proteins from their lipid environment and then replace that environment without too much disruption to the native structure of the protein. Mixed detergent-lipid micellar systems are also in use for membrane-protein study, and often provide a more stabilising environment

than detergent micelles alone (reviewed in Seddon *et al.*, 2004). Despite their small size and high surface curvature, micelles have been used extensively as biomimetic systems for membrane proteins and peptides, utilising techniques such as high-resolution nuclear magnetic resonance (NMR), Fourier transform infrared spectroscopy and circular dichroism (CD) (Jelinek and Kolusheva, 2005).

Bicelles are a form of mixed detergent-lipid micelle, but have a much higher lipid component (Sanders and Prosser, 1998). Usually short chain lipids such as dimyristoylphosphatidylcholine (DMPC) are used with detergents such as dihexanoylphosphatidylcholine (DHPC; Sanders and Schwonek, 1992) or a zwitterionic bile salt derivative, 3-[(3-cholamidopropyl)dimethylammonio]-2-hydroxyl-1-propanesulfonate (CHAPSO; Sanders and Prestegard, 1990). Mixed in the correct composition and the correct temperature, the detergent-lipid mixture forms edge-stabilised, bilayered, discoidal structures known as bicelles (Figure 1.4). They are used primarily in NMR studies because of the fact that they can be magnetically aligned (Sanders and Landis, 1995).

Planar lipid systems such as bilayers and monolayers aim to model the phospholipid ordering within cellular membranes and to mimic the lateral organisation of cell surfaces (Greenhall *et al.*, 1998). Phospholipid monolayers deposited at the air-water interface of aqueous solutions (Langmuir monolayers) are used as model membrane systems for studying the interactions of certain peptides and membrane proteins with membranes. Thermodynamic and microscopy techniques such as pressure-area isotherms and fluorescence microscopy can be used to investigate, for example, structural disruption and phase separation caused by peptides incorporated into the monolayers (Chen *et al.*, 2003). Phospholipid monolayers can also be used in so-called “tip-dip” electrophysiology experiments, whereby a monolayer is spread on the surface of an aqueous bath, and a glass pipette passed repeatedly through the monolayer until the resistance reaches a certain level (e.g. in Harrop *et al.*, 2001; Warton *et al.*, 2002). The relevant membrane-insertion-competent protein is then added to the bath and electrophysiological recordings made. The most common use of planar

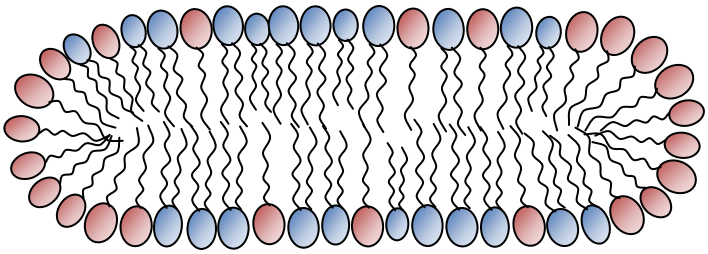

Figure 1.4. Schematic structure of a bicelle.

Cross-section of a bicelle composed of a mixture of phospholipids (blue) and detergent (red). The detergent molecules stabilise the edge of the disc.

lipid bilayers is as black lipid membranes. These consist of thin lipid films placed across small apertures separating baths containing ionic solutions (Winterhalter, 2000). Conductance measurements are then undertaken to study the formation of pores and ion channels in the membrane, their relative permeability and their ion selectivity.

Liposomes are bilayered lipid vesicles which enclose an aqueous space separate from the external solution. There are four major classes of liposomes: small unilamellar vesicles (SUVs), large unilamellar vesicles (LUVs), giant unilamellar vesicles (GUVs) and multilamellar vesicles (MLVs). SUVs range in size up to about 100 nm, averaging between 30-70 nm, and are generally prepared by sonication of MLVs (Papahadjopoulos and Miller, 1967). LUVs have hydrodynamic diameters of 100-1000 nm, and can be prepared by a number of methods, including sonication (Lasch *et al.*, 2003), reverse-phase evaporation (Szoka and Papahadjopoulos, 1978), extrusion (Olsen *et al.*, 1979; Hope *et al.*, 1985; MacDonald *et al.*, 1991) and detergent dialysis (Mimms *et al.*, 1981) (Figure 1.5). GUVs can range up to 100 µm, but are generally of the order of up to 10 µm. They are prepared by electroporation (Angelova and Dimitrov, 1986). MLVs consist of multiple concentric bilayers and are formed by hand-shaking of a dried lipid film hydrated with aqueous buffer (Lasch *et al.*, 2003). The surfaces and properties or liposomes can be modified by the choice of phospholipid, as

well as by the incorporation of proteins such as lectins and glycoproteins, or even synthetic polymers (Jones, 1995).

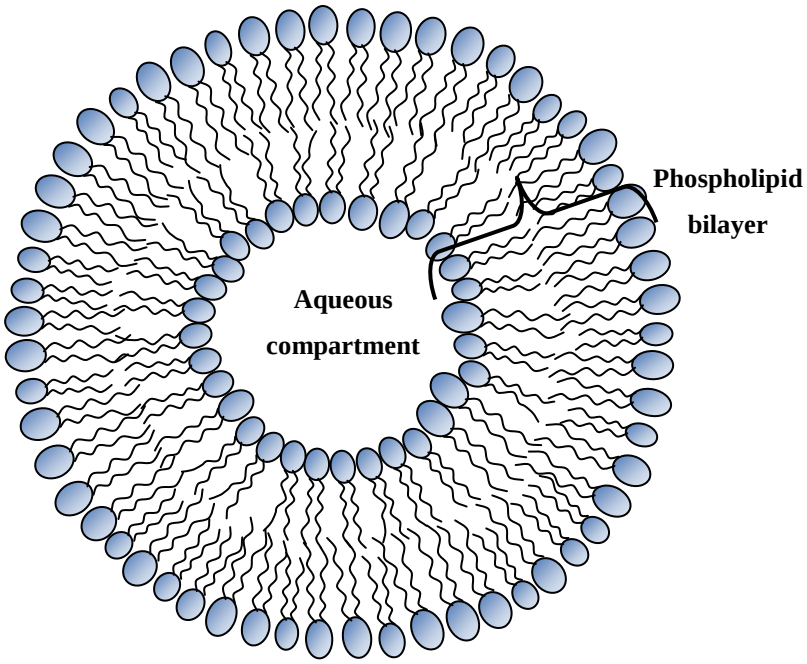

Figure 1.5. Schematic structure of an LUV.

Large unilamellar vesicle showing enclosed aqueous compartment enclosed by phospholipid bilayer.

An enormous amount of research has gone into the formation, structure, properties and applications of liposomes, and a search of the PubMed database at NCBI retrieves 33 433 results of articles with the word “liposomes” in their text. This intense interest is driven by the fact that liposomes so closely resemble the biological cell and as such can be used to study cellular processes such as transport phenomena, and their biological compatibility also means that they are particularly useful as drug delivery systems (Jones, 1995). Liposomes have been used to deliver chemotherapeutic agents (Leyland-Jones, 1993), antiviral drugs (Phillips, 1992), antibacterials (Škalko *et al.,* 1992), and have also been used for gene therapy (Li and Huang, 2006; Karmali and Chaudhuri, 2007). They have

also been used as cosmetic agents for the delivery of moisturisers or anti-inflammatory agents to the skin (Puglia *et al.*, 2004; Betz *et al.*, 2005; Nasr *et al.*, 2008). Generally, larger vesicles are preferred for structural and functional studies of membrane-incorporated proteins because of the closer resemblance of the surface curvature of these vesicles to that of biological cells, and because of the larger encapsulated volume inside these vesicles (Matsuda *et al.*, 1997; Kahya *et al.*, 2000).

1.1.2. Membrane proteins

It has been estimated that up to 45 % of drugs in current use target membrane proteins (Drews, 2000; Terstappen and Reggiani, 2001), and the greatest proportion of pharmaceutical sector research funds are targeted toward membrane components (Lee, 2005), yet the structures of membrane proteins account for less than 1 % of the known high resolution protein structures (White, 2004). Membrane proteins are involved in a vast array a cellular functions, working as ion and protein transport channels, receptors, signal transducers and proton pumps, amongst many other functions. Determination of high resolution structures of membrane proteins has been stymied by the difficulty of obtaining enough pure protein for structural studies and by the obvious necessity of providing an appropriate membrane-like environment for reconstitution of the native structure and function of the protein. Recent developments in the field have facilitated the high resolution structural determination of a small number of membrane proteins which include tightly bound endogenous lipids with assigned head groups (http://www.mpibp-frankfurt.mpg.de/michel/public/memprotstruct.html). The lipids are co-purified with the protein, despite the use of detergents in extraction and purification. From these structures it can be seen that certain lipid molecules bind tightly to membrane proteins in a specific manner, and in so doing, ensure that the integrity of the membrane and its properties as a permeability barrier are not compromised by the presence of the protein protruding through it (Lee, 2003; Lee, 2005; Hunte, 2005; Hunte and Richers, 2008). The interactions of lipids with membrane proteins have been classed into

three types of binding modes: a) “annular lipids” form a shell around the surface of the protein and resemble the lipid bilayer; b) “non-annular surface lipids” nestle into and bind tightly to clefts and cavities in the protein surface, particularly at interfaces between adjacent subunits; and c) “integral protein lipids” are found within membrane proteins or protein complexes, often in unusual positions, such as with the head group below the membrane plane (Hunte, 2005). The crystal structure of tetrameric aquaporin-0 from sheep lens shows an almost complete representation of annular lipids surrounding the protein (Gonen *et al.*, 2005). The identified phospholipids were 1,2-dimyristoyl-rac-glycero-3-phosphocholine (Figure 1.6). The bacterial potassium channel KcsA crystal structure shows two non-annular surface lipids, modelled as a fatty acid and a diacylglycerol molecule, bound into grooves on the surface of the protein close to Trp87, with the diacylglycerol bound at the interface of two monomers (Doyle *et al*., 1998; Zhou *et al.*, 2001) (Figure 1.7). Integral protein lipids have been observed in the yeast cytochrome bc_1 complex (Lange *et al.*, 2001) and in cytochrome *c* oxidase from *Rhodobacter sphaeroides* (Svensson-Ek *et al.*, 2002) (Figure 1.8). It is considered that these may be important for folding and assembly, and additionally, in the case of cytochrome *c* oxidase, may act to stabilise subunit IV by indirect contacts via lipid molecules.

Evidence for specific binding of lipids to membrane proteins and structural rearrangement of the bilayer around membrane proteins is not unexpected. The membrane-spanning portions of integral membrane proteins are more hydrophobic than typical soluble structures and the layers of lipids that form around and within the protein prevent any compromise of the membrane permeability barrier. Internal hydrogen bonding of membrane-traversing segments is maximal, since the energetic cost of transferring a non-hydrogen bonded peptide bond from water to the interior of the membrane is estimated at about 6 kcal/mol, but is only about 0.6 kal/mol when hydrogen bonded (Roseman, 1988). The structures that allow the formation of the maximum number of hydrogen bonds are α-helices and β-sheets, and thus, it is these structures that the regions spanning the membrane adopt (Lee, 2005). β-barrel type structures are

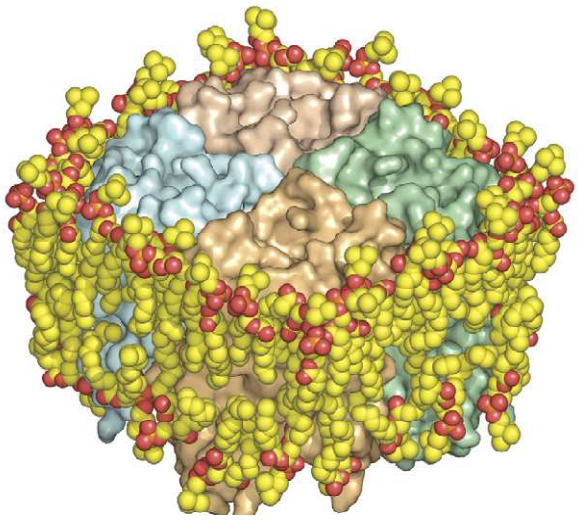

Figure 1.6. Annular phospholipids in close contact with protein.

Annular phospholipids surrounding aquaporin-0 tetramer from sheep lens. Each aquaporin monomer surface is coloured differently. Lipid molecule carbons are yellow, oxygens are red, phosphorus orange. Figure from Hunte and Richers, 2008.

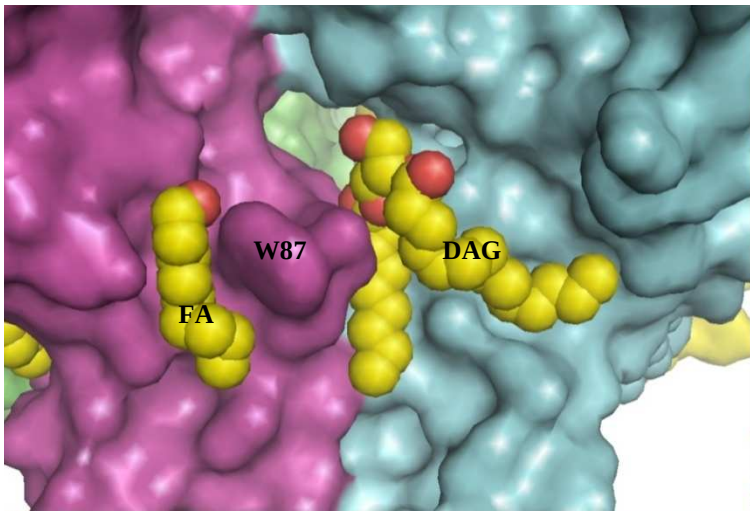

Figure 1.7. Non-annular surface lipids bound to a potassium channel.

Two partial lipid molecules, modelled as a fatty alcohol (FA) and a diacylglycerol (DAG) molecule, are shown bound to grooves in the surface of KcsA, a bacterial potassium channel. The lipids are on the extracellular side of the membrane and the DAG molecule is found at the interface of two subunits (purple and blue). Trp87 is situated just inside the membrane-water interface. The lipid carbons are shown in yellow, oxygens in red. PDB code 1K4C (Zhou *et al.*, 2001); modelled using PyMOL™ v. 0.99 (DeLano Scientific, 2006).

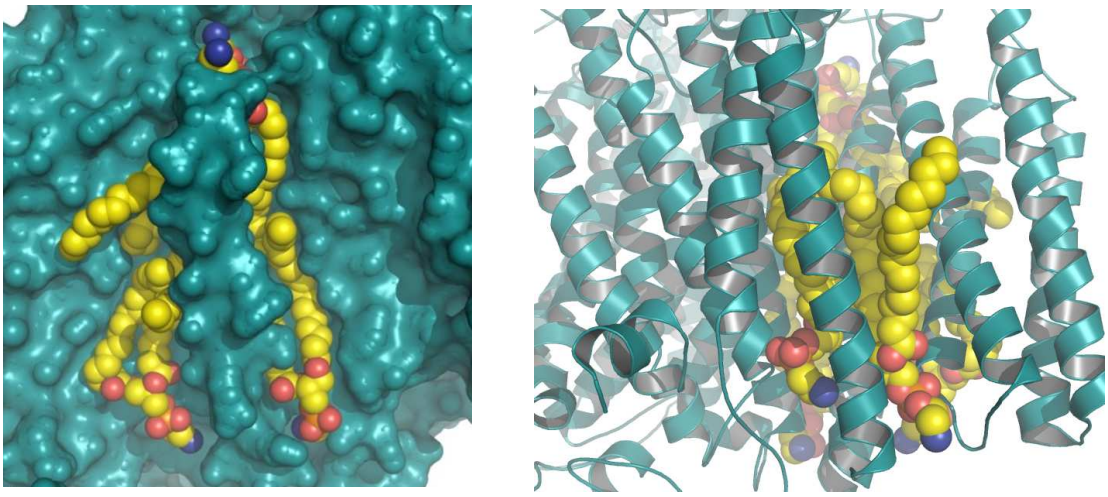

Figure 1.8. Integral protein lipids in cytochrome *c* oxidase.

Surface (left) and ribbon (right) diagrams of cytochrome *c* oxidase from *Rhodobacter sphaeroides* showing how lipids integrate into the structure, aiding in stability of the molecule in the membrane via steric effects and specific interactions. The lipids are di-stearoyl-3-*sn*-phsphatidylethanolamine molecules. Carbons are yellow, oxygen atoms red and nitrogen atoms blue. PDB code 1M56 (Svensson-Ek *et al.*, 2002). Figures modelled using PyMOL™ v. 0.99 (DeLano Scientific, 2006).

found in bacterial outer coat membrane proteins, and all other known integral membrane proteins adopt single or multiple α-helical transmembrane structures (Lee, 2005). A characteristic of membrane protein helices is that they are longer than about 20 Å, sufficiently long to span the membrane (White and Whimley, 1999). Fascinatingly, an almost standard feature of transmembrane helices in particular is the presence of Trp (and often Tyr) residues at the interfacial region, with their non-polar portions embedded in the hydrocarbon plane just inside the membrane-water interface, and their polar amide (or hydroxyl) groups protruding into the aqueous region. With its large hydrophobic surface, considerable dipole moment and ability to act as a hydrogen bond donor, Trp is uniquely suited to interacting at the polar-apolar interface. Trp and Tyr are proposed to anchor the helices within the lipid bilayer (Landolt-Marticorena *et al.*, 1993; Ulmschneider and Sansom, 2001), and can participate in specific interactions with phospholipid head groups (Lee, 2005; Hunte, 2005). The preference for Trp and Tyr for the

membrane interface is even more pronounced in single spanning membrane protein helices (Landolt-Marticorena *et al.*, 1993).

Another prominent feature at the membrane interface, specifically at the cytoplasmic surface, is the presence of clusters of charged residues, especially positive residues (Arg, Lys). The common presence of these positively charged residues on the protein surface on the negative side of the membrane gave rise to the "inside positive" rule (von Heijne, 1986). These residues participate in strong stabilising interactions with phospholipid head groups and possibly ester groups, as exhibited by the much higher resolution in crystal structures of electronegative membrane surface head groups, and may function as a "plug" to fix the membrane protein in place (von Heijne, 1986; Hunte, 2005). In many cases their long, flexible, hydrophobic side chains are buried in the hydrophobic core of the membrane from where they "snorkel" up to the surface to expose their charged groups (Segrest *et al.*, 1990). They may also play a role in membrane binding events for certain proteins (Gouaux *et al.*, 1997). Thus the presence of both charged and aromatic groups in the interface region implies a combination of electrostatic and hydrophobic interactions at the membrane interface serve to stabilise membrane proteins.

The Born energy barrier greatly disfavours the translocation of charged residues into or across the membrane, and yet charged residues are found in transmembrane segments. The surface dipole potential, which arises from the carbonyl ester groups that link the lipid fatty acid chains to the glycerol backbone of the phospholipids, and internal membrane potentials, positive inside, favour the anionic residues by about 5 kcal/mol and disfavour cationic residues by about the same (Flewelling and Hubbell, 1986). The favouring of anionic residues has been explained as being a result of a positive shift in the p*K* values of these groups due to dielectric effects and to electrostatic effects arising from the negative charge at the surface of the membrane and in the interfacial layer, rendering a greater proportion of acidic residues neutral (Krishtalik and Cramer, 1995). Also, the lower pH at the surface of the membrane favours protonation of carboxylate

groups. Nonetheless, the energy barrier for all charged residues remains high: approximately 25 kcal/mol for Asp and Glu, 35 kcal/mol for Arg and 43 kcal/mol for Lys (Krishtalik and Cramer, 1995). Thus it is likely that translocation of most of these residues occurs with them in a neutralised form, such as in ion pairs.

The high electrostatic barrier to the movement of polar molecules across the membrane engenders the requirement for the cell to possess some other means of transporting essential ions into and out of the cell and its organelles, in order to maintain specific intracellular ion concentrations and the required pH. Two major classes of specialised ion transporters are the carrier proteins and channel proteins (Honig *et al.*, 1986; Alberts *et al.*, 2002). Carriers are able to transport solutes across the membrane by binding the specific solute to be transported and then undergoing a series of conformational changes in order to transfer it to the other side of the membrane. This process may occur by facilitated diffusion "downhill" across the concentration gradient, or via active transport, which requires the input of energy from ATP. Channel proteins transport inorganic ions of appropriate size and charge only in a passive manner, via facilitated diffusion across electrochemical or concentration gradients. Incredibly, they can transport up to 100 million ions per second in this manner (Alberts *et al.*, 2002)! Channel proteins normally form narrow, selective, hydrophilic pores that can exist in open and closed states – their pores are much narrower than those of the pore-forming toxins discussed in Section 1.2. Their gating status is regulated by such factors as voltage and mechanical stress (Jentsch *et al.*, 2002). In order to decrease the Born electrostatic energy barrier ions would face when crossing the membrane, the pores of channel proteins are lined with polar or oppositely charged residues that effectively raise the dielectric constant within the membrane in that region, thus compensating for the loss of solvation energy the ions would encounter otherwise (Honig *et al.*, 1986).

1.2. Soluble to membrane-partitioning proteins

A number of proteins have the unique capability of existing in both soluble and integral membrane conformations. These include bacterial pore-forming toxins (PFTs), some of the pro- and anti-apoptotic mitochondrial proteins and the chloride intracellular channel protein family (CLICs). Transformation from a soluble cytosolic or nucleoplasmic conformation with hydrophilic surface residues to an integral membrane-inserted conformation with a hydrophobic or amphiphilic surface requires a dramatic structural rearrangement, and challenges the notion that primary sequence determines a unique three-dimensional structure. A better understanding of how this transformation occurs offers unique opportunities to study protein refolding. In many cases, however, only the soluble structures of these proteins are known, and although the basic steps involved in pore-formation are fairly well-understood, mechanisms for their insertion are still sketchy. The following briefly covers what is known about the structures and insertion mechanisms of various classes of pore-forming proteins.

1.2.1. Classes

1.2.1.1. Pore-forming toxins

At least a third of the approximately 300 protein toxins characterised to date act by disrupting membranes (Alouf, 2001). Many of these are bacterial, but cytolytic toxins are produced by other organisms too, including certain insects, poisonous reptiles and stinging marine invertebrates (Parker and Feil, 2005). Bacterial PFT toxic activity is realised via the pore-mediated release of cellular nutrients required for the growth of extracellularly multiplying bacteria, or by a systematic attack on host defences, such as phagocytes and other immune system cells (Geny and Popoff, 2006). Many PFTs act simply by penetrating the membrane to form a pore, thereby disrupting the cell's permeability barrier, destroying the transmembrane potential and leading eventually to cell death via necrosis or apoptosis; others penetrate the host cell membrane in order to translocate

themselves into the cell to act on a cytosolic target (Parker and Feil, 2005). Either way, for penetration to occur, these PFTs, which are secreted in a water-soluble form, need to undergo fairly major structural changes in order to expose hydrophobic surfaces which are able to penetrate the hydrophobic core of the host cell membrane. While the exact structures formed during this process are unknown, the mode of action is common, and includes: binding, oligomerisation, insertion, and assembly of the functional pore (Menestrina *et al*., 2003) (Figure 1.9).

Binding of the toxin to the cell surface involves exploiting a host cell surface molecule, such as a protein, lipid (such as cholesterol in the case of the cholesterol-dependent cytolysins) or sugar for use as a receptor. This may serve to concentrate the toxin on the membrane surface, following which it oligomerises and inserts into the membrane, or inserts and then oligomerises (Parker and Feil, 2005). The functional channel is then formed. Binding to the membrane is driven by electrostatic and/or hydrophobic events. Insertion occurs via a pH-dependent process either by the neutralisation of acidic surface residues, whereby the hydrophobicity of the protein is increased, or by the formation of a molten globule state, whereby the energy barrier to insertion is lowered. Electrostatics may also play a role in insertion, since charged residues have been found to play a role in the insertion mechanisms of a number of PFTs (Parker and Pattus, 1993).

PFTs have been classified as α-PFTs and β-PFTs, based on certain structural features (Gouaux, 1997). The α-PFTs include the colicins (Parker *et al.*, 1989), exotoxin A (Allured *et al.*, 1986), the insecticidal Cry δ-endotoxins (Li *et al.*, 1991) and diphtheria toxin (DT) (Choe *et al.*, 1992). These toxins form α-helical transmembrane structures. The β-PFTs are rich in β-sheets and form β-barrel transmembrane structures. They include aerolysin (Parker *et al.*, 1994), *Clostridium septicum* α-toxin (Ballard *et al.*, 1995), *Staphylococcus aureus* α-hemolysin (Song *et al.*, 1996), anthrax protective antigen (Petosa *et al.*, 1997), some insecticidal δ-endotoxins (Li *et al.*, 1991) and cholesterol-dependent cytolysins (CDCs) (Tweten *et al.*, 2001).

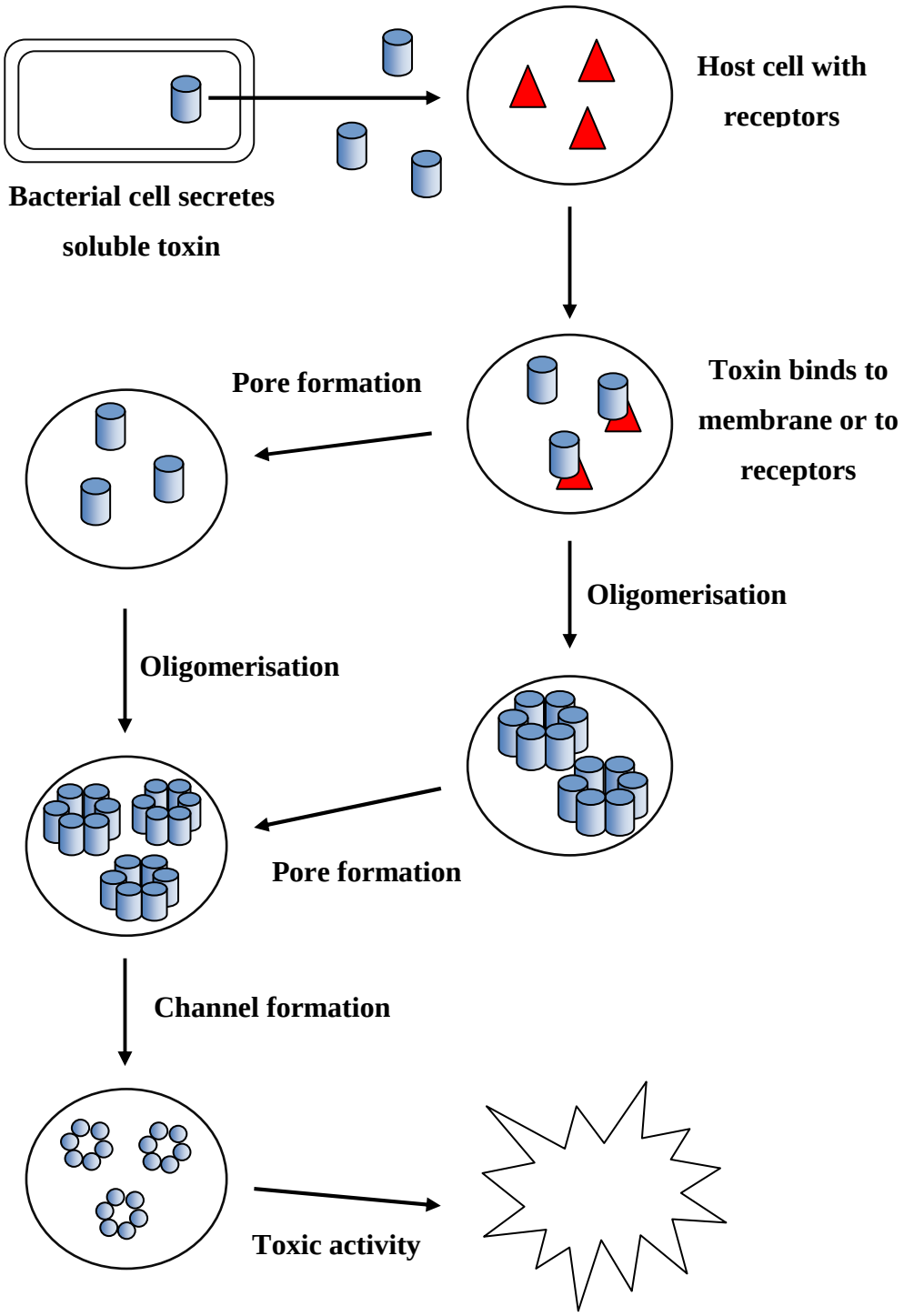

Figure 1.9. General schematic of PFT insertion and infection.

Water-soluble toxins are secreted by the bacterium. Once bound to the host cell, depending on the toxin, they either oligomerise and then form a pore, or form a pore as monomers and then oligomerise to assemble the functional channel conformation. Schematic adapted from Gilbert, 2002; Parker and Feil, 2005.

A common feature of the membrane interacting domains of the α-PFTs is a bundle of α-helices (from six in exotoxin A to ten in colicin A) arranged in three layers of two or more antiparallel amphipathic or hydrophobic helices (Figure 1.10). The core in many cases is made up of a highly hydrophobic helical hairpin, which is usually longer than about 30 Å, and is thus long enough to span a typical membrane (reviewed in Parker and Feil, 2005). This hydrophobic hairpin structure is the membrane-insertion component of the toxins, and is present in the colicins and diphtheria toxin (van der Goot *et al.*, 1991; Parker *et al.*, 1992) and in the Cry δ-endotoxins to a lesser extent (Grochulski *et al.*, 1995). The pore-forming domain of exotoxin A is made up of six α-helices, two of which are long enough to span the membrane (Allured *et al.*, 1986), although, in fact, there are no stretches of hydrophobicity long enough to actually do so (Parker and Feil, 2005). Nevertheless, the protein does form pores (Menestrina *et al.*, 1991) and it is well-established that helical pore-forming toxins can have membrane-inserted segments that are not as hydrophobic as normal integral membrane proteins (Rosconi and London, 2002).

Another feature of α-PFTs is that many of them require receptors to bind to the surface of the cell, although others can form pores in model membranes, suggesting that receptors are not a primary requirement for pore-formation (Parker and Feil, 2005). Electrostatic interactions between charged residues on the surface of PFTs and receptors or membranes may play a role in receptor recognition. Receptor-binding is usually accomplished by a specific domain and may serve to concentrate the toxin molecules on a targeted cell surface, thereby facilitating oligomerisation and/or pore-formation (Parker and Feil, 2005). Helical PFTs known to form dimers or oligomers are diphtheria toxin (Bennet *et al.*, 1994), some of the Cry δ-endotoxins (Puntheeranurak *et al.*, 2005) and equinatoxin, which, incidentally, requires no receptor and binds directly to the membrane surface, utilising clusters of aromatic residues on its surface to do so (Belmont *et al.*, 1993, Tejuca *et al.*, 1996). The colicins bind receptors, but are believed to form monomeric transmembrane channels, although there is still debate about whether a colicin monomer provides sufficient protein to form the

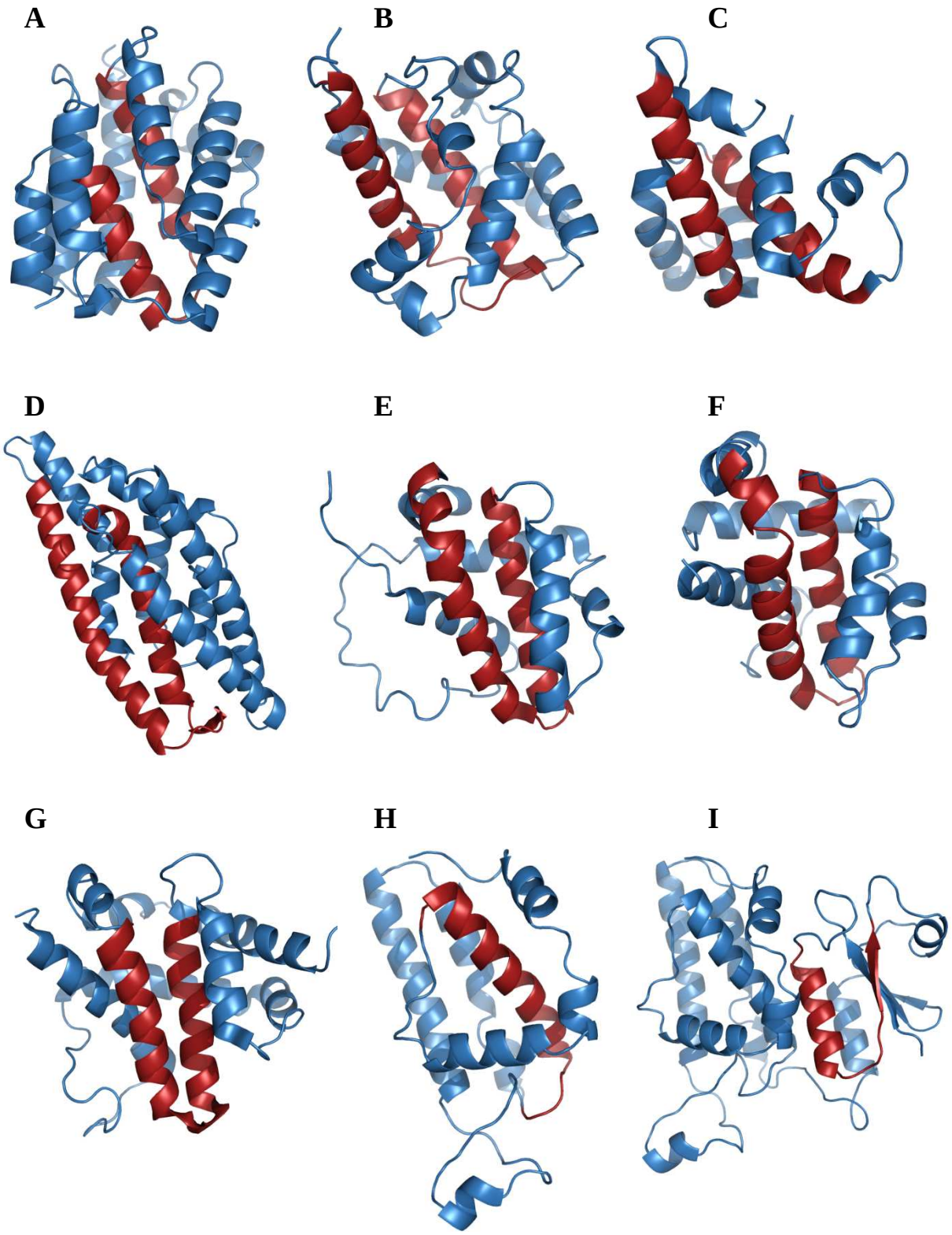

Figure 1.10. Comparison of topology of various pore-forming protein classes. Ribbon representations of the translocation regions of four bacterial pore-forming toxins (**A-D**), three apoptosis-regulating proteins (**E-G**) and CLIC1 (**H**, **I**). Helices/strands highlighted in red are the proposed membrane-traversing regions. In almost all cases a

hairpin is formed from sequential portions in the protein sequence, except for exotoxin A and the CLIC1 proposed C-terminal domain helix. (**A**) Pore-forming domain of colicin A; PDB code 1col (Parker *et al.*, 1992). (**B**) Transmembrane domain of diphtheria toxin; PDB code 1ddt (Bennet *et al.*, 1994). (**C**) Pore-forming domain II of exotoxin A; PDB code 1ikq (Wedekind *et al.*, 2001). (**D**) Pore-forming domain I of insecticidal Cry δ-endotoxin; PDB code 1ciy (Li *et al.*, 1991). (**E**) The anti-apoptotic Bcl-x_L; PDB code 1maz (Muchmore *et al.*, 1996). (**F**) The anti-apoptotic Bcl-2; PDB code 1g5m (Petros *et al.*, 2001). (**G**) The pro-apoptotic Bax; PDB code 1f16 (Suzuki *et al.*, 2000). (**H**) The all-helical C-terminal domain of CLIC1; PDB code 1k0m (Harrop *et al.*, 2001). (**I**) N- and C-terminal domains of CLIC1; PDB code 1k0m. Figures modelled using PyMOL™ v. 0.99 (DeLano Scientific, 2006).

well-defined channels detected (Levinthal *et al.*, 1991; Tory and Merrill, 1999).

The fundamental requirement for PFTs to successfully bind the membrane and insert into it to form pores is that they must be able to undergo a conformational change which will expose or generate hydrophobic surfaces which are able to cross the membrane interior. In the case of the colicins, a spiral of cavities within the hydrophobic core of the protein is suggested to prime the structure for conformational change (Parker *et al.*, 1992). In addition, eight positively charged residues form a ring around the hydrophobic hairpin, possibly ensuring that the protein is properly oriented for insertion via electrostatic interactions with negatively charged lipids (Lakey *et al.*, 1994). The key factor contributing to the conformational change undergone by α-PFTs in their conversion to membrane-inserted forms is the low pH found at the surface of the membrane. Acidic residues in particular play important roles, in that they act as "pH sensors". Neutralisation of these residues at low pH not only increases the hydrophobicity of certain segments, facilitating hydrophobic interactions with the membrane, but can also disrupt salt bridges and hydrogen bonds which may be critical to the stability of the protein. For example, in colicin E1, local unfolding of a helix is caused by disruption of a critical salt bridge and hydrogen-bonding network formed by three conserved Asp residues (Musse and Merrill, 2003). Acid-induced neutralisation of the charge on an Asp residue at the end of a helix in exotoxin A causes helix unfolding that exposes a Trp residue involved in insertion of the pore-forming domain (Mere *et al.*, 2005). Several α-PFTs form a molten globule state at low pH (see Section 1.3.3). These include colicin A (van der Goot *et al.*, 1991), exotoxin A (Jiang and London, 1990), diphtheria toxin (Jiang *et al.*, 1991; Choe *et al.*, 1992; London, 1992), Cyt1A δ-endotoxin (Manceva *et al.*, 2004) and equinatoxin (Ulrih *et al.*, 2004). The molten globule state is characterised in part by a conserved secondary structure and a loss of tertiary structure (Haynie and Freire, 1993), rendering the surface much more hydrophobic than that of the native state. This then greatly lowers the energy barrier to conversion to a membrane-competent form and to insertion into the membrane. In fact, PFTs are able to insert much more rapidly into membranes than integral membrane proteins

because they proceed from a partially unfolded, rather than a fully unfolded state (Kleinschmidt and Tamm, 1996). The acid-induced insertion of the translocation domain of diphtheria toxin into the membrane involves first hydrophobic and then electrostatic interactions (Chenal *et al.*, 2002). At low pH, DT partially unfolds to form a molten globule state. This exposes the buried hydrophobic helical hairpin made up of helices α8 and α9, which binds to the membrane and probably inserts at this point. Electrostatic interactions involving a combination of attractions and repulsions between residues of the highly charged helices 1-4 of the translocation domain and the phospholipid head groups then bring about permeabilisation of the membrane and formation of the pore. Two charged acidic residues at the tip of the hairpin on the loop between helices α8 and α9 are probably neutralised at the membrane surface prior to insertion, but then become charged again in the cytosol of the target cell. This would help to lock the protein in the membrane (Kaul *et al.*, 1996). Both DT and the colicins have been shown to follow an "umbrella" model of insertion, whereby hydrophobic interactions of the central hairpin with the membrane initiate insertion, followed by an opening up of the outer layers of helices to lie flat on the surface of the membrane with their hydrophobic faces embedded into it (Parker *et al.*, 1990; Choe *et al.*, 1992).

The β-PFTs have three features in common, despite their large structural dissimilarities: they are rich in β-sheets, in general there are no extended regions of hydrophobic residues which could form transmembrane regions, and they all require oligomerisation in order to form a pore (Parker and Feil, 2005). Oligomerisation facilitates the formation of a closed β-barrel structure, which aids the generation of large enough hydrophobic surfaces for membrane-insertion. Most commonly, the β-PFTs form heptamers (Parker and Feil, 2005; Tilley and Saibil, 2006). In general, they require receptors, in many cases as yet unidentified, to bind to membranes. In the case of the CDCs, the receptor is cholesterol. The CDCs are the only β-PFTs that switch secondary structure from an α-helical bundle in the soluble monomer to a β-hairpin in the membrane-bound oligomer (Tilley and Saibil, 2006).

1.2.1.2. Apoptotic proteins

Some of the members of the Bcl-2 family of apoptosis regulators make up another group of channel-forming proteins. In particular, the anti-apoptotic proteins Bcl-2 and Bcl-x_L, and the pro-apoptotic Bax, which normally reside in the cytosol (Bax) or at the mitochondrial membrane surface (Bcl-2 and Bcl-x_L), are able to insert into the membrane upon receiving an apoptotic signal (Schendal *et al.*, 1998; Shimizu *et al.*, 1999; Shimizu *et al.*, 2000). Their integral membrane functions involve acting as moderately selective ion and/or protein channels for the release of apoptotic factors from the mitochondrion (Gross *et al.*, 1999). Members of the Bcl-2 family are divided into three groups based on their functions and on whether they possess certain homology domains, BH1-BH4 (Adams and Cory, 1998; Gross *et al.*, 1999). Type-I members, whose function is anti-apoptotic, include Bcl-2 and Bcl-x_L, and contain all four homology domains. They localise to the surface of mitochondrial, ER and nuclear membranes (Bcl-2) or only to the mitochondrial outer membrane (Bcl-x_L) (Janiak *et al.*, 1994; Kaufmann *et al.*, 2003). They are anchored to the membrane by a hydrophobic C-terminal domain (Nguyen *et al.*, 1993; Adams and Cory, 1998). The Type-II proteins are pro-apoptotic and contain only the first three domains, such as Bax and Bak. Members of the Type-III group are also pro-apoptotic but contain only BH3. Both types exist in a soluble form in the cytosol, but translocate to the mitochondrial outer membrane when apoptotic stimuli are received, where they promote the release of apoptogenic factors (Wolter *et al.*, 1997; Desagher *et al.*, 1997).

Despite wide sequence diversity and extensive diversity of function, members of the Bcl-2 family have a remarkably similar fold. This fold consists of six or seven amphipathic α-helices surrounding two hydrophobic α-helices forming a helical hairpin at the core of the bundle (Muchmore *et al.*, 1996; Suzuki *et al.*, 2000; Petros *et al.*, 2001) (Figure 1.10). These central helices are generally α5 and α6. A striking similarity exists between the structures of the Bcl-2 family and the translocation domains of the PFTs, particularly diphtheria toxin and the colicins. In addition, like the PFTs, these apoptotic regulators have been shown to exhibit

channel-forming activity, particularly under acidic conditions and in the presence of anionic membranes (Minn *et al.*, 1997; Shimizu *et al.*, 1999; Saito *et al.*, 2000; Vander Heiden *et al.*, 2001). In the case of Bax, the functional channel is formed by a large multimer, although Bax is a monomer in solution (Antonsson *et al.*, 2000, 2001). Most of these proteins also happen to have low p*I* values, ranging between 4 and 5 (Epand *et al*., 2002; Thuduppathy *et al.*, 2006). Their channel-forming activity has been demonstrated in vitro with recombinant protein and synthetic lipid model membranes, so insertion may not be receptor-mediated (Minn *et al.*, 1997; Basanez *et al.*, 2001). The structural similarity of the Bcl-2 proteins to the PFTs, and the requirement for acidic conditions for their insertion into membranes led to speculation that they followed a similar insertion mechanism, i.e. via a molten globule state intermediate. However, it was subsequently shown that, although the solution to membrane conformational change of Bcl-x_L is pH-dependent, the protein does not form a molten globule (Thuduppathy and Hill, 2005). However, it is proposed to follow a similar "umbrella" or "inside-out" model of insertion (Thuduppathy *et al.*, 2006). The energy barrier to insertion into the membrane is reduced by acidification of the side chains, as opposed to acid-induced destabilisation of the solution conformation as in the case of the toxins (Ramsay *et al.*, 1989; Schendal and Cramer, 1994; Sathish *et al*., 2002; Thuduppathy and Hill, 2005). The solution to membrane conformational change of Bcl-x_L is therefore driven by electrostatic interactions, whereby the free energy of binding to the membrane is reduced upon protonation of acidic residues (Thuduppathy and Hill, 2005). The proton gradient intrinsic to mitochondrial function may play a role in the process, as well as the fact that cytosolic pH decreases slightly upon induction of apoptosis (Matsuyama *et al.*, 2000).

The exposed location of the Bcl-2 proteins on the mitochondrial or other organellar surfaces may have driven the evolution of a different conformational conversion process from that of the toxins due to their susceptibility to intracellular proteases in those locations (Thuduppathy and Hill, 2005). Diphtheria toxin, for example, would not be exposed to proteases in the endosome

in which it enters the cell, and thus would be perfectly safe forming a molten globule intermediate, which would normally be rapidly targeted by proteases (Draper and Simon, 1980).

1.2.1.3. CLIC proteins

The chloride intracellular channel proteins (CLICs) make up a unique class of chloride channels which have the special characteristic of being able to exist, like the PFTs and apoptotic proteins discussed above, in dual soluble and membrane-inserted forms. They are the fourth class of chloride channels characterised to date, the others being the chloride channel family (CLC), the cystic fibrosis transmembrane conductance regulator family (CFTR) and the ligand-gated gamma-aminobutyric acid (GABA) and glycine receptor family (Jentsch *et al.*, 2002). A less well-characterised family is the calcium-activated chloride channels (CaCC). Chloride channels have been implicated in a broad array of functions, including cell volume regulation, regulation of electrical excitability across membranes, transepithelial transport (Jentsch *et al.*, 2002), acidification of intracellular compartments, accumulation or dissipation of a membrane potential via chemi-osmotic coupling (Al-Awqati, 1995) and exocytosis (Redhead *et al.*, 1997). Chloride channel malfunction leads to a number of diseases such as cystic fibrosis (Riordan *et al.*, 1989), Dent's disease (Lloyd *et al.*, 1996), Bartter's syndrome (Simon *et al.*, 1997) and several myotonias (Koch *et al.*, 1992).

The CLIC nomenclature was initiated by Heiss and Poustka (1997) because of the apparent channel activity of earlier members, but recently there have been suggestions for a review of this terminology, due to the relatively poor selectivity of more recently cloned members and the fact that some of the members do not appear to manifest pore-forming abilities (Friedli *et al.*, 2003; Ashley, 2003; Singh *et al.*, 2007). This is despite high sequence similarity in the family.

CLIC proteins have been found expressed ubiquitously in different cells and tissues, and can localise to the plasma membrane or to the membranes of many different organelles (Chuang *et al.*, 1999; Duncan *et al.*, 1999; Edwards, 1999;

Valenzuela *et al.*, 2000). They are involved in a wide variety of functions, as anion channels or modulators of ion channels or other proteins, including signal transduction (Qian *et al.*, 1999; Berryman and Goldenring, 2003; Saeki *et al.*, 2005), kidney function (Tulk and Edwards, 1998), regulation of the cell cycle (Valenzuela *et al.*, 2000; Berryman and Goldenring, 2003), water secretion (Nishizawa *et al.*, 2000), bone resorption (Schlesinger *et al.*, 1997), spermatozoa function (Myers *et al.*, 2004), cell division (Tonini *et al.*, 2000; Warton *et al.*, 2002), apoptosis (Fernandez-Salas *et al.*, 2002; Suh *et al.*, 2005), cellular growth control (Qian *et al.*, 1999), chaperone activity (Maeda *et al.*, 2008) and cardiac function (Jalilian *et al.*, 2008).

The CLIC proteins are highly unusual for ion channels in that they exist mostly in a soluble form, and in that they are actually very small for typical channel proteins (most are around 25-30 kDa). Cellular and subcellular localisation studies have found CLICs abundantly expressed in the cytoplasm of cells of various tissue types, although the soluble to membrane-bound proportions seem to vary according to cell type (Valenzuela *et al.*, 1997; Tulk and Edwards, 1998; Berryman and Bretscher, 2000; Ulmasov *et al.*, 2007). In comparison to the CLC family of chloride channels, for example, which form dimers with ten to twelve transmembrane domains each (Dutzler *et al.*, 2004; Dutzler, 2006), the single putative transmembrane domain of the CLICs was considered an unlikely candidate for channel formation. The CFTR family have twelve transmembrane domains and the GABA receptors contain four transmembrane domains which oligomerise to form a pentameric structure 230-270 kDa in size (Jentsch *et al.*, 2002). Nevertheless, conclusive ion channel activity has been demonstrated for p64 (CLIC5B) (Landry *et al.*, 1993), CLIC1 (Tonini *et al.*, 2000; Harrop *et al.*, 2001; Tulk *et al.*, 2000, 2002; Singh and Ashley, 2006; Singh *et al.*, 2007), CLIC2 (Cromer *et al.*, 2007), CLIC4 (Singh and Ashley, 2007; Singh *et al.*, 2007) and CLIC5A (Berryman *et al.*, 2004; Singh and Ashley, 2007), in some cases, such as CLIC1 and CLIC4, *in vitro* in the absence of any other proteins.

To date, six human CLIC family members have been identified: CLIC1 (Valenzuela *et al.*, 1997), CLIC2 (Heiss and Poustka, 1997), CLIC3 (Qian *et al.*, 1999), CLIC4 (Duncan *et al.*, 1997), CLIC5 (A and B splice variants, CLIC5B being the homologue of bovine p64) (Berryman and Bretscher, 2000), and CLIC6 (the homologue of parchorin) (Nishizawa *et al.*, 2000; Friedli *et al.*, 2003). They consist of a highly conserved core (40-80 % sequence identity) of about 230 amino acids (Figure 1.11), while CLIC5B and CLIC6 have hydrophilic N-terminal extensions of 200-400 residues which are not evolutionarily conserved (Friedli *et al.*, 2003). Furthermore, CLIC homologues have been identified in other mammals, amphibians, birds, fish, nematodes, insects and may even exist in sea squirts (Berry *et al.*, 2003; Littler *et al.*, 2007). Despite their ubiquity across species, tissues and cell types and organelles, the biological function of CLICs remains obscure, but is speculated to be related to their ion channel activity, which has been implicated in several disease processes. Increased functional expression of CLIC1 was observed in brain microglia exposed to the β-amyloid peptide implicated in Alzheimer's disease (Novarino *et al.*, 2004; Milton *et al.*, 2008), and is overexpressed in colon cancer (Petrova *et al.*, 2008). Antisense suppression of CLIC4 induced an antitumour response via a pro-apoptotic pathway in several cell types *in vitro* and retarded tumour growth *in vivo* (Suh *et al.*, 2005).

The CLICs are all acidic proteins, with p*I* values lower than 5.4, except for CLIC3, whose p*I* is slightly higher. Those CLICs for which channel activity has been demonstrated have shown this activity to occur more readily and to a greater extent at low pH (~5) (and also, incidentally, at high pH) than at physiological pH (Warton *et al.*, 2002; Tulk *et al.*, 2002; Berry and Hobert, 2006; Cromer *et al.*, 2007). CLIC proteins also all share two major hydrophobic domains as determined by hydrophobicity plots (Kyte and Doolittle, 1982). The crystal structures of soluble CLIC1, CLIC2, CLIC4, a *Drosophila melanogaster* CLIC homologue, *Dm*CLIC, and a *Caenorhabditis elegans* CLIC homologue, EXC-4, have been solved (Harrop *et al.*, 2001; Littler *et al.*, 2005; Li *et al.*, 2006; Littler *et al.*, 2007; Cromer *et al.*, 2007). All structures bear the same canonical fold,

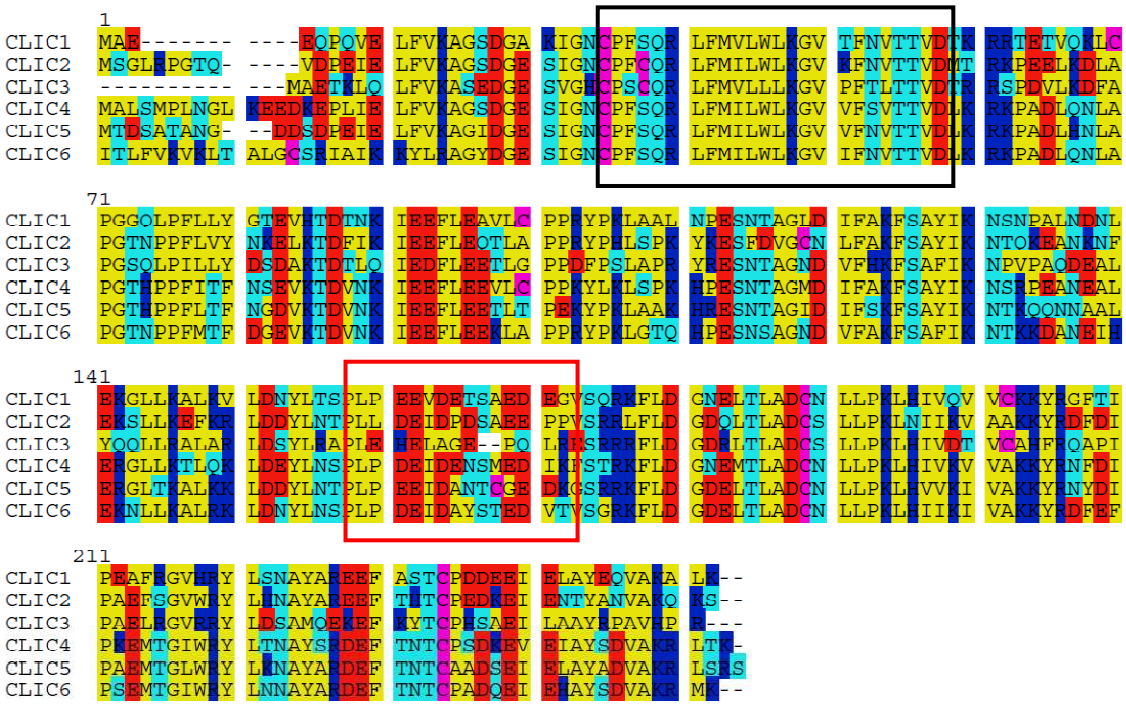

Figure 1.11. Multiple alignment of human CLIC sequences.

ClustalW alignment of the six human CLIC sequences, showing the high degree of conservation within the family. The extended N-terminal region of CLIC6 was omitted. The putative transmembrane region is boxed in black. The sequences within this region are practically invariant. The acidic "foot loop" region is boxed in red. Non-polar residues are yellow, polar residues are cyan, basic residues are dark blue, acidic residues are red and cysteines are pink.

which is that of the glutathione *S*-transferase (GST) superfamily (Wilce and Parker, 1994; Armstrong, 1997; Board *et al.*, 2000; Harrop *et al.*, 2001). For example, Figure 1.12 shows a structural alignment between CLIC1 and a monomer of Omega class GST (GST O1-1), the GST with which it shares the highest structural homology. It is likely, based on sequence similarity, that the CLIC structures not yet solved will exhibit the same or similar homology to GST structure. The known CLIC structures all have the same or similar thioredoxin fold in the N-terminal region consisting of a *βαβαββα* topology, and an all-helical C-terminal domain. The N-terminal *β*-sheet is between two *α*-helices on one side and one *α*-helix on the other. CLIC sequence identity with the GSTs is low, though, being up to only 16 % with GST O1-1 (Dulhunty *et al.*, 2001), and the

redox-active cysteine in the N-terminal domain is not conserved throughout. Also, the CLICs are monomeric, while the GSTs are dimeric.

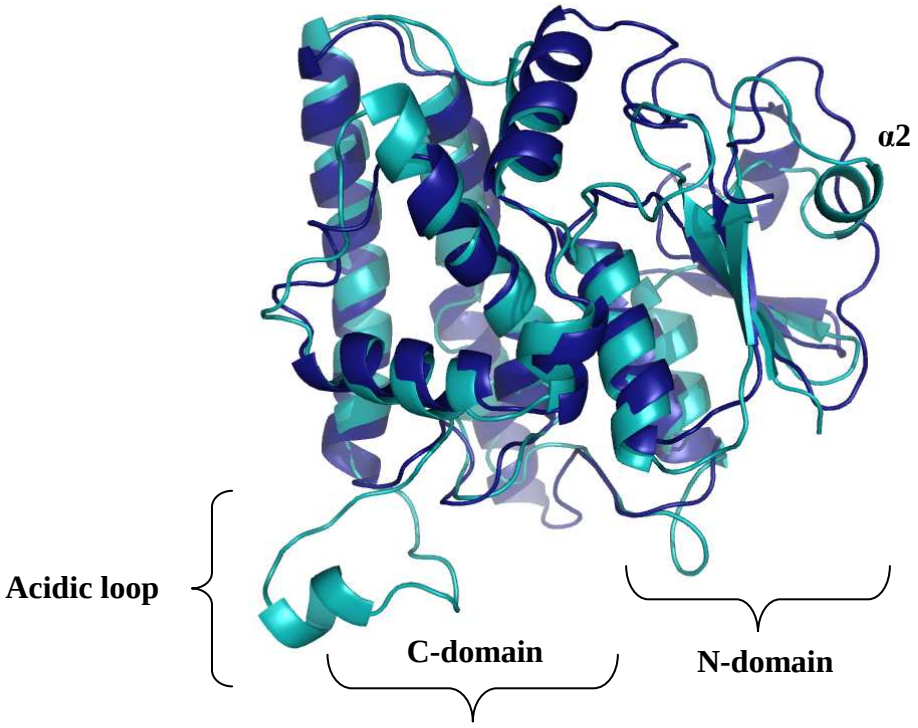

Figure 1.12. Structural alignment of CLIC1 with GST O1-1.

CLIC1 (cyan) alignment with a monomer of GST O1-1 (blue), with RMSD = 1.65 Å. The structure is remarkably conserved, with the N-domains aligning only slightly less than the C-domains. The major differences are in helix (top right) and in the acidic loop region of CLIC1, which is absent in GST O1-1. The alignment was performed using the MultiProt server (http://bioinfo3d.cs.tau.ac.il/MultiProt/) (Shatsky *et al.*, 2004) and PDB codes 1k0m (Harrop *et al.*, 2001) and 1EEM (Board *et al.*, 2000). Image rendered using PyMOL™ v. 0.99 (DeLano Scientific, 2006).

The question as to how, or even *why*, CLIC proteins rearrange themselves to generate a membrane-competent conformation remains highly speculative. A number of models for this transition have been proposed (Harrop *et al.*, 2001; Cromer *et al.*, 2002; Littler *et al.*, 2004; Singh and Ashley, 2006; Berry and Hobert, 2006; Fanucchi *et al.*, 2008), but until a membrane-inserted structure is

solved, the subject remains relatively obscure. An extensive structural rearrangement involving either the N- or C-terminal hydrophobic domains would be required. These correspond roughly to strand β2 and helix α1 in the N-domain or helix α6 in the C-domain (Figure 1.10). Various studies have narrowed the putative transmembrane region (PTM) down to the N-terminal domain region. These include immunological, electrophysiological and proteolytic studies which show that the membrane-inserted forms cross the bilayer an odd number of times (Duncan *et al.*, 1997; Tonini *et al.*, 2000; Singh and Ashley, 2006; Singh and Ashley, 2007). A truncated form of CLIC4 with only the first 61 residues of the N-terminal domain exhibited channel activity much like that of the native protein (Singh and Ashley, 2007). The N-terminal domain of EXC-4, the nematode CLIC homologue, has been shown to be necessary for membrane localisation and function, and surprisingly, the same study showed that beyond the PTM, the C-terminal region of invertebrate and vertebrate CLICs was functionally interchangeable (Berry and Hobert, 2006). Not only that, but the equivalent C-domain regions of Omega GST and Sigma GST, proteins which do not exhibit any membrane interactions, were also interchangeable! This certainly does appear to indicate that the proposed N-terminal PTM is indeed the region of CLIC proteins that traverses the membrane, where, it is believed, based on electrophysiological evidence, the functional structure is a tetramer or higher order multimer (Warton *et al.*, 2002; Littler *et al.*, 2004; Singh and Ashley, 2006, 2007). None of the CLICs has a membrane localisation signal sequence.

The first human CLIC protein, CLIC1, the subject of this study, was isolated from a human myelomonocytic line (Valenzuela *et al.*, 1997). It has 241 amino acids and a p*I* of 4.85. Bovine (p64) and rat brain (p64H1) CLIC homologues had been isolated prior to CLIC1 (Redhead *et al.*, 1992; Landry *et al.*, 1993; Howell *et al.*, 1996), but CLIC1 was interesting in that it localised to nuclear membranes, an unexpected locale at the time (Valenzuela *et al.*, 1997; Tonini *et al.*, 2000; Valenzuela *et al.*, 2000). It had been believed previously that nuclear ion channels were redundant, since nuclear pore complexes dealt with exchange of large molecules between the nucleus and the cytoplasm, whilst small ions and

metabolites diffused passively across the nuclear membrane (Miller *et al.*, 1991; Stochaj and Silver, 1992; Goldberg and Allen, 1995). However, this nuclear localisation has since proved to be tissue- and cell type-dependent. In a recent study using CLIC1 antibodies, CLIC1 expression was found in a non-polarised pattern throughout the cytoplasm of non-polarized cells such as basal epithelial cells of the upper gastrointestinal tract, skeletal muscle, and cultured Panc1 cells, with a small proportion present in the plasma membrane (Ulmasov *et al.*, 2007). In polarised epithelial cells, however, CLIC1 expression is polarised to the apical domain of the cells, with the vast majority membrane-inserted. Insertion is not into the plasma membrane, though, but to the membranes of subapical vesicles of the endocytic/recycling compartment (i.e., not to membranes of the ER, Golgi or trans-Golgi network). The suggestion, therefore, was that CLIC1 may play a role in the acidification of compartments along this pathway. Other areas where CLIC1 may play a role is in cell division, via regulation of chloride concentrations and therefore regulation of cell volume, or cell cycle regulation (Valenzuela *et al.*, 2000) and kidney function (Tulk and Edwards, 1998), while its direct interaction with F-actin implicates it in functions such as cell movement or division, endo- or exocytosis, intracellular vesicle fusion and apoptosis (Singh *et al.*, 2007).

The appearance of novel ion conductance in the presence of CLIC1 has been observed time and again, in cultured cells, nuclei, planar lipid bilayers, lipid monolayers and liposomes (Valenzuela *et al.*, 1997; Tonini *et al.*, 2000; Valenzuela *et al.*, 2000; Harrop *et al.*, 2001; Warton *et al.*, 2002; Tulk *et al.*, 2002; Littler *et al.*, 2004; Singh and Ashley, 2006; Singh *et al.*, 2007). The lipid mixture seems to be important for the readiness with which CLIC1 inserts (Singh and Ashley, 2006), but the functional protein has been reconstituted in a number of different mixtures. Channel activity is regulated by redox conditions (Littler *et al.*, 2004; Singh and Ashley, 2006), and can be abolished by the chloride channel blocker indanyloxyacetic acid 94 (IAA-94) (Tulk *et al.*, 2000; Tulk *et al.*, 2002; Warton *et al.*, 2002). There can no longer be any doubt that CLIC1 is an ion channel, but its poor selectivity suggests that it is not necessarily a chloride ion channel *per se* (Singh and Ashley, 2006).

The ubiquitous tissue and cellular distribution of CLIC1 mRNA, its conservation across species and the fact that it is present in foetal and adult cells imply some fundamental biological role for CLIC1. Exactly what this is is yet to be determined, but its apparent involvement in Alzheimer's disease (Novarino *et al.*, 2004; Milton *et al.*, 2008), colon cancer (Petrova *et al.*, 2008) and possibly in cystic fibrosis (Edwards, 2006) indicate that it may be a potentially important therapeutic target.

CLIC2 was identified in the telomeric Xq28 region of the human X chromosome, a region linked to X-linked mental retardation and X-linked epilepsy (Heiss and Poustka, 1997). It is expressed in most tissues, with particularly high levels in the lung and spleen, but is not expressed in the brain (Board *et al.*, 2004). CLIC2 inhibits cardiac ryanodine receptor (RyR2) Ca^{2+} channels in the sarcoplasmic reticulum in a redox-dependent manner, implicating it as a therapeutic target for ischemia-induced cardiac cellular damage (Dulhunty *et al.*, 2005; Jalilian *et al.*, 2008). This function of CLIC2 is interesting because GST O1-1, the GST to which the CLICs bear the most structural homology, while not able to form channels in its own right, *also* modulates RyR2 Ca^{2+} channels (Dulhunty *et al.*, 2001). CLIC2 is small (243 residues, ~ 27 kDa) with a p*I* of 5.24. It has the same canonical fold as the other CLICs for which structures are available, and shares 60 % sequence identity with CLIC1 and 63 % with CLIC4. The overall root mean square distance (RMSD) between CLIC2 and CLIC1 is 1.8 Å (for 224 residues) including the flexible so-called "foot loop" region of acidic residues in the C-terminal domain (Harrop *et al.*, 2001), and 0.9 Å excluding this region. Helix α2 is disordered in the CLIC2 structure. The RMSD between CLIC2 and CLIC4 is 0.8 Å (for 211 residues). The foot loop is disordered in the CLIC4 structure. The redox-active glutathione (GSH) binding site seen in CLIC1 is absent in CLIC2, replaced by an intramolecular disulphide bond between Cys30 (Cys24 in CLIC1) and Cys33 in an interdomain crevice dubbed the "mouth region" (Cromer *et al.*, 2007). In both crystal forms solved, the foot loop of one symmetry-related molecule inserts into the mouth region of another, giving rise to a so-called "foot-in-mouth" interaction (Figure 1.13). This may be how CLIC2 interacts with

RyR2 channels (Cromer *et al.*, 2007). Electrophysiological studies showed that CLIC2 forms redox-sensitive functional channels in bilayers with the probability of observing single-channel conductance increasing as the pH was lowered. Addition of 5 mM dithiothreitol (DTT) abolished channel activity (Cromer *et al.*, 2007). In CLIC1 and CLIC4, *oxidation* at the *trans* side of the membrane, where the redox-active cysteine would be located, lowered channel activity, although some gating of CLIC1 was noted with 1 mM DTT (Singh and Ashley, 2006; 2007).

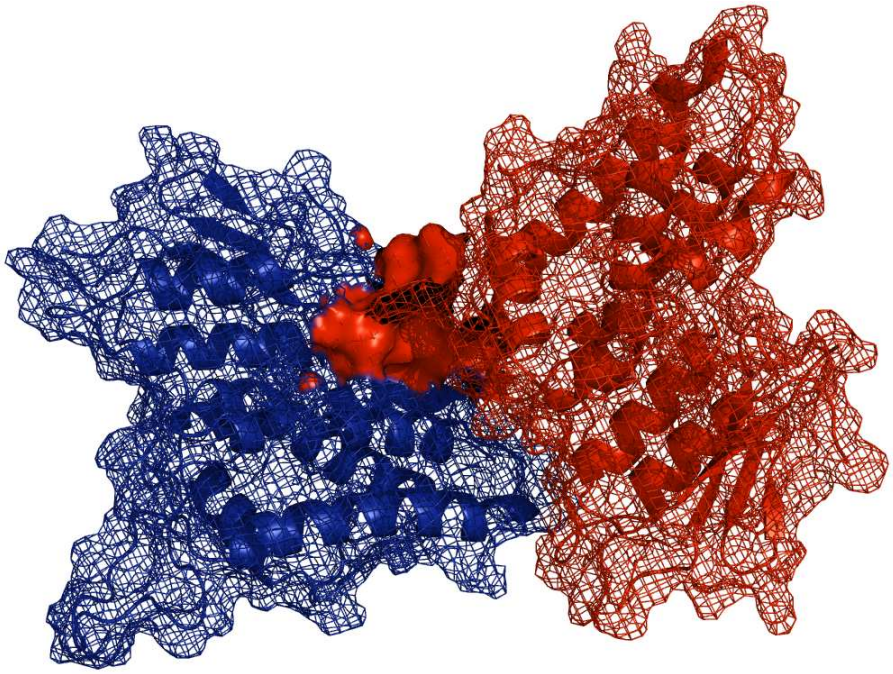

Figure 1.13. Structure of CLIC2.

Ribbon structure of symmetry-related CLIC2 molecules, showing the so-called "foot-in-mouth" interaction between the acidic foot loop of one molecule with the interdomain crevice of another molecule. PDB code 2R4V was used (Cromer *et al.*, 2007). Image rendered using PyMOL™ v. 0.99 (DeLano Scientific, 2006).

CLIC3, with 236 residues, is slightly smaller than CLIC1 and CLIC2, and shares 49 % sequence identity with CLIC1. Its mass is 26.6 kDa and its p*I* is 5.99. It was originally isolated in foetal brain tissue by Qian *et al*. (1999) during a search for proteins which interact with ERK7, a member of the mitogen-activated protein

(MAP) kinase superfamily. Co-immunoprecipitation of CLIC3 and ERK7 confirmed their interaction in mammalian cells, but CLIC3 is not a direct substrate of ERK7. CLIC3 localises predominantly to the nucleus, but also to the cytoplasm and the plasma membrane, where its presence induces novel chloride ion channel activity. However, CLIC3 lacks a significant N-terminal hydrophobic domain, and therefore is proposed to multimerise to form channels, if indeed it does form channels (Qian *et al*., 1999). The protein is expressed in human lung, heart, skeletal muscle, kidney and pancreas, and is abundantly expressed in human placenta (Money *et al.*, 2007). Its interaction with a MAP kinase superfamily member is unique amongst the CLICs, and may play a role in cell growth regulation (Qian *et al*., 1999).

CLIC4 is slightly larger than the first three CLICs, at 253 residues, with a calculated mass of about 28.7 kDa and a p*I* of 5.45. It shares 67 % sequence identity with CLIC1. Rat (p64H1) and mouse (mtCLIC) homologues were first identified by Duncan *et al*. (1997) and Fernández-Salas *et al*. (1999), respectively. They were widely expressed in different tissues, and they were found in both soluble and intracellular membrane-associated forms. The expression of mitochondrial mouse CLIC, mtCLIC, is regulated by the tumour suppressor, p53, and tumour necrosis factor α (TNFα). The human homologue, CLIC4, was identified in the apical regions of proximal tubule cells (Edwards, 1999). Mammalian CLIC4 mRNA is expressed in many different tissues: lung, liver, skeletal muscle, testis and skin (Duncan *et al.*, 1997; Fernández-Salas *et al.*, 1999). Membrane-associated rat brain CLIC4 was shown by proteolytic digestion studies to be a single-pass integral membrane protein, a small portion of whose N-terminal domain protruded into the lumen while the larger C-terminal domain remained cytoplasmic (Duncan *et al.*, 1997). The cytoplasmic domain of membrane-inserted CLIC4, corresponding to the C-terminal domain, forms complexes with a number of other proteins, such as brain actin, dynamin I and tubulin (Suginta *et al.*, 2001). Cytoplasmic CLIC4 co-localises with A-kinase anchoring proteins (AKAPs) including centrosomes and the cortical actin cytoskeleton (Berryman and Goldenring, 2003). CLIC4 enhances cell surface

expression of histamine H3 receptor (H3R), one of the G-protein coupled receptors (GPCRs) (Maeda *et al.*, 2008). This function is thought to occur by the electrochemical balancing of proton transport into endosomes by chloride conductance of CLIC4, thus enhancing recycling of H3R back to the plasma membrane. Mouse CLIC4 levels are enhanced by p53 and TNFα, which induces p53-mediated apoptosis marked by depolarisation of the mitochondrial membrane potential and release of cytochrome *c* (Fernández-Salas *et al.*, 1999, 2002). This fact links CLIC4 function to that of the Bcl-2 family, particularly Bax, which is a target for p53 transcription (Miyashita and Reed, 1995). CLIC4 may act as an alternative to Bax for ion flux regulation, and its apparent function in apoptosis may mark it as a potential anti-cancer target (Fernández-Salas *et al.*, 2002). CLIC4 membrane localisation is diverse. It has been found in the ER and outer nuclear membrane (Duncan *et al.*, 1997; Suh *et al*., 2004), caveolae (Edwards, 1999), mitochondria (Fernández-Salas *et al.*, 1999), large dense core vesicles (Chuang *et al.*, 1999) and the plasma membrane (Edwards, 1999, Proutski *et al.*, 2002). It has been functionally reconstituted into planar lipid bilayers and displays redox-sensitive, poorly selective ion selectivity (Singh and Ashley, 2007; Singh *et al.*, 2007).

The structure of soluble CLIC4 has been resolved as a monomer with a 16-residue C-terminal extension, referred to as CLIC4(ext) (Littler *et al.*, 2005) and as a homotrimer where the subunits associate via hydrophobic and hydrogen-bonded contacts (Li *et al.*, 2006) (Figure 1.14). The only significant difference between the CLIC1, CLIC4(ext) and CLIC4 trimer structures is in helix α2, which does not align closely in CLIC1 and CLIC4(ext), and is wholly or partially disordered in the CLIC4 trimer (as in the CLIC2 structure, too). This intrinsic flexibility may play a role in the conformational transition of the CLICs to their membrane-inserted forms (Li *et al.*, 2006). The acidic foot loop region is disordered in CLIC4 and CLIC4(ext). Whether the soluble trimeric structure of CLIC4 is indicative of its membrane-inserted conformation or not is speculative, but electrophysiological studies indicate CLIC4 may be a tetramer or higher order multimer (Singh and Ashley, 2007).

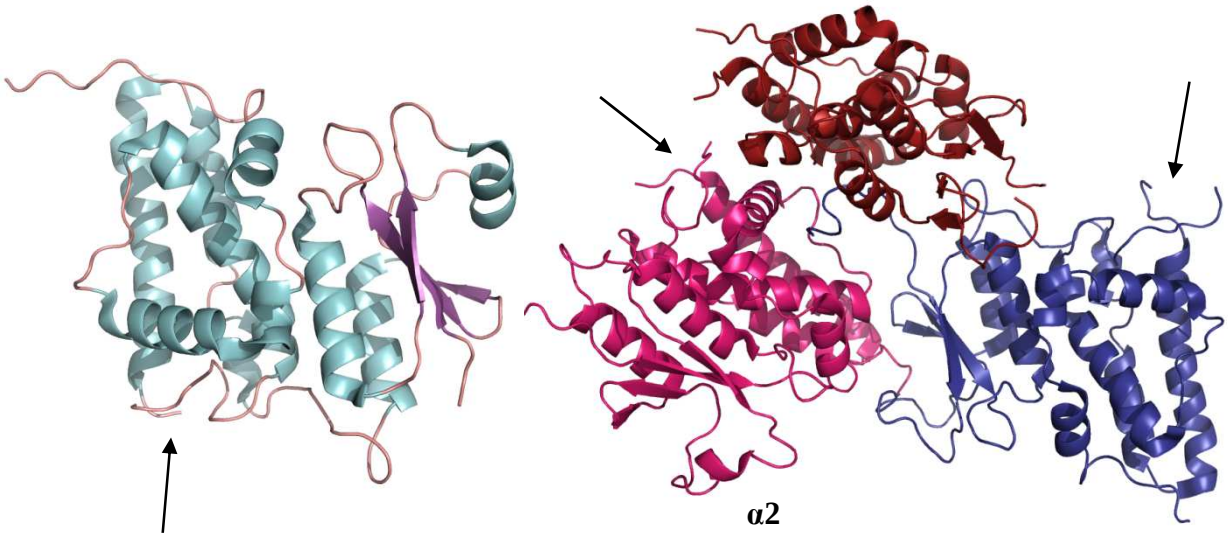

Figure 1.14. Structure of CLIC4.

Monomeric (left) and trimeric (right) crystal forms of CLIC4. The canonical thioredoxin fold is present in the N-terminal domains. Helix α2 is only really apparent in one of the trimer molecules (pink), and the flexible acidic foot loop region is disordered in both crystal structures (arrows). PDB codes 2AHE and 2D2Z were used (Littler *et al.*, 2005; Li *et al.*, 2006). Images rendered using PyMOL™ v. 0.99 (DeLano Scientific, 2006).

CLIC5 (strictly CLIC5A) has 251 resides with a predicted molecular mass of approximately 28.1 kDa. Its p*I* is 5.44. It displays 63 % overall identity with CLIC1. CLIC5 was isolated in a pull-down assay used to identify proteins that bind to the C-terminal domain of the AKAP ezrin, a membrane-cytoskeleton linking protein of placental microvilli (Berryman and Bretscher, 2000). CLIC5 bound tightly to either ezrin or to F-actin in the cytoskeleton of these polarised cells. CLIC5 was detected in a number of tissues, including heart and skeletal muscle, with lower levels in kidney, lung and placenta (Berryman and Bretscher, 2000). CLIC5 reconstituted into phospholipid liposomes exhibited chloride conductance that could be inhibited by indanyloxyacetic acid-94 (IAA-94) (Berryman *et al.*, 2004), but ionic selectivity was poor (Singh *et al.*, 2007). More recently it has been shown that CLIC5 (and CLIC1, but not CLIC4) interacts directly with F-actin and that F-actin regulates its ion channel activity (Singh *et*

al., 2007). F-actin inhibition of CLIC1 and CLIC5 channel activity was specifically from the cytosolic side, implying that the C-domains of CLICs play a role in channel regulation. Inhibition was abolished by F-actin disassembly.

CLIC6, the human homologue of parchorin (Nishizawa *et al.*, 2000), is the largest of the CLIC proteins, but its p*I* is the lowest of them all, at 4.29. With 704 amino acid residues, corresponding to a molecular mass of approximately 73 kDa, it seems strangely out of place in the CLIC family. Yet approximately the last 240 residues of the C-terminal domain have high sequence identity with the rest of the CLICs. Its extended N-terminal domain is highly hydrophilic, and contains 14 copies of a decapeptide repeat (Friedli *et al.*, 2003). CLIC6 is found in the cytoplasm and perinuclear region of water-secreting cells and endocrine cells (Griffon *et al*., 2003; Friedli *et al.*, 2003). It interacts with scaffolding proteins and a dopamine receptor to form a multimeric complex (Griffon *et al*., 2003). No ion conductance could be detected in transfected oocytes, leading to the conclusion that CLIC6 is either not an ion channel protein or requires other proteins for its function which were not present in the cells used (Friedli *et al.*, 2003). This is interesting, because parchorin does exhibit channel activity (Nishizawa *et al.*, 2000).

At this point it can probably be said that there is little doubt that most, if not all, of the CLIC proteins form functional ion channels in the cellular and subcellular membranes of a wide variety of cells and tissues, and that their ion channel activity is wholly or partly related to their numerous essential biological functions. Their sequence and structural similarity as well as their overlapping cellular locations suggest that there is a certain amount of functional redundancy built into the family. It is practically indisputable that it is the N-terminal PTM domain that traverses the membrane, although this does not exclude the possibility that the C-terminal domain may also have membrane-inserted regions. Structurally and functionally they bear more resemblance to the Bcl-2 family of apoptotic regulators than to the pore-forming toxins.

1.3. Protein folding

Protein folding has been studied for over 80 years, and is a vast and complex field. Over the years the methodology has moved from a more purely experimental basis to a synthesis of experimental and computational approaches. Ever since Anfinsen postulated that the three-dimensional structure of a protein is determined by its primary sequence (Anfinsen, 1973), the so-called "protein folding problem" has been of concern. The primary questions raised by Anfinsen's postulate are how, exactly, does the amino acid sequence of a protein code for a unique three-dimensional structure; and how do polypeptides fold as rapidly as they do into their native conformations despite, in theory, having to search through an infinitely large conformational space, a random search of which would take longer than the age of the universe? This is the Levinthal paradox (Levinthal, 1968).

The folding of most proteins to their biologically active conformations occurs spontaneously as the polypeptide comes off the ribosome in the cell, despite molecular crowding effects. However, the protein may not remain in its folded state. Many cellular processes, such as the translocation of proteins across membranes and cell cycle regulation require that proteins fold and unfold, and so it can be expected that proteins within the cell will exist in a variety of different states (Dobson and Karplus, 1999). The ability to fold and unfold is required for the function of some proteins (Plaxco and Gross, 1997), but the chances of aggregation and proteolytic digestion are greatly increased the longer a protein remains in an unfolded conformation. The speed with which proteins fold is probably an evolutionary development to avoid competition with aggregation, which is a relatively slow process (Lomakin *et al.*, 1996; Dobson and Karplus, 1999). Misfolded aggregates are a component in the appearance of the amyloid fibrils and plaques associated with neurodegenerative toxicity in diseases such as the prion-associated spongiform encephalopathies and Alzheimer's disease (Kelly, 1998, Uversky *et al.*, 1999a, 1999b). The study of protein folding seeks to understand how and why proteins fold to the conformations that they do, and how this information can be used to predict protein folding and function, as well as to design polypeptides *de novo* for use in the biotechnological and medical fields.

1.3.1. Forces stabilising proteins

Globular proteins are only marginally stable. Estimates of their conformational stabilities range from 5 kcal/mol to 15 kcal/mol (Pace, 1990). Conformational stability is defined as the difference in free energy between the native and unfolded conformations, denoted $\Delta G_{(H2O)}$. Apparently there is an evolutionary advantage to having such low stabilities, and this almost certainly has to do with function (Becktel and Schellman, 1987). There are three dominant forces that contribute to the stability of the native structure of a protein: electrostatic interactions (including ionic interactions and van der Waals forces), hydrogen bonds and hydrophobic interactions, the latter two contributing the most (Matthew, 1985; Dill, 1990; Pace *et al.*, 1996). These forces can be up to two orders of magnitude weaker than typical covalent bonds, but it is their very weakness that is their strength in maintaining the dynamic stability of the functional protein. The interplay of their interactions results in a robust network of surface and buried contacts that acts to overcome their greatest opposing force, conformational entropy (Dill, 1990).

1.3.1.1. Electrostatic interactions

Electrostatic interactions can be either charge-charge interactions between charged species (ionic interactions) or dipole-dipole type interactions between electrically neutral species (van der Waals forces) (Voet and Voet, 2004). In proteins, the charged carboxylate groups of acidic (Glu, Asp) and amino groups of basic (Lys, Arg, His) residues can participate in specific ionic interactions with each other, forming salt bridges (or ion pairs). These interactions occur at distances of the charged species from each other of ≤ 4 Å, and can additionally result in hydrogen bonds if the species are closer, at about ≤ 3.5 Å. Salt bridges are the strongest of the forces stabilising proteins. Their contribution to protein stability depends upon their geometry, including how the side chains are positioned relative to one another, and where they are located in the protein itself. The electrostatic potential between two charges varies with the distance between

the two and the dielectric constant of the medium they are in, as described by Coulomb's law:

$$U = k\frac{q_i q_j}{\varepsilon r_{ij}} \qquad \textbf{Equation 1-2}$$

where k is a conversion factor to the desired energy units, q_i and q_j are the two charges, ε is the dielectric constant of the medium and r is the distance between the charges. The equation shows that the attraction between the charges is higher in a low dielectric medium such as the interior of a protein, where the dielectric constant is estimated to be between 3 and 5, depending on the degree of flexibility of the polypeptide backbone (Honig *et al.*, 1986). Estimations of the number of ion pairs buried in the interior of proteins range from 17 % (Barlow and Thornton, 1983) to approximately 33% (Kumar and Nussinov, 1999) to 53 % (Lesser and Rose, 1990). Salt bridges can be stabilising or destabilising in proteins because of the balance between the favourable charge-charge interactions and the unfavourable loss of solvation and structural ordering (Bosshard *et al.*, 2004). This was shown quite neatly with a study of the conformers in nuclear magnetic resonance (NMR) structures of proteins, where ion pairs were lost in some conformers and other ion pairs were gained, with some of the interactions being stabilising and others destabilising (Kumar and Nussinov, 2001). This study also illustrated that the networks of interactions within proteins are in constant dynamic equilibrium.

The net contribution of surface ion pairs is of the order of 10 kcal/mol (Matthew, 1985), and these pairs are less likely to be conserved than buried pairs (Kumar and Nussinov, 2002). The contributions of buried ion pairs to overall stability vary depending on their geometries and the extent of burial, but can be quite high (~5 kcal/mol or higher) (Honig *et al.*, 1986; Kumar and Nussinov, 2002). Complete ion pairs, where there are two interactions between the same two residues, are more numerous and stronger than so-called "incomplete" ion pairs, where one residue has interactions with two different residues (Gowri Shankar *et al.*, 2007). This could allow for local flexibility. However, incomplete ion pairs are able to

form networks, and are therefore likely to contribute to the stability of the protein. Ion pairs contribute to the stability of secondary structures such as α-helices and β-turns, but are more important for anchoring tertiary structure than secondary structure (Gowri Shankar *et al.*, 2007).

The fact that the species making up salt bridges are titratable means that ion pair interactions are pH-dependent. Addition of protons to the solution will change the ionisation status of the charged groups according to their pK_a values, which may be shifted in the protein environment from that of model compounds. The pK_a values of Lys and Arg are high, so these residues are protonated at physiological pH. The pK_a values for the carboxyl groups on Asp and Glu are around 4, so they are negatively charged at physiological pH. His, with a pK_a value around 6.1 for the imidazole group, is a critical potential "pH sensor" within proteins, since it will be neutralised below its pK_a. Deviations in pK_a values of charged residues of up to 2 to 3 units have been observed in some proteins compared to model compounds, shifts that are attributed to electrostatic interactions and the local dielectric environment of the charged species (Matthew, 1985). Amino acids with anomalously shifted pK_a values contribute significantly to the electrostatic component of stability (Pace *et al.*, 1990).

The conformational state of a protein which has the higher affinity for protons will be the state stabilised with a drop in pH (Pace, 1990; Whitten and García-Moreno, 2000). Thus if the acidic residues in the native state have a higher affinity for protons than those in the unfolded state, the native state will be stabilised with a decrease in pH, and *vice versa*. Much research has been done on the effect of pH on proteins, with the unsurprising conclusion that pH has a profound effect on the structure and stability of proteins. Additionally, in many cases, an acid-induced intermediate state is found to be stabilised by a drop in pH (Jiang *et al.*, 1991; Muga *et al.*, 1993; Fink *et al.*, 1994; Whitten and García-Moreno, 2000; Chenal *et al.*, 2002; Nolan *et al.*, 2005).

Van der Waals forces are much weaker than ionic interactions, and arise from electrostatic interactions between molecules with permanent and/or induced dipoles. The carbonyl and amide groups of the peptide backbone have permanent dipole moments, an important fact for α-helices, since the arrangement of the backbone in the helix results in a macrodipole, positive toward the N-terminus and negative toward the C-terminus (Voet and Voet, 1995). Thus, despite the relative weakness of these interactions, which attenuate with r^{-3}, their number and arrangement within the low dielectric constant interior of a protein, means that they are a significant force in protein stability. Transient dipole moments can arise in non-polar groups due to fluctuating electron motion. Interactions between these transient dipoles are termed London dispersion forces. These are extremely weak interactions, and attenuate with r^{-6}, such that they are only significant between contacting atoms. Correct packing of the side-chains of the protein ensures that there are a large number of interatomic contacts, and it is this which makes these forces an important factor in maintaining stability, although they are not a dominant force in folding (Liang and Dill, 2001).

1.3.1.2. Hydrogen bonding

Hydrogen bonds are a type of electrostatic interaction. They arise from dipole-dipole interactions between a weakly acidic donor group and an acceptor group that bears a lone pair of electrons (Voet and Voet, 1995). In proteins in aqueous solution, the donor and acceptor groups can be the highly electronegative nitrogen, oxygen or sulphur atoms found in side chain residues and in the peptide backbone. The interaction is linear, directional, and occurs within a distance range of 2.7-3.1 Å. Linearity is not always a given, though, and significant deviation can occur within hydrogen bonding networks in proteins where donors and acceptors can be multiply bonded to other donors and acceptors (Voet and Voet, 1995). Hydrogen bond strengths range from 2-10 kcal/mol, depending on the geometry of the interactions (Dill, 1990). A large majority of the hydrogen bonding interactions in globular proteins (68 %) are between the amide hydrogen and the carbonyl oxygen in the peptide group (Stickle *et al.*, 1992), and only 11 % of carbonyl oxygens and 12 % of amide nitrogens are not hydrogen bonded

(Baker and Hubbard, 1984). Since the two major secondary structures in proteins, α-helices and β-sheets, depend on backbone hydrogen bonding for their structures, this is no surprise. The desolvation penalty of about 2.5 kcal/mol for burying a hydrogen bonded peptide group is offset by burial of a non-polar surface area (Baldwin, 2003). Like van der Waals forces, although the individual energetic contribution of hydrogen bonds to conformational stability may be small, their sheer number means they are a formidable force. Early views of the contribution of hydrogen bonds to the stability of proteins were that they were the most important factor (Mirsky and Pauling, 1936). By 1959, however, Kauzmann had brought the emphasis around to hydrophobic interactions as the dominant force for maintaining protein stability (Kauzmann, 1959). Current views hold that both hydrogen bonding and hydrophobic effects are the major forces involved in stabilisation of the native state (Pace *et al.*, 1996; Baldwin, 2003).

1.3.1.3. The hydrophobic effect

The hydrophobic effect, as mentioned in Section 1.1.1.1. comes about due to water molecules having a much stronger attraction to each other than to hydrocarbon molecules, an attraction that is also much stronger than that of hydrocarbon molecules to each other. This results in a exclusionary effect, such that non-polar molecules in aqueous solutions minimise their contact with water, an effect that is observed in bilayer lipid membranes, micelles and bicelles, and significantly, in proteins. The process (at room temperature) is entropically driven since the addition of non-polar molecules to water disrupts the hydrogen bonded structure of water. Thus water molecules order themselves around the non-polar molecules to maximise their contacts with each other and minimise their contacts with the non-polar substance (Geiger *et al.*, 1979; Stillinger, 1980). The vast majority (81 %) of non-polar residues in proteins are buried in the core (Lesser and Rose, 1990). Their close packing, aided by direct interatomic van der Waals forces, minimises the surface area exposed to the solvent (Pace, 1996). The sheer abundance of hydrophobic interactions results in a significant contribution to protein stability. The hydrophobic free energy contribution to protein stability is estimated at about 60 kcal/mol (Dill *et al.*, 1989). A fascinating observation that

appears to pinpoint the hydrophobic effect as the dominant force in protein folding is that jumbled protein sequences with only their correct hydrophobic and polar patterning retained, fold to their expected native states (Kamtekar *et al.*, 1993; Cordes et al., 1996; Kim *et al.*, 1998; Hecht *et al.*, 2004).

1.3.1.4. Conformational entropy

The principle force opposing the conformational stability of proteins is conformational entropy (Dill, 1990). As a protein folds, so its side chains lose rotational degrees of freedom, decreasing entropy, so the unfolded state is favoured by conformational entropy. Conformational entropy is large: about 50 kcal/mol, mostly because of the vast difference in the number of conformations available to the native state, where the protein is at its thermodynamic state of lowest free energy, compared to the unfolded state (Chan and Dill, 1990). Thus the net stability of the protein is mostly the difference between the large contributions from hydrophobic free energy and conformational entropy. The free energy of stabilisation of the native state is summarised with the standard thermodynamic equation:

$$\Delta \boldsymbol{G} = \Delta \boldsymbol{H} - \boldsymbol{T}\Delta \boldsymbol{S} \qquad \textbf{Equation 1-3}$$

where ΔH is the sum of the enthalpic effects of bond formation, T is the temperature and ΔS is the entropy term, which is composed of the favourable entropy of solvation for when hydrophobic side chains are removed from water, and the unfavourable conformational entropy, which opposes the ordering of the structure as the protein folds. The formation of the maximum number of interatomic and intramolecular (within the protein) interactions and bonds will maximise the negative enthalpic term. The more negative this term becomes, the better it will balance the opposing entropic term to maximise the free energy of stabilisation. Thus, the dense packing inside proteins contributes to its stability (Harpaz *et al.*, 1994).

1.3.2. Protein folding models

A number of models have been developed over the years to explain the rapid, highly cooperative process of the folding of proteins to their native states. Early models, for example, proposed that protein folding took place over a defined hierarchical pathway of discrete steps, with distinct intermediates and transition states, much in the way chemical reactions occur (Ptitsyn, 1973; Honig *et al*., 1976). The protein folding hierarchy corresponds to the hierarchy of protein structure. A similar model, the diffusion-collision model, proposed that the protein chain is composed of many unstable secondary structural microdomains which simultaneously search through conformational space before they coalesce into higher order structures (Karplus and Weaver, 1976). The nucleation-condensation model considers that secondary and tertiary structures are formed concurrently (Fersht, 1995; 1997). A nucleus of marginal stability is formed with some correct secondary and tertiary structural interactions. The rest of the structure is then able to condense around these structures, using them as a template and reducing the number of conformations the polypeptide has to search. This model is still currently in use, with adaptations to account for some of the features of older and newer models (Nölting and Agard, 2008). The hydrophobic collapse model (Dill, 1985) follows on from the theories of Kauzmann (1959), and sees the polypeptide initially collapse cooperatively due to long range hydrophobic interactions, followed by the formation of secondary and tertiary structures. While aspects of many of these models are probably correct, some of them fail to account for essential features of the folding process. Hydrophobic collapse, for example, cannot account convincingly for structural features due to the primary sequence of the protein (Roder and Colon, 1997).

Current models approach the problem in terms of statistical ensembles of states (Wolynes *et al.*, 1995; Dill and Chan, 1997; Dobson and Karplus, 1999) and describe folding using a multidimensional energy function known as a “folding funnel” or folding energy landscape (Honig, 1999) (Figure 1.15). The width of the funnel represents the conformational entropy of the polypeptide chain, while the depth represents the free energy of stabilisation. The native state exists at the

free energy minimum at the bottom of the funnel. As the polypeptide transits through various conformational states within the energy landscape it may encounter intermediate states and/or kinetic traps, but ultimately the landscape implies that there are *many alternate routes* to the native state. This approach encompasses some aspects of the older models as descriptors for events, but primarily sees folding as a transition from disorder to order, not as a transition from a reactant to a product (Dill *et al*., 2008). The denatured state exists as an ensemble of an unknown number of poorly structured conformations (not random coils) (Shortle, 1996), which the funnel model adequately encompasses within its presentation of conformational heterogeneity. Furthermore, the folding funnel model rationally accounts for the existence of ensembles of structurally and energetically non-equivalent intermediate states.

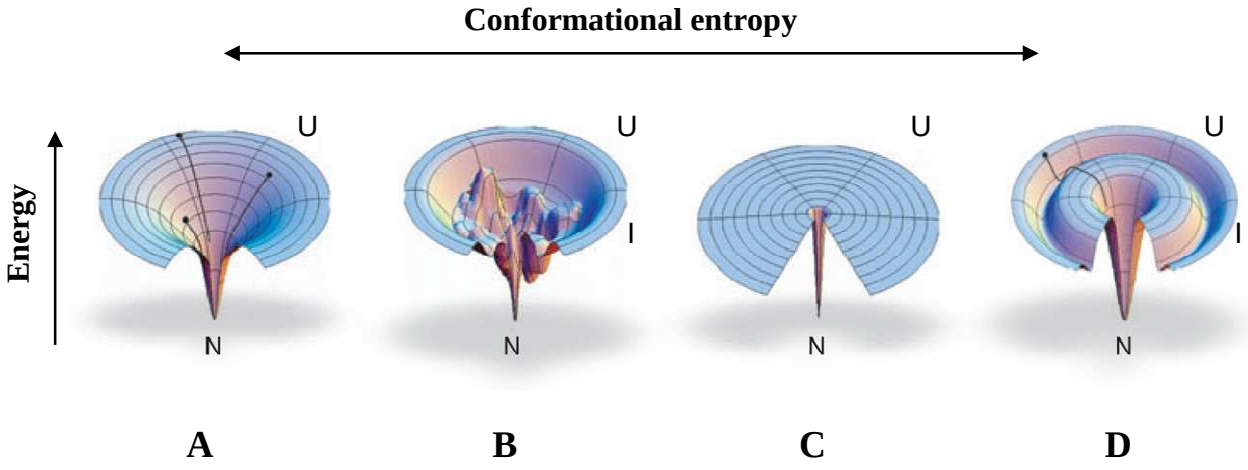

Figure 1.15. Different types of folding energy landscapes.

Folding funnel diagrams depicting (**A**) a smooth energy landscape for a fast folding polypeptide, (**B**) a rugged landscape that contains kinetic traps, (**C**) a smooth "golf course" energy landscape where the conformational search is diffusional, and (**D**) a moat style landscape, where the protein has no choice but to go through an intermediate state (I) in order to get to the native conformation (N). U represents the unfolded state ensemble. Image adapted from Dill *et al*. (2008).

1.3.3. Intermediate states

For many years analyses of denaturation curves of proteins were premised upon the two-state assumption, i.e., that the curve was populated by only one, or a mixture, of two possible states, the native state (N) or the unfolded state (U). However, in the late 1960s and the 1970s, the detection of acid-induced intermediate states led to the hope that some kind of universal folding intermediate existed that would help to solve the Levinthal paradox (Aune *et al.*, 1967; Tanford *et al.*, 1967; Tanford, 1970a; Kuwajima, 1977). Further evidence for intermediates that formed at low pH and often in mild denaturing conditions showed that they were a distinct group of species which had more of the characteristics of the native state than the unfolded state (Ohgushi and Wada, 1983; Ptitsyn, 1987; Kuwajima, 1989; Baldwin and Roder, 1991; Chyan *et al.*, 1993; Fink *et al.*, 1993; Ptitsyn and Uversky, 1994; Ptitsyn, 1995a). This intermediate state was designated the "molten globule" (Ohgushi and Wada, 1983), and defined as having the following general characteristics: a) the intermediate is compact, with dimensions slightly larger than those of the native state, but much smaller than those of the unfolded state; b) the average secondary structural content approximates that of the native state; c) the environments of the interior side chains is homogeneous, unlike the asymmetric environments of the native state side chains; d) interior amide groups are more accessible to hydrogen exchange, and exchange hydrogen atoms with the solvent more rapidly than those of the native state, and more slowly than those of the unfolded state; e) the enthalpy of the molten globule is close to that of the native state, but very different from that of the unfolded state; f) the molten globule state interconverts with the native state slowly and cooperatively, but interconverts rapidly and non-cooperatively with the unfolded state (Creighton, 1990; Ptitsyn, 1987, 1992). Another distinct characteristic of molten globules is that they have a much higher affinity for the fluorescent hydrophobic probe 1-anilino-naphthalene-8-sulphonate (ANS) than either the native or unfolded states do (Semisotnov *et al.*, 1991). This affinity is derived from the higher accessibility of the hydrophobic core of the intermediate protein conformation to the dye, since the packing of the native state is too rigid to allow this accessibility, and the loss of clusters of hydrophobicity in

the unfolded state precludes binding of the dye. Furthermore, the molten globule state has been characterised as having a "tertiary fold", a conformation wherein the spatial arrangement of α-helices and β-sheets is native-like, but without the specific side-chain packing of the native state (Peng and Kim, 1994). The term "compact intermediate" is sometimes preferentially used to describe the molten globule state because it may exist at one end of a continuum of partially unfolded conformations, and many of the so-called molten globules have differing structural properties (Creighton, 1990).

Classic examples of proteins that form molten globular intermediate states are α-lactalbumin (Kuwajima, 1977; Dolgikh *et al.*, 1981; Griko *et al.*, 1994), equine lysozyme (van Dael *et al.*, 1993; Griko *et al.*, 1995), staphylococcal nuclease (Dill and Shortle, 1991; Shortle, 1993, 1995, 1996) and apomyglobin (Cocco *et al.*, 1992; Barrick and Baldwin, 1993). What is of particular interest with these four proteins, as well as with some others that form molten globules, is that one domain or subdomain of the partially unfolded protein remains folded, while the other is unfolded (Freire *et al.*, 1992; Freire, 1995; Privalov, 1996; Vreuls *et al.*, 2004). In general, one of the domains is intrinsically less stable than the other. For example, the β-domain of α-lactalbumin is less stable than the α-domain, and has been found to be the unfolded portion of the molten globule, while the α-domain retains a native-like fold, without the extensive side-chain packing seen in the native state (Peng and Kim, 1994; Chyan *et al.*, 1993). In the equine lysozyme intermediate the α-domain side chains are largely immobilised and therefore must be closely packed, while the Gibbs energy of stabilisation of the β-domain is very low, and NMR experiments show it to be unstructured (van Dael *et al.*, 1993; Morozova *et al.*, 1995). In phosphoglycerate kinase, the N-domain contains fewer hydrogen bonds per residue than the C-domain, and is found to be stabilised by its interactions with the C-domain (Freire *et al.*, 1992). The intermediate state of this protein has a folded, native-like C-domain, while the N-domain is unfolded (Adams, *et al.*, 1985; Freire *et al.*, 1992).

Other intermediate species that do not exactly fit the criteria of a molten globule state have been identified (reviewed in Ptitsyn, 1995b). These have been designated pre-molten globule states or highly ordered molten globule states, depending on their level of native-like structural content, reflecting the statement made above that various similar, but different, intermediates may simply exist on a continuum between the native and unfolded states.

1.4. CLIC1 structure and properties

1.4.1. Primary, secondary and tertiary structure

CLIC1 is a relatively small, monomeric protein, with 241 residues and a calculated molecular mass of 26.9 kDa. The crystal structure of soluble, monomeric CLIC1 was solved at 1.4 Å resolution at pH 5.0 (Harrop *et al.*, 2001) (Figure 1.16). The structure is relatively flat, with dimensions of 55 x 52 x 23 Å. It has two domains, a mixed α-helical/β-sheet N-terminal domain containing a thioredoxin fold, and an all α-helical C-terminal domain. The structure is 47 % α-helical and 8 % β-sheet, with the remainder in turns. The sequence contains one tryptophan residue, Trp35, in the N-terminal domain near the domain interface, and eight tyrosine residues, two in the N-domain and six in the C-domain. There are 35 acidic and 27 basic residues in the CLIC1 sequence, giving the protein a net negative charge of -7 at physiological pH. CLIC1 has six cysteine residues, three in each domain. One of these, Cys24, is redox-active, and forms the centre of a glutaredoxin-like active site, although CLIC1 has not exhibited any catalytic activity (Harrop *et al.,* 2001). Cys24 is able to form a mixed disulphide bond with glutathione (GSH), but binding overall is weak. A *cis*-proline residue conserved in almost all GSTs and CLICs creates the appropriate active-site geometry for GSH binding (Harrop *et al.,* 2001). CLIC2 and CLIC3 contain the second Cys of the thioredoxin/glutaredoxin redox motif Cys-Xaa-Xaa-Cys, but unexpectedly, the recently solved crystal structure of CLIC2 shows that the GSH binding residues present in CLIC1 are absent in CLIC2, and GSH-binding is thus abolished

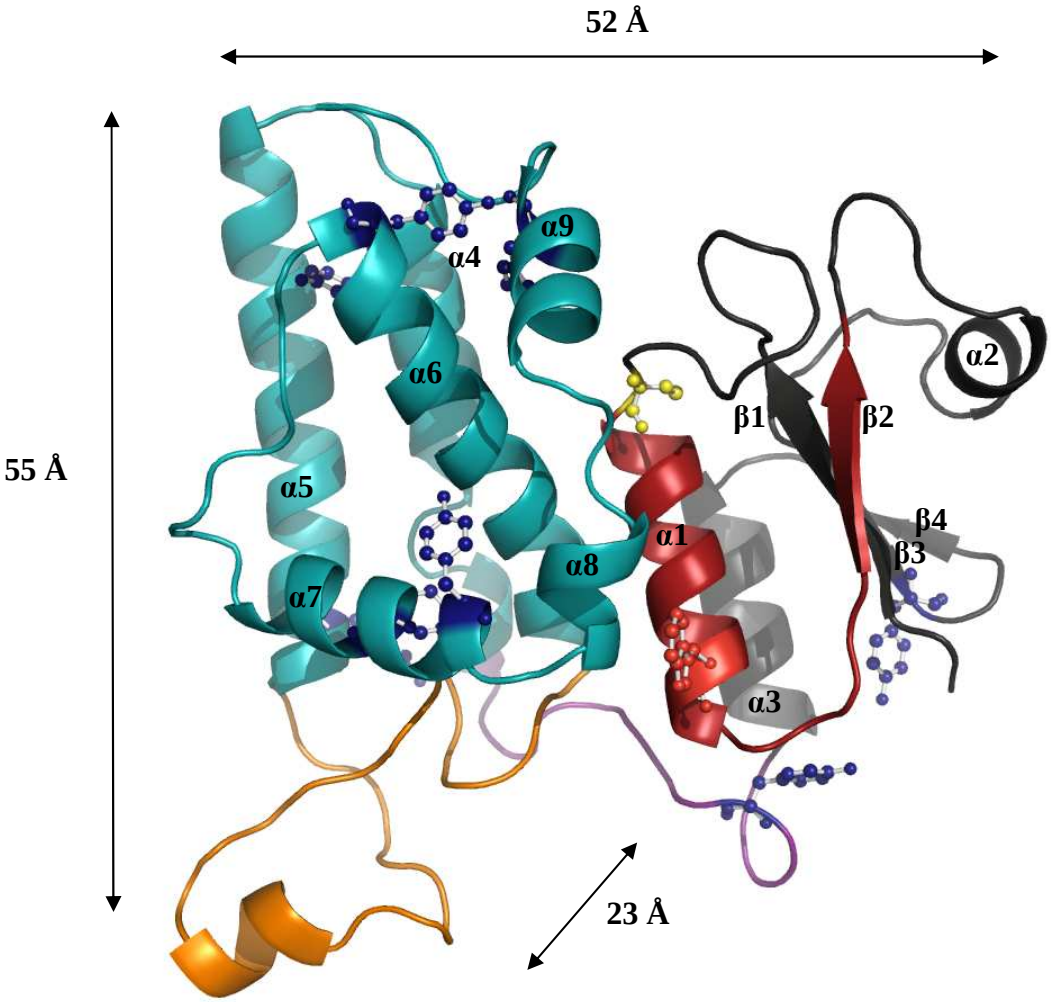

Figure 1.16. CLIC1 crystal structure.

Ribbon diagram of the crystal structure of reduced, soluble CLIC1. The N-domain is shown in red and grey, and the C-domain in green and orange. The domain linker is shown in purple. The putative transmembrane region is coloured red and the acidic "foot loop" is shown in orange. Selected residues are shown in ball and stick models. The single Trp residue (Trp35) is shown in red, the eight Tyr residues in blue and the redox-active Cys24 in yellow. PDB code 1k0m (Harrop *et al.*, 2001). Image rendered using PyMOL™ v. 0.99 (DeLano Scientific, 2006).

(Cromer *et al.*, 2007). CLIC1 has two putative nuclear localisation sequences, KRR (residues 49-51) and KKYR (residues 192-195) in its sequence, as well as a cAMP phosphorylation site and several putative protein kinase phosphorylation

sites (Valenzuela *et al.*, 1997). A hydrophobic patch on the protein surface is probably a protein interaction domain (Ashley, 2003), but may also be involved in membrane binding.

Upon oxidation, CLIC1 is able to transform reversibly to an all α-helical non-covalent dimeric conformation during which an intramolecular disulphide bond forms between Cys24 and Cys59, which are usually distant from each other (Littler *et al.*, 2004) (Figure 1.17). The C-domain undergoes little change, but the N-domain exhibits a major structural transition, proving the theory that it is intrinsically more susceptible to structural change than the C-domain. The dimer interface is mainly hydrophobic, and could form part of a membrane-docking interface if exposed *in vivo*. The dimer does not resemble those of the GSTs.

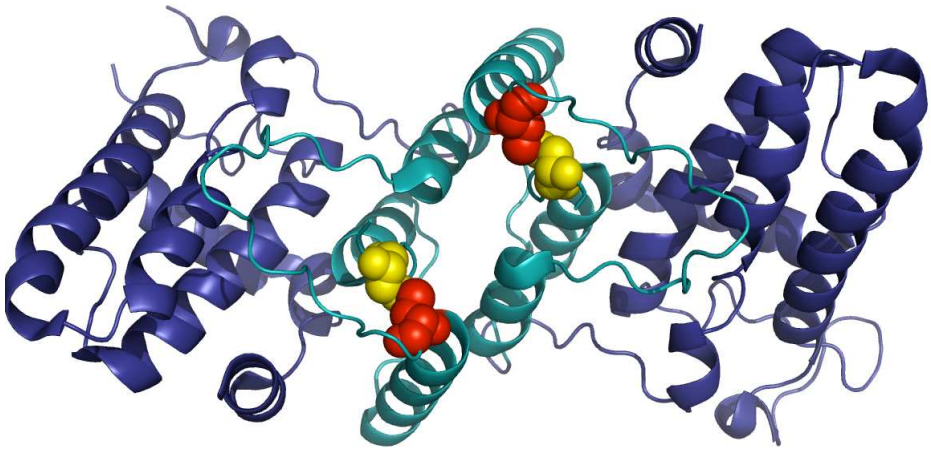

Figure 1.17. Structure of oxidised CLIC1.

Oxidised CLIC1 undergoes a major structural transition to form a dimer with intramolecular disulphide bonds between Cys24 (yellow) and Cys59 (red). The C-domain (blue) structure changes very little, while the N-domain (cyan) transforms completely from a mixed α-helical/β-sheet conformation to an all α-helical conformation. PDB code 1irk was used (Littler *et al.*, 2004). Image rendered using PyMOL™ v. 0.99 (DeLano Scientific, 2006).

Functional studies on Cys mutants showed that Cys24 and Cys59 are both essential for channel formation and for dimerisation of CLIC1 (Littler *et al.*, 2004). Cys24 is conserved only in vertebrates and Cys59 is conserved in neither vertebrates nor invertebrates, leading to speculation that the oxidatively regulated conformational change undergone by CLIC1 is specific for CLIC1 only (Berry and Hobert, 2006). The biological significance of the dimer formation may only be relevant at specific times though, when the normally reducing environment of the cell becomes oxidised, such as during cell cycle changes or even apoptosis.

As already mentioned, CLIC1 bears strong structural homology with GST O1-1. However, the CLIC proteins all have an acidic loop region in the C-terminal domain (Pro147 – Thr174, CLIC1 numbering), which is not present in GST O1-1. This region appears to be very flexible and the highly negatively charged region Pro147-Gln164 is speculated to be involved in protein-protein interactions (Harrop *et al.*, 2001). This is borne out by the recently resolved crystal structure of CLIC2, where the acidic loop of one molecule interacts with the groove formed at the active site region of Cys30 of a symmetry-related molecule (Cromer *et al.*, 2007) (Figure 1.13). The flexibility of this region within the family in general is attested to by its lack of electron density in two of the crystal forms of CLIC1 and both the CLIC4(ext) and CLIC4 trimer structures (Harrop *et al.*, 2001; Littler *et al.*, 2005; Li *et al.*, 2006). An additional region which has a high density of negative charge is near the C-terminus, in helix α9. This region contains six negatively charged residues. The profoundly negative nature of CLIC1 in general, with spots of basicity, give the molecule a distinct dipolar character (Figure 1.18). This may be important for its orientation prior to insertion into the membrane.

Another region of pronounced flexibility is the proline-rich linker loop between the N-domain and C-domain (Cys89 – Asn100). Pro91 exists as a major *cis* or minor *trans* conformer in the A and B monomers of the 1k0m crystal structure, respectively. The minor conformer shifts helices α1 and α3 somewhat relative to their conformation in the major conformer, giving the domain interface a certain

degree of plasticity which is speculated to be related to the structural alterations that would be required for CLIC1 function in vivo (Harrop *et al*., 2001).

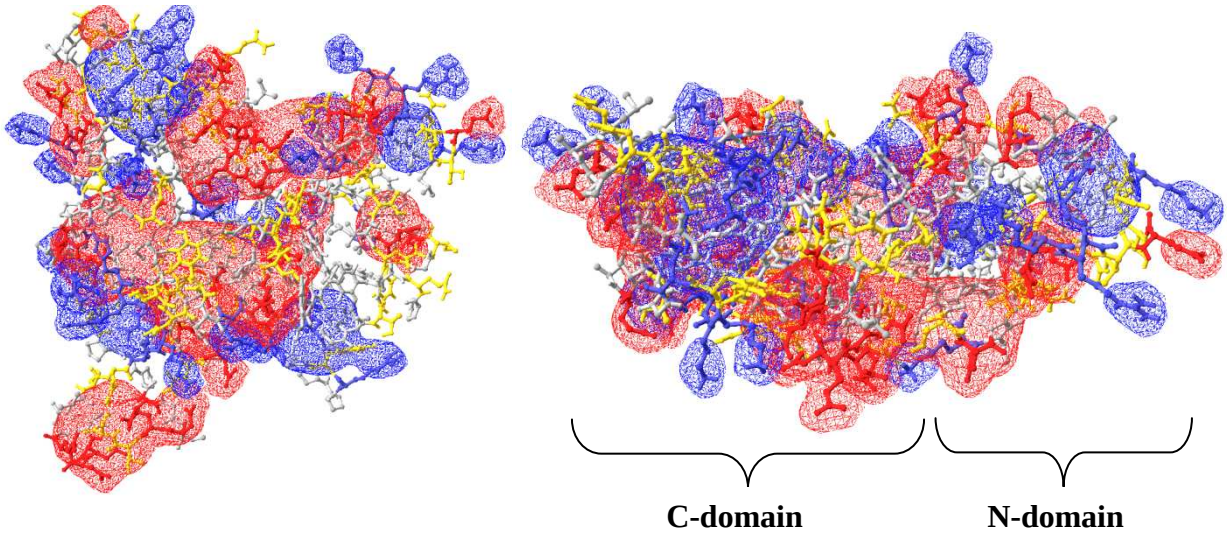

Figure 1.18. Electrostatic potential of CLIC1.

Side (left) and top (right) views of CLIC1 showing the electrostatic potential. Negative charge is red, positive charge is blue. Residues are coloured according to type: acidic – red; basic – blue; polar – yellow; non-polar – grey. The acidic nature of CLIC1 is evident. The view on the right shows that the electrostatic potential is somewhat biased toward one side of the molecule. Electrostatic potential was calculated using Swiss PDB Viewer v. 4.0.1. (Guex *et al.*, 1995) with solvent dielectric constant = 80, protein dielectric constant = 4, ionic strength = 0.05 M, and default pH = 7.0.

1.4.2. CLIC1-membrane interactions and insertion mechanism

It is no longer disputed that CLIC1 is an ion channel, or that it exists in dual soluble and membrane-inserted forms. The exact nature of the membrane-bound form and its significance within the wider biological function of CLIC1 are matters still receiving much attention. The structure of the CLIC1 channel is unknown, but is generally proposed to be tetrameric (Warton *et al.*, 2002), or even a multimer of up to 16 subunits (Singh and Ashley, 2006). This is because of the

rather varying single-channel conductances noted by different research groups, which have been suggested to represent different substates of the channel (Singh and Ashley, 2006). It was also suggested that the appearance of different substates may be related to the type of lipids used in the membrane system (Singh and Ashley, 2006), or to the chloride concentrations used (Tonini *et al.*, 2000).

The conserved putative transmembrane region (Cys24 – Val46) of CLIC1 is significantly hydrophobic, and like all of the human CLICs, but not necessarily the invertebrate CLICs, has an amphipathic character which is ideal for a membrane-traversing ion channel helix (Littler *et al.*, 2007). The proven membrane-insertion ability and functionality of the invertebrate CLICs would tend to suggest that this amphipathic character is not an absolute requirement for channel formation and function (Littler *et al.*, 2007). Cys24 is located at the N-cap position of helix α1, and would be present just on the outside of the membrane in the membrane-inserted conformation. Its location there was proposed, and has been shown, to regulate channel activity via redox control, with Pro25 possibly acting as a hinge region for opening and closing the channel (Harrop *et al.*, 2001; Singh and Ashley, 2006). Channel activity of CLIC1 reconstituted in bilayers was lowered in the presence of 5 mM *trans* GSH or 1 mM dithiothreitol (DTT). The channels also remained open or closed longer. However, *trans* oxidation with oxidised glutathione (GSSG) greatly reduced channel activity, and *cis* GSSG had no effect on function. The thiol-reactive reagent *N*-ethylmaleimide (NEM) blocked channel activity from the *trans* side, but had no effect from the *cis* side, and a Cys24 mutant was insensitive to the effects of NEM. These results are somewhat in conflict with those of Littler *et al*. (2004), who found that oxidation was essential for dimer formation and channel activity. In their experiments, oxidation greatly increased channel activity, and this activity of oxidised CLIC1 was abolished in the presence of 5 mM DTT. Thus, the exact role of oxidation in the function of CLIC1 is still being studied.

While studies of the truncated N-domain of CLIC1 have yet to appear, work on the truncated N-domains of CLIC4 and the nematode CLIC homologue EXC-4

have shown that this portion of the protein is all that is required for function (Berry and Hobert, 2006; Singh and Ashley, 2007). Truncated CLIC4 formed channels less readily and with reduced conductance and selectivity, but nevertheless functioned reproducibly in every experiment. They demonstrated the same redox sensitivity as the full-length protein. This would indicate that the extramembranous C-domain region serves only to orient the protein and act as a concentrating vestibule for ions travelling through the channel (Singh and Ashley, 2007). A vestibule-like function would greatly aid the efficient functioning of the channel, given that a negative surface potential depletes the surface concentration of anions, as discussed in Section 1.1.1.2. It is likely that the conserved KRR motif acts as a "plug" to anchor the protein in the membrane surface and possibly to direct ions toward the channel opening.

A study on EXC-4, a *Caenorhabditis elegans* excretory canal cell CLIC protein showed that deletion of strand *β*2 in the PTM region resulted in decreased membrane localisation, and that mutation of a highly conserved Leu46 in helix α1 (also in the PTM region) to a helix-breaking Proline disrupted membrane localisation, indicating that these secondary structural elements are important for membrane insertion of CLIC proteins (Berry *et al.*, 2003). The crystal structures of CLIC2 and trimeric CLIC4 show helix α2 to be disordered, and slight differences exist in this helix in the different crystal forms of CLIC1, suggesting a possible susceptibility to conformational change in this region leading to membrane docking (Li *et al.*, 2006; Cromer *et al.*, 2007). Structural rearrangement of the N-terminal domain would require the β1α1β2 supersecondary motif to detach from the rest of the protein, extend and refold into a helical membrane-traversing structure (Fanucchi *et al.*, 2008). Inherent plasticity in the domain interface and the proven ability of the N-domain to form an all α-helical conformation show that this may certainly be possible (Harrop *et al.*, 2001; Littler *et al.*, 2004). The protein may oligomerise either prior to or post-insertion, but appears to function as a monomer anyway (Warton *et al.*, 2002).

Further to studies that showed that CLIC1 activity occurred more readily and with greater conductance at low pH (Warton *et al.*, 2002; Tulk *et al.*, 2002), a recent study from our laboratory investigated the structural properties and conformational stability of CLIC1 as a function of pH in the absence of membranes (Fanucchi *et al.*, 2008). A highly populated intermediate species with a solvent-exposed hydrophobic surface was detected at acidic pH (≤ pH 5.5) under mildly denaturing conditions. An intermediate with the same properties was detected at pH 7.0 and 37 °C. Thus it was proposed that the negative potential and acidic environment encountered at the surface of the membrane could alter local and long range electrostatic interactions within the protein structure, priming it for membrane insertion via a lowering of the energy barrier for its conversion from a soluble to a membrane-bound conformation.

1.5. Objectives

The exact mechanism whereby CLIC1 transforms from a soluble cytosolic/nucleoplasmic protein to an integral membrane-bound channel is unknown. All models proposed to date agree that a dramatic structural rearrangement of the N-domain would be required for the transformation to occur.

The objectives of this project are threefold: The first is to characterise CLIC1 in terms of its secondary and tertiary structure, the second is to investigate its conformational stability using urea-induced equilibrium unfolding, and the third is to characterise a model membrane system that can be used for studies on the membrane-bound form of CLIC1. A reliable system of this sort has not yet been established in our laboratory. The aim is to characterise the structure and stability of CLIC1 at physiological pH and at the pH found at the membrane surface in order to detect if these conditions would have an effect on the structure and stability of CLIC1 *in vivo*. This may help to provide an explanation for how the protein is able to undergo the structural changes that would be required for its insertion into membranes.

CHAPTER 2. EXPERIMENTAL PROCEDURES

2.1. Materials

The cDNA encoding wild-type GST-CLIC1 fusion protein cloned into the pGEX-4T-1 vector was a gift from Dr. S. N. Breit, Centre of Immunology, St. Vincent's Hospital and University of New South Wales, Sydney, Australia (Valenzuela *et al.*, 1997). *Escherichia coli* XL1-Blue cells (Stratagene, USA) transformed with the pGEX-4T-1 plasmid encoding wild-type CLIC1-GST fusion protein were donated by Stoyan Stoychev, Protein Structure-Function Research Unit, University of the Witwatersrand. *Escherichia coli* BL21(DE3)pLysS chemically competent cells were obtained from Stratagene (USA). E. Cloni® 10G chemically competent cells were from Lucigen. Dithiothreitol (DTT), reduced glutathione (GSH), bovine plasma thrombin (T3399 and T6884) and glutathione-agarose were purchased from Sigma-Aldrich (USA). L-α-phosphatidylethanolamine Type IV, L-α-phosphatidylserine, L-α-phosphatidylcholine, L-α-phosphatidylinositol, sphingomyelin, cholesterol and asolectin were also from Sigma-Aldrich. Ultrapure urea was purchased from Merck (South Africa). The SDS-PAGE markers #SM0431 and #SM0661 and isopropyl-1-thio-β-D-galactopyranoside (IPTG) were obtained from Fermentas. Blue Dextran 2 000 000 was supplied by Sigma-Aldrich (USA), and the GeneJet Kit for plasmid DNA purification was obtained from Fermentas. Electron microscopy (EM) grade uranyl acetate was supplied by Merck (Germany) and EM grade glutaraldehyde was purchased from SPI-Chem™ Chemicals (USA). All other chemicals used were of analytical grade.

2.2. Experimental Procedures

2.2.1. Plasmid purification and insert identification

Glycerol stocks of XL1-Blue cells (Stratagene, USA) transformed with the pGEX-4T-1 plasmid containing the cDNA encoding wild-type GST-CLIC1 fusion

protein were plated on sterile Luria-Bertani (LB)-ampicillin agar (per 100 mℓ dH_2O: 1 g tryptone, 0.5 g yeast extract, 0.5 g NaCl, 1.5 g agar and 100 μg/mℓ ampicillin, added to cooled LB agar) and grown overnight at 37 °C. The high copy number pGEX-4T-1 plasmid contains an ampicillin resistance (amp^r) region coding for β-lactamase. This enzyme is able to destroy ampicillin by cleavage of the β-lactam ring in the ampicillin structure. It is used in the pGEX system as a selectable marker. A single colony was used to inoculate 100 mℓ sterile LB medium (1 g tryptone, 0.5 g yeast extract, 0.5 g NaCl per 100 mℓ dH_2O) containing 100 μg/mℓ ampicillin. The culture was grown overnight in a shaking incubator at 250 rpm and 37 ˚C.

The XL1-Blue strain is endonuclease (*endA*) and recombination (*recA*) deficient. These mutations improve plasmid DNA purification quality and insert stability. The overnight culture was used for small-scale plasmid DNA purification. GeneJet Kit (Fermentas) was used for the purification. The kit employs a standard alkaline lysis procedure (Birnboim and Doly, 1979; Ish-Horowicz and Burke, 1981; Sambrook *et al*., 1989). Briefly, the procedure uses alkali (NaOH) and detergent (sodium dodecyl sulphate (SDS)) treatment to lyse bacterial cells and denature chromosomal DNA and proteins. These and other cell debris are removed by centrifugation. Supercoiled DNA is not denatured and is thus not precipitated. The kit protocol was followed as written, except that initial cell culture volume was 4.5 mℓ, as opposed to 1.5mℓ. The presence and purity (in terms of chromosomal DNA) of the plasmid was verified by running 5 μℓ of purified plasmid DNA on a 1% agarose gel. GelRed™ (Biotium) was added to the loading buffer at 0.5 μℓ/100 μℓ and 2 μℓ of this was added to 5 μℓ of sample and marker DNA. GelRed™ is a fluorescent dye that intercalates between the stacked base pairs of DNA, allowing visualization of the DNA under ultraviolet light. The electrophoretic buffer used was 0.04 M Tris base and 2.54 x 10^{-3} M ethylenediaminetetra-acetic acid (EDTA), titrated to pH 8.5 with glacial acetic acid. A spectrum of a 21x dilution of the purified plasmid DNA was recorded from 220-300 nm on a Jasco V-550 UV/VIS spectrophotometer, and the concentration was determined using a NanoDrop™ ND-1000 spectrophotometer

(Thermo Scientific, USA). The NanoDrop™ measures various types of samples including nucleic acids and proteins, and can determine the concentration of as little as 1 μℓ of sample. It utilises surface tension to keep the sample in place. The optical density (OD) output is given for a cell of path length 1 cm. Five μℓ purified plasmid DNA was sent to Inqaba Biotec (Pretoria, South Africa) for sequencing of the insert using the 5'and 3' pGEX primers which bind at nucleotides 869-891 and 1041-1019 of the plasmid, respectively. The resulting sequence was aligned with the known CLIC1 ORF nucleotide sequence (Genbank AC: BC064527) using the global alignment tool, *NEEDLE*, in the EMBOSS suite of bioinformatics tools (Rice *et al*., 2000). The nucleotide sequence was also translated using *TRANSEQ* and the resulting peptide sequence aligned with the known CLIC1 peptide sequence (GenBank AC: O00299) (Rice *et al*., 2000).

2.2.2. Transformation of *Escherichia coli* BL21(DE3)pLysS cells with pGEX-4T1-CLIC1

Transformation of *Escherichia coli* BL21(DE3)pLysS cells (Stratagene, USA) with the pGEX vector containing the CLIC1 insert was performed using a one-step transformation method described by Chung *et al*. (1989). The control was pUC19 DNA. Fifty μℓ competent BL21(DE3)pLysS cells were thawed on ice for 10 minutes. One hundred ng of dsDNA was added to the cells and the reaction mixture stored on ice for 30 minutes. The cells were heat-shocked for 60 seconds at 42 °C and then immediately placed on ice for 2 minutes. Nine hundred and fifty μℓ of 37 °C 2x yeast tryptone (YT) medium (1.6 g tryptone, 1.0 g yeast extract, 0.5 g NaCl per 100 mℓ dH_2O) was added to the reaction mixture, which was then incubated on a shaking incubator at 37 °C for 1.25 hours. Stock and concentrated samples were spread onto LB-ampicillin (LB-amp) agar plates. For the stock sample, 100 μℓ of the reaction mixture was plated. For the concentrated sample, the remaining 900 μℓ cells were centrifuged at 13 000 rpm in an Eppendorf MiniSpin for one minute, 800 μℓ of supernatant aspirated and discarded and the cells resuspended in the remaining 100 μℓ 2xYT medium. The

resuspension was plated on LB-amp agar, and the plates were incubated for 16 hours at 37 °C.

E. Cloni® 10G chemically competent cells were transformed with pGEX-4T-1-CLIC1 in the same manner for plasmid maintenance and purification stocks.

2.2.3. CLIC1 heterologous over-expression and purification

Heterologous over-expression of recombinant CLIC1 was enabled by the inducible expression vector system, pGEX-4T-1, into which the CLIC1 cDNA was cloned. The system uses a strong promoter, *pTac*, a hybrid of two other strong promoters, *trp* and *lac*UV5 (Amann *et al*., 1983). *pTac* contains the -10 region of the *lac*UV5 promoter and the -35 region of the *trp* promoter (Amann *et al*., 1983). *Lac*UV5 is repressed by the *lac*I^q gene product, which itself is inactivated by the lactose analogue, IPTG. Thus, expression is repressed by lacI^q until IPTG is added in the early- to mid-log phase of cell growth to induce expression. The amount of expression by *pTac* should be proportional to the amount of IPTG added (Amann *et al*., 1983), although clearly there are limits. BL21(DE3)pLys cells carry a chromosomal copy of the T7 RNA polymerase gene under the control of the *lac*UV5 promoter. They also contain the coding sequence for T7 lysozyme, a bifunctional protein which is a natural inhibitor of T7 RNA polymerase (Moffat and Studier, 1987), and also cleaves specific bonds in the peptidoglycan cell wall of *Escherichia coli* cells (Inouye *et al.*, 1973). Pre-induction basal expression can thus be limited, and gentler sonication cycles employed. BL21(DE3) strains are particularly useful for high-level protein expression because they are ompT and Lon protease deficient. Target proteins are therefore less vulnerable to protease cleavage than in host strains not deficient in these proteases (Studier *et al*., 1990). CLIC1 is expressed as a fusion protein with a 26-kDa GST (*Sj*GST) encoded by the parasitic helminth *Schistosoma japonicum* (Smith and Johnson, 1988). *Sj*GST is a well-characterised protein, which can be purified on a GSH-agarose affinity column with a fairly high degree of confidence and yield (Smith and Johnson, 1988). The pGEX-4T-1 plasmid is engineered

with a thrombin cleavage site between the GST and the target protein, allowing on- or off-column cleavage of the target, CLIC1, from the GST with thrombin.

CLIC1 over-expression and purification were based upon the methods used by Tulk *et al*. (2000). Sterile LB (400 mℓ) containing 100 μg/mℓ ampicillin was inoculated with 50 μℓ/100 mℓ *Escherichia coli* BL21(DE3)pLys cells transformed with the pGEX-4T-1 plasmid containing the cDNA encoding for the fusion protein GST-CLIC1. The cells were incubated overnight at 37 °C with shaking at 250 rpm. Fresh sterile 2xYT medium (4 ℓ) containing 100 μg/mℓ ampicillin was inoculated with 20x dilutions of the overnight cultures. The cultures were grown for approximately 2 hours after inoculation, to an OD_{600} of ~0.6. Protein over-expression was induced with 0.8 mM IPTG, and cells were allowed to continue growing for a further 4-5 hours. The cells were then harvested by centrifugation in a Sorvall RC5C centrifuge using an SLA3000 rotor at 5000 rpm for 15 minutes at 4 °C. The pellet was resuspended in approximately 8 mℓ culture resuspension buffer, pH 7.5 (10 mM Tris, 200 mM NaCl, 1 mM EDTA, 0.02% NaN_3 and 1 mM DTT added fresh) per litre of original culture and frozen at -20 °C to initiate cell lysis.

The frozen cells were thawed on a rotator at 4 °C. One μℓ of 1 M $MgCl_2$, 1 μℓ of 100 mg/mℓ DNase and 10 μℓ of 10 mg/mℓ lysozyme were added per mℓ of cells. Cells were rotated at 4 °C for a further 20-25 minutes. They were lysed by sonication on ice for 3 cycles of 30 seconds, pulsed (intensity 3, pulse 0.5 sec) on a Sonicator™ Ultrasonic Processor XL (Misonix Inc.). Cell debris was removed by centrifugation in an SS34 rotor at 15 000 rpm for 30 minutes at 4 °C. The supernatant containing soluble proteins was diluted with an equal volume of culture resuspension buffer, pH 7.5, and filtered through a 0.45 μm filter to remove any remaining cell debris.

2.2.3.1. GST-CLIC1 fusion purification and cleavage

GST fusion proteins can be purified a number of ways, including cation exchange and affinity chromatography. The high specificity of affinity chromatography,

however, makes it an attractive purification option despite its cost. A specific ligand is covalently immobilised on a suitable matrix (agarose). Only molecules in the mobile phase that have an affinity for the immobilised ligand will be bound to the column. This principle was used to bind soluble GST-CLIC1 fusion protein in the supernatant of *Escherichia coli* BL21(DE3)pLysS lysate to a glutathione (GSH)-agarose column, where GSH and GST-CLIC1 are the immobilised ligand and the target molecule, respectively (Figure 2.1). The binding of CLIC1 to GSH is too weak to immobilise CLIC1 alone on a GSH-agarose column (Harrop *et al*., 2001). Purification and all experimental procedures were performed under reducing conditions, using 1 mM DTT, to prevent oxidative dimerisation of the protein (Littler *et al*., 2004).

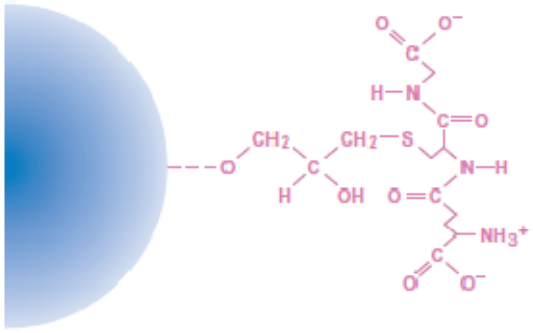

Figure 2.1. Glutathione immobilised to Sepharose.

Glutathione is coupled to Sepharose™ via the oxirane group using epoxy activation (image from GST Gene Fusion System Handbook, Amersham Biosciences).

A 20 mℓ GSH-agarose column was equilibrated at 4 °C with 300 mℓ GSH-equilibration buffer, pH 8.0 (10 mM Tris, 200 mM NaCl, 1 mM EDTA, 0.02% NaN_3 and 1 mM DTT added fresh). The diluted supernatant was loaded onto the column at a flow rate of approximately 1.5 mℓ/min. This was to ensure adequate binding of the *Sj*GST to the GSH. Flow-through was collected and reloaded at the same flow rate. Bacterial proteins and any unbound GST-CLIC1 were removed by washing the column with 300 mℓ GSH-equilibration buffer pH 8.0, followed

by 300 mℓ GSH-equilibration buffer pH 8.0 containing 1 M NaCl. The column was then equilibrated with 125 mℓ thrombin cleavage buffer, pH 8.4 (20 mM Tris, 150 mM NaCl, 2.5 mM $CaCl_2$, 0.02% NaN_3). To cleave the CLIC1 from the bound GST, a solution of 25 mℓ thrombin cleavage buffer pH 8.4 containing 80 µℓ of 1000U/mℓ bovine thrombin per litre of cell culture was added to the column, which was then sealed and digestion allowed to occur for 16 hours at 20 °C on a rotator. The GSH-agarose was allowed to settle for ~30 minutes post-digestion and the flow-through containing the CLIC1 cleaved from the GST and the thrombin used for cleavage (thrombin+CLIC1) was collected and pooled. The GST remained bound to the column. The column was subsequently washed with a 50-75 mℓ diethylaminoethyl (DEAE) equilibration buffer, pH 6.5 (20 mM Tris, 0.02% NaN_3, 1 mM DTT added fresh) and the flow-through collected and pooled. The GST was eluted from the GSH-agarose column with 50-100 mℓ GSH-agarose elution buffer pH 8.0 (50 mM Tris, 0.02% NaN_3, 10 mM GSH added fresh). The column was regenerated according to the manufacturer's instructions. During purification, samples of whole cell, supernatant, pellet, supernatant flow-through, washes, thrombin+CLIC1 elution and GST elution were collected for analysis on SDS-PAGE (section 2.2.3.3).

2.2.3.2. CLIC1 purification

CLIC1 was separated from the thrombin used for GST-CLIC1 cleavage by anion-exchange chromatography. Anion-exchange chromatography is based on the attraction between molecules with opposite charges. Depending on the pH, a protein may carry a net positive or net negative charge. This is determined by the isoelectric point (p*I*) of the protein. At a pH above or below its p*I*, a protein carries a net negative or positive charge respectively. A 30 mℓ Fast Flow™ diethylaminoethyl-agarose (DEAE) column (Amersham) was used to purify CLIC1 from the thrombin used to cleave it from GST. The column is positively charged within a fairly narrow pH range, and binds negatively charged molecules. The column was equilibrated at 20 °C at 3 mℓ/min with 300 mℓ DEAE-equilibration buffer, pH 6.5 (20 mM Tris, 0.02% NaN_3, 1 mM DTT added fresh), using an ÄKTAprime protein purification system (Amersham Biosciences). At

pH 6.5, CLIC1 (p*I* ~4.85) has a net negative charge and bovine thrombin (p*I* 9.3) has a net positive charge, as determined by the ProtParam tool on the ExPASy proteomics server (Gasteiger *et al*., 2005). Thus CLIC1 binds to the column and thrombin does not. The thrombin+CLIC1 eluted from the GSH-agarose column was loaded onto the DEAE column at 2.5 mℓ/min. The column was washed with 120 mℓ DEAE equilibration buffer, pH 6.5, to elute the thrombin. CLIC1 was eluted from the column with ~80 mℓ DEAE-elution buffer, pH 6.5 (20 mM Tris, 300 mM NaCl, 0.02% NaN_3, 1 mM DTT added fresh) and 2 mℓ fractions collected. The DEAE column was regenerated with 300 mℓ 1 M NaCl. Alternate fractions coinciding with the ÄKTAprime elution profile peak were analysed on SDS-PAGE to assess protein purity and approximate molecular mass. Fractions with significant bands (A_{280} higher than ~0.1) were pooled and dialysed into CLIC1 storage buffer, pH 7.0 (50 mM sodium phosphate, 0.02% NaN_3, 1 mM DTT added fresh) using Snakeskin™ Pleated Dialysis Tubing MWCO 10 000 (Pierce). Thereafter, CLIC1 protein stock was extensively dialysed every 6-7 days into 2-3 changes of storage buffer (1 ℓ/10 mℓ protein) containing 1 mM fresh DTT to maintain a reducing environment. High concentrations of CLIC1 (over ~120 µM) dialysed and stored at pH 5.5 tended to aggregate somewhat. If this occurred, the protein was centrifuged for 30 minutes at 13 400 rpm in an Eppendorf Minispin benchtop centrifuge at 4 °C and aggregates removed before concentration was determined and experimental work undertaken. All buffers were filtered through a 0.45 µm or sometimes 0.22 µm pore-size membrane to remove dust particles or other large contaminants prior to spectroscopic work being undertaken.

2.2.3.3. Sodium dodecyl sulphate polyacrylamide gel electrophoresis

Complex mixtures of proteins can be separated and characterised using SDS-PAGE. The method relies on the fact that charged particles in an electric field will move toward the electrode of opposite sign. Mobilities of different ions will differ in an area of the same field strength, so relative concentrations will adjust to maintain current (Wilson and Walker, 2005). The discontinuous system described by Laemmli (1970) was used for all SDS-PAGE analyses in this study. The

system utilises differences (discontinuities) in stacking and separating gel acrylamide concentrations, and differences in ionic strengths and pH values of the stacking and separating gel buffers, to "stack", or concentrate protein-SDS complexes between leading and trailing ions in the stacking gel. Once the trailing ions move into the higher pH of the separating gel, they gain higher mobility and move ahead of the protein-SDS complexes. The proteins then separate out according to their sizes. Some proteins run more slowly on SDS-PAGE gels than their calculated molecular weights would suggest they should, giving them a higher apparent molecular weight. This may have to do with variable binding of SDS to the protein due to higher numbers of charged groups (Reynolds and Tanford, 1970).

SDS is an anionic detergent that binds to proteins in a ratio of approximately 1.4 g SDS/g protein, although binding ratios may vary in glycosylated proteins or those with very high or very low isoelectric points (Pitt-Rivers and Impiombato, 1968; Reynolds and Tanford, 1970). The large negative charge of the bound SDS effectively masks the native net charge of the protein, conferring upon all proteins in the sample the same charge:mass ratio (Makowski and Ramsby, 1997). Proteins are denatured by SDS, and 2-mercaptoethanol is added to the sample buffer to reduce any inter- or intramolecular disulphide bonds. Thus, proteins are separated purely on the basis of size, due to the molecular sieving effect of the gel.

The stacking gels (4% T, 0.36% C) used were composed of 0.125 M Tris-HCl, pH 6.8, 0.1% (w/v) SDS, 0.1% (w/v) ammonium persulphate and 0.1% TEMED (w/v). Separating gels (15% T, 1.3% C) consisted of 0.375 M Tris-HCl, pH 8.8, 0.1% (w/v) SDS, 0.1% (w/v) ammonium persulphate and 0.1% (w/v) TEMED. Sample buffer was composed of 40% (w/v) glycerol, 0.02% (w/v) SDS, 0.05% (w/v) 2-mercaptoethanol, 0.05% (w/v) bromophenol blue and 0.0625 M Tris-HCl, pH 6.8, and was added to samples in a 1:4 sample to sample buffer ratio. Electrophoretic buffer, pH 8.3, was 0.192 M glycine, 0.124 M Tris base and 0.5% (w/v) SDS. The molecular mass markers (Fermentas #SM0431) used were: β-galactosidase (116 kDa), bovine serum albumin (66.2 kDa), ovalbumin (45 kDa),

lactate dehydrogenase (35 kDa), restriction endonuclease *Bsp*98I (25 kDa), β-lactoglobulin (18.4 kDa) and lysozyme (14.4 kDa). Another set of molecular mass markers used was #SM0661 (Fermentas), with sizes ranging from 25-200 kDa. Protein identities were not included in the product literature for these. Samples were boiled for 5 minutes to ensure denaturation and 20-30 μℓ of each sample was loaded on the gels. The gels were run at 140 V for 2-3 hours. They were stained for 3-16 hours in Coomassie Blue stain solution made up of 0.25% (w/v) Coomassie Brilliant Blue R250, 45% (v/v) methanol and 10% (v/v) glacial acetic acid. Gels were destained in 25% (v/v) ethanol and 10% (v/v) glacial acetic acid for 5-16 hours. Images of the gels were analysed using Labworks™ Image Acquisition and Analysis Software v.4.5 (UVP Bioimaging Systems, California, USA).

2.2.3.4. Protein concentration determination

Purified CLIC1 concentration was determined by ultraviolet (UV) absorbance spectroscopy using the Beer-Lambert law:

$$\mathbf{A = \varepsilon_{\lambda} c l} \qquad \textbf{Equation 2-1}$$

where A is the absorbance, ε is the molar extinction coefficient of the absorber at wavelength λ, c is the concentration of the absorbing solution and *l* is the cuvette path length. The molar extinction coefficient of CLIC1 was determined using the method of Perkins (1986), based on the molar extinction coefficients of tryptophan, tyrosine and cystine:

$$\begin{aligned} \varepsilon_{280}\ (\mathbf{M^{-1}cm^{-1}}) &= \mathbf{5550\Sigma Trp + 1340\Sigma Tyr + 150\Sigma Cys} \qquad \textbf{Equation 2-2} \\ &= \mathbf{5550(1) + 1340(8) + 150(6)} \\ &= \mathbf{17\ 170\ M^{-1}cm^{-1}} \end{aligned}$$

An apparently more rigorous method by Pace *et al*. (1995) gives an ε_{280} value of 17 420 M^{-1} cm^{-1} for CLIC1, but this value results in less than 1% difference in calculated protein concentration, and this laboratory utilises the method by

Perkins. A buffer-corrected standard curve was constructed from A_{280} readings for five or more dilutions of stock CLIC1 and the concentration of the stock calculated from linear regression analysis of the curve. Dilution factors were expressed as the ratios of the final fractional concentration of the diluted solutions to the initial concentration of the stock solution, where the latter was taken as 1 (Reed *et al.*, 2003). For example, the dilution factor for a fivefold dilution, using 1 part stock protein solution and 4 parts buffer, is expressed as 1/5, or 0.2. The A_{280} readings were corrected for absorbance by any aggregates at 340 nm by using the following calculation:

$$\mathbf{A_{280(\mathit{corrected})} = (A_{280(\mathit{protein})} - A_{280(\mathit{buffer})}) - (A_{340(\mathit{protein})} - A_{340(\mathit{buffer})})} \quad \textbf{Equation 2-3}$$

A spectrum from 240-340 nm of 4x diluted CLIC1 was recorded on a Jasco V-550 UV/VIS spectrophotometer. A quartz cuvette of 1 cm path length was used for all readings.

2.2.4. Spectroscopic methods

2.2.4.1. Circular dichroism spectroscopy

Circular dichroism (CD) relies upon the differential absorption of left- or right-handed circularly polarised light by optically active chromophores. The chromophore must either be intrinsically chiral or be in an optically asymmetric environment (Pain, 2004). The relevant optically active molecules in proteins are the peptide backbone, disulphide groups and aromatic residues (Woody, 1995). Circularly polarised light with equal right and left components is passed through the absorbing substance at a particular wavelength. An asymmetric chromophore or chromophore in an asymmetric environment will not absorb both components equally. The difference gives a resultant vector that is elliptical (Woody, 1996). The signal in the far-UV region (170-250 nm) arises predominantly from the peptide backbone, while the near-UV signal (250-340 nm) is dominated by characteristic absorption bands of the aromatic residues, specifically Phe, Tyr and

Trp, but also His to a certain extent. The signal is caused by the transition of an electron from a filled ground state orbital (n or π) to an empty excited state orbital (π*) with higher energy. Far-UV spectra are highly specific for specific secondary structures (Adler *et al*., 1973). Proteins with high α-helical content exhibit characteristic minima at 222 nm and 208 nm, with a strong positive band around 190 nm (Woody, 1995). The negative band with a 222 nm minimum has been assigned to the amide nπ* transition, while the 208 nm negative band and the 190 nm positive band result from exciton splitting of the ππ* absorption band into long- (208 nm) and short-wavelength (190 nm) components polarised along and perpendicular to a right-handed helix axis respectively (Woody, 1996).

Near-UV absorption and CD bands of proteins are much weaker than far-UV bands, but are, in a sense, more sensitive to assignation of specific features due to fine vibronic structure and wavelength differences. The Platt classification system characterises the electronic components of the electric dipole transition moments of the aromatic residues as ^1L_a and ^1L_b (Woody and Dunker, 1996). These transitions are perpendicular and parallel to the axis of rotation of the phenolic ring, respectively (Woody and Dunker, 1996). Strickland (1974) identified the peak wavelengths of these transitions for Phe, Tyr and Trp, with the ^1L_b transitions of Phe and Tyr occurring around 262 nm and 268 nm (Phe) and 277 nm and 283 nm (Tyr). The broad, somewhat featureless ^1L_a transition for Trp overlaps the ^1L_b transition of Phe, while the ^1L_b transition of Trp occurs above 275-285 nm up to about 300 nm and has much more fine structure. The fine structure is due to transitions between the ground state and different vibronic levels of the excited state, where 0-0 is a transition from the ground state to the lowest excited state vibronic level, 0 + 420 cm^{-1} is a transition from the ground state to the 420 cm^{-1} vibronic level in the excited state, and so on (Strickland, 1974). Coupling between two electronic transitions in different residues near to each other (up to 10 Å or even 15 Å (Strickland, 1974)) is a major mechanism contributing to aromatic near-UV CD bands, thus clustering of these residues will greatly influence the spectrum shape (Vuilleumier *et al*., 1993). The sign and magnitude of near-UV CD signals is determined by side-chain orientations and

the tertiary environments of certain residues under different conditions. Assignation of specific bands to specific residues is most easily achieved with multiple site-directed mutants; nonetheless, a certain amount of information about tertiary structure can be gleaned from the spectra of the same protein under different conditions. CLIC1 has 14 Phe, 8 Tyr and one Trp residues, the latter of which makes assignation of the ^1L_b Trp transition signal relatively uncomplicated.

All circular dichroism measurements were undertaken on a Jasco J-810 spectropolarimeter constantly flushed with nitrogen, and using Spectra Manager software v. 1.5.00. A 2 mm path length quartz cuvette was used for all far-UV CD measurements. Protein concentration was 2 µM CLIC1 in CLIC1 storage buffer (50 mM sodium phosphate, 0.02% NaN_3, 1 mM DTT added fresh), pH 7.0 or pH 5.5. All spectra were the result of 10 accumulations recorded at 50 nm/min with standard sensitivity (100 mdeg) over the range of 185-250 nm at 20 °C. The bandwidth was set at 0.5 nm, with a response of 1 sec and data pitch of 0.1 nm. Since most buffers above 10-20 mM and any buffer containing urea are not transparent below about 210 nm, CLIC1 storage buffer was diluted 10x for native spectra to reduce the noise signal at the lower end of the spectrum. All spectra were buffer-corrected and the raw signal in mdeg converted to mean residue ellipticity (MRE) [Θ] (deg.cm^2.dmol^{-1}.residue^{-1}) using the following equation:

$$[\Theta] = (100\ \theta)/cnl \qquad \textbf{Equation 2-4}$$

where θ is the raw signal in mdeg, c is the concentration of the protein (mM), n is the number of residues in the protein and *l* is the path length (Woody, 1995). Native spectra were smoothed using the negative exponential function in Sigmaplot v. 11.0 with a sampling proportion of 0.1 and a first degree polynomial. This function applies a Gaussian weight function to weight the data and a quadratic fit. Far-UV CD at 222 nm (E_{222}) was also used to monitor changes in secondary structure during urea-induced unfolding transitions (see Section 2.2.5.). E_{222} was used because CLIC1 is known to be predominantly α-helical, with 10 α-helices and 4 β-strands.

Near-UV CD spectra were recorded at 5 °C over a wavelength range of 250-340 nm at a scanning speed of 100 nm/min. The temperature was maintained by a Jasco PTC-423S Peltier-type temperature control system. A 1 cm path length cuvette was used, sensitivity was set at high (10 mdeg), data pitch was 0.05 nm, response 1 sec, bandwidth 0.5 nm, and each spectrum was the result of 10 accumulations. Protein concentration was 50 µM in 50 mM sodium phosphate, 0.02% NaN_3, 1 mM DTT added fresh. Low temperature CD measurements on proteins sharpen the CD bands because of lowered motility of the side-chains, and at very low temperatures (77 K) increase the intensity of the signal (Strickland, 1974). Near-UV CD signal data were not converted to MRE since only four types of residues contribute to the signal, making averaging over all residues unjustified. However, the HT voltage data for the near-UV CD spectra were converted to optical density (OD) using the Spectra Manager software in order to compare the absorbance and CD spectra.

2.2.4.2. Fluorescence spectroscopy

Fluorescence is the other side of absorbance, or the fate of a molecule after it has been excited to a higher energy state by the absorbance of light. The phenomenon is best explained with a standard Jabłoński energy diagram. Molecules in their ground energy state are excited by the absorption of light of a specific wavelength to a higher energy state, from where they can fall back down to the ground state by several processes: initially by loss of heat by internal conversion, which is loss of energy within an energy state, across vibronic levels; and then via non-radiative or radiative transitions (Van Holde *et al.*, 1998). The radiative transitions are either fluorescence or phosphorescence. Phosphorescence is a comparatively slow process and thus relatively rare. Fluorescence is thus basically the loss of electronic energy by emission of light, which emission occurs at a longer wavelength than the excitation radiation. This loss of energy between absorption and emission of light is termed “Stokes’ shift” and is due to processes including dissipation of vibrational energy and solvent-fluorophore interactions (Lakowicz, 1999). Generally speaking, the delocalised electrons in π orbitals of aromatic ring

structures are most easily excited to higher energy states, and these molecules are prone to fluoresce.

The tertiary structure of a protein can be characterised by fluorescence spectroscopy because of the presence of the intrinsic aromatic fluorophores, Tyr and Trp in just about every protein molecule. Fluorescence spectroscopy gives information about the packing and local environment of Tyr and Trp (Lakowicz, 1999), although protein fluorescence spectra are generally dominated by tryptophan emission. The quantum yields for Tyr and Trp - basically the ratio of the number of photons emitted to the number absorbed - are not that different (0.14 vs. 0.13 respectively) (Lakowicz, 1999), but the molar extinction coefficient for Trp is much higher, resulting in greater total yield. The indole ring of Trp is highly sensitive to solvent polarity because of the complexity of the electronic transitions to the ^1L_a and ^1L_b states and the relative orientations of the absorbing and emission states (Lakowicz, 1999). Proteins exhibit characteristic fluorescence spectra according to the environment within which the main fluorescing species are packed. Fluorescence intensity varies according to the polarity of the environment, but the fluorescence wavelength does not change for tyrosine (Lakowicz, 1999). The contribution of tyrosine can be undetected in the folded protein, due to energy transfer to tryptophan residues, or to quenching by nearby groups, but will often become apparent in a denatured sample (Lakowicz, 1999). Fluorescence emission intensity and wavelength for tryptophan change according to the polarity of the environment within which the tryptophan is found, and the degree of quenching experienced by the fluorophore as a result of that environment (Lakowicz, 1999). The greater the exposure of Trp to the polar aqueous environment, the longer its wavelength of maximum emission will be, since the polar solvent molecules lower the energy of the excited state (Royer, 1995). Tryptophan can be selectively excited at 295 nm since Tyr absorbs well below this wavelength. CLIC1 has eight Tyr and one Trp residue. The tyrosine residues are mostly in the C-terminal domain, with only two in the N-terminal domain, and Trp35 is in the putative transmembrane region in the N-terminal domain, acting as a local reporter for that region.

2.2.4.2.1. Intrinsic fluorescence

All fluorescence measurements on CLIC1 were performed on a Jasco FP6300 spectrofluorometer with Spectra Manager v. 1.54.03 software, using a quartz cuvette. Scan speed was 200 nm/min over a wavelength range of 280-450 nm using a quartz cuvette of path length 1 cm. Excitation was at 280 nm (Ex.280) or 295 nm (Ex.295), with excitation and emission slit widths at 5 nm. Sensitivity was set to manual with the photomultiplier (PMT) voltage set to 350 V, and response set to *fast*. The data pitch was 0.5 nm. Native and unfolded spectra of 2 μM CLIC1 in CLIC1 storage buffer (50 mM sodium phosphate, 0.02% NaN_3, 1 mM DTT), pH 7.0 and pH 5.5, and in 3.8 M and 8.0 M urea made up with CLIC1 storage buffer, were measured. All data were buffer-corrected.

2.2.4.2.2. Extrinsic fluorescence

8-Anilino-1-naphthalene sulphonate (ANS) (Figure 2.2), an amphipathic dye with a tendency to bind hydrophobic surfaces, has long been used as an extrinsic fluorescent probe of protein conformations because of its greatly enhanced quantum yield upon binding to exposed hydrophobic patches (Rosen and Weber, 1969; Brand and Gohlke, 1972). In particular, ANS is widely used for probing intermediate states in the unfolding transitions of proteins since clusters of hydrophobic residues not normally exposed in the native conformation of the protein become available for ANS binding (Semisotnov *et al.*, 1991). ANS has complex photophysical properties. The polarity of the environment affects both the quantum yield and energy of emission (and thus wavelength of emission) of the molecule (Gasymov and Glasgow, 2007). In aqueous solution the dye's fluorescence is quenched, but in a hydrophobic environment the intensity of fluorescence is greatly enhanced, and the maximum emission wavelength (λ_{max}) is blue-shifted. This is due to different excited states of the molecule. The first excited state – the non-polar (NP) state - is localised on the naphthalene ring, and high energy emission from this state occurs in non-polar solvents (Kosower and Kanety, 1983; Kosower, 1986). If the solvent is more polar, an intramolecular electron-transfer reaction from the NP state forms the charge-transfer state (CT), a

low energy state. In aqueous solution, intermolecular electron-transfer results in electron solvation and subsequent radiationless decay from the CT state, explaining the low quantum yield in aqueous solution (Kosower and Kanety, 1983; Kosower, 1986).

Figure 2.2. The structure of ANS.

ANS is charged, but is highly hydrophobic due to its triple ring structure. Electronic transitions of the delocalised π electrons within these rings are the basis of its fluorescent properties, but the polarity of the solvent will affect electron transfer reactions which determine the energy and intensity of emission.

ANS stocks were made up to between 2 mM and 6 mM using the 50 mM sodium phosphate storage buffer, 0.02 % NaN_3 with 1 mM fresh DTT into which CLIC1 had been dialysed that week. Separate stocks were prepared using pH 5.5 or pH 7.0 buffers. The stocks were warmed slightly during stirring and then filtered through 0.45 µm filters because ANS does not dissolve easily in aqueous solution, and black precipitate remains even after extensive stirring. The pH was checked and adjusted using NaOH and the ANS concentration was confirmed spectrophotometrically using a series of dilutions of stock ANS and an extinction coefficient of ε_{350} = 5000 M^{-1} cm^{-1} (Weber and Young, 1964). Dilution factors were expressed as the ratios of the final fractional concentration of the diluted

solutions to the initial concentration of the stock solution, where the latter was taken as 1 (Reed *et al.*, 2003).

Fluorescence spectra of ANS in the presence and absence of CLIC1 in 0.0 M, 3.8 M and 8.0 M urea were recorded at pH 5.5 and pH 7.0 on a Jasco FP6300 spectrofluorometer with Spectra Manager v. 1.54.03 software, using a 1 cm quartz cuvette. The scan speed was 200 nm/min over a wavelength range of 400-650 nm. Excitation was at 390 nm, with excitation and emission slit widths at 5 nm. Sensitivity was set to manual with PMT voltage at 350 V, and response set to *fast*. The data pitch was 0.5 nm.

Equilibrium unfolding in the presence of ANS was performed by allowing 2 µM samples of CLIC1 to unfold in 0-8 M urea for 1-2 hours as described in Section 2.2.5.4. The samples were then brought to 200 µM ANS and incubated at room temperature (20 °C) for a further hour before performing measurements. Equivalent samples containing no CLIC1 were prepared and treated in the same manner. These are necessary to correct for the increasing free ANS emission signal in increasing concentrations of urea. Samples were excited at 390 nm and the emission signal monitored at 460 nm (F460) using the time drive function on a Perkin Elmer LS50-B spectrofluorometer (pH5.5) or spectrum measurement on a Jasco FP6300 spectrofluorometer (pH 7.0). A quartz cuvette with a 1 cm path length was used, and both excitation and emission monochromator slit widths, respectively, were set to 5 nm on both machines. On the Perkin Elmer LS50-B, recordings were made at a data pitch of 0.5 sec for 60 seconds, and the free ANS-corrected F460 plotted as the average emission over this time period. On the Jasco FP6300, scan speed was 200 nm/min, data pitch 0.5 nm, response *fast* and sensitivity manual with PMT voltage at 350 V. F460 data were extracted, corrected for free ANS and plotted as a function of urea concentration using Sigmaplot v. 11.0.

The binding affinity of ANS for CLIC1 was determined by titrating aliquots of 2 mM stock ANS into 2 µM CLIC1 in 50 mM sodium phosphate buffer, 0.02 %

NaN_3 and 1 mM DTT at pH 5.5 and 7.0 in the presence and absence of 3.8 M urea. The same titrations were performed in the absence of CLIC1 to correct for free ANS. Data were collected on a Perkin Elmer LS50-B spectrofluorometer using the time drive function with excitation at 390 nm and emission at 460 nm. Recordings were made for 60 secs at a data pitch of 0.5 sec, with excitation and emission slit widths both at 5 nm. The averaged time drive data was corrected for free ANS and plotted using Sigmaplot v. 11.0.

2.2.5. Urea-induced equilibrium unfolding

2.2.5.1. Urea solution

Equilibrium unfolding was performed using ultrapure urea in CLIC1 storage buffer (50 mM sodium phosphate, 0.02% NaN_3, 1 mM DTT), pH 7.0 or pH 5.5, as the denaturant. Stock urea solutions of approximately 10 M were made up using 0.45 µm-filtered dialysis buffers into which CLIC1 stocks had been freshly dialysed and the pH adjusted by titration with orthophosphoric acid. The stock urea concentration was determined using the following equation from Pace *et al*. (1986):

$$\mathbf{[Urea] = 117.66(\Delta \mathit{N}) + 29.753(\Delta \mathit{N})^2 + 185.56(\Delta \mathit{N})^3} \qquad \textbf{Equation 2-5}$$

where (ΔN) is the difference between the refractive indices of the denaturant solution and water. Urea stocks were then kept at -20 °C until required, but for no longer than a week, because cyanate and ammonium ions form during the decomposition of urea, the former of which can chemically modify the amino groups of proteins (Stark, 1965). Once thawed, any unused urea was discarded.

2.2.5.2. Recovery

The reversibility of protein unfolding must be established before equilibrium unfolding studies can be performed. The shift in equilibrium toward the unfolded species that occurs in the presence of a chemical denaturant allows for the accurate determination of the equilibrium constant, K_{eq}, which is required to calculate ΔG and other thermodynamic parameters which define the stability of proteins. Fluorescence with excitation at 280 and 295 nm and far-UV CD (see section 2.2.4.) were used to follow refolding. At pH 7.0, triplicate 1 mℓ samples of 10 μM CLIC1 in 8 M urea were allowed to unfold for 2 hours at 20 °C. They were diluted 10x with CLIC1 storage buffer, pH 7.0 (50 mM sodium phosphate, 0.02% NaN_3, 1 mM DTT), and allowed to refold for 2 hours before spectra were recorded. Controls consisted of 1 μM CLIC1 in 0.8 M urea. At pH 5.5, triplicate 1 mℓ samples of 5 μM CLIC1 in 8 M urea were allowed to unfold for 1 hour at 20 °C. They were diluted 10x with CLIC1 storage buffer, pH 5.5 (50 mM sodium phosphate, 0.02% NaN_3, 1 mM DTT), and allowed to refold for 1 hour before spectra were recorded. Controls consisted of 0.5 μM CLIC1 in 0.8 M urea. Averages of triplicate spectra were buffer-corrected and plotted using Sigmaplot v. 11.0.

2.2.5.3. Equilibrium unfolding

The aim of equilibrium unfolding studies is to characterise the relationship between observed experimental results and the thermodynamic properties of a system by estimating the values of parameters which describe this relationship according to an applied denaturation model. Three denaturation models are in common use: Tanford's model, which makes use of data on the solubility of amino acid analogues upon transfer from water to aqueous urea or guanidine hydrochloride (GdnHCl) solutions (Tanford, 1970b); the denaturant binding model, which assumes that urea or GdnHCl molecules bind to amino acid side chains or the peptide group, and calculates thermodynamic parameters from the difference in the number of binding sites between native (N) and unfolded (U) states (Aune and Tanford, 1969); and the linear extrapolation method, which is

based upon the linear dependence of the free energy of unfolding on denaturant concentration (Schellman, 1978), and extrapolates this dependence from the transition region to zero denaturant concentration (Greene and Pace, 1974). This last method is the method used here, and is the most widely used for two reasons: additional parameters such as those representing the transfer of protein residues into denaturant or the binding behaviour of denaturant molecules are not required; and agreement between estimates of the change in Gibbs free energy of unfolding in the absence of denaturant ($\Delta G_{(H2O)}$) from urea and GdnHCl denaturation is the closest (Greene and Pace, 1974). This method always gives the lowest estimate of $\Delta G_{(H2O)}$ (Greene and Pace, 1974), and relies on a number of assumptions: reversibility of unfolding, that the transition is two-state, that the assumption of linear dependence of the free energy of unfolding on denaturant concentration is valid, and that $\Delta G_{(H2O)}$ is independent of denaturant, i.e. is a property of the protein system itself (Santoro and Bolen, 1988).

Denaturation curves are useful for several reasons: for determining the conformational stability of proteins, for inferring the folding mechanism of a protein, for inferring the structure of a protein (e.g. number of domains) and the relative stabilities of domains (Pace, 1986), for detecting the existence of stable unfolding intermediates and for comparing differences in conformational stabilities among proteins. The elucidation of unfolding pathways and typical parameters should someday allow for the development of reliable models for the prediction of protein folding pathways. The conformational stability of a folded protein refers to the free energy change, ΔG, for the unfolding of a protein from its native to denatured states (Schellman, 1978). The native conformations of proteins have been found to be only marginally more stable (approximately a few hydrogen bonds in terms of free energy change) than denatured, biologically inactive conformations (Tanford, 1970b; Privalov and Gill, 1988; Pace, 1990; Pace *et al.*, 1996). Forces that contribute to the conformational stability of proteins are van der Waals forces, electrostatic forces, hydrophobic interactions and hydrogen bonding (Dill, 1990; Lins and Brasseur, 1995; Pace *et al.*, 1996). Chemical denaturation by chaotropic agents such as urea or GdnHCl can be

monitored by a number of methods, including fluorescence (Brand and Witholt, 1967), CD (Adler *et al*., 1973), UV difference spectroscopy (Donovan, 1973; Herskovits, 1967) and nuclear magnetic resonance spectroscopy (NMR) (Wüthrich *et al*., 1980). Urea is believed to exert its denaturing effect either directly, by binding to the protein, or indirectly, by altering the solvent environment (Bennion and Daggett, 2003). It thus alters the equilibrium between the folded (N) and unfolded (U) states of the protein: $N \leftrightarrow U$.

2.2.5.4. Probes

The probes used in this study were fluorescence and far-UV CD spectroscopies (see Section 2.2.4.). These techniques are complementary because far-UV CD measures secondary structure (Adler *et al*., 1973) while fluorescence spectra can indicate changes in the tertiary environments of Tyr and Trp residues (Lackowicz, 1983; Brand and Witholt, 1967). The simultaneous use of both of these probes is convenient because both require very low concentrations of protein and are relatively straightforward to execute. In addition, intermediate states along the transition curves are likely to be detected because of differences in the transitions obtained by monitoring both secondary and tertiary structural changes.

Triplicate 1 mℓ samples of 2 μM CLIC1 in urea concentrations ranging from 0.0-8.0 M in 0.2 M intervals were prepared by adding denaturant slowly to protein and mixing by gentle inversion 3 times. Samples were allowed to unfold at 20 °C for 1 hour at pH 5.5 and for 2 hours at pH 7.0. Unfolding was followed using fluorescence with excitation at 280 and 295 nm and far UV-CD (see Section 2.2.4.). Fluorescence spectra were recorded on a Jasco FP6300 spectro-fluorometer with Spectra Manager v. 1.54.03 software, using a 1 cm quartz cuvette. The scan speed was 200 nm/min, data pitch 0.5 nm, response *fast* and sensitivity manual with PMT voltage at 350 V. CD data were collected by monitoring the signal at 222 nm on a Jasco J-810 spectropolarimeter. Data were collected for 60 sec at a data pitch of 0.1 sec with standard sensitivity, bandwidth of 0.5 nm and response of 1 sec. Fluorescence emission and CD spectra of 0.0-8.0 M solutions of urea prepared with CLIC1 storage buffer were measured to check

background signal. Light scatter for each sample, which indicates the presence of aggregates, was recorded with both excitation and emission wavelengths set at 340 nm. Data were collected for 60 sec at a data pitch of 0.2 sec with slit widths of 2.5 nm. Sensitivity was set to *high* and response to 2 sec. All data were buffer-corrected, and were plotted in SigmaPlot v. 11.0.

2.2.5.5. Equilibrium unfolding data-fitting

Calculation of thermodynamic parameters from unfolding data can only be carried out if 2 conditions have been met: the reversibility of the reaction has been established and the reaction was at equilibrium before measurements were undertaken (Pace, 1986).

The fluorescence unfolding data were presented and analysed in 3 ways:

i. The maximum emission wavelength (λ_{max}), i.e., the wavelength at which each spectrum peaked, was plotted against urea concentration.
ii. The emission intensities at the wavelength at which the native species peaked were plotted against urea concentration.
iii. The emission intensities at a number of different wavelengths along the rising, peak, and falling portions of the spectra were plotted against urea concentration.

Averages of triplicate data sets were used in each case. Data sets were first overlaid to ensure that their transition regions in particular were superimposable.

The circular dichroism data was plotted as the average of triplicate data sets (which had been confirmed to superimpose) of ellipticity at 222 nm as a function of urea.

The unfolding data at pH 7.0 was fitted to a *two-state monomer* (N ↔ U) unfolding model. The pH 5.5 data was fitted to a *three-state monomer* (N ↔ I ↔ U) unfolding model. The fits were calculated by global analysis (Beecham, 1992) using the program Savuka v. 6.2.26 (Zitzewitz *et al.*, 1995; Bilsel *et al.*, 1999) and a Poisson probability distribution. The program uses a Marquardt-Levenberg type

non-linear least squares routine to analyse simultaneously multiple data sets from different experiments in terms of internally consistent sets of fitting parameters (Beecham, 1992), thus minimising error. The test statistics generated are the chi-squared (χ^2) and goodness-of-fit parameters.

2.2.5.5.1. Two-state monomer fit

In a two-state monomer unfolding transition, only two species exist: the native species (N), and the unfolded species (U), N ↔ U.

A two-state unfolding curve has three regions (Pace and Stoltz, 1997):

i. The pre-transition region, in which the native state predominates.
ii. The transition region, where native and unfolding species exist in varying concentrations, and cooperative unfolding occurs
iii. The post-transition region, in which the unfolded state predominates.

The sum of the fraction of protein in the native conformation (f_N) and the fraction of protein in the unfolded conformation (f_U) will always be 1:

$$f_N + f_U = 1 \qquad \textbf{Equation 2-6}$$

The physically observed signal, recorded using circular dichroism and fluorescence in this study, is represented by *y*, which at any point in the curve will be:

$$y = y_N f_N + y_U f_U \qquad \textbf{Equation 2-7}$$

where y_N and y_U represent the measured properties of the folded and unfolded states, respectively. y_N and y_U for the transition region are calculated by linear extrapolation of the pre- and post-transition regions. Equations 2-6 and 2-7 are combined to give:

$$f_U = \frac{(y_N - y)}{(y_N - y_U)} \qquad \textbf{Equation 2-8}$$

The Gibbs-Helmholtz equation relates the Gibbs free energy for the transition, ΔG, to the equilibrium constant, K_{eq}:

$$\Delta G = -RTlnK_{eq} \qquad \textbf{Equation 2-9}$$

where R is the universal gas constant (1.987 cal mol^{-1} K^{-1}) and T is the absolute temperature. For a two-state monomer transition:

$$K_{eq} = \frac{f_U}{f_N}$$

$$= \frac{f_U}{(1 - f_U)}$$

$$= \frac{(y_N - y)}{(y - y_U)} \qquad \textbf{Equation 2-10}$$

Substituting into Equation 2-9:

$$\Delta G = -RT\, ln\left(\frac{y_N - y}{y - y_U}\right) \qquad \textbf{Equation 2-11}$$

The method assumes a linear relationship between ΔG and denaturant concentration (Greene and Pace, 1974) such that $\Delta G_{(H2O)}$ can be determined by extrapolation from a plot of ΔG vs. [urea] according to:

$$\Delta G = \Delta G_{(H2O)} - m[\text{urea}] \qquad \textbf{Equation 2-12}$$

The *m*-value is the slope of the plot described by Equation 2-12, and is defined as the dependence of the free energy of unfolding on denaturant concentration:

$$\boldsymbol{m = \frac{\delta \Delta G}{\delta [\text{urea}]}} \qquad \textbf{Equation 2-13}$$

It is an indication of the difference in solvent accessible surface area (ΔASA) between the native and unfolded states of the protein (Green and Pace, 1974). It can indicate the presence of intermediates in the unfolding pathway, and indicates the level of cooperativity of the unfolding process (Schellman, 1978; Shortle, 1995; Soulages, 1998; Luque *et al*., 2002).

Changes in solvent accessible surface area (ΔASA) upon unfolding in urea were calculated according to Myers *et al.* (1995), whereby:

$$\textbf{ΔASA (Å}^2\textbf{) = -907 + 93(\#res)} \qquad \textbf{Equation 2-14}$$

Predicted values for *m* were calculated according to Myers *et al.* (1995) from the ΔASA upon unfolding in urea, whereby:

$$\boldsymbol{m = 374 + 0.11\ (\Delta ASA)} \qquad \textbf{Equation 2-15}$$

Predicted C_m values (the midpoints of the transition curves) were calculated using the experimentally derived $\Delta G_{(H2O)}$ values and the above predicted *m*-values, such that:

$$\mathbf{C_m} = \frac{\Delta \boldsymbol{G}_{(\boldsymbol{H2O})}}{\boldsymbol{m}} \qquad \textbf{Equation 2-16}$$

For a two-state model to be applicable, the unfolding curve needs to be monophasic, with no shoulders or inflections in the transition. Also, the curves generated by different techniques should be superimposable. A three-state fit can be applied if these conditions are not met.

2.2.5.5.2. Three-state monomer fit

A three-state monomer fit can be applied to data where an intermediate species (I) can be detected at equilibrium (Pace, 1986), whereby the equilibrium equation becomes N ↔ I ↔ U. In this case, the equilibrium constant for the N ↔ I transition is K_1, and is K_2 for the I ↔ U transition:

$$\boldsymbol{f_N + f_I + f_U = 1} \qquad \textbf{Equation 2-17}$$

$$\boldsymbol{K_1 = \frac{f_I}{f_N}} \qquad \textbf{Equation 2-18}$$

$$\boldsymbol{K_2 = \frac{f_U}{f_I}} \qquad \textbf{Equation 2-19}$$

$$\boldsymbol{K_U = \frac{f_U}{f_N} = K_1 K_2} \qquad \textbf{Equation 2-20}$$

Here, the sum of the fraction of protein in the native conformation (f_N), the fraction of protein in the intermediate conformation (f_I) and the fraction of protein in the unfolded conformation (f_U) is 1. The N ↔ U equilibrium constant is represented by K_1K_2. The observed signal, y, is represented as:

$$\boldsymbol{y = y_N f_N + y_I f_I + y_U f_U} \qquad \textbf{Equation 2-21}$$

where y_I are the measured properties of the intermediate.

To get f_U in terms of K_1 and K_2, equations 2-17 to 2-20 are combined:

$$\boldsymbol{f_U + \frac{f_U}{K_1 K_2} + \frac{f_U}{K_2} = 1}$$

$$\therefore f_{\mathrm{U}} = \frac{K_1 K_2}{K_1 K_2 + 1 + K_1} \qquad \textbf{Equation 2-22}$$

Similarly:

$$f_{\mathrm{I}} = \frac{K_1}{K_1 K_2 + 1 + K_1} \qquad \textbf{Equation 2-23}$$

and:

$$f_N = \frac{1}{(K_1 K_2 + 1 + K_1)/(K_1 K_2)} \qquad \textbf{Equation 2-24}$$

We know from Equations 2-9 and 2-12 that: $\Delta G = -RT\ln K_1$

and: $\Delta G1 = \Delta G1_{(H2O)} - m1[\mathrm{urea}]$

therefore:

$$K_1 = e^{(m1[\mathrm{urea}] - \Delta G1_{(H2O)})/RT} \qquad \textbf{Equation 2-25}$$

and similarly for K_2:

$$K_2 = e^{(m2[\mathrm{urea}] - \Delta G2_{(H2O)})/RT} \qquad \textbf{Equation 2-26}$$

Substituting Equations 2-22 to 2-26 into Equation 2-21 gives the model for the final fit:

$$y = \frac{\left[y_{\mathrm{N}} + y_{\mathrm{I}}\left(e^{(m1[\mathrm{urea}] - \Delta G1_{(H2O)})/RT}\right) + y_{\mathrm{U}}\left(e^{(m1[\mathrm{urea}] - \Delta G1_{(H2O)})/RT}\right)\left(e^{(m2[\mathrm{urea}] - \Delta G2_{(H2O)})/RT}\right)\right]}{\left[1 + e^{(m1[\mathrm{urea}] - \Delta G1_{(H2O)})/RT} + \left(e^{(m1[\mathrm{urea}] - \Delta G1_{(H2O)})/RT}\right)\left(e^{(m2[\mathrm{urea}] - \Delta G2_{(H2O)})/RT}\right)\right]}$$

2.2.6. Liposome preparation

2.2.6.1. Freeze-thaw extrusion method

A number of methodologies are in use for lab- and large-scale preparation of unilamellar and multilamellar liposomes ranging from 20 nm to several µm in diameter (reviewed in Mozafari, 2005). Some of the more common methods are detergent dialysis (Millsman *et al.*, 1978), sonication (Papahadjopoulos and Watkins, 1967), reverse-phase evaporation (Szoka and Papahadjopoulos, 1978), high pressure homogenisation (Mayhew *et al.*, 1984) and extrusion (Olsen *et al.*, 1979; Hope *et al.*, 1985). Clearly the method chosen depends very much on the intended application of the liposomes, particularly since residual organic solvents or detergents could prove severely problematic in certain downstream applications. Regardless of the method used though, the underlying principle of how liposomes form remains the same: hydrophilic/hydrophobic interactions between lipid-lipid and lipid-water molecules in a system perturbed by some physical means such as shaking, sonication, extrusion, etc., cause the spontaneous arrangement of the lipid and water molecules into the most energetically favoured conformation: the bilayered vesicle form (Mozafari, 2005).

Consideration of the expected applications of a model membrane system that would be used to characterise the structural and functional interactions of CLIC1 with membranes (in future work in this laboratory) generated five basic requirements for the model membrane system under study here:

i) The system had to be as biomimetic as possible in terms of lipid composition and size, which affects the extent of membrane curvature.

ii) The encapsulation capacity of the liposomes had to be large enough to enclose experimentally significant quantities of protein or other molecules, such as fluorescent dye or chemical modifiers.

iii) The size distribution had to be as narrow as possible to prevent the generation of extraneous noise in certain experiments (such as isothermal titration calorimetry, for example).

iv) The liposomes had to be relatively stable over time, especially in light of the prohibitive cost of purified phospholipids. Having to discard any portion of a single preparation is not ideal.

v) The system had to be amenable to different buffer conditions which would be used to explore the ideal environment for a large fraction of CLIC1 to insert into the membrane.

With these conditions in mind, the *extrusion method* of liposome preparation first described by Olsen *et al.* (1979) and improved by Hope *et al.* (1985) was chosen, using a freeze-thaw protocol and 400 nm polycarbonate membranes. The development of the small volume extrusion apparatus by MacDonald *et al.* (1991) appreciably extended the applicability of this method. Large unilamellar vesicles prepared by the extrusion technique (LUVETs) have no residual organic solvent or detergents, have a sharp size distribution, can be prepared in sizes ranging from 50-1000 nm, resemble biological membranes in that they are unilamellar and have a relatively good encapsulation efficiency, are relatively stable in that their lipid arrangement is at equilibrium, and are reasonably easy to prepare (MacDonald *et al.*, 1991).

Three types of lipid composition were used for LUVETs in this study:

i) Asolectin (Sigma-Aldrich product number 11145), a crude and relatively inexpensive extract from soybean comprising approximately 20-24 % phosphatidylcholine (PC), 18-22 % phosphatidyl-ethanolamine (PE), 12-15 % phosphatidylinositol (PI) and 4-7% phosphatidic acid (PA). This product was used initially to optimise the extrusion process and encapsulation of fluorescent dye. Asolectin (Sigma P5638) was successfully used by Tulk *et al.* (2000) to demonstrate functional reconstitution of CLIC1 into liposomes and planar lipid bilayers.

ii) A combination of ~60 % PC, ~10 % PI, ~10 % PE, ~10 % phosphatidylserine (PS), ~10 % cholesterol and the remainder sphingomyelin, based on approximate values gained from several

studies of typical nuclear membrane lipid compositions (Table 1). This lipid mixture is attractive for its resemblance to typical nuclear membrane composition, but in practice is almost impossible to reproduce batch to batch due to the very small masses being weighed out and the extreme stickiness of the lipids themselves. Thus this mixture was only used once or twice.

iii) A 4:1:1 mol/mol ratio of PE:PS:cholesterol (hereafter referred to simply as PE:PS:chol) determined by Singh and Ashley (2006) to produce the most reproducible ion channel activity in the presence of CLIC1 of all lipid mixtures tested. While Singh and Ashley (2006) used palmitoyloleoyl phosphatidylethanolamine (POPE) and palmitoyloleoyl phosphatidylserine (POPS), the phospholipids used in this study were purified L-α-PE Type IV and L-α-PS from soybean (*Glycine max*) (Sigma-Aldrich P8193 and P0474, respectively). Oleoyl is a monounsaturated C18:1 fatty acid, and palmitoyl a 16-carbon (C16:0) saturated fatty acid chain. The exact fatty acid composition of L-α-PE Type IV is unknown, but it contains 65 % C18 unsaturated fatty acids, primarily linoleic acid (C18:2), and 12.5-28.5 % saturated fatty acids. The fatty acids in the L-α-PS used are primarily linoleic acid. L-α-PE Type IV and L-α-PS rather than POPE and POPS were used in this study simply because of the logistical reason of availability, but they were chosen because their fatty acid chain lengths were at least similar.

Glassware used in the preparation of liposomes was cleaned thoroughly in phosphate- and chlorine-free detergent (Contrad™), rinsed in distilled water (dH_2O), twice in deionised water (DI water) and twice in methanol to remove excess water. Tubes and beakers were then sealed with parafilm and stored for no longer than 30 days prior to use. LUVET preparation followed the basic protocol described by MacDonald *et al.* (1991). Lipids were stored at -20 °C and brought to room temperature prior to opening the containers. Lipid mixtures were made up in concentrations from 20-100 mg/mℓ. The appropriate mass was weighed out

under nitrogen as far as possible and the storage container then flushed gently with nitrogen and sealed with parafilm before being placed back in the -20 °C freezer. Asolectin was solubilised in 1 mℓ chloroform and PE:PS:chol in 2:1 chloroform:methanol. For stocks, no more than four batches of lipids were solubilised and then stored layered under nitrogen in a Schott bottle with the lid sealed with parafilm at -70 °C. The lipids were dried under a gentle stream of nitrogen while rotating the tube by hand or using a vortex mixer. Residual nitrogen was removed overnight under vacuum of at least 300-500 mtorr. The lipid film was hydrated while shaking at a temperature above the phase transition temperature (T_m) (~18 °C for asolectin and less than that for PE:PS:chol) in 30-500 mM potassium acetate or potassium nitrate in CLIC1 storage buffer (50 mM sodium phosphate, 0.02 % NaN_3, 1 mM DTT), pH 5.5 or 7.0, used for dialysis that week; or in 200 mM KCl in CLIC1 storage buffer. In cases where *N*-(ethoxycarbonylmethyl)-6-methoxyquinolinium bromide (MQAE) was encapsulated in liposomes, the hydration buffer contained 10 mM MQAE. The hydration phase with shaking or vortexing causes the formation of multilamellar vesicles (MLVs) as the lipid film lifts off the inner surface of the glass tube (Figure 2.3).

Once it could be seen that the lipid film had been fully removed from the inner surface of the tube by the hydration buffer, the solution was subjected to 10 freeze-thaw cycles in an ethanol/ice bath and lukewarm water bath (45 °C for asolectin, 30 °C for PE:PS:chol). Cycles were 1-3 minutes each for asolectin, or 1-2 minutes freezing and very brief thawing for PE:PS:chol. The freeze-thaw cycles ensure equilibration between trapped and bulk solutions (Mayer *et al.*, 1985) and have also been shown to increase encapsulation efficiency of liposomes (Manojlovic *et al.*, 2008). Extrusion was performed using an Avanti Mini-Extruder (Avanti Polar Lipids, Alabaster, USA) equipped with two 1 mℓ Hamilton syringes with removable needles (The Hamilton Company, Nevada, USA). The mini-extruder apparatus fits into a heating block which was maintained at 42 °C for asolectin and 22 °C for PE:PS:chol during extrusion.

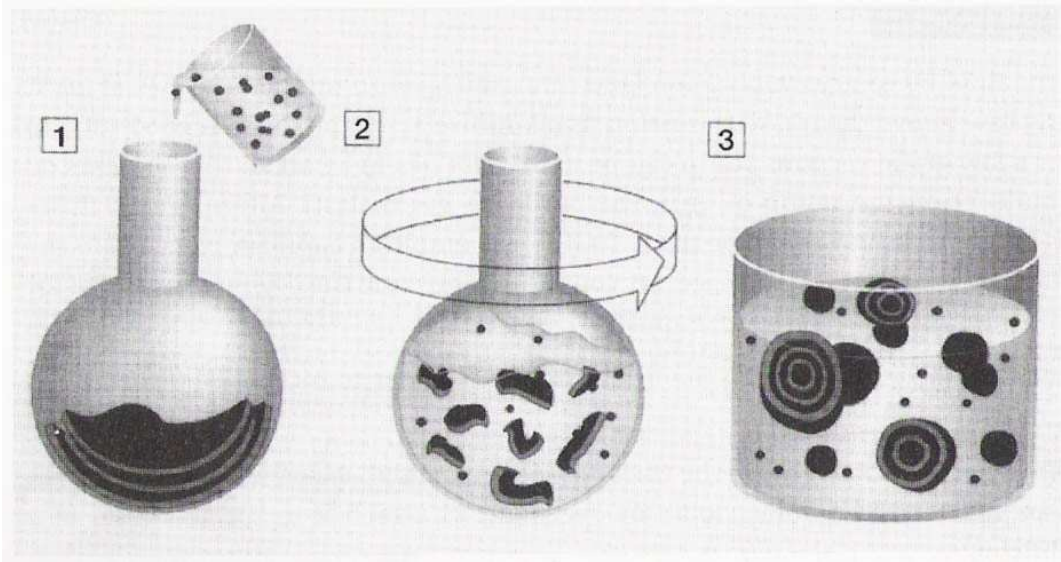

Figure 2.3. Multilamellar vesicles formed during hydration of vacuum-dried lipid film.

(1) A lipid mixture solubilised in organic solvent is dried to a film around the bottom of a glass tube under a stream of nitrogen. The tube is rotated or vortexed while drying, resulting in layers of lipid drying over each other. (2 and 3) When hydrated in aqueous buffer these layers peel off to form multilamellar vesicles. Image from Lasch *et al.* (2003).

Multilamellar dispersions were extruded through a single 400 nm Nuclepore polycarbonate track-etched membrane (Whatman) 11-75 times. Dead space was reduced by pre-wetting the extruder parts by passing 0.22 µm-filtered buffer through the apparatus several times prior to extruding lipids. An odd number of passes was always used so that any large particles or other contaminants remaining after extrusion would be left in the first syringe. After extrusion the asolectin liposome suspensions were centrifuged at 13 400 rpm in a benchtop Eppendorf Minispin for 30 minutes to pellet larger particles. The PE:PS:chol mixture was found not to form any pellet at this stage so these mixtures were not centrifuged in subsequent preparations. The supernatant was aspirated into a clean tube, layered with nitrogen and the lid sealed with parafilm. Liposomes were

stored at 4 °C sealed under nitrogen at all times. They were used within 3-4 days of preparation.

2.2.6.2. Encapsulation of fluorescent dye, MQAE, in liposomes

The fluorescent dye, MQAE (Figure 2.4), is collisionally quenched by chloride ions via a charge-transfer quenching mechanism (Jayaraman and Verkman, 2000). Collisional quenching is the deactivation of the excited state of a fluorophore by contact with a quencher molecule in solution (Lakowicz, 1999). The decrease in fluorescence intensity is described by the Stern-Volmer equation:

$$\frac{F_0}{F} = 1 + K_{SV}[Q] \qquad \textbf{Equation 2-27}$$

where F_0 is the fluorescence intensity in the absence of quencher, F is the fluorescence intensity in the presence of quencher, K_{SV} is the Stern-Volmer quenching constant and [Q] is the quencher concentration.

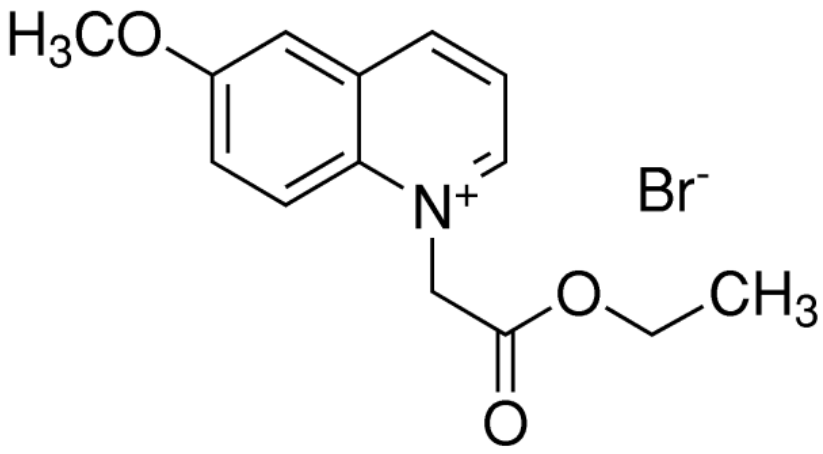

Figure 2.4. The structure of MQAE.

The basis of the molecule's fluorescent properties is the quinolinium ring structure. MQAE was designed as an analogue to 6-methoxy-*N*-[3-sulfopropyl] quinolinium (SPQ) as a more sensitive chloride indicator, which it is. This is probably due to the deletion of the negative charge of the sulphonate of SPQ (Verkman *et al.*, 1989a).

One of the objectives of this project was to ensure that the model membrane system characterised would be viable later for functional studies of CLIC1. All functional work on CLIC1 to date has been done using electrophysiology (Valenzuela *et al.*, 1997; Tonini *et al.*, 2000; Valenzuela *et al.*, 2000; Harrop *et al.*, 2001; Tulk *et al.*, 2000; Warton *et al.*, 2002; Tulk *et al.*, 2002; Littler *et al.*, 2004; Singh and Ashley, 2006; Singh *et al.*, 2007). This type of electrophysiology requires much investment in highly specialised equipment and some technical skill. It was considered for this project that it may be possible to develop a fluorescence-based functional assay that could be performed relatively easily and could be used to compare CLIC1 and CLIC1 mutant-mediated chloride flux into liposomes. The aim of the assay would be simply to indicate that CLIC1 was actually inserted into the membrane and was functioning to allow quantifiable chloride conductance across the membrane. This is not an entirely novel application within the CLIC family. Nishizawa *et al*. (2000) used the quinolinium-based MQAE analogue 6-methoxy-*N*-[3-sulfopropyl] quinolinium (SPQ) to detect parchorin-mediated chloride efflux from LLC-PK1 cells. This was done by monitoring *un*quenching of the signal as chloride was transported out of SPQ-loaded cells. The assay proposed here would monitor quenching of the MQAE signal as chloride flowed into MQAE-loaded liposomes. Demonstrating quantifiable function would be a fundamental prerequisite for any structural studies on the membrane-inserted form of CLIC1, in addition to the rather more formidable requirement that most or all of the CLIC1 be in its integral membrane form. This latter point, though, is rather beyond the scope of this project at present. Verkman *et al*. developed a number of quinolinium-based chloride-sensitive fluorescent indicators (reviewed in Verkman, 1990) which they showed to be able to measure, quantifiably, chloride flux across liposomal membranes (Illsley and Verkman, 1987; Verkman *et al*., 1989a; Verkman *et al.*, 1989b). The principle is simple: the fluorescent dye (MQAE in this case) is encapsulated inside the liposomes and the extravesicular dye removed by size exclusion chromatography. The chloride channel protein is introduced to the liposome suspension with extravesicular chloride and the signal monitored at the emission maximum of the fluorescent molecule. If the channel protein (CLIC1 in this case)

is inserted into the membrane and transporting chloride ions across it, the MQAE signal will be quenched. If not, the signal will remain the same and it can be assumed that the protein is not functioning as a chloride channel. The system can be calibrated in the sense that initial chloride concentration is known, the baseline signal for total quenching can be measured by lysis of the liposomes with Triton X-100, and rates of flux can therefore be calculated from a line fitted to the initial drop in signal. MQAE is quenched by Cl^-, Br^-, I^-, SCN^- and citrate (Verkman *et al.*, 1989a). It is unaffected by Na^+, K^+, Ca^+ or pH in the range 4-8 (Verkman *et al.*, 1989a). It is highly water-soluble and its net positive charge probably prevents leakage across the membrane.

Ten mM MQAE was encapsulated in LUVETs by preparing it in the buffer used for hydration of the dried lipid. The buffer was always the most recent CLIC1 storage buffer used for dialysis (50 mM sodium phosphate, 0.02 % NaN_3, 1 mM DTT), pH 5.5 or 7.0, containing 30-500 mM potassium acetate or potassium nitrate. Buffer was filtered through a 0.22 µm filter prior to use.

2.2.6.3. MQAE fluorescent dye concentration determination

MQAE concentration was determined using the Beer-Lambert law (Equation 2-1) and a molar extinction coefficient of ε_{350} = 2 800 M^{-1} cm^{-1} (Verkman *et al.*, 1989a). Ten to 15 serial dilutions of the MQAE stock were measured at 350 nm using a Jasco V-550 UV/VIS spectrophotometer. A quartz cuvette of 1 cm path length was used for all readings. Readings were buffer-corrected, plotted as a function of dilution factor and the concentration determined from the line fitted by linear regression. Dilution factors were expressed as the ratios of the final fractional concentration of the diluted solutions to the initial concentration of the stock solution, where the latter was taken as 1 (100 %) (Reed *et al.*, 2003). An absorbance spectrum of approximately 0.1 mM MQAE was recorded from 250-450 nm.

2.2.6.4. Determination of MQAE Stern-Volmer chloride quenching constant

All fluorescence measurements of MQAE were performed on a Jasco FP6300 spectrofluorometer with Spectra Manager v. 1.54.03 software. The Stern-Volmer chloride quenching constant for MQAE was determined in order to ascertain appropriate Cl^{-1} concentrations to use in a functional assay based on the use of this dye. Ten mM MQAE in CLIC1 storage buffer (50 mM sodium phosphate, 0.02 % NaN_3, 1 mM DTT), pH 7.0, containing 30 mM potassium nitrate was titrated with approximately 5 mM aliquots of 2 M KCl. Excitation was at 350 nm, and the emission signal was monitored for 40 seconds at 450 nm using the time drive function. Sensitivity was set to *high*, the data pitch was 0.2 sec, excitation and emission slit widths were both 5 nm, and the response was 2 sec. A 1 cm quartz cuvette was used. Data were buffer-corrected and plotted as the average intensity over 40 secs, and duplicate sets of data were collected. The same experiment was carried out with 10 mM MQAE in dH_2O. Fluorescence spectra of MQAE in the same buffer as above and in dH_2O were recorded from 350-600 nm at 200 nm/min with sensitivity set to *high*, the data pitch 0.5 sec, excitation and emission slit widths both 5 nm, and the response set to *fast*.

2.2.6.5. Removal of extravesicular MQAE

Complete removal of any unencapsulated dye is necessary for the success of downstream experimental work. This was achieved by size-exclusion chromatography. Initially an 85 mℓ Sephadex G25 column pre-equilibrated in CLIC1 storage buffer (50 mM sodium phosphate, 0.02 % NaN_3, 1 mM DTT), pH 7.0 or pH 5.5, containing 30-500 mM potassium chloride was used for the separation of liposomes containing MQAE and extravesicular dye. Liposomes were applied manually to the column and chased with two column volumes of equilibration buffer. Eluate was collected in 1.5 mℓ fractions from shortly before the liposome fraction could be seen to reach the bottom of the column (the asolectin formulation is yellow and the PE:PS:chol liposome mixture is white). Later, an 82 mℓ Sephacryl™ 300 High Resolution (S300HR) (Amersham

Biosciences) column was used on the ÄKTAprime protein purification system (Amersham Biosciences) to achieve higher resolution between liposome and MQAE fractions. The void volume of this column was determined by passing 2 mℓ of 2 mg/mℓ Blue Dextran 2 000 000 (Sigma-Aldrich) through it. The column was equilibrated with 300 mℓ CLIC1 storage buffer (50 mM sodium phosphate, 0.02 % NaN_3, 1 mM DTT), pH 7.0 or pH 5.5, containing 30-500 mM KCl. One-two mℓ of extruded liposomes were injected onto the column at 2 mℓ/min and were eluted with up to 150 mℓ equilibration buffer. Fractions which were visibly cloudy and which were 2-3 fractions into the liposome elution peak visualised by the ÄKTAprime software (PrimeView™ v. 1.0, Amersham) were pooled in a clean tube, layered with nitrogen and the lids sealed with parafilm. Extravesicular MQAE was collected in 2 mℓ fractions and an absorbance spectrum from 250-450 nm recorded to confirm that it was indeed MQAE. MQAE-containing liposomes were stored under nitrogen at 4 °C in the dark, and were kept in the dark until just prior to experiments.

Fluorescence emission spectra of MQAE-containing liposomes and the extravesicular MQAE fraction were recorded on a Jasco FP6300 spectrofluorometer using the same settings as detailed for MQAE spectra in Section 2.2.6.4. above.

2.2.6.6. Basal leakage study

The usefulness of fluorescent-dye-containing liposomes only extends so far as the dye does not leak out of the vesicles. The lipid bilayer is fluid, dynamic and permeable, and is more or less so depending on the lipid composition (Finkelstein, 1976; de Gier, 1993; Albi *et al.*, 1997; Manojlovic *et al.*, 2008; Mathai *et al.*, 2008), particularly in relation to cholesterol, the so-called "packing lipid" (Carruthers and Melchior, 1983; Lande *et al.*, 1995). While permeability is a unique and critical property of biological membranes, minimisation of this property was highly desirable for this study. Once extravesicular MQAE had been removed from the liposome dispersion, basal leakage rates were monitored to indicate for how long the liposomes could be used before the MQAE signal

dropped too significantly. Aliquots of the prepared liposomes were stored protected from light at 4 °C or at room temperature (20 °C). Quenching was monitored by fluorescence emission intensity with the wavelength fixed at 440 nm on a Hitachi Model 650 fluorescence spectrophotometer. A 1 cm path length quartz cuvette was used. The excitation wavelength was 350 nm, and excitation and emission monochromator slit widths were set at 10 nm. Measurements were taken every few hours for the first few days, and then once or twice a day subsequent to that. Percentage leakage was calculated after complete release of all dye from the vesicles with 0.1 % Triton X-100, which lyses the vesicles.

2.2.7. Phospholipid concentration determination

A number of sensitive methods are available for the determination of phospholipid concentration, most based upon the colorimetric determination of organic phosphorus, such as the Barlett assay (Bartlett, 1959), the Fiske and Subbarow assay (Fiske and Subbarow, 1925) and a method by Chalvardjian and Rudnicki (1970). The Stewart assay (Stewart, 1980) relies upon the complexation of ammonium ferrothiocyanate with phospholipids. The method used here was based on that of Chen *et al.* (1956) and is a total phosphorus assay. Although it cannot directly account for cholesterol, which does not have a phosphate head group, the cholesterol concentration can be calculated from the molar ratio once the phosphorus concentration is known. The phosphorus assay is a colorimetric assay for inorganic phosphate which involves acid hydrolysis of phospholipids followed by conversion of inorganic phosphate to phospho-molybdic acid with the addition of ammonium molybdate. This compound is then reduced while heating by ascorbic acid to form a blue-coloured complex whose absorbance is read at 820 nm. The more phosphorus present, the deeper blue the colour development.

A standard curve was constructed from triplicate samples of 0.0-0.228 µmol phosphorus made up from 0.65 mM stock phosphorus solution (Sigma-Aldrich 661-9). Glassware was washed as described in Section 2.2.6.1. The standard samples and triplicate samples of asolectin liposomes prepared in 20 mM Tris-

HCl pH 7.0 were acid-hydrolysed by addition of 0.45 mℓ 8.9 N H_2SO_4 to each tube with heating in an aluminium block at 200-215 °C for 25 mins. The tubes were removed from the heating block and allowed to cool for five minutes before 150 µℓ H_2O_2 was added to each tube. Heating was continued above 200 °C for a further 30 minutes. DI water (3.9 mℓ) was added to each tube, followed by 0.5 mℓ 2.5 % ammonium molybdate (VI) tetrahydrate solution. All tubes were vortexed five times, 0.5 mℓ 10 % ascorbic acid added, and vortexed five times each again. Tubes were covered with marbles to prevent evaporation and heated at 100 °C for 7 minutes. Once cooled to room temperature (20 °C) the absorbance at 820 nm of all standards and samples was determined. The 0.0 µmol phosphorus standard was used for blank-correction and triplicate averages plotted at a function of phosphorus amount. The phosphorus concentration, and thus the phospholipid concentration of the samples were determined from the equation of a regression line fitted to the data.

Of great interest was the determination of whether dried weight would give a relatively reliable concentration estimation if all lipid lost during the liposome production process was accounted for. This was desirable not only because most phospholipid concentration determination methods are lengthy and rather unwieldy processes not really suited to frequent and ongoing use, but also because the protein storage buffer used throughout this study for storage, assays and LUV preparation, is a phosphate buffer, chosen for its relatively wide buffering range – the range concentrated on in this study. Clearly a phosphate buffer cannot be used in a total phosphorus assay, but the assay itself was perfectly suited in all other aspects. Thus it was decided to use dried weight estimates if it could be confirmed that the phosphorus assay and dried weight values corresponded. All glassware and other tubes used during the LUV production process were weighed prior to lipid solubilisation and after vacuum drying. Residual lipid left in tubes was vacuum dried and the tubes weighed again. Total loss from the original mass was accounted for and the lipid concentration calculated from an average molecular mass estimated for the lipid mixtures. Unfortunately, small volume losses during extrusion could not be perfectly accounted for.

2.2.8. Liposome size determination

The size of LUVs was determined, in most cases, straight after extrusion and again after passage through the S300HR column. Size was determined using dynamic light scattering (DLS). DLS is based on the principle that the speed of the motion of a molecule in solution can be used to estimate its size. Molecules in solution undergo constant random bombardment from the molecules of the solution surrounding them. These collisions cause movement termed Brownian motion (Harding, 1997). The smaller and more compact a molecule is, the faster its Brownian motion is likely to be than that of a large, asymmetric, extended molecule. In DLS, laser light is scattered by macromolecules in solution and the scatter pattern detected. Fluctuations in the intensities within the scatter pattern caused by Brownian motion of the macromolecules are recorded and correlated by the computer (Harding, 1997). A diffusion coefficient (*D*) is produced from an exponential fit to the correlation data and a size distribution calculated. The Stokes-Einstein equation, which relates the speed of motion of molecules in solution to their size, is then used to calculate the size of the particles:

$$\boldsymbol{D_{\mathrm{H}} = \frac{kT}{f} = \frac{kT}{3\pi\eta D}} \qquad \textbf{Equation 2-28}$$

where D_{H} is the hydrodynamic diameter, k is the Boltzmann constant, T is the absolute temperature, f is the particle frictional coefficient, η is the solvent viscosity and D is the diffusion coefficient (Harding, 1997). The hydrodynamic diameter is given as the *Z*-average. The polydispersity index (PDI) provides a measure of how broad the distribution is. A value lower than 0.3 is generally acceptable.

Size measurements of LUVs were performed using a Zetasizer Nano-S Zen 1500 light scattering instrument (Malvern Instruments, UK) equipped with a 633 nm laser with backscatter detection at 173°. The sample was in a 1 cm glass cuvette. Manual measurement settings were used with dispersant as phosphate buffer with potassium nitrate or potassium chloride, measurement type as size, material as

lipid, equilibration time as 3 min, temperature 20 °C, and the result calculation as general purpose. Each *Z*-average was the average of five measurements, with each measurement the result of approximately 12 iterations.

A melting curve of PE:PS:chol liposomes was also measured using DLS from 4-80 °C to determine their heat stability.

2.2.8.1. Entrapped volume calculation

The volume of aqueous buffer entrapped within the liposomes during extrusion was estimated from the measured sizes according to:

Entrapped volume (ℓ/mol lipid) = (500/3)ANR **Equation 2-29**

where A is the area of the membrane occupied by one lipid (in m^2), N is Avogadro's constant (6.022×10^{23} mol^{-1}) and R is the radius of the vesicles (in m) (Zuidam *et al.*, 2003). This is basically a modification of the standard volume of a sphere equation (V=R/3 x A), with 500 used as a conversion factor. The lipid mixture was taken as 4:1:1 mol/mol PE:PS:chol. Average liposome size was taken as 200 nm. Average areas of phospholipid head groups were taken as 0.57 nm^2 for PE, 0.65 nm^2 for PS and 0.30 nm^2 for cholesterol (Zuidam *et al.*, 2003; Mathai *et al.*, 2008).

2.2.9. Electron microscopy

Asolectin LUVETs were visualised using transmission electron microscopy (TEM) in order to get a visual size comparison with the DLS sizing data, and also to get a sense of the morphology of the liposomes. Electron microscopy (EM) works by accelerating a beam of electrons in a vacuum at a sample which is stained with some electron-dense material (Alberts *et al*., 2002). This material scatters electrons directed at it, and they are lost from the beam. Areas of reduced electron flux show up as dark in the image. An electron microscope with an

accelerating voltage of 100 keV allows for a theoretical resolution of 0.002 nm because of the tiny wavelength of electrons at high velocity, but in practice this resolution is closer to 0.1 nm (Alberts *et al*., 2002).

Asolectin liposomes of 200-230 nm diameter as determined by DLS were prepared by extrusion as described in Section 2.2.6.1. A saturating solution (2 %) of uranyl acetate (Merck) was prepared and centrifuged for 10 minutes at 13 400 rpm in a benchtop Eppendorf Minispin centrifuge. This solution was protected from light at all times. Five µl of liposomes were gently pipetted onto a carbon film-coated copper EM grid and allowed to dry for a few seconds. Excess liquid was carefully blotted off the grid, and the sample was then negatively stained with 2 % uranyl acetate for 10 seconds in the dark. Excess liquid was once again blotted, and the grid placed in a JEOL 100S transmission electron microscope operating at an accelerating voltage of 80 keV. Images were recorded at magnifications from 25 000x-100 000x.

CHAPTER 3. RESULTS

3.1. CLIC1 purification

3.1.1. Plasmid purification and verification

Several small-scale plasmid DNA purifications from XL1-Blue cells or E. cloni® cells harbouring the pGEX-4T-1-CLIC1 plasmid yielded DNA concentrations of between 104 ng/μℓ and 177 ng/μℓ, giving total amounts of 5.2 μg to 8.9 μg. A_{260}/A_{280} ratios were 1.78 to 1.93 (Figure 3.1), indicating high purity of the DNA. The ideal value indicating low to no protein contamination is 1.8 (Brown, 1986), below which significant protein contamination can be assumed. A 1% agarose gel showed the plasmid DNA to be free of chromosomal DNA and to have been treated gently enough during the purification to maintain the plasmid largely in covalently closed circular form (Figure 3.2). The size cannot be determined from the gel because the plasmid was not linearised prior to electrophoresis, but the expected size is approximately 5 600 bp. The sequencing result translated to the correct CLIC1 sequence. There are two expected additional residues (Gly, Ser) at the N-terminus which form part of the thrombin cleavage site between the *Sj*GST and CLIC1 fusion (Harrop *et al.*, 2001). Transformation of competent BL21(DE3)pLysS cells with plasmid DNA yielded approximately 90 000 transformants/μg. No growth was seen on control plates.

3.1.2. CLIC1 expression and purification

Purification of CLIC1 was carried out following the general method of Tulk *et al.* (2000), using affinity chromatography followed by DEAE-anion exchange chromatography. The purity of CLIC1, as well as the success of each step of the purification protocol, was assessed using 15% acrylamide SDS-PAGE gels. Figure 3.3A and Figure 3.4B show representative SDS-PAGE gels of samples collected throughout the purification process. A band corresponding to approximately 60 kDa in Figure 3.3A, lanes 1-4, indicates the position of the

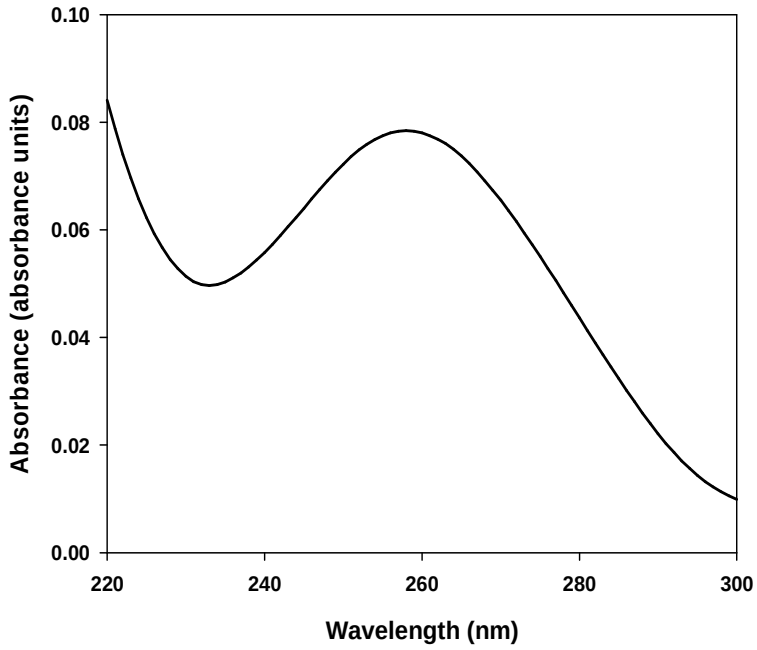

Figure 3.1. Representative absorbance spectrum of pGEX-4T-1-CLIC1 plasmid DNA.

DNA was diluted 21 times in distilled water and scanned from 220-300 nm. The A_{260}/A_{280} ratio was 1.78, indicating low protein contamination. The spectrum was recorded on a Jasco V-550 UV/VIS spectrophotometer at 20 °C.

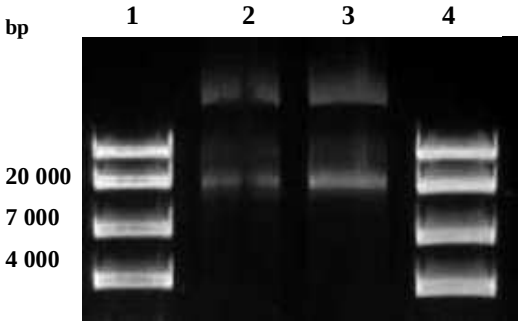

Figure 3.2. Purified pGEX-4T-1-CLIC1 cDNA agarose gel analysis.

Samples, 5 µℓ of purified 104 ng/µℓ (Lane 2) and 177 ng/µℓ (Lane 3) plasmid DNA were analysed on a 1% agarose gel. GelRed™ was added to the loading buffer at 0.5 µℓ/100 µℓ and 2 µℓ of this was added to 5 µℓ of sample and marker DNA. Lanes 1 and 4 are marker DNA.

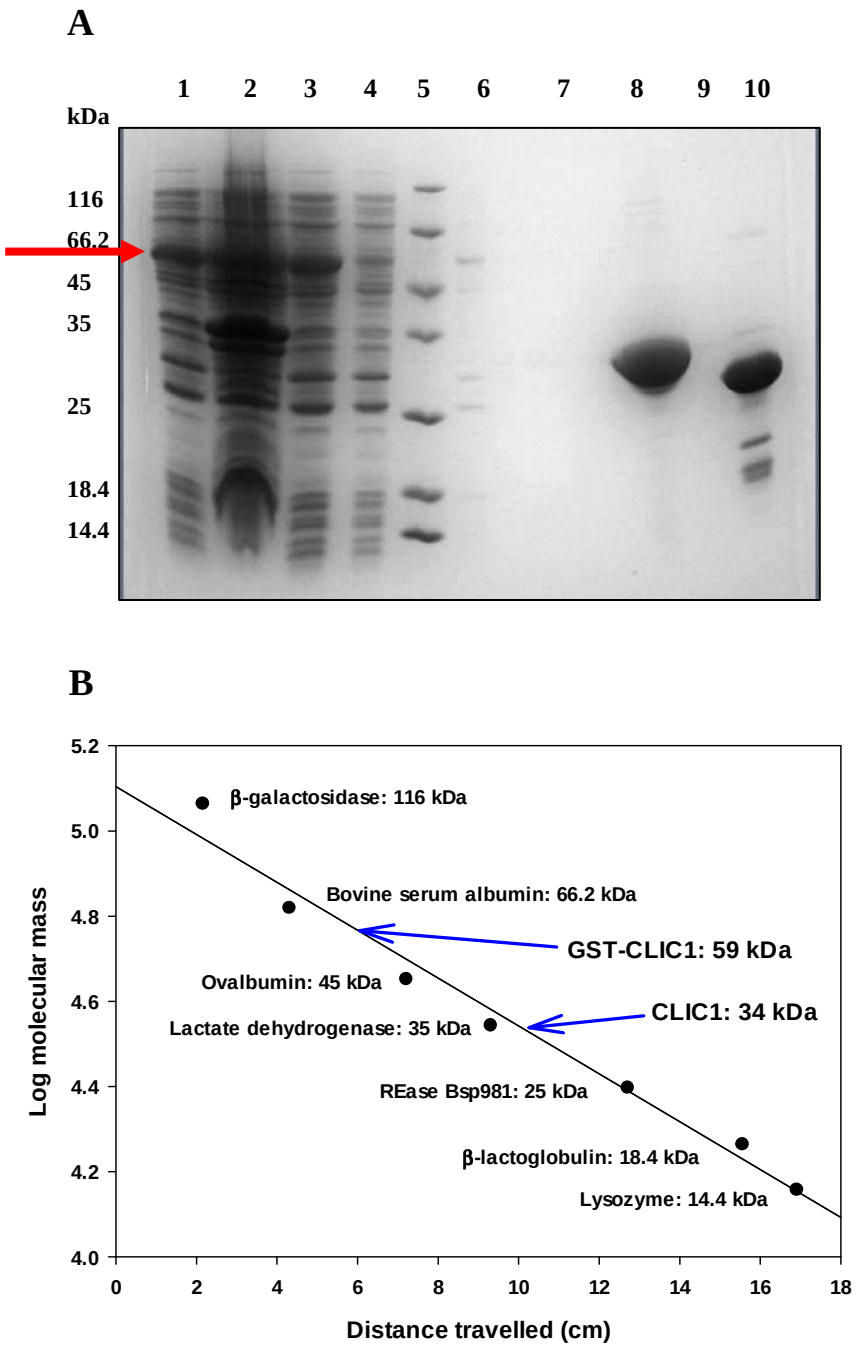

Figure 3.3. GST-CLIC1 purification.

(A) 15% SDS-PAGE gel showing samples collected from GSH-agarose affinity column purification: total lysate, 40x dilution (lane 1); pellet, 40x dilution (lane 2); supernatant, 40x dilution (lane 3); supernatant flow-through, 40x dilution (lane 4); MW marker (lane 5); wash 1 (lane 6); wash 2 (lane 7); thrombin+CLIC1 elution (thrombin not visible) (lane 8); thrombin wash from DEAE column (lane 9); GST elution (lane 10). The red **arrow** shows the position of the GST-CLIC1 fusion protein. **(B)** Calibration curve constructed from mobilities of molecular mass standards on 15% SDS-PAGE, indicating the positions within the curve of GST-CLIC1 and CLIC1 (r^2 = 0.98).

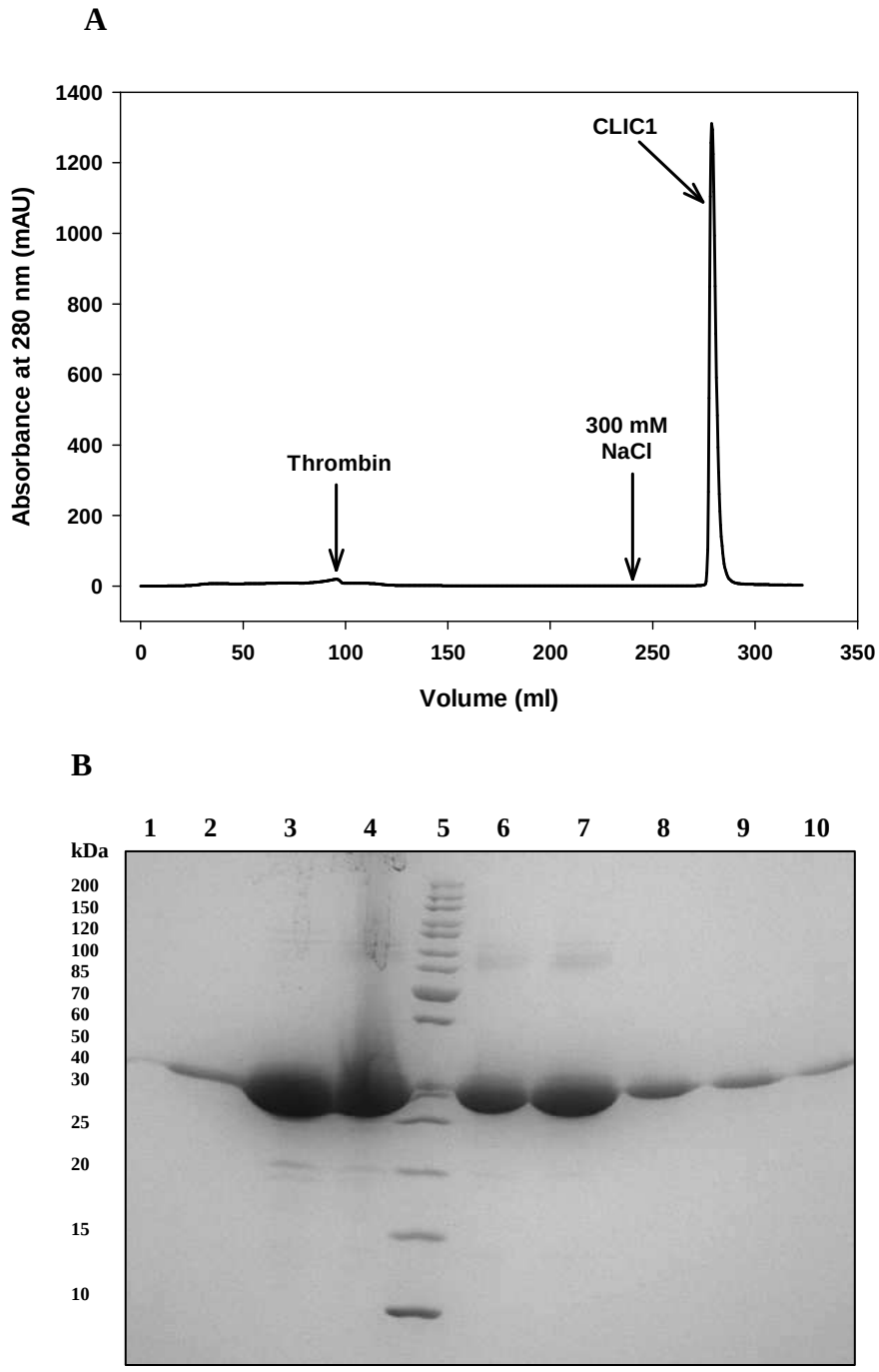

Figure 3.4. CLIC1 purification.

(A) Elution profile of CLIC1 from DEAE column. The thrombin signal was very weak. CLIC1 was eluted in 2 mℓ fractions using DEAE elution buffer, pH 6.5 (20 mM Tris, 300 mM NaCl, 0.02% NaN_3, 1 mM DTT). **(B)** 15% SDS-PAGE gel showing fractions eluted from DEAE-agarose anion exchange column. Lanes 1-4, 6-10: alternate fractions from 272 mℓ – 294 mℓ (CLIC1 peak as in panel A above); lane 5: MW marker. Sizes of the MW marker are shown in kDa on the left hand side of (A) and (B).

GST-CLIC1 fusion protein and shows it was mostly expressed in a soluble form. Some fusion protein remained in the insoluble pellet fraction (Figure 3.3, Lane 2), but soluble yields were sufficient to preclude a pellet wash. In Figure 3.3, lane 4, it can be seen that the fusion protein bound to the GSH-agarose column successfully, since the supernatant flow-through contains very little of the GST-CLIC1 fusion. Increased wash volumes improved the final purity of CLIC1. A sample from the NaCl wash in Figure 3.3, lane 7 indicates that practically all of the bacterial proteins were washed off the column.

The CLIC1 fractions eluted from the DEAE-agarose column shown in Figure 3.4B are mostly contaminant-free, with densitometric analysis indicating that contaminants constitute less than 3 % of the total lane density. Standard curves constructed from measurement of distances travelled on SDS-PAGE gels by the molecular mass markers gave average calculated sizes for the GST-CLIC1 fusion and CLIC1 of approximately 59.2 kDa and 34.4 kDa respectively (n=3) (Figure 3.3B). Linear regression analysis of only the linear portion of the curve gave sizes slightly smaller (53.1 and 32.7 kDa respectively (n=5)). The predicted sizes are 53 kDa for the fusion protein and 27 kDa for CLIC1, so even within an approximate 10 % error margin for sizes from SDS-PAGE (Weber and Osborn, 1969), CLIC1 travels anomalously slowly (17-22 % error). This appears to be a general characteristic of CLIC family proteins, though, and others have found the same to be true (Redhead *et al*., 1997; Edwards, 1999; Tulk *et al*., 2000; Tulk *et al.*, 2002). It is most likely that the acidic nature of CLIC1 interferes with SDS binding, lowering the mass:charge ratio and leading to lower than expected mobility (Pitt-Rivers and Impiombato, 1968; Dunker and Rueckert, 1969; Reynolds and Tanford, 1970; Lehtovaara, 1978). CLIC1 has 35 negatively charged residues, an overall charge of -7 at pH 7.0 and a p*I* near 5, so this is the most likely explanation. CLIC1 eluted off the DEAE-agarose column in a narrow peak between fractions 20 and 37 (Figure 3.4A). In most cases, fractions 22-30 were concentrated enough to pool, and protein yields were 20-30 mg/ℓ of culture. In most cases this was 2-8 times those previously reported (Tulk *et al*., 2000; Tulk *et al*., 2002). Concentrations of stock CLIC1 solutions ranged from 100–250 µM.

A UV absorbance spectrum of purified CLIC1 was recorded, and showed a peak at 278 nm and an A_{280}/A_{260} ratio of 1.63 (Figure 3.5). There was little to no aggregation as shown by the low A_{340} value of 0.0495 AU.

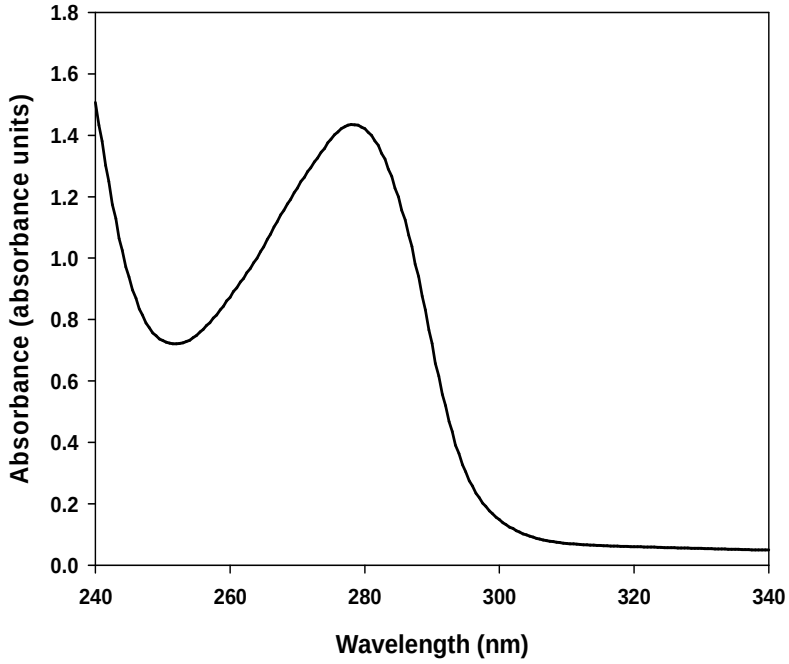

Figure 3.5. Absorbance spectrum of purified CLIC1.

Stock CLIC1 was scanned from 240-340 nm, yielding the above absorbance spectrum. The spectrum was recorded in 50 mM sodium phosphate buffer, 1 mM DTT, 0.02 % NaN_3 on a Jasco V-550 UV/VIS spectrophotometer at 20 °C.

3.1.3. Protein concentration determination

Protein concentration was determined after every purification and each time protein was dialysed. Buffer- and scatter-corrected absorbances at 280 nm for a series of dilutions of stock CLIC1 were plotted and the equation of the linear fit to the data used to calculate protein concentration (Figure 3.6). A_{340} values were subtracted in order to correct for scatter, which can contribute to an

overestimation of protein concentration if there is aggregation. In most cases this made less than $1x10^{-2}$ μM difference to the concentration determination, but CLIC1 was nonetheless maintained at lower stock concentrations when at pH 5.5 because of its tendency to aggregate at this pH. Generally speaking, concentration determinations throughout were consistently reliable, with r^2 values for almost all plots in the region of 0.999-0.9999.

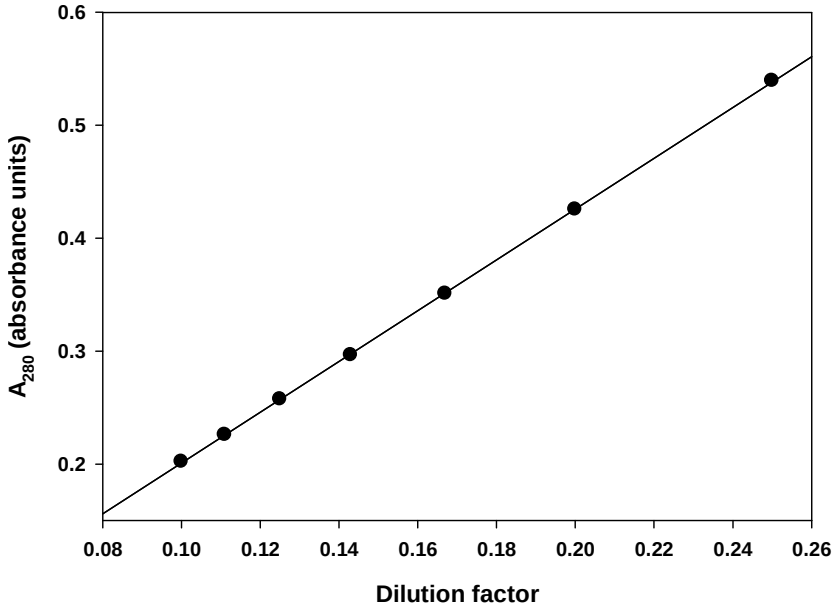

Figure 3.6. CLIC1 concentration determination.

Representative plot showing corrected absorbance readings at 280 nm for 4x-10x dilutions of purified stock CLIC1. In this case, stock concentration was calculated from regression analysis as 130 μM. r^2 = 0.99995.

3.2. Structural characterisation of CLIC1

3.2.1. Secondary structure of native and unfolded CLIC1

Secondary structural characterisations of CLIC1 at pH 7.0 and 5.5 were obtained using far-UV CD. Two µM native and unfolded CLIC1 CD spectra were recorded between 180 and 250 nm (Figure 3.7). There are clear troughs at 208 and 222 nm in the CD spectra for native CLIC1, as well as a strong, positive peak around 190 nm, the characteristic markers of α-helical proteins. The double negative bands at 208 nm and 222 nm are characteristic of proteins with high α-helical content (Johnson, Jr. and Tinoco, 1972; Brahms and Brahms, 1980), but specifically the deeper 208 nm trough indicates proteins with α-helical and β-sheet content in different domains (Venyaminov and Yang, 1996). The minimum at 208 nm is less negative than that at 222 nm for all α-helical proteins. The crystal structure of CLIC1 has 10 α-helices and 4 β-strands, in different domains, so the spectra are as expected. The spectra for CLIC1 unfolded in 8.0 M urea average close to zero up to about 212 nm, beyond which the signal-to-noise ratio becomes too low for accurate data recording. Clearly there is a total or almost total loss of secondary structure under these conditions and CLIC1 exists essentially in an unfolded conformation.

CLIC1 has been studied in this work at pH 7.0 and pH 5.5 because these values represent pH values close those found in the cytoplasm and near the membrane, respectively (Menestrina *et al.*, 1989; van der Goot *et al.*, 1991; Bortoleto and Ward, 1999; Chenal *et al.*, 2002). Although the spectra for native CLIC1 at pH 5.5 and pH 7.0 have the same idiosyncratic shape, the pH 5.5 spectrum shows a lower degree of secondary structure than that for CLIC1 at pH 7.0, with an approximately 12 % loss in signal intensity. This is highly significant within the parameters of the J-810 instrument, which has a photometric accuracy of ± 0.01 absorbance units (AU), a CD resolution of 0.01 mdeg at ±200 mdeg full scale, and a wavelength repeatability of ± 0.05 nm between 163-250 nm. The consistently reliable concentration determinations throughout this study make it unlikely that the lower signal for pH 5.5 is due to concentration differences, and a 16 % loss in

signal from pH 7.0 to pH 5.5 has been observed previously (Fanucchi *et al.*, 2008). This type of acid-induced loss of secondary structure is actually quite unusual in pore-forming proteins, and has not been observed in, for example, α–toxin (Vecsey-Semjen *et al.*, 1996), diphtheria toxin (Chenal *et al.*, 2002) or Bcl-x_L (Thuduppathy *et al.*, 2006).

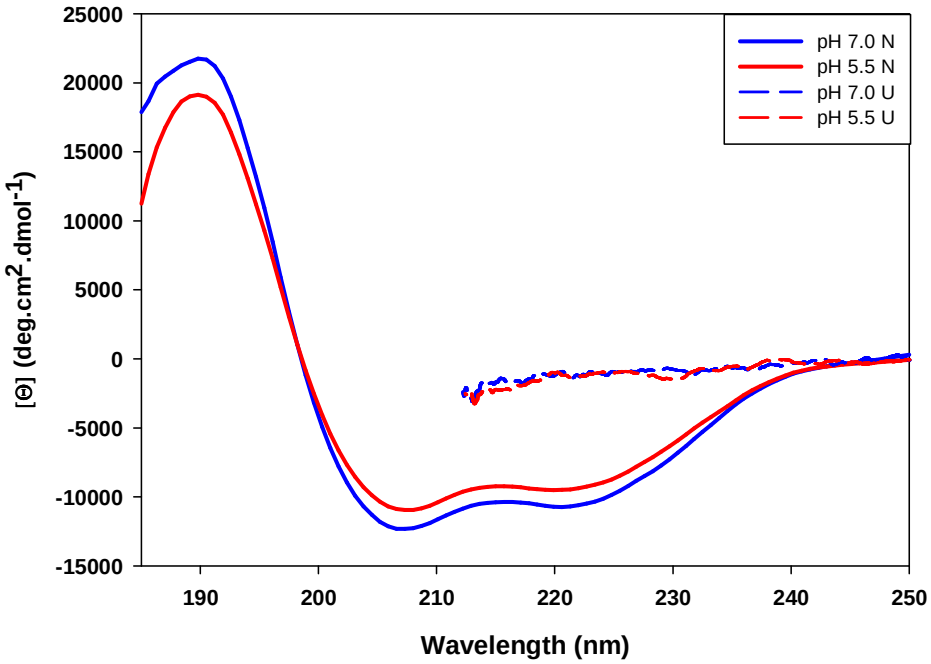

Figure 3.7. Far-UV CD spectra of native and unfolded CLIC1.
Circular dichroism spectra of 2 µM CLIC1 in 5 mM sodium phosphate buffer, 0.1 mM DTT at pH 7.0 (blue) and pH 5.5 (red), at 20 °C. Native spectra are shown with solid lines and spectra for CLIC1 unfolded in 8.0 M urea are shown with dashed lines. Data were plotted with Sigmaplot v. 11.0 and native spectra smoothed using the negative exponential method.

3.2.2. Tertiary structure of native and unfolded CLIC1

3.2.2.1. Fluorescence

The tertiary structure of CLIC1 was explored using two probes: intrinsic fluorescence and near-UV CD. Excitation with light at 280 nm excites tyrosine

and tryptophan residues, while excitation at 295 nm excites only tryptophan. The eight tyrosines in CLIC1 are spread relatively evenly around the protein and its lone tryptophan is localised at the C-terminal end of the α1 helix in the putative transmembrane region (PTM) of the N-terminal domain (Figure 1.16). This region is proposed to traverse the membrane when CLIC1 is in its integral membrane form (Harrop *et al.*, 2001; Berry and Hobert, 2006; Singh and Ashley, 2006). Trp's exquisite sensitivity to solvent polarity and environment, its higher molar absorptivity at 280 nm and thus greater quantum yield, and the fact that excitation of Tyr residues in the vicinity of Trp result in fluorescence resonance energy transfer (FRET) to Trp (which can occur over distances up to 18 Å (Lakowicz, 1999)), mean that the Ex.280 spectrum will be dominated by Trp anyway. However, this is not to say that the Ex.280 and Ex.295 spectra are the same, not by any means. The two different excitation wavelengths give slightly different pictures of the tertiary structure of CLIC1 in relation to Trp35, and the spectra do differ quite significantly. Excitation at 295 nm of the lone tryptophan in CLIC1 gives a much lower intensity signal than excitation of the eight tyrosines and the tryptophan at 280 nm (Figure 3.8). The wavelength of maximum emission (λ_{max}) for Ex.295 is slightly red-shifted from that for Ex.280 (1-2 nm), and while this is a small change and probably within error, it was consistent across multiple data sets and different instruments. At pH 7.0 the λ_{max} of native CLIC1 excited at 280 nm is 341 nm, and is 342 nm for Ex.295. At pH 5.5 λ_{max} for the native protein is 340 nm for Ex.280 and 342 nm for Ex.295. For CLIC1 at pH 7.0 and pH 5.5 unfolded in 8.0 M urea the λ_{max} are 345 nm and 348 nm for Ex.280 and Ex.295 respectively. The maximum emission wavelength of 340-342 nm is indicative of a partially buried Trp, which is seen in the crystal structure, where Trp is ~26 % exposed.

The contribution of tyrosine residues to the spectrum excited at 280 nm is invisible until the protein is unfolded, when a shoulder is revealed at around 305 nm. The much higher quantum yield of Trp35, possibly also due to fluorescence resonance energy transfer (FRET), swamps the Tyr contribution in the native state (Lakowicz, 1999), but when the protein unfolds there is uncoupling of energy

transfer from the Tyr residues to Trp35 as they move apart spatially. This peak is not apparent when Trp35 is selectively excited at 295 nm. Tyrosine is relatively unaffected by differences in solvent polarity and generally emits at the same wavelength no matter the environment, whilst the indole ring of Trp is particularly sensitive to environmental polarity (Lakowicz, 1999).

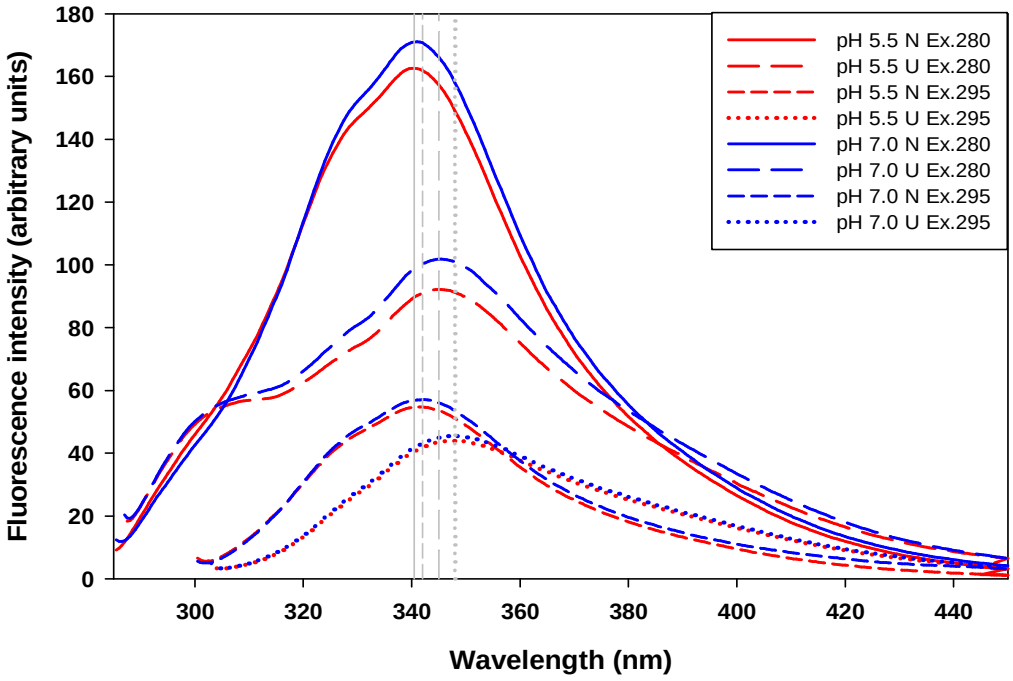

Figure 3.8. Fluorescence emission spectra of native and unfolded CLIC1.

Fluorescence emission spectra of 2 µM CLIC1 in 50 mM sodium phosphate buffer, 1 mM DTT at pH 7.0 (blue) and pH 5.5 (red), at 20 °C. Excitation at 280 nm is shown with solid lines and long dashes. Excitation at 295 nm is shown with short dashes and dots. Native spectra are shown with solid lines and short dashes, and spectra for CLIC1 unfolded in 8.0 M urea are shown with long dashes and dots. The drop lines indicate peak wavelengths for the spectra: solid: native (Ex.280); long dashes: unfolded (Ex.280); short dashes: native (Ex.295); dots: unfolded (Ex.295). The emission peak wavelengths for Ex.295 N and U are slightly longer than those for Ex.280.

3.2.2.2. Near-UV circular dichroism

Near-UV circular dichroism was the second probe used to investigate the tertiary structure of CLIC1. This technique provides information about the packing environments of the aromatic residues Phe, Tyr and Trp. The fact that CLIC1 is a single-Trp protein is rather useful at this juncture, since assigning its band should be easy. The native spectra at pH 5.5 and pH 7.0 were plotted with the HT voltage (the voltage applied to the photomultiplier tube) to OD converted data in order to show the small increase in visible vibronic structure in the absorbance spectra that occurs at the lower temperature used for these measurements, compared to the absorbance spectrum shown in Figure 3.5, and how these relate to the CD bands for the corresponding residues (Figure 3.9). The native pH 5.5 spectrum exhibits clear positive bands at 261 nm, 267 nm and 283 nm, with smaller peaks at 276 nm and 294 nm. There are strong negative bands at 279 nm and 287 nm. The native pH 7.0 spectrum also has strong bands at 261 nm and 268 nm, but has a lower intensity between 265 nm and 290 nm. Instead of one broad band peaking at 283 nm, the pH 7.0 spectrum has 2 peaks in this region, one at 280.5 nm and another at 283 nm. There is also some finer detail resolved at 292 nm and 295 nm, which in the pH 5.5 spectrum is seen as one broad band peaking at 295 nm. Both spectra have deep troughs at 287 nm. The absorbance spectra give an indication of the likely side-chain assignations of the CD bands. Absorbance by Phe is responsible for bands in the lower region: the shoulder at 257 nm and the two peaks at 261 nm and 267 nm. Tyr is probably responsible for the 276 nm and 283 nm bands, and Trp35's contribution is between 280 nm and 300 nm (Strickland, 1974), with the vibronic structure in the 275-290 nm bands arising from the ^1L_b transition. Trp35's 0-0 ^1L_b transition is prominent at 287 nm, and the negative band at 280 is probably due to its 0 + 850 cm^{-1} ^1L_b transition. This band, according to Strickland (1974), is about 7 nm short of the 0-0 band and is of the same sign. The 287 nm band corresponds to the shoulder seen at this wavelength in the absorbance spectrum in Figure 3.9. What is very clear from these spectra is that there appears to be a fairly significant loss of structure around Trp35 and possibly some of the Tyr residues at pH 5.5.

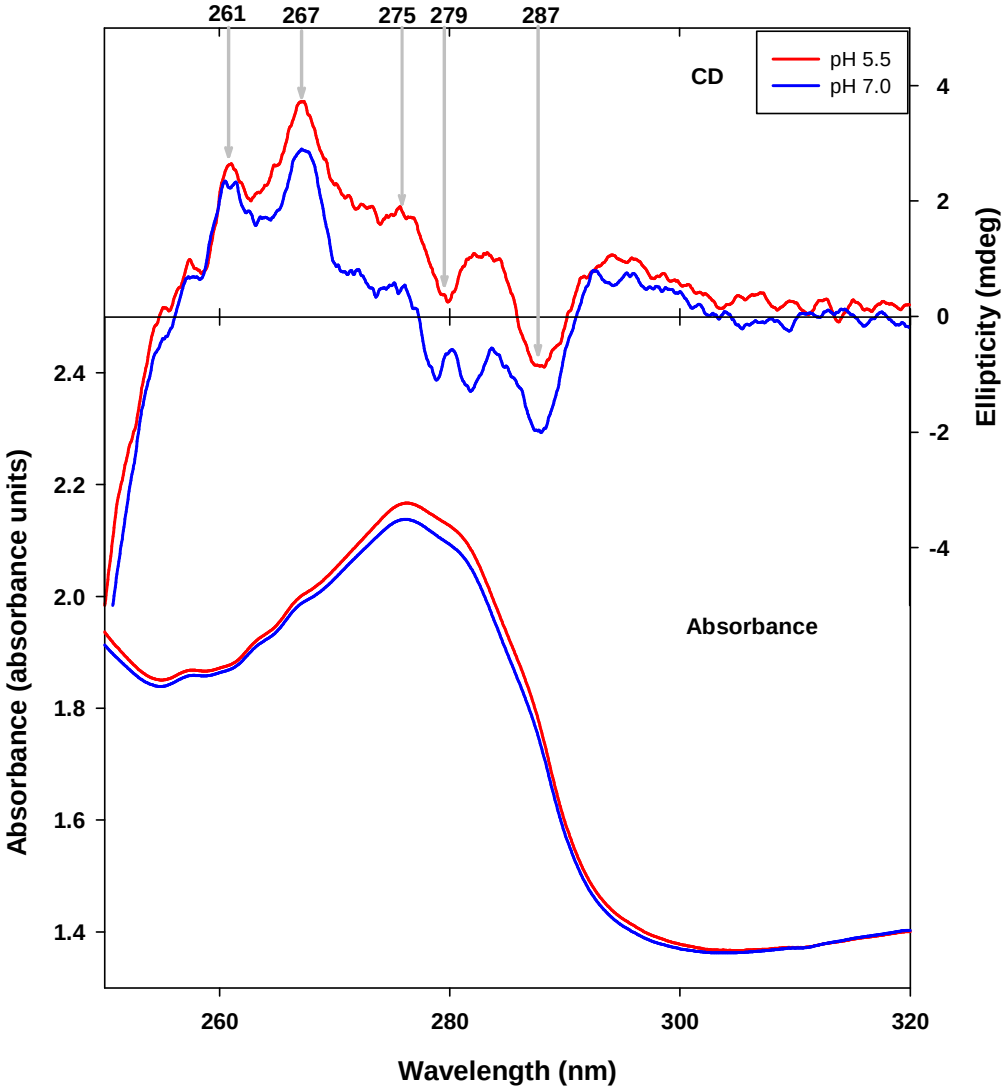

Figure 3.9. Near-UV CD and absorbance spectra of CLIC1.

Near-UV circular dichroism (upper) and absorbance (lower) of 50 µM native CLIC1 at pH 5.5 (red) and pH 7.0 (blue) in 50 mM sodium phosphate buffer, 1 mM DTT. The CD spectra HT voltage data were converted to OD data using the instrument software. The corresponding absorbance bands for the relevant residues can be seen in the CD spectra. Spectra were recorded on a Jasco J-810 spectropolarimeter at 5 °C with a data pitch of 0.05 sec, response of 1 sec and bandwidth of 0.5 nm.

Unfolding CLIC1 in high urea concentrations abolishes much of the near-UV CD intensity at pH 7.0 and pH 5.5, except for some low-intensity structured bands around 261 nm and 268 nm, the Phe bands (Figure 3.10). These may be due to small residual pockets of structure around some Phe residues caused by hydrophobic or charge-charge interactions.

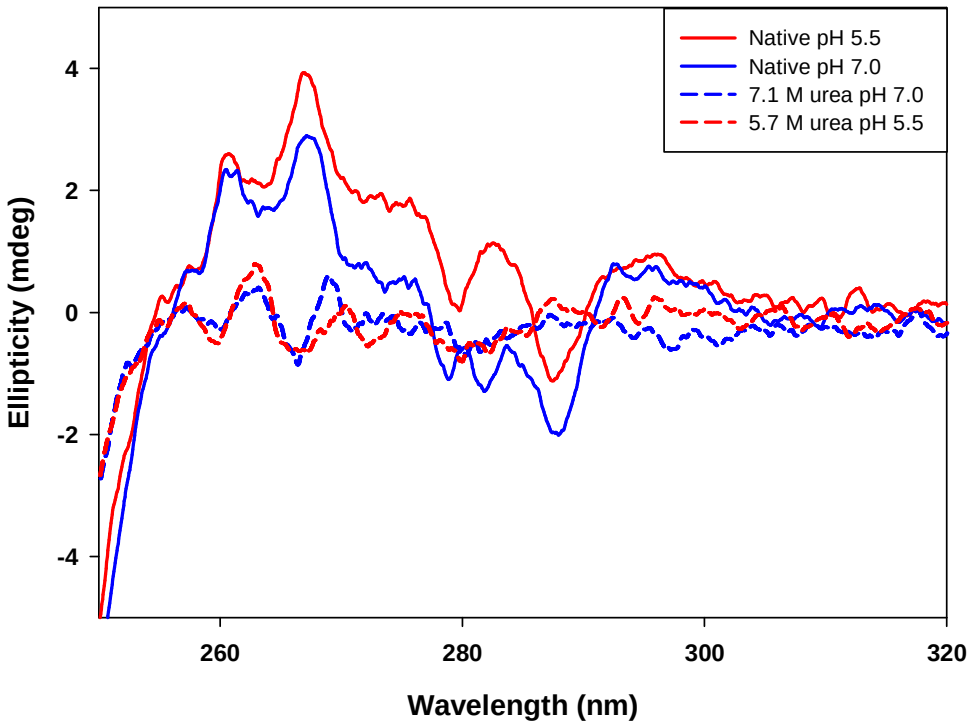

Figure 3.10. Near-UV CD spectra of native and unfolded CLIC1.

Near-UV circular dichroism of 50 µM native and unfolded CLIC1 at pH 5.5 (red) and pH 7.0 (blue) in 50 mM sodium phosphate buffer, 1 mM DTT. Native spectra: solid lines; unfolded spectra: dashed lines. Spectra were recorded on a Jasco J-810 spectropolarimeter at 5 °C with a data pitch of 0.05 sec, response of 1 sec and bandwidth of 0.5 nm.

3.3. Urea-induced equilibrium unfolding

3.3.1. Recovery of native fold

Equilibrium unfolding transitions can only be analysed in terms of their thermodynamic parameters if it has been established that the unfolding reaction is reversible and that the native fold can be recovered (Pace, 1986). CLIC1 secondary and tertiary structural recovery at pH 7.0 and pH 5.5 was monitored using fluorescence with excitation at 280 nm and 295 nm (Figure 3.11) and with circular dichroism with ellipticity at 222 nm. Unfortunately, the low concentrations used resulted in very noisy CD spectra, so only the fluorescence recovery spectra are shown here. These indicate almost complete recovery of the tertiary structure at both pH 7.0 and pH 5.5. At pH 7.0, Ex.280, 96 % recovery of the native fold was achieved, and 100 % was achieved with excitation at 295 nm. At pH 5.5, the recovery was 92 % with Ex. 280 and was 100 % at Ex.295. Thus the equilibrium unfolding transitions of CLIC1 at pH 7.0 and pH 5.5 can be analysed to determine the thermodynamic parameters which will indicate the stability of CLIC1: the free energy of unfolding in the absence of denaturant ($\Delta G_{(H2O)}$) and the *m*-value.

3.3.2. Effect of pH on CLIC1 conformational stability

The conformational stability of 2 µM CLIC1 at pH 7.0 and pH 5.5 was analysed using equilibrium unfolding curves monitoring changes in secondary (far-UV CD) and tertiary (fluorescence) structure simultaneously. The beauty of using both techniques at once on the same samples is that any differences in the transitions can be reliably attributed to changes in the protein conformation itself, as opposed to differences in the samples. Figure 3.12 shows the E_{222} data overlayed against the Ex.280 emission peak fluorescence data at pH 7.0 and pH 5.5. At pH 7.0, the curves are sigmoidal and monophasic, with no indication of any shoulders or inflections anywhere along the curves. The CD and fluorescence data superimpose

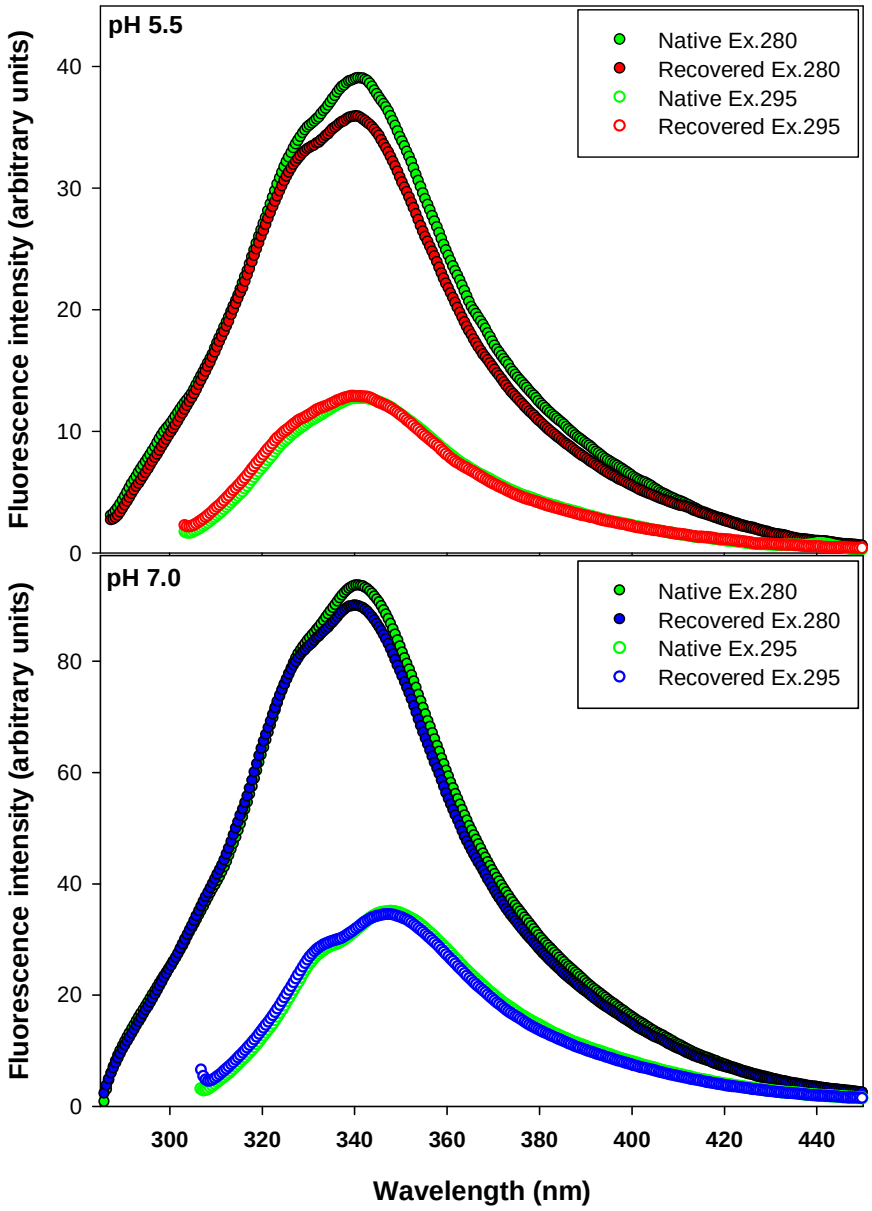

Figure 3.11. Recovery of native fold.

Fluorescence spectra for CLIC1 unfolded in 8.0 M urea and then refolded at pH 5.5 (upper) and pH 7.0 (lower). Triplicate samples of 5 µM CLIC1 (pH 5.5, red) or 10 µM CLIC1 (pH 7.0, blue) were unfolded for 1 hour (pH 5.5) or 2 hours (pH 7.0) in 8.0 M urea in 50 mM sodium phosphate buffer, 1.0 mM DTT, 0.02 % NaN3, then diluted 10x with buffer and allowed to refold for 1 hour (pH 5.5) or 2 hours (pH 7.0). Baseline spectra of 0.5 µM CLIC1 (pH 5.5) or 1.0 µM CLIC1 (pH 7.0) in 0.8 M urea were collected to act as a native reference (green).

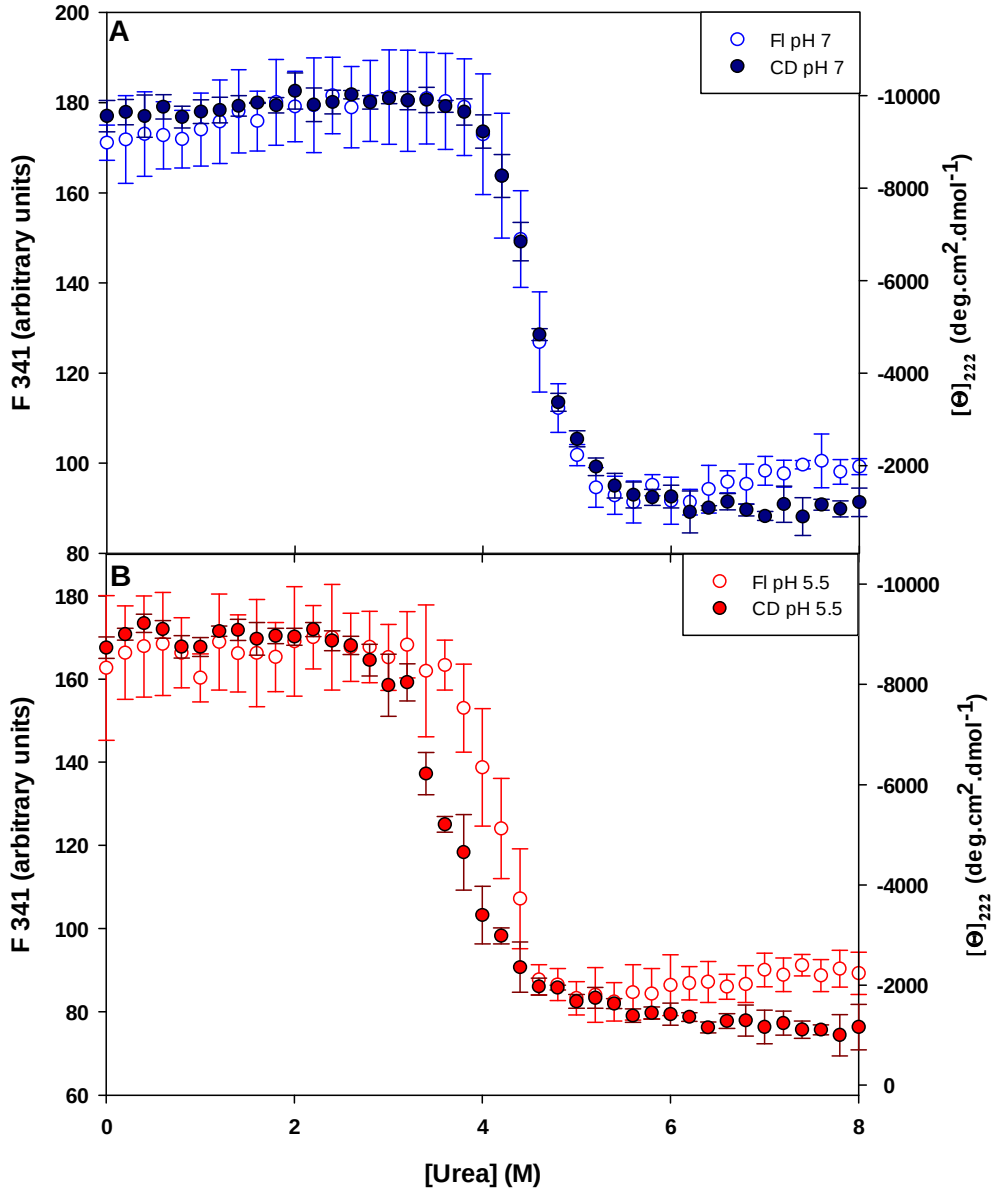

Figure 3.12. Overlays of fluorescence and CD unfolding data.

Fluorescence- and CD-monitored equilibrium unfolding for 2 µM CLIC1 in 50 mM sodium phosphate buffer, 0.02% NaN_3, 1 mM DTT, pH 7.0 (**A**), and pH 5.5 (**B**) as a function of urea concentration. Fluorescence excitation was at 280 nm (open circles) and CD data were collected at 222 nm (closed circles).

perfectly in the transition region, whose steepness indicates a highly cooperative unfolding transition. At pH 5.5, however, the curves separate from one another in the transition region and the transition occurs over a broader range of urea concentrations. The slope in the transition region is less steep than that at pH 7.0, suggesting a drop in cooperative unfolding. The CD-monitored transition at pH 5.5 begins at least one urea concentration unit lower than at pH 7.0, and the fluorescence-monitored transition at pH 5.5 also begins at lower concentrations of urea than at pH 7.0, implying that the structure at pH 5.5 is more susceptible to urea denaturation than at pH 7.0. What is rather unusual about the pH 5.5 plots is that the CD-monitored transition occurs at lower urea concentrations than the fluorescence-monitored transition, indicating that more secondary structure is lost at lower urea concentrations in the transition than tertiary structure. This could be significant in terms of the nature of the structural changes the protein undergoes as it unfolds, but also may be related to the nature of fluorescence as a probe, given the complexity of the electronic transitions within the indole ring in particular. Lack of superimposition usually indicates some kind of intermediate species in the unfolding pathway. This is borne out by Figure 3.13, where the wavelength at which each spectrum in the curve peaked (λ_{max}) was plotted as a function of urea concentration. Although this type of plot cannot be used to determine thermodynamic parameters because it does not depend upon protein concentration, it is a useful means of qualitatively analysing the data. Again, the pH 7.0 data shows a monophasic, sigmoidal transition, but the pH 5.5 data is dramatically different, showing a clear dip in the unfolding transition which represents a blue shift in the λ_{max} between 2.8-3.8 M urea followed by a red shift at urea concentrations above 3.8 M. A blue shift indicates a change to a more hydrophobic environment of Trp35.

To ensure that the blue shift in the pH 5.5 data in Figure 3.13 was not simply the result of large, sticky, hydrophobic aggregates forming, light scatter at 340 nm was monitored along the entire unfolding curve (shown in Figure 3.17). There was no significant increase in scatter anywhere along the curves for either pH 7.0

(Figure 3.14) or pH 5.5 (Figure 3.17), so it can safely be concluded that the blue shift observed at pH 5.5 is due to a stable intermediate species.

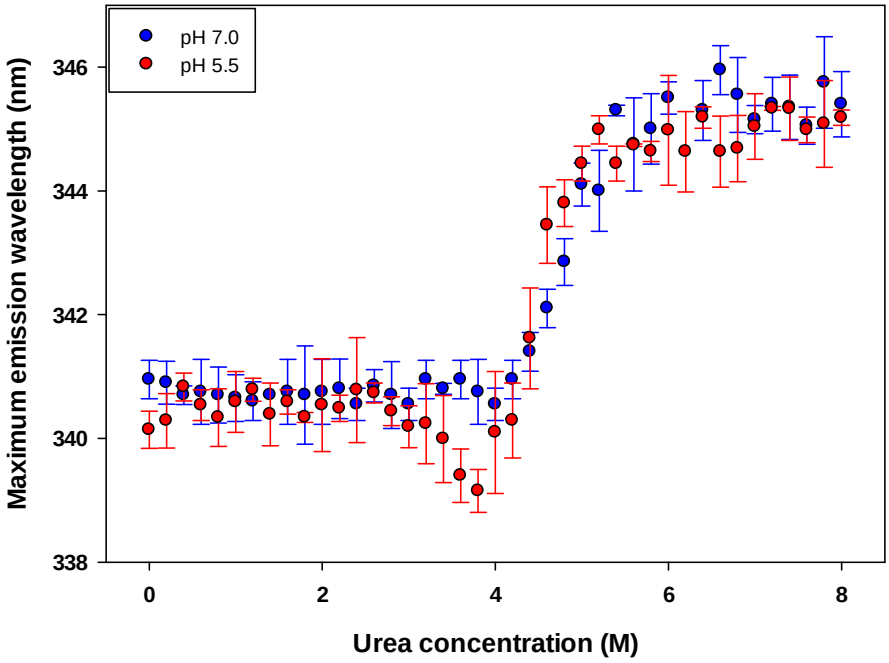

Figure 3.13. CLIC1 equilibrium unfolding monitored by maximum emission wavelength.

Fluorescence-monitored equilibrium unfolding curves for 2 µM CLIC1 in 50 mM sodium phosphate buffer, 0.02% NaN_3, 1 mM DTT, pH 5.5 (red) and 7.0 (blue) with increasing concentrations of urea. Excitation was at 280 nm.

3.3.2.1. Data-fitting

The pH 7.0 and pH 5.5 data were fitted to monomeric models (described in Section 2.2.5.5.). There is extensive data to indicate that CLIC1 exists as a monomer under reducing conditions within a range of pHs (Tulk *et al.*, 2000; Fanucchi *et al.*, 2008), and the crystal structure of CLIC1 is monomeric (Harrop *et al.*, 2001). Since the pH 7.0 data obeys the criteria outlined for a two-state

transition, the Ex.280 pH 7.0 fluorescence intensity data at 305 nm (F305), F310, F315, F325, F330, F341, F345, F355 and F365, as well as the E_{222} data were fitted to a two-state monomer model ($N \leftrightarrow U$) using global analysis to perform the fit (Beecham, 1992) (Figure 3.14A). Ex.295 data at the same wavelengths with E_{222} data were also globally fit (Figure 3.14B). The thermodynamic parameters obtained from the fits are listed in Table 2, and residuals for the fits are shown in Figure 3.15 and Figure 3.16. The reduced χ^2 values for the fits at pH 7.0 were 0.8 and 0.2 for Ex.280 + CD and Ex.295 + CD data, respectively. Goodness of fit for both fits was 1.

Deviation from a two-state model can be ascertained, in addition to any obvious visible variations in the unfolding curves, by checking the following criteria outlined by Whitten and García-Moreno (2000) that indicate conformity with a two-state process:

i) Fits to data obtained with different probes must yield the same $\Delta G_{(H2O)}$ values.

ii) Statistical tests of the quality of the fit, such as r^2 and χ^2 values, must show it to be good. Dependencies of the variables should also be low.

iii) The curves obtained from monitoring with different probes should superimpose, since the properties monitored by the different probes should change simultaneously.

iv) The unfolding curve must be sigmoidal, with no shoulders or inflections to imply intermediate species.

v) No other compact species besides the native state should be detectable by size-exclusion chromatography along the unfolding transition.

vi) The ratio of the calorimetric to van't Hoff enthalpies must be close to one.

This study did not include size-exclusion or calorimetric work, but certainly (i) – (iv) hold true for the pH 7.0 data. None of (i) – (iv) hold true for the pH 5.5 data, and dynamic light scattering data has detected a compact intermediate species in

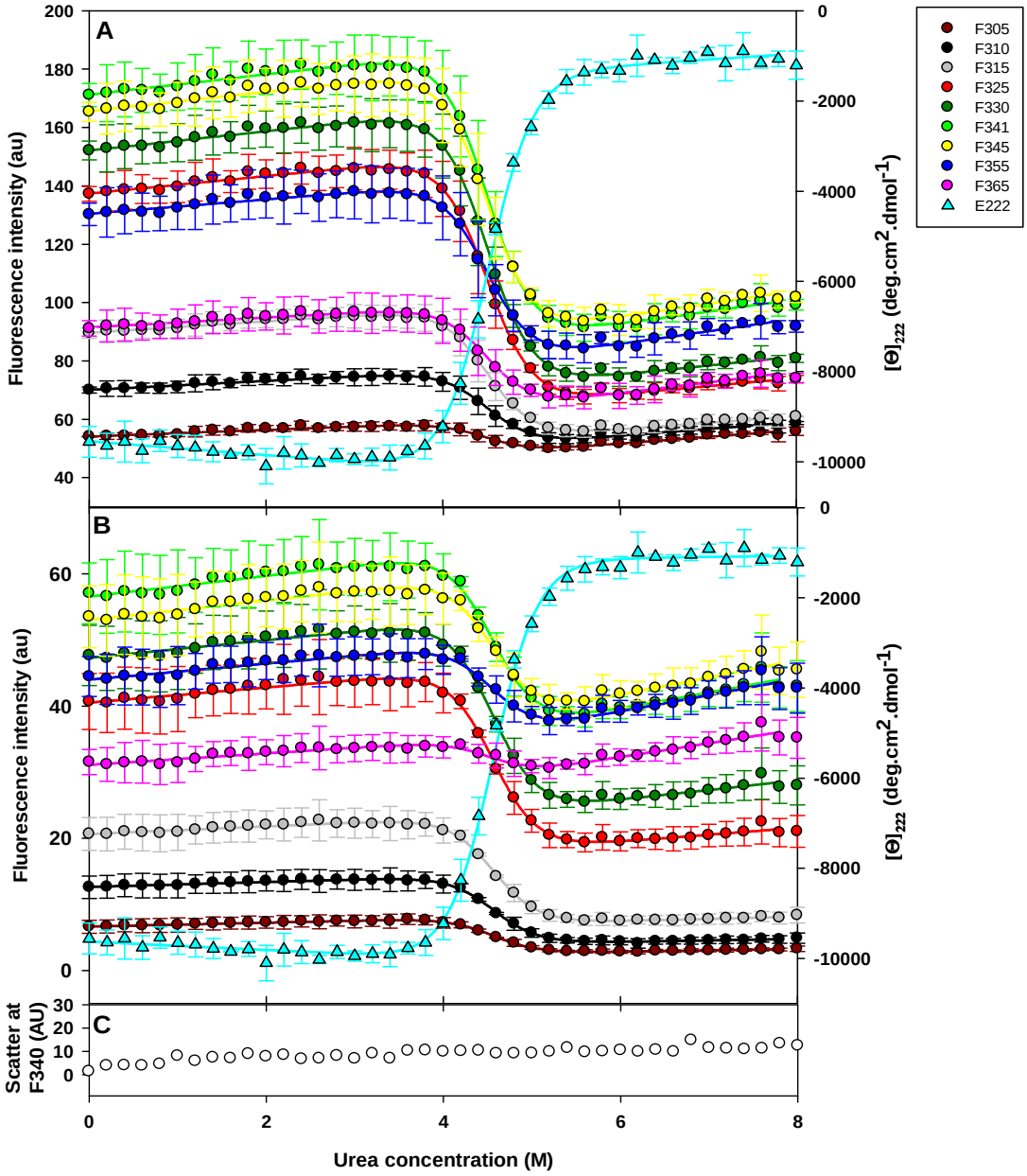

Figure 3.14. CLIC1 equilibrium unfolding at pH 7.0.

Fluorescence- and CD-monitored equilibrium unfolding for 2 µM CLIC1 in 50 mM sodium phosphate buffer, 0.02% NaN_3, 1 mM DTT, pH 7.0, as a function of urea concentration. Fluorescence excitation was at 280 nm (**A**) and 295 nm (**B**). CD data were collected at 222 nm. Scatter data for the detection of aggregation was monitored with excitation and emission at 340 nm (**C**). Buffer-corrected data were plotted as the average of 3 data sets at specific wavelengths: F305 (brown), F310 (black), F315 (gray), F325 (red), F330 (dark green), F340 (lime green), F345 (yellow), F355 (blue), F365 (pink) and E_{222} (cyan), as a function of urea concentration. Global analysis was applied to the data using Savuka v. 6.2.26 (Beecham, 1992; Zitzewitz *et al.*, 1995). The lines represent the fits.

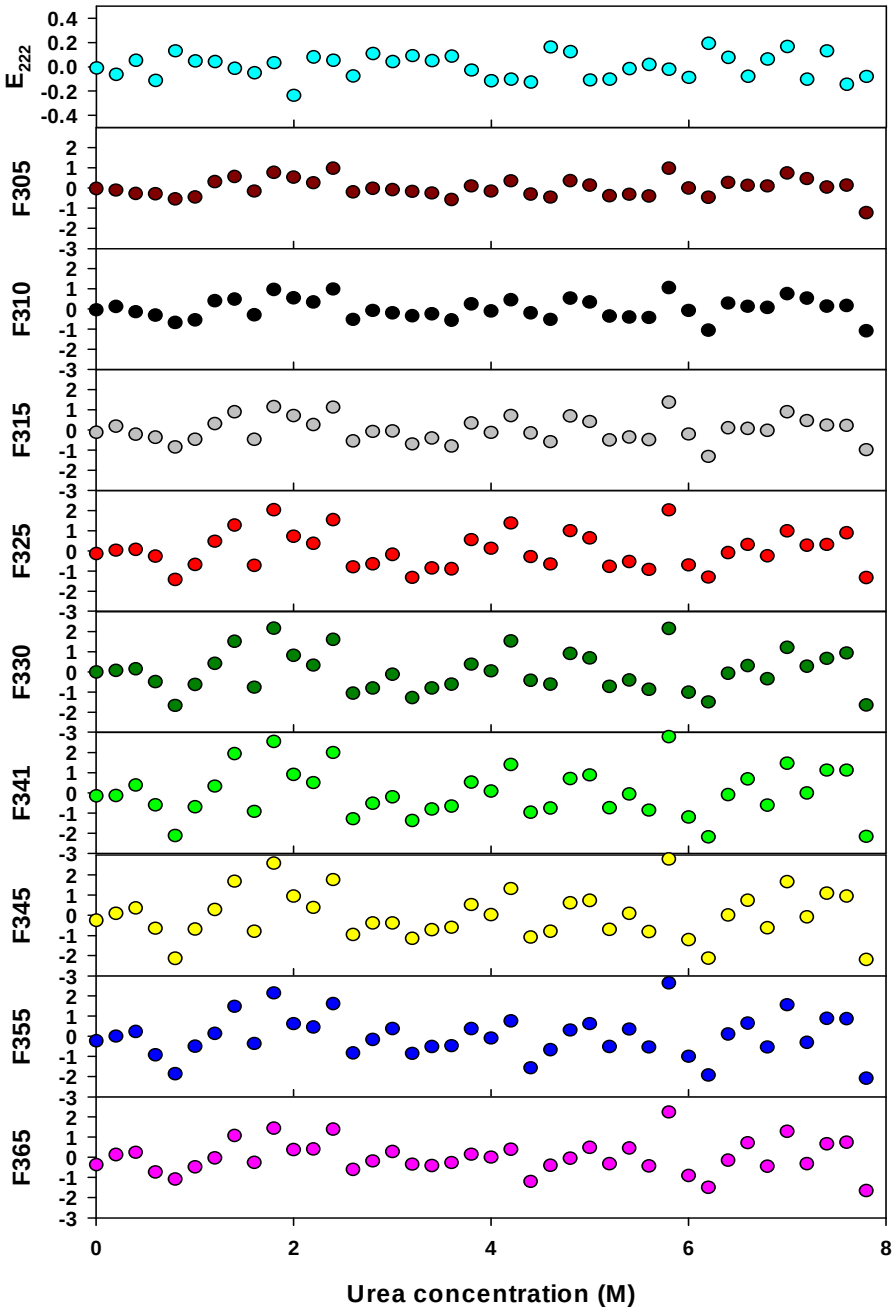

Figure 3.15. Residual plots for pH 7.0 Ex.280 + CD global fits.

Residual data for each of the data sets used for global analysis of CLIC1 equilibrium unfolding at pH 7.0, Ex.280 + CD (see Figure 3.14).

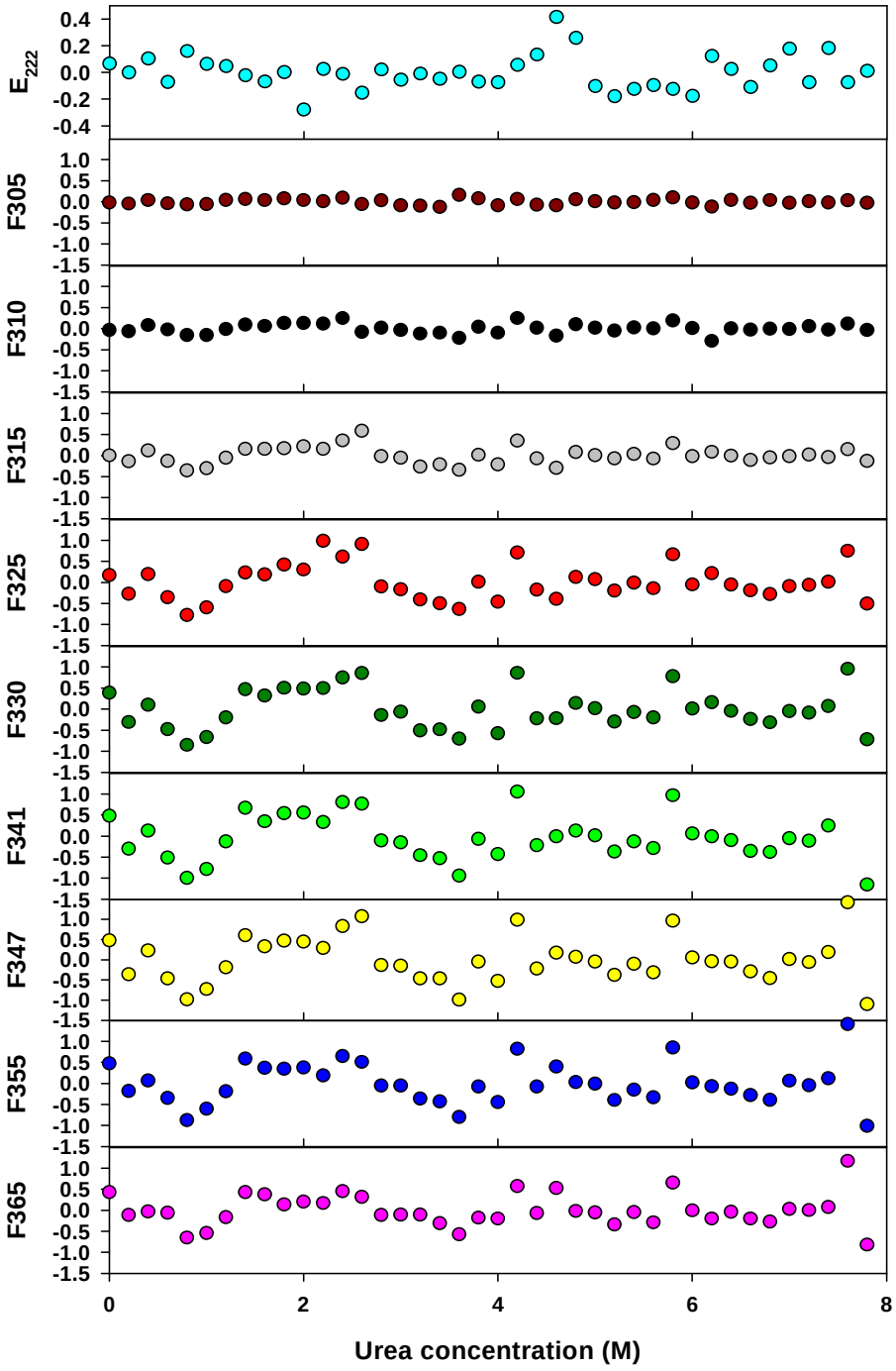

Figure 3.16. Residual plots for pH 7.0 Ex.295 + CD global fits.

Residual data for each of the data sets used for global analysis of CLIC1 equilibrium unfolding at pH 7.0, Ex.295 + CD (see Figure 3.14).

the transition at pH 5.5 (Fanucchi *et al.*, 2008). Therefore, a three-state monomer model (N ↔ I ↔ U) was applied to the pH 5.5 data using global analysis (Beecham, 1992) (Figure 3.16). The data sets used were Ex.280 F310, F315, F325, F340, F345, F355, F365 and E_{222}. Residual plots for this data are shown in Figure 3.18. Ex.295 fluorescence data at F305, F310, F315, F325, F342, F348, F355 and F365 were also fit. Residual plots for Ex.295 data are shown in Figure 3.19. The thermodynamic parameters obtained are listed in Table 2. The reduced χ^2 values for the fits were 0.02 and 0.01 for the Ex.280 + CD and Ex.295 data, respectively. Goodness of fit for both fits was 1. The thermodynamic parameters obtained for the fits at pH 7.0 and pH 5.5 were used to calculate fractional populations of each species from the equilibrium constants (see Section 2.2.5.5.) (Figure 3.20).

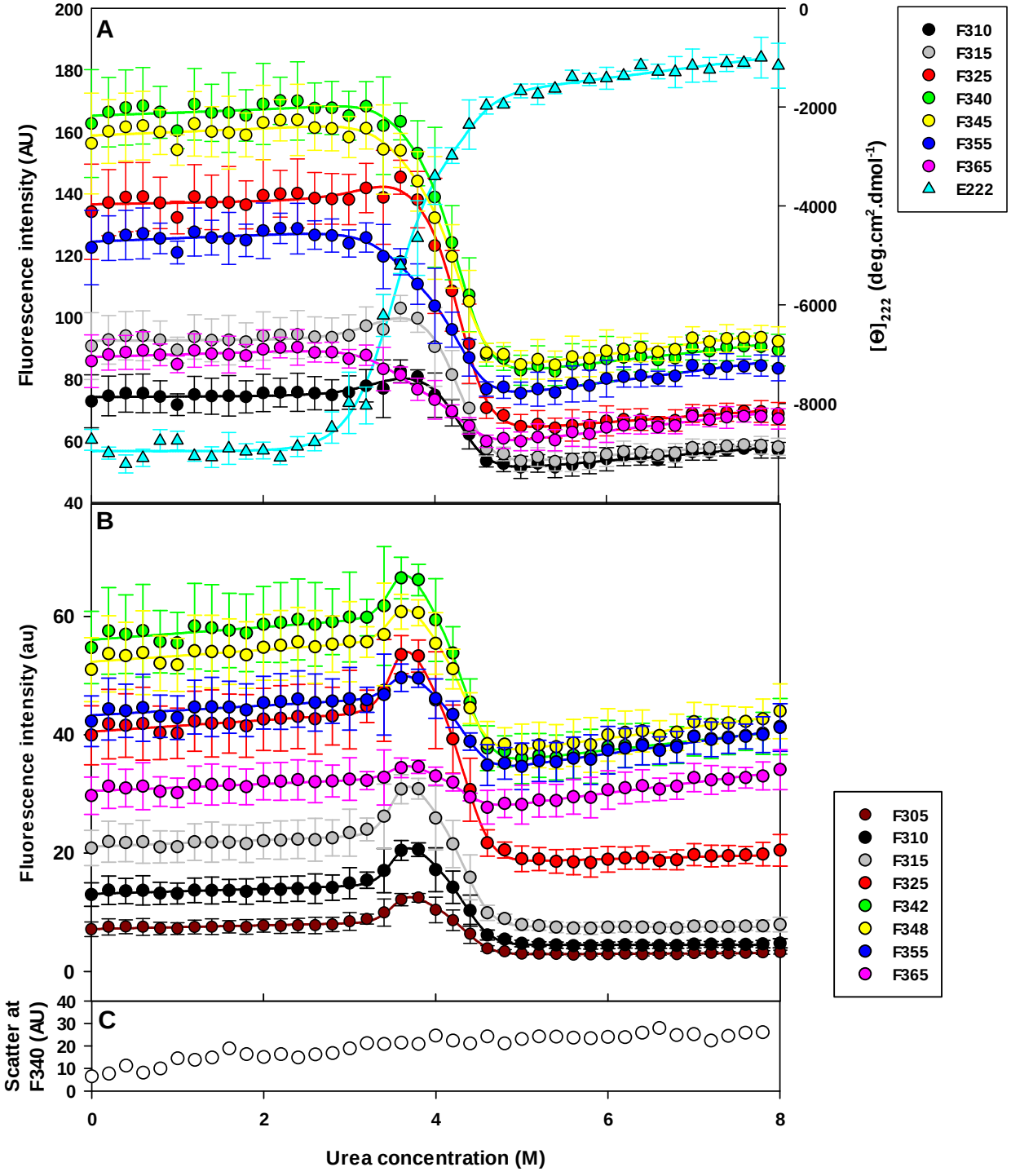

Figure 3.17. CLIC1 equilibrium unfolding at pH 5.5.

Fluorescence- and CD-monitored equilibrium unfolding for 2 µM CLIC1 in 50 mM sodium phosphate buffer, 0.02% NaN_3, 1 mM DTT, pH 5.5, as a function of urea concentration. Fluorescence excitation was at 280 nm (**A**) and 295 nm (**B**). CD data were collected at 222 nm. Scatter data for the detection of aggregation was monitored with excitation and emission at 340 nm (**C**). Buffer-corrected data were plotted as the

average of 3 data sets at specific wavelengths: F305 (F310 (black), F315 (gray), F325 (red), F340 (green), F345 (yellow), F355 (blue), F365 (pink) and E222 (cyan), as a function of urea concentration. Global analysis was applied to the data using Savuka v. 6.2.26 (Zitzewitz et al., 1995). The lines represent the fits.

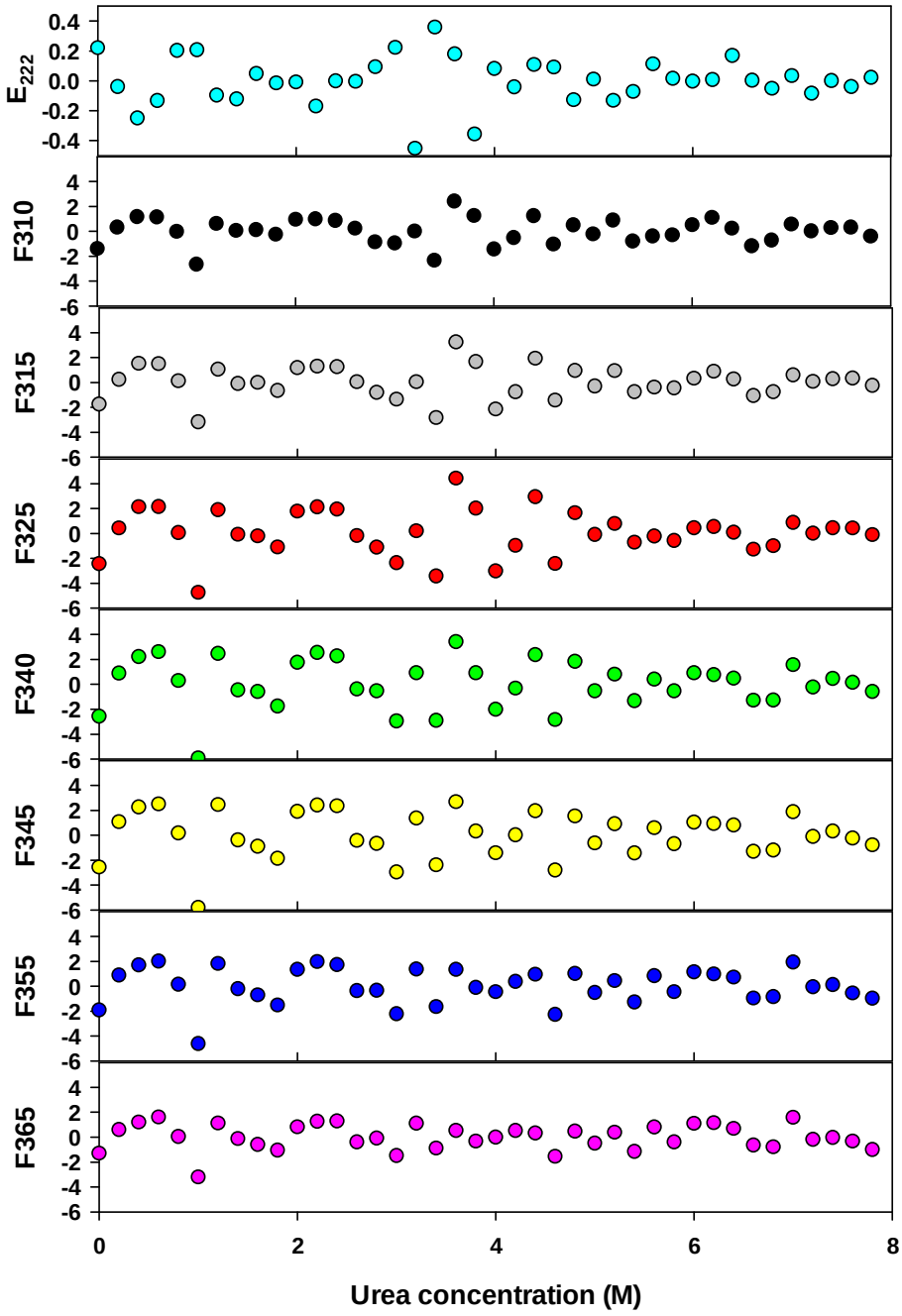

Figure 3.18. Residual plots for pH 5.5 Ex.280 global fits.

Residual data for each of the data sets used for global analysis of CLIC1 equilibrium unfolding at pH 5.5, Ex.280 + CD (see Figure 3.17).

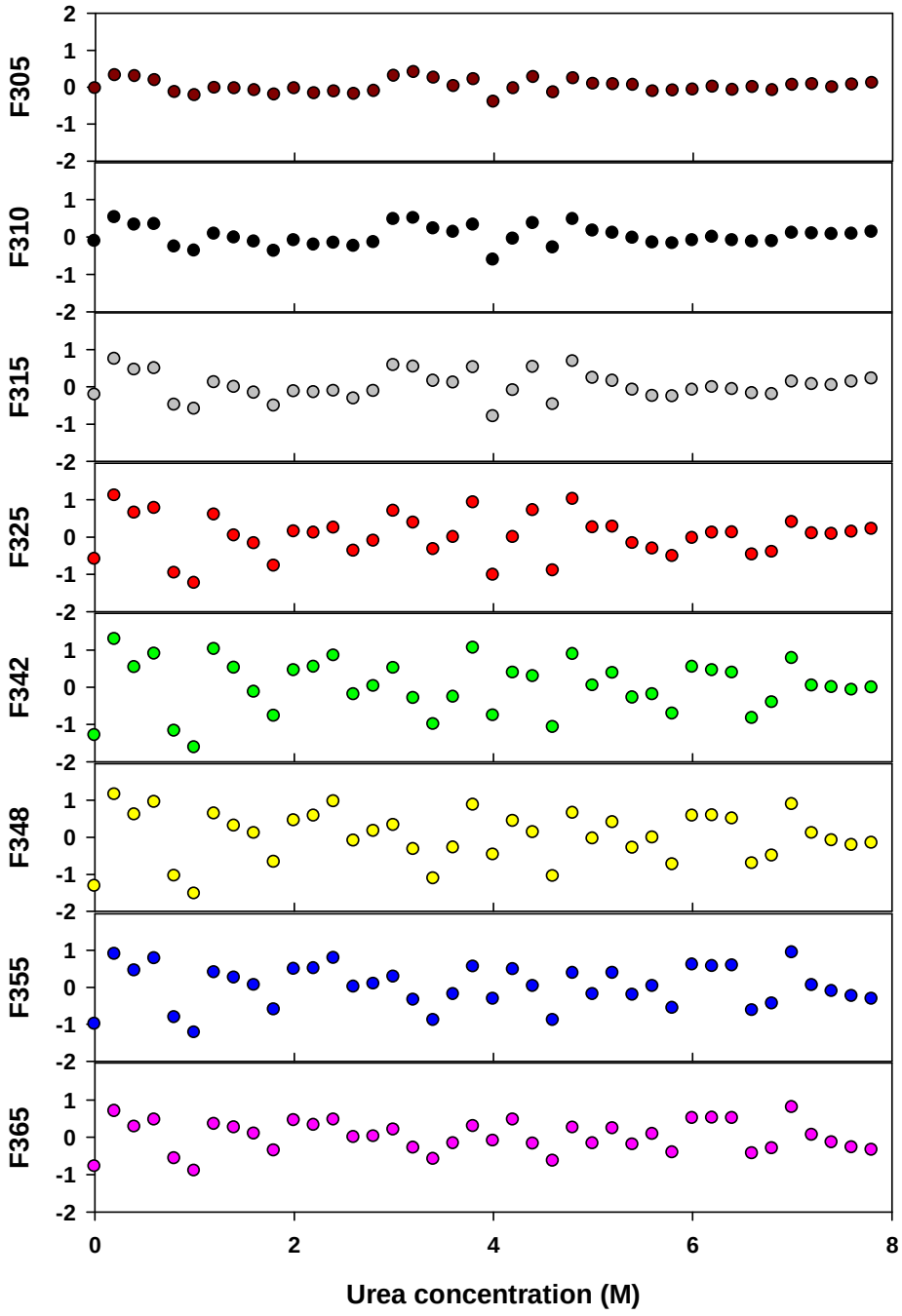

Figure 3.19. Residual plots for pH 5.5 Ex.295 global fits.

Residual data for each of the data sets used for global analysis of CLIC1 equilibrium unfolding at pH 5.5, Ex.295 (see Figure 3.17).

Table 2. Comparison of $\Delta G_{(H2O)}$, *m*-values and C_m values obtained with 2-state monomer and 3-state monomer fits to equilibrium unfolding data for CLIC1 in increasing concentrations of urea at pH 7.0 and pH 5.5.

Parameters	pH 7.0 (2-state monomer fit)	
	Fluorescence (Ex.280) and CD	**Fluorescence (Ex.295) and CD[a]**
$\Delta G_{(H2O)}$ (kcal/mol) N → U	10.3 ± 0.1	10.6 ± 0.2
***m* (kcal/mol/M urea)**	2.3 ± 0.0	2.3 ± 0.0
C_m (M urea)[b]	4.5 ± 0.0	4.6 ± 0.1
m_{pred} (kcal/mol/M urea)	2.7	2.7
C_{mPred} (M urea)[c]	3.8	3.9
	pH 5.5 (3-state monomer fit)	
$\Delta G_{(H2O)}1$ (kcal/mol) N → I	8.0 ± 0.8	21.3 ± 1.8
***m*1 (kcal/mol/M urea)**	2.3 ± 0.3	6.0 ± 0.5
C_m1 (M urea)	3.5 ± 0.1	3.6 ± 0.0
$\Delta G_{(H2O)}2$ (kcal/mol) I → U	14.6 ± 1.0	16.6 ± 1.0
***m*2 (kcal/mol/M urea)**	3.4 ± 0.2	3.7 ± 0.2
C_m2 (M urea)	4.3 ± 0.0	4.5 ± 0.0
m_{pred} (kcal/mol/M urea)	2.7	2.7
C_m1_{Pred} (M urea)	3.0	7.9
C_m2_{Pred} (M urea)	5.4	6.1

[a] CD data was not included in pH 5.5 Ex.295 fit.

[b] $C_m = \Delta G_{(H2O)}/m$

[c] $C_{mPred} = \Delta G_{(H2O)}/m_{pred}$

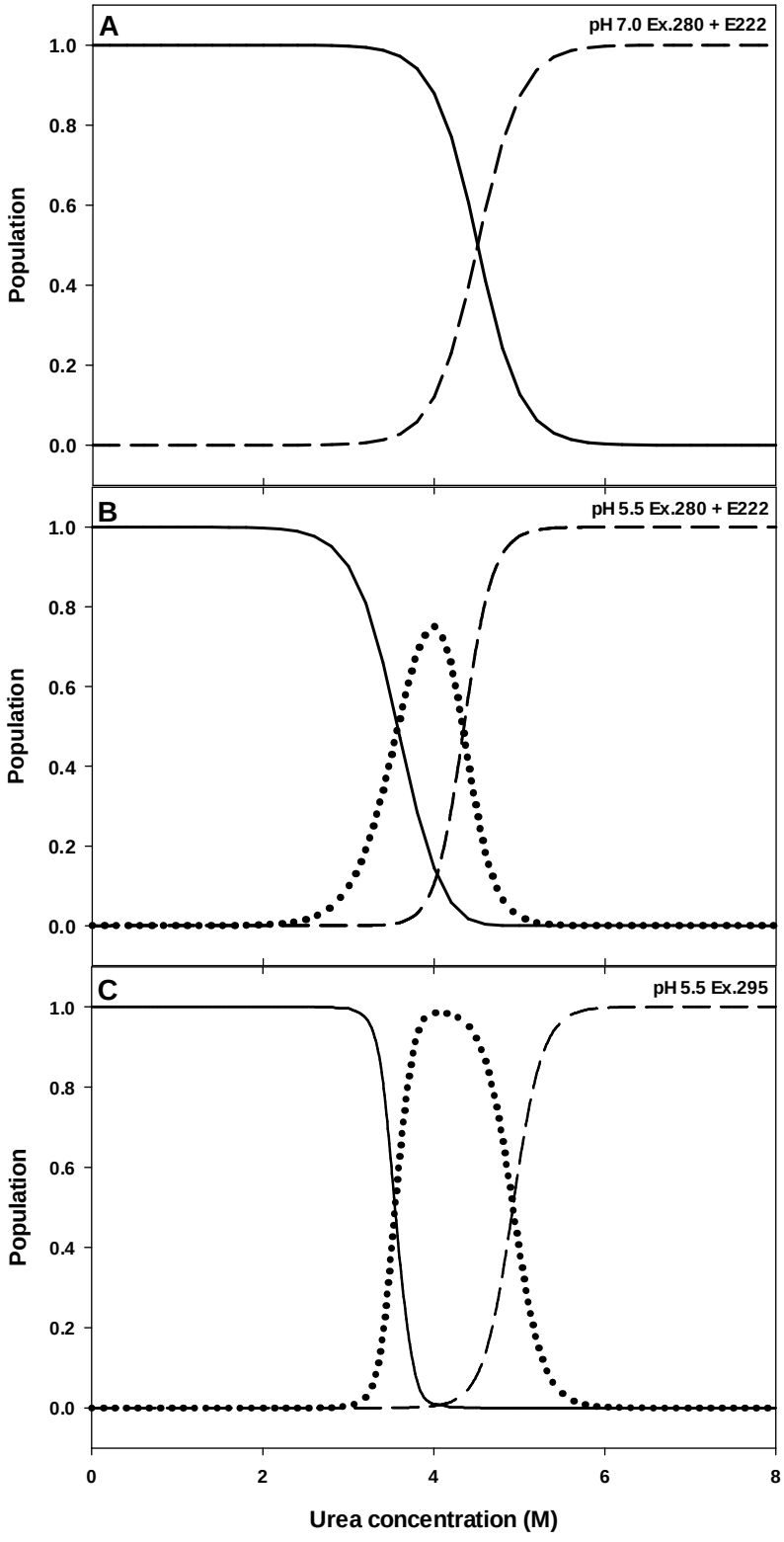

Figure 3.20. Fractional populations of native, intermediate and unfolded species.

Fractional populations of native (solid line), intermediate (dotted line) and unfolded (dashed line) species as a function of urea concentration were calculated from the

thermodynamic parameters obtained from global fits to the unfolding data. Only the Ex.280 data for pH 7.0 is shown (**A**), as Ex.295 was basically the same. Populations of N and U species are equal at approximately 4.5 M urea. The fit to E_{222} data and fluorescence data with excitation at 280 nm, pH 5.5 (**B**) differed markedly from that to pH 5.5 data with excitation at 295 nm (**C**), with the I species existing in much greater proportion in the latter case.

It is clear from Figure 3.20 and Table 2 that the thermodynamic parameters obtained from the fits to the Ex.280 and Ex.295 data at pH 5.5 differ quite markedly. The values obtained from the pH 7.0 fits are very similar, and within the range expected for a monomeric protein (6-14 kcal/mol) (Pace, 1990). For the pH 5.5 data, the rather baffling difference between the thermodynamic parameters obtained for fits to Ex.280 + CD and Ex.295 data seems to indicate that there is a distinct disparity between what is happening in the protein as a whole during unfolding, and what is occurring in the N-terminal domain, where Trp35 resides. Ex.295 fluorescence data only were fitted in order to see if "global" and "local" actually *are* appropriate terminology for the Ex.280 *vs.* Ex.295 transitions, considering that, on the whole, the Ex.280 spectra are generally taken to be dominated by Trp anyway, as discussed in Section 3.2.2.1. Including the E_{222} data in the Ex.295 fit did not change the derived values much, except that the χ^2 is much higher, and neither did fitting the data to a three-state dimeric model ($N_2 \leftrightarrow I_2 \leftrightarrow 2U$), except that the error was much larger. A $2N \leftrightarrow I_2 \leftrightarrow 2U$ or $nN \leftrightarrow I_n \leftrightarrow nU$ model is not available. Residual plots from all fits (Figure 3.15, Figure 3.16, Figure 3.18, Figure 3.19) do not indicate any systematic problems with the fits.

Figure 3.20 indicates that the intermediate species detected with Ex.295 appears at slightly higher urea concentrations, exists until higher urea concentrations, and is much more heavily populated than when detected with Ex.280. This correlates with the spectra at different urea concentrations, where the intermediate can clearly be seen in the rising spectra. This increased signal, which occurs to a much smaller extent with Ex.280 (see Figure 3.17), and does not occur at pH 7.0 anywhere along the unfolding curve, can only be accounted for by Trp35 moving

to a microenvironment where it is either less exposed to the polar solvent, or removed from the vicinity of potential quenching residues such as Lys or Arg. Only the former accounts for the blue shift seen in Figure 3.13. The Ex.295 thermodynamic parameters show the transition to the intermediate species is less energetically favourable, but more cooperative than the parameters obtained for the transition from Ex.280 data. It is not unthinkable to imagine that during unfolding of the entire protein the localised region of the N-terminal domain is undergoing some kind of structural rearrangement whereby it gains some hydrophobic contacts with the N-terminal domains of other partially unfolded CLIC1 molecules. Once a critical level of unfolding and hydrophobic contacts is reached, CLIC1 collapses highly cooperatively into a stable intermediate conformation that may exist as a partial dimer or oligomer, connected only at the N-domain regions. The N ↔ I transition monitored by Ex.280 emission is much less cooperative than that for Ex.295 – in fact, the *m*-values for pH 5.5 Ex.280 N ↔ I and pH 7.0 N ↔ U are the same.

3.3.3. Properties of the intermediate

The unfolding intermediate detected at pH 5.5 in 3.8-4.0 M urea was further characterised.

3.3.3.1. Secondary and tertiary structural properties

The secondary structure of the CLIC1 intermediate formed at 3.8 M urea, pH 5.5 was probed using far-UV circular dichroism (Figure 3.21). In comparison to the native spectra, the signal for the intermediate at 3.8 M urea is significantly reduced in intensity (~56 %) compared to the difference between native CLIC1 and CLIC1 in 3.8 M urea at pH 7.0 (~19 %). This correlates to a loss of secondary structure in 76 out of 136 residues in CLIC1 that are packed into defined α-helices and β-strands, although obviously the β-strands contribute less to the E_{222} signal than α-helices do.

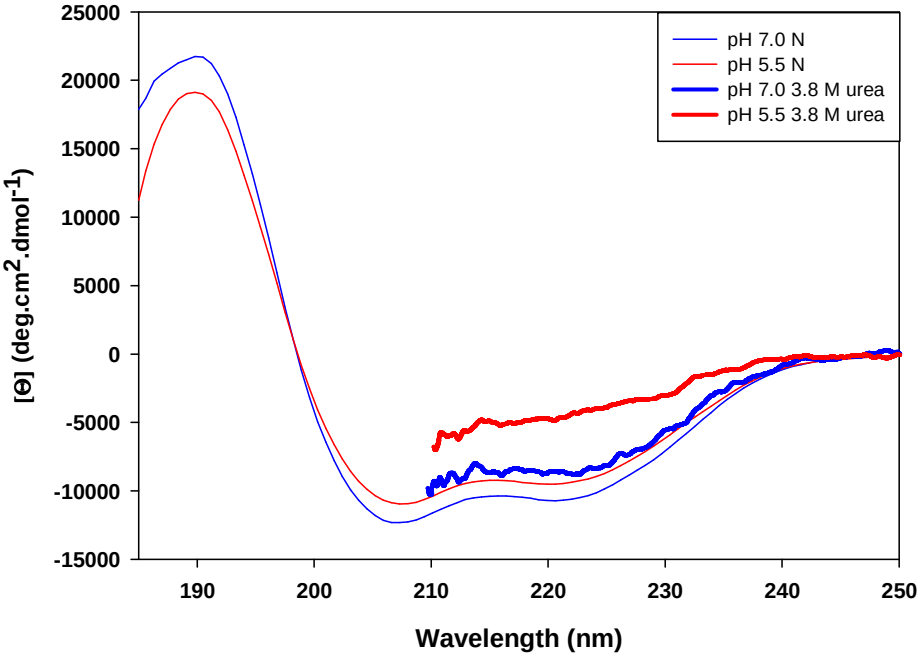

Figure 3.21. Far-UV CD spectra of native and intermediate conformations of CLIC1.

Far-UV circular dichroism spectra of 2 µM CLIC1 in 5 mM sodium phosphate buffer, 0.1 mM DTT at pH 7.0 (blue) and pH 5.5 (red), at 20 °C. Native spectra are shown with fine lines and spectra for CLIC1 in 3.8 M urea are shown with bold lines. Data could not be recorded below about 210 nm for the samples in urea due to low transparency of the solutions at lower wavelengths, resulting in low signal-to-noise ratios. Spectra were plotted with Sigmaplot v. 11.0 and native spectra smoothed using the negative exponential method.

The tertiary structural properties of native CLIC1 and CLIC1 in 3.8 M urea, as reflected in the packing of the side-chains of tyrosine, phenylalanine and tryptophan, were investigated using near-UV CD (Figure 3.22). The signal for the intermediate at pH 5.5 is reduced in comparison to those of native CLIC1 and CLIC1 at pH 7.0 in 3.8 M urea. The fine structure around the Trp35 transitions at 280 nm and 287 nm is gone, and the signal is much reduced. The sharp peaks

around the Phe bands between 260 and 270 nm are flattened. This does not necessarily imply a *loss* of structure, since changes in packing could lead to new degenerate dipole-dipole couplings which cancel out the signal (Strickland, 1974), but it *does* imply a change in packing which is not apparent for CLIC1 in 3.8 M urea at pH 7.0, and which is not the same as the loss of signal seen for unfolded CLIC1.

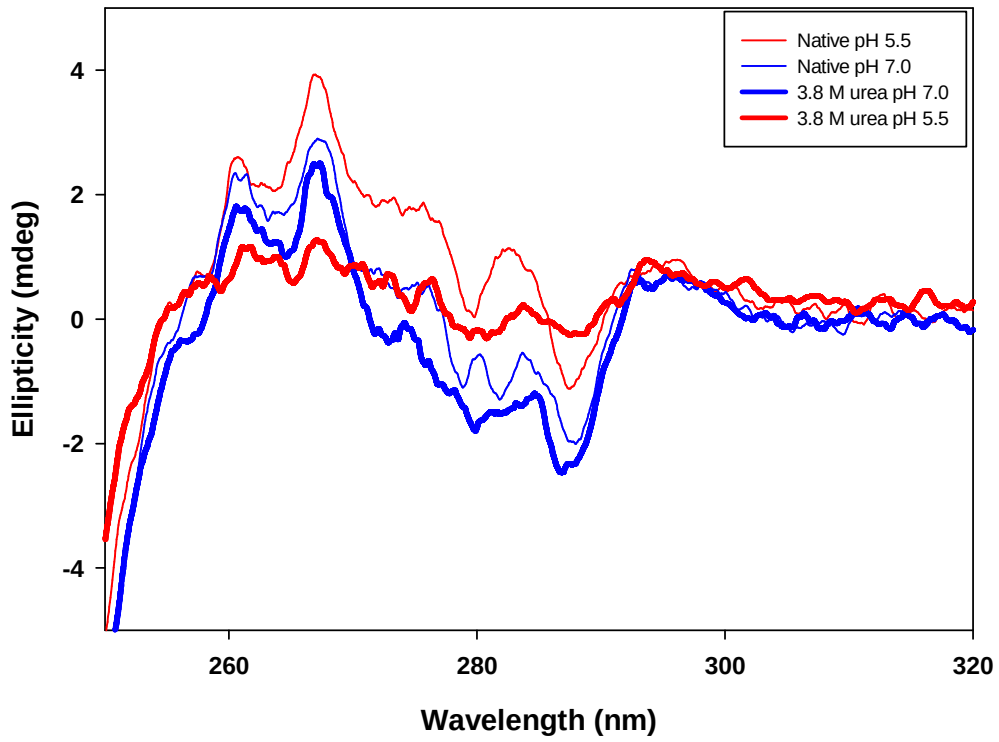

Figure 3.22. Near-UV CD spectra of native CLIC1 and CLIC1 in 3.8 M urea. Near-UV circular dichroism of 50 µM native CLIC1 (fine lines) and CLIC1 in 3.8 M urea (bold lines) at pH 5.5 (red) and pH 7.0 (blue) in 50 mM sodium phosphate buffer, 1 mM DTT. Spectra were recorded on a Jasco J-810 spectropolarimeter at 5 °C with a data pitch of 0.05 sec, response of 1 sec and bandwidth of 0.5 nm.

Fluorescence emission spectra for native, intermediate and unfolded CLIC1 at pH 5.5 indicate a slight blue shift in the spectrum peak for the intermediate at 3.8 M urea, compared to the native protein (Figure 3.23). This correlates with the blue shift seen in Figure 3.13. While this 1 nm shift is possibly not significant within the parameters of the instrument, especially using a 5 nm slit width, it certainly is a consistent observation over tens of spectra collected for the intermediate, and has been recorded as being up to 3-5 nm on a different instrument (Fanucchi *et al.*, 2008). A blue shift is consistent with a move of Trp35 into a more hydrophobic environment. The intensity of the signal with excitation at 280 nm is slightly lower than the native signal, probably indicating a loss of energy transfer from Tyr residues to Trp35. This may indicate a relaxing of the structure such that the polar solvent has more access to Trp35. The signal for the intermediate with Ex.295, however, is *greater* than that for the native. In the absence of aggregation, which was shown not to be a factor, an increased signal would generally suggest a move to a *less* quenching environment, such as into a more buried position, which would be consistent with the blue shift observed, or away from charged residues such as Lys, Arg and His, the latter of which would be positively charged at pH 5.5, which could be responsible for quenching.

3.3.1.2. ANS-binding properties

ANS was used to probe for the intermediate species detected in the unfolding transitions. The blue shift in the fluorescence spectrum peak exhibited by this species implied it is more hydrophobic than the native species. Measurements of CLIC1 incubated in increasing concentrations of urea and 200 µM ANS were performed at pH 7.0 and pH 5.5 to determine if there was a pH dependence to ANS binding that may be observed along the unfolding transition. At pH 5.5, fluorescence intensity is dramatically enhanced between 2.5 and 5.2 M urea, peaking at 3.8-4.0 M urea (Figure 3.24A). This is within the same concentration range at which the intermediate species is most populated in the unfolding transitions. There is no enhancement of the signal at any point along the unfolding curve at pH 7.0, indicating that ANS does not bind CLIC1 at that pH.

Light scatter at 340 nm did not detect the presence of any aggregates (Figure 3.24B).

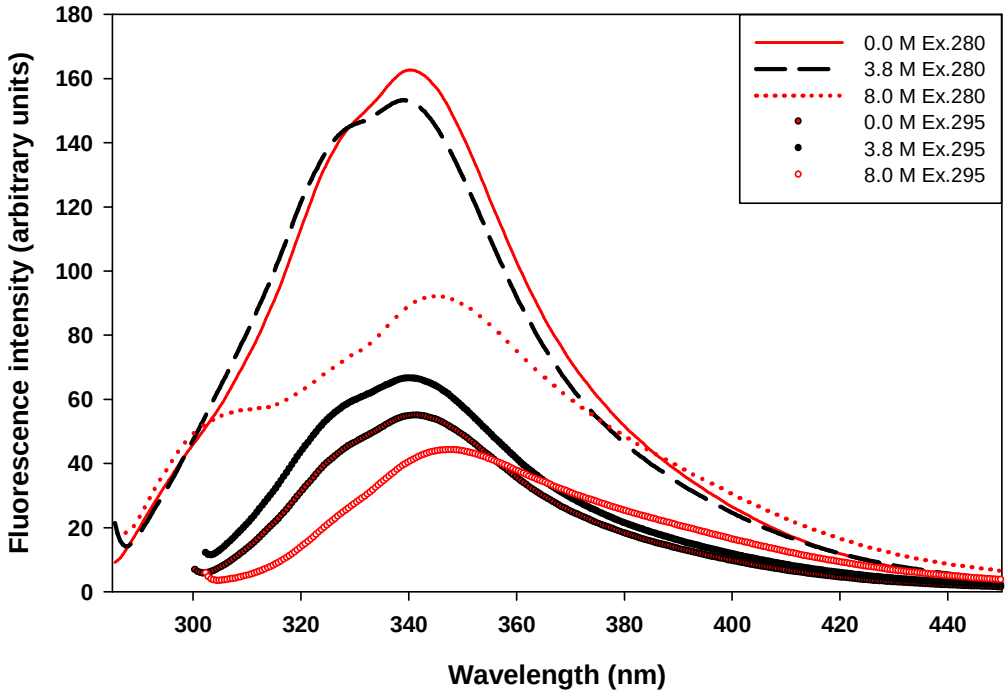

Figure 3.23. Fluorescence emission spectra of native, intermediate and unfolded CLIC1.

Ex.280 (solid, dashed, dotted lines) and Ex.295 (circles) fluorescence emission spectra of native (red solid line, filled red circles), unfolded (red dotted line, red open circles) and intermediate (black dashed line, black circles) CLIC1 at pH 5.5. 2 µM CLIC1 in 50 mM sodium phosphate buffer, 0.02% NaN_3, 1 mM DTT and 0.0, 3.8 or 8.0 M urea was allowed to unfold for 1 hour and then spectra recorded on a Jasco FP6300 spectrophotometer.

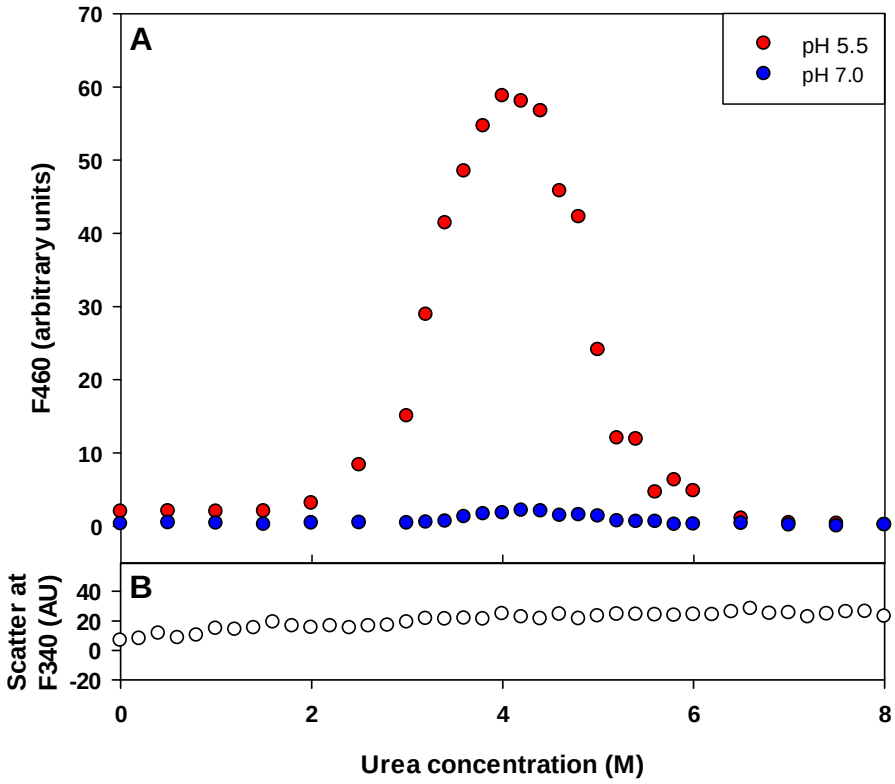

Figure 3.24. CLIC1 equilibrium unfolding in the presence of ANS.

(**A**) Fluorescence emission enhancement at 460 nm was monitored during equilibrium unfolding of 2 µM CLIC1 in 50 mM sodium phosphate buffer, 0.02% NaN_3, 1 mM DTT at pH 5.5 (red) and pH 7.0 (blue) in the presence of 200 µM ANS. At pH 5.5 CLIC1 began to bind ANS after 2.5 M urea and fluorescence enhancement reached a peak at 4.0 M urea, after which it declined again. Scatter data for pH 5.5 with excitation and emission at 340 nm (**B**) indicate that there is no aggregation along the unfolding transition.

The spectrum for free ANS peaks at 518 nm and the spectra at pH 7.0 and pH 5.5 are identical, so there is no pH-dependent change in free ANS emission signal (Figure 3.25). The peak emission wavelength shifts from 518 nm to 476 nm when ANS binds the CLIC1 intermediate, and the substantially enhanced signal intensity is much higher than that of free ANS in solution.

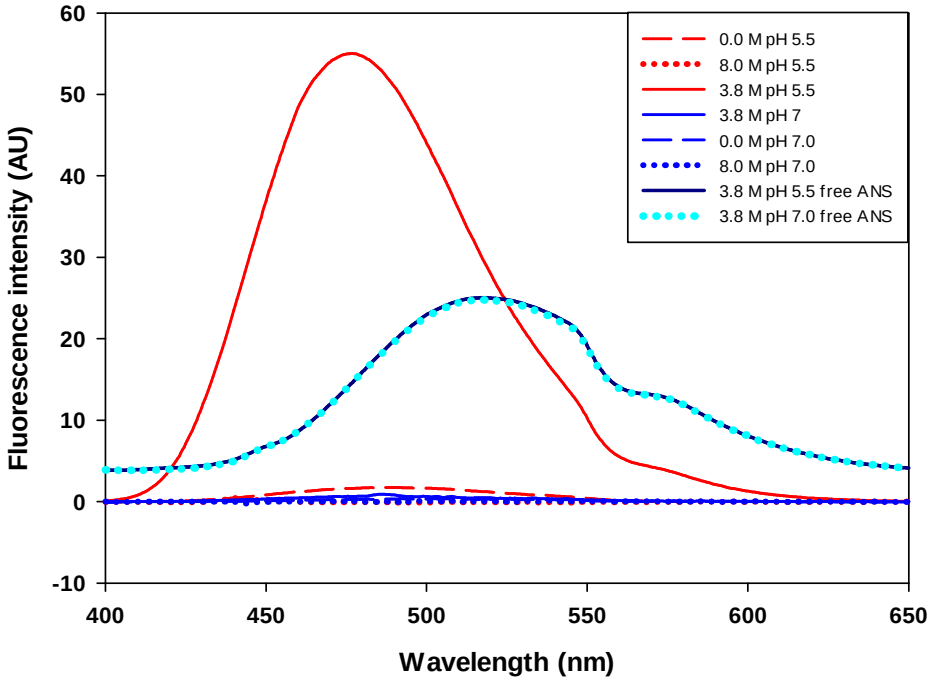

Figure 3.25. ANS binding to CLIC1.

Fluorescence emission spectra of CLIC1 in the presence of 200 µM ANS in 50 mM sodium phosphate buffer, 0.02% NaN3, 1 mM DTT, at pH 5.5 (red), pH 7.0 (blue). Free ANS in the same buffer at 3.8 M urea is shown in navy blue (pH 5.5) and in cyan dots (pH 7.0). Native and unfolded CLIC1 at pH 5.5 and pH 7.0 and CLIC1 in 3.8 M urea at pH 7.0 do not bind ANS, but the significant enhancement of the emission signal for CLIC1 in 3.8 M urea at pH 5.5 indicates binding of ANS. All data were corrected for free ANS. Data were recorded on a Jasco FP6300 spectrophotometer.

The binding affinity of ANS for the intermediate species was determined by titrating aliquots of 2 mM stock ANS into 2 µM CLIC1 at pH 5.5 and 7.0 in the presence and absence of 3.8 M urea (Figure 3.26). Significant fluorescence enhancement occurred only with CLIC1 in 3.8 M urea at pH 5.5. Fitting of the data to a rectangular hyperbole produced a K_d of 20 ± 2 µM.

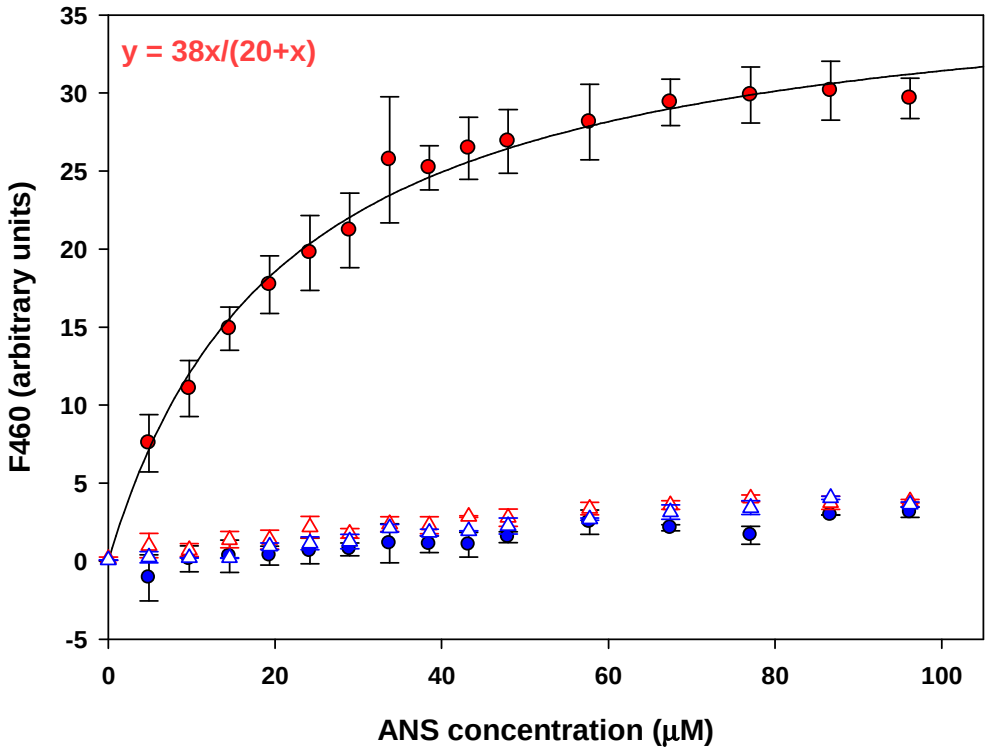

Figure 3.26. Determination of the dissociation constant for the binding of ANS to CLIC1.

ANS titration of 2 µM CLIC1 in 50 mM sodium phosphate buffer, 0.02% NaN_3, 1 mM DTT, pH 5.5 (red) and pH 7.0 (blue), with 3.8 M urea (circles) and without urea (triangles). ANS did not bind to CLIC1 at pH 7.0, or at pH 5.5 in the absence of urea, but significant signal enhancement was noted for CLIC1 at pH 5.5 in 3.8 M urea. A single rectangular hyperbola was fitted to the data (solid line) and a K_d of 20 µM determined from the equation. r^2= 0.98.

3.4. Model membrane studies

CLIC1 has been shown, incontrovertibly, to exist in both soluble and chloride-conducting membrane-inserted conformations (Valenzuela *et al*., 1997; Tulk *et al.*, 2000; Tonini *et al*., 2000; Valenzuela *et al.*, 2001; Harrop *et al*., 2001; Tulk *et al.*, 2002; Warton *et al.*, 2002; Littler *et al.*, 2004; Ulsamov *et al*., 2007). The crystal structure of the soluble form is known (Harrop *et al.*, 2001), but little structural knowledge of the membrane-inserted conformation is available. A compact, hydrophobic, stable equilibrium unfolding intermediate has been identified at pH 5.5 in 3.8 M urea and at pH 7.0 at 37 °C, which is proposed to resemble the pre-insertion conformation of CLIC1 (Fanucchi *et al.*, 2008). A critical aspect of unravelling the enigma of CLIC1's dual-state existence is to study in much greater depth its membrane-bound conformation. To do this a stable, biomimetic model membrane system with the potential for an array of different applications is required. In addition to characterising soluble CLIC1, this project aimed to characterise the preparation and properties of a model membrane system which can be used by this laboratory for structural work on membrane-inserted CLIC1. Furthermore, a possible fluorescence-based functional assay is proposed which could allow for a reasonably rapid determination of the relative level of functionality of CLIC1 mutants.

3.4.1. Liposome preparation

LUVETs were prepared using the freeze-thaw extrusion method (Olsen *et al.*, 1979; Hope *et al.*, 1985; MacDonald *et al.*, 1991). Vesicles were made up of either asolectin, which comprises roughly equal proportions of phosphatidyl-choline (PC), phosphatidylethanolamine (PE) and phosphatidylinositol (PI) along with minor amounts of other phospholipids and polar lipids, or a specific 4:1:1 mol/mol ratio of phosphatidylethanolamine, phosphatidylserine and cholesterol (PE:PS:chol) (see Section 2.2.6.1.). Asolectin, for economic reasons, was used initially to optimise the resuspension and extrusion process, after which most studies were carried out using the PE:PS:chol mixture. Preparation of liposomes

took, on average, one night and one-and-a-half days. It was established that overnight vacuum drying was the minimum drying time required to ensure successful resuspension of lipids in aqueous buffer, particularly in the case of the PE:PS:chol mixture. This was the time required for the vacuum to reach 500-300 mtorr. The lower the vacuum pulled, the more successful was the resuspension. Lipids dried in a vacuum down to ~1000 mtorr (~4 hours, the typical drying time used in many protocols) aggregated completely upon addition of aqueous buffer and had to be discarded.

Asolectin resuspended rapidly and little lipid was left adhering to the inner surface of the glass tube, and the resuspension was relatively homogeneous. This made the extrusion process rapid and trouble-free. Initial dried films of the PE:PS:chol mixture, on the other hand, adhered steadfastly to the inner surface of the glass tube upon resuspension and required hours of vigorous vortexing to remove, at which point a glutinous gel would form which would be almost impossible to solubilise homogeneously. The problem was compounded if the mixture was warmed. In theory, the gel to liquid-crystalline phase transition temperature (T_m) for the PE:PS:chol mixture is low (< 20 °C), since the PE and PS are comprised mainly of C18 unsaturated fatty acids, primarily linoleic acid (~65 %), a C18:2 fatty acid with very low melting point. Unfortunately, the supplier does not specify the nature of the saturated fatty acids making up the rest of the composition. The T_m for these could be up to 68 °C. The unsolubilised particles contributed to a problematic extrusion process, in that large lipid particles clogged the membrane, leading to high back pressure and often, a ruptured membrane, leakage and spillage. Resuspension was less problematic in phosphate buffer containing higher concentrations of potassium acetate or potassium nitrate (200-300 mM) than lower concentrations (30-50 mM). Lower concentrations of lipid were likely to resuspend more easily and also produced more homogeneously sized populations of liposomes (see section 3.4.2). One hundred mg/mℓ produced populations with fairly high polydispersity, although still within an acceptable range, and 50 mg/mℓ produced extremely homogeneous populations with PDI less than 0.15. Further experimentation with temperature produced a facile solution to

the solubility problem – if rapidly frozen in ethanol-ice, warmed just slightly enough to liquefy, and immediately vortexed, the dispersion immediately formed a milky white suspension that solubilised almost all of the lipid in the tube. This modified freeze-thaw protocol was then adopted for all further work with PE:PS:chol. Clearly the previously-used thaw temperature (40-45 °C) had been too high. Despite the initial problems mentioned, however, highly monodisperse populations of phospholipid liposomes at very adequate concentrations were achieved (Sections 3.4.2.1. and 3.4.2.4).

Freeze-thawing before extrusion appeared to make little difference to the size or homogeneity of either asolectin or PE:PS:chol liposomes. If anything, at first its only effect was to make resuspension of PE:PS:chol lipid mixture more troublesome, although the actual extrusion process was somewhat easier with freeze-thawed dispersions than those not given this treatment. Once the thaw temperature was optimised with immediate vortexing, though, freeze-thawing turned out to be an extremely useful addition to the protocol because of the total solubilisation achieved with its use. Unfortunately, a comparison of encapsulation volumes and efficiencies of liposomes prepared with or without freeze-thawing was not undertaken, but Manojlovic *et al.* (2008) reported significantly increased encapsulation efficiencies of mistletoe lectin into liposomes prepared with freeze-thawing. MacDonald *et al.* (1991) found that the uptake of a fluorescent dye into liposomes was significant after freeze-thawing and prior to extrusion, but that subsequent extrusion augmented this gain considerably. In accordance with other studies (MacDonald *et al.*, 1991; Sou *et al.*, 2003; Manojlovic *et al.*, 2008), in this study the main contributor to size and population narrowing was the number of times the suspension was extruded (Figure 3.27).

3.4.2. Liposome characterisation

Liposomes were characterised in terms of size using dynamic light scattering and size and morphology using electron microscopy. Phospholipid concentrations were determined from a total phosphorus assay. Encapsulated volumes were calculated from average measured sizes and published average values for

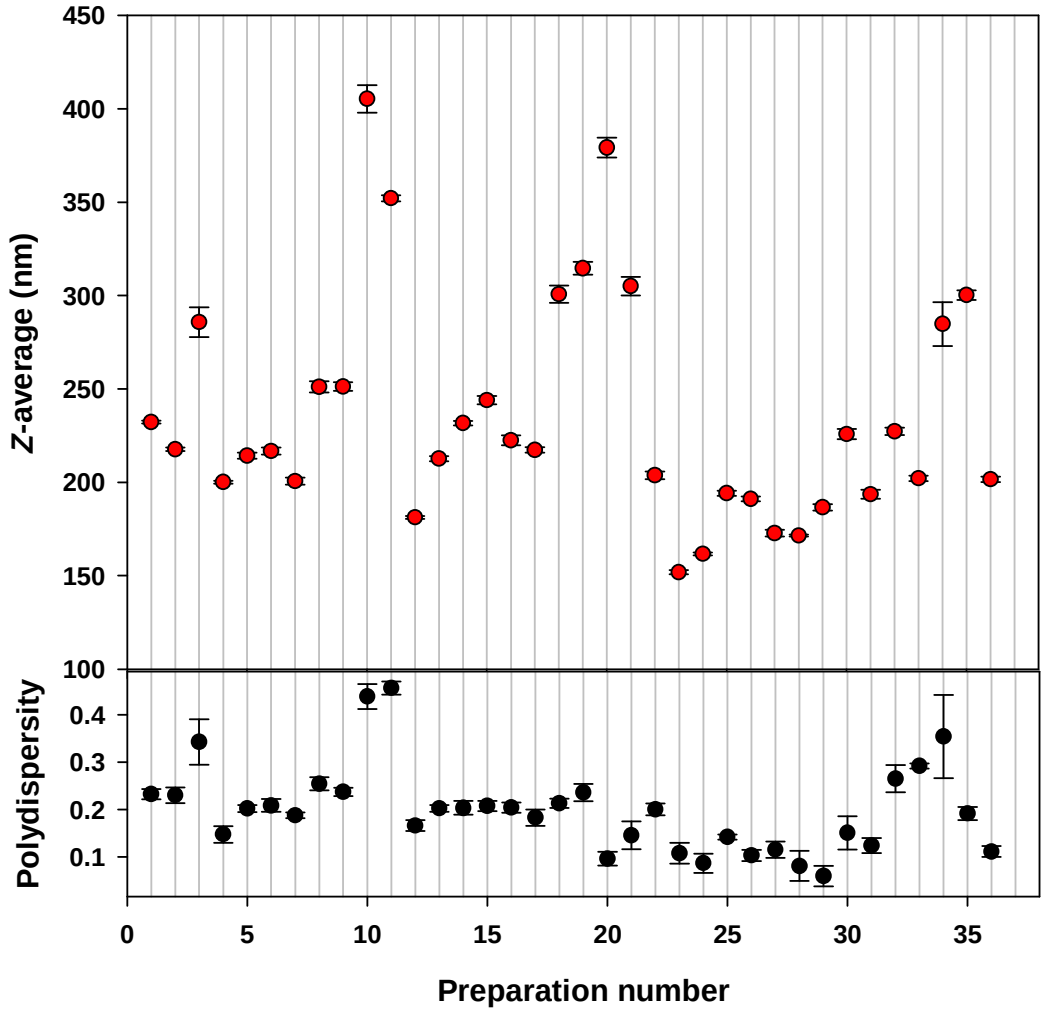

Figure 3.27. Sizes of asolectin and PE:PS:chol liposomes.

Most of the initial preparations (~#20) were asolectin made up at 20-100 mg/mℓ in 50 mM sodium phosphate buffer, 1 mM DTT, 0.02 % NaN_3 and 200-500 mM potassium nitrate or potassium acetate, pH 5.5 or 7.0, often with 10-13 mM MQAE. Most preparations were freeze-thawed prior to extrusion, and extruded 11-31x. Their average size is approximately 230 nm. Later preparations were made up with PE:PS:chol at 50 mg/mℓ in the same buffer as above, but with 20-30 mM potassium nitrate, pH 5.5 or 7.0, usually with 13 mM MQAE. Fewer of these preparations were freeze-thawed and were extruded 61-101x. The *Z*-average for these liposomes was 180-200 nm. Sizing was done using a Zetasizer Nano S with a 633 nm beam detecting backscatter at 173°. Size was an average of 5 measurements.

phospholipid head group area sizes and their molar ratios making up the liposome compositions. Predicted encapsulated concentrations were calculated from these volumes. A melting curve was performed with monitoring of size to determine at what temperature the LUVs completely lost structural integrity. Basal leakage of Cl^- into vesicles and/or MQAE out of them was monitored to establish the useful working lifespan of MQAE-loaded LUVs.

3.4.2.1. Liposome size determination

The size of liposomes was checked on a Zetasizer Nano S (Malvern, UK) directly after extrusion and usually again after size exclusion chromatography. In most cases the liposome populations were highly homogeneous with low PDI values (< 0.3 and often < 0.15) (Figure 3.27, Figure 3.28), although lipid concentrations above ~50 mg/mℓ increased the polydispersity to up to 0.45 (Figure 3.29). Homogeneity appeared to be most affected by the number of passes during extrusion, and this also affected the size of the liposomes. In Figure 3.28 the PDI drops from about preparation 20 onwards. The size, correspondingly, drops from an average of about 200 nm to an average of about 180 nm. Preparations prior to #20 were mostly made up from asolectin and were extruded ~31x. From #20 onwards, liposomes were made up from 50 mg/mℓ PE:PS:chol, and were extruded 61-101x because of the lower solubility of this lipid composition. Liposome size was found to be fairly dynamic, and some preparations whose size was checked twice often registered smaller sizes on the Zetasizer after addition of different components or buffers. PE:PS:chol liposomes of 194 ± 1.3 nm shrank to 173 ± 1.8 nm after being diluted approximately 1.6 times in the same buffer. On the other hand, phospholipid liposomes of 315 ± 3.5 nm in 50 mM sodium phosphate buffer, 1 mM DTT, 0.02 % NaN_3, 500 mM KCl expanded to 379 ± 5.3 nm when passed through a size exclusion column equilibrated in the same buffer without KCl. Clearly this demonstrates the highly dynamic osmotic properties of these vesicles, and also aptly demonstrates the futility of any study aiming to ascertain binding of protein to liposomes by measuring variation in hydrodynamic volume. The osmotic properties and permeabilities of lipid vesicles have been studied by a number of researchers (Bangham *et al.*, 1967; Alhanaty and Livne, 1974; Blok *et*

al., 1976; de Gier, 1993; Mui *et al.*, 1993) and have been found to be highly variable and dependent on a number of factors which will be discussed in Section 4.1.1.

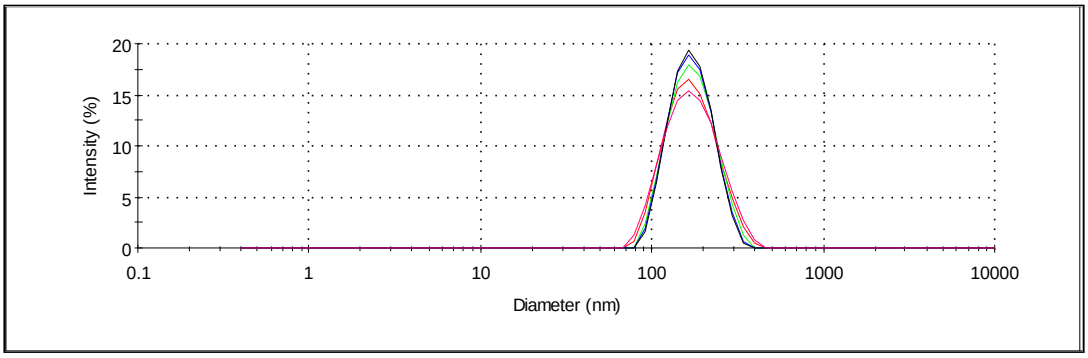

Figure 3.28. Size distribution of PE:PS:chol liposomes.

Representative plot showing the size distribution for PE:PS:chol liposomes made up at 50 mg/mℓ in 50 mM sodium phosphate, 1 mM DTT, 0.02 % NaN_3, 50 mM potassium nitrate and 13 mM MQAE, pH 5.5, freeze-thawed 9x and extruded 61x at 40 °C through a 0.4 µm polycarbonate membrane (Whatman Nucleopore). Most liposome preparations were extremely monodisperse. The *Z*-average in this case from 5 measurements on a Zetasizer Nano S was 161.7 ± 0.8 nm with a PDI of 0.09 ± 0.02.

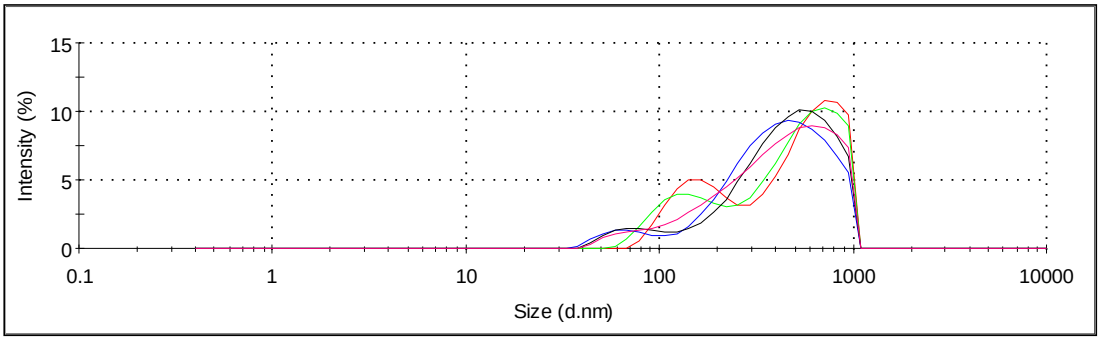

Figure 3.29. Increased polydispersity of liposomes prepared at high lipid concentrations.

Liposomes prepared at lipid concentrations greater than approximately 50 mg/mℓ tended to have reduced size homogeneity and increased polydispersity. These asolectin liposomes prepared at 105 mg/mℓ had an average diameter of 352.1 ± 1.6 nm (5 measurements) with a PDI of 0.456 ± 0.01. They were not freeze-thawed prior to extrusion, and were extruded 31x at 45 °C through a 0.4 µm polycarbonate membrane (Whatman Nucleopore).

The temperature stability of PE:PS:chol liposomes was tested by means of a melting curve monitored by dynamic light scattering. Figure 3.30 shows the size of the vesicles increasing steadily from 207 nm to 298 nm between 4 °C and 51 °C while maintaining a single intensity peak (not shown) and low polydispersity indices. This expansion is probably due to the thermal expansion of encapsulated aqueous solution and membrane components. From 52 °C to 57 °C, however, the PDI began to climb rapidly, and a new peak appeared with a much greater hydrodynamic diameter (2500-5000 nm). Vesicles are beginning to fuse and aggregate here. Between 57-66 °C the large diameter peak became the main peak, while a lower intensity peak maintained a size around 300 nm. Beyond 66 °C a single peak appeared once more, with an average size of 3150 nm, and the PDI decreased again, indicating total aggregation of the sample. While these data cannot identify the T_m of the PE:PS:chol LUVETs, because they would still maintain their structural integrity at temperatures some way beyond the gel to

liquid-crystalline phase transition, it clearly does indicate that these liposomes can safely be used in experimental work up to a temperature of about 50 °C without fusing or aggregating. It would probably be advisable before doing such work, though, to ascertain if the time period for which they can be maintained at high temperatures is limited.

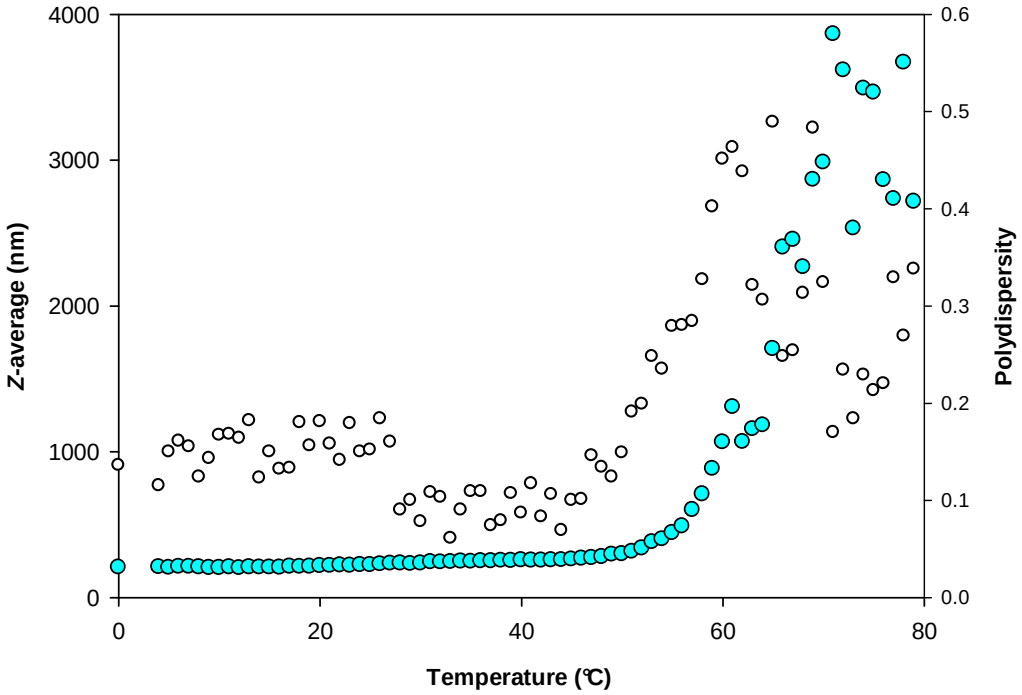

Figure 3.30. Melting curve of PE:PS:chol liposomes.

PE:PS:chol liposomes maintain their size (cyan) quite steadily under increasing temperature conditions, until about 50-55 °C, when they rapidly increase in size by more than a factor of 10. The polydispersity of the sample (white circles) increases dramatically over the same range and then drops again as the sample aggregates completely. The size of liposomes in 50 mM sodium phosphate buffer containing 30 mM potassium nitrate, 10 mM MQAE, 1 mM DTT and 0.02 % NaN_3 at pH 7.0 was monitored by dynamic light scattering as the temperature was increased.

3.4.2.2. Electron microscopy

Transmission electron microscopy was used to visualise liposomes after extrusion and to correlate dynamic light scattering data with visual data. Asolectin liposomes of 200-230 nm diameter as determined by DLS were prepared by extrusion. Five µl of this preparation were negatively stained with 2 % uranyl acetate for 10 seconds on a carbon film-coated copper EM grid as described in section 2.2.9., and then placed in the electron microscope.

Initially it took quite some time to find and identify the liposomes on the grid, since the uranyl acetate was not centrifuged for initial attempts, and tended to leave much artefactual debris on the grid, particularly if left to stain for too long. It was found that the liposomes were not evenly dispersed across the whole grid, but tended to clump in certain areas, particularly near the edges of the squares on the grid, in the shadow of the grid, where they would mass thickly in layers amongst uranyl acetate debris, making it particularly challenging to find them. It was found that with centrifugation of the stain and shortened staining times, as opposed to dilution of the stain, the best results were achieved (Figure 3.31). On the whole, measured sizes of liposomes under EM correlated very well with *Z*-averages obtained on the Zetasizer, with 200 nm *Z*-averaged liposomes coming out at ~200 nm when back-calculated for magnification, considering the margin of error for manual measurement of micrographs is relatively high.

One interesting point noted about one of the preparations visualised under EM was an odd “doughnut-like” shape, indicating that the liposomes are not necessarily spherical, as one would tend to assume, but that their shapes are flexible and probably vary greatly depending on conditions. It was interesting, too, how they tended in some cases to cling together in bead-like strings along the creases in the carbon film. Talmon *et al*. (1990) and Mui *et al*. (1993) found that vesicles prepared by extrusion were non-spherical. Manojlovic *et al*. (2008) observed that the lipid composition and concentration of vesicles prepared by extrusion influenced the size, shape and lamellarity of the vesicles as visualised using cryo-EM. In general, they found that a greater percentage of unsaturated

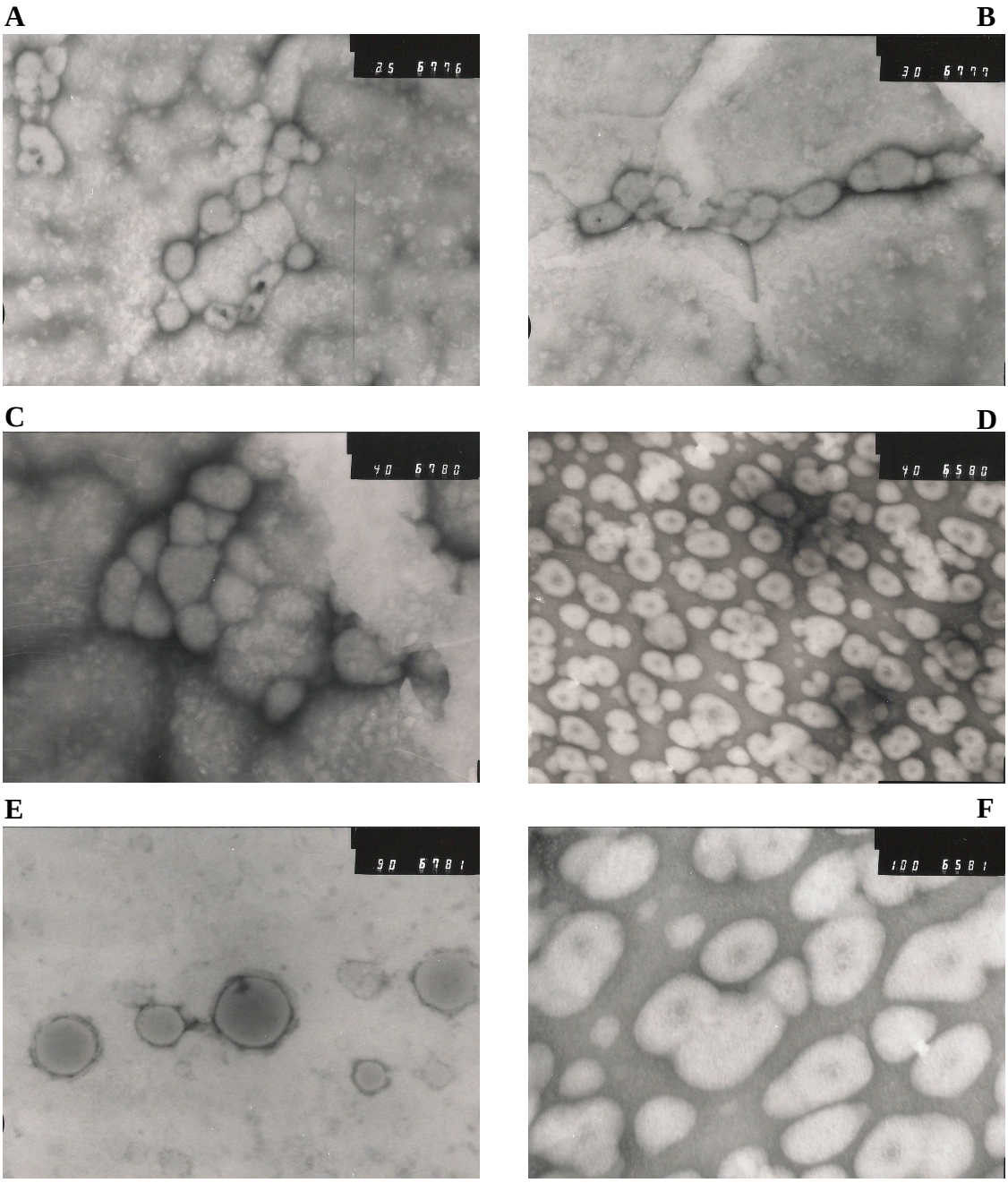

Figure 3.31. Transmission electron micrographs of asolectin liposomes.

Asolectin liposomes were prepared at 50 mg/mℓ with 10x freeze-thaw and 51x extrusion in 50 mM sodium phosphate buffer, 1 mM DTT, 0.02 % NaN_3 and 50 mM KCl, pH 7.0. DLS gave a *Z*-average of 202 nm. Liposomes were negatively stained with 2 % uranyl acetate for 10 seconds on a carbon film-coated copper EM grid and visualised in a JEOL 100S transmission electron microscope operating at 80 keV. Magnification was as follows: (**A**) 25 000x, (**B**) 30 000x, (**C**) 40 000x, (**D**) 40 000x, (**E**) 90 000x, (**F**) 100 000x. Representative measured diameters here are as follows: (A) 240 nm, (B) 200 nm, (C) 200 nm, (D) 150 nm, (E) 144 nm, (F) 160 nm.

lipids resulted in more spherical, unilamellar vesicles, and as the saturated lipid content and the overall concentration increased so did deformity, lamellarity and aggregation.

3.4.2.3. Phospholipid concentration determination

A rapid and sufficiently reliable method of estimating liposome suspension concentrations was required. In order to establish whether the use of dried mass concentration calculations were adequate for the purposes of this study and for future use, concentrations of liposome suspensions were determined both by calculation from dried mass of lipids after solubilisation and vacuum-drying (using an average M_r based on the lipid composition), and by a total phosphorus assay. The phosphorus assay (Chen *et al.*, 1956), being lengthy and unwieldy, was not suited to regular, rapid lipid concentration determinations, and was especially inappropriate in that CLIC1 storage buffer, in which liposomes were made up, is a phosphate buffer. Nonetheless, it was the best-suited of the concentration assays considered, and it turned out to be reliable. An inorganic phosphorus standard curve was generated as described in Section 2.2.7. and experimental sample concentrations calculated from the equation of a fitted regression line (Figure 3.32). Clearly, the assay cannot account for cholesterol, but in theory, this can be calculated once phosphorus concentration is known, given the known molar ratio.

On average, it was found that there was a 4-8% decrease in mass from the initial weighed amount of lipid to the mass after resolubilisation in organic solvent and vacuum drying (n=5). Actual lipid loss during the production process, particularly in the case of post-extrusion centrifugation of asolectin liposomes, and initially in the case of pre-extrusion resuspension of PE:PS:chol, often amounted to an additional 20-35 % mass decrease, and in some unfortunate cases, up to 70 % loss. Thus, in a typical preparation of asolectin or PE:PS:chol liposomes of 50 mg/mℓ weighed mass, approximately 45 mg would be actual lipid mass with an expected concentration of 61 mM, using an average M_r of 740. The experimentally determined actual final concentration would be approximately 35-

40 mM, up to 45-48 mM when accounting for cholesterol. Given a further 20-30 % mass loss during production, this is exactly what would be expected from dried mass-based concentration calculations. Using dried mass as an estimate of lipid concentration was therefore fairly accurate, so long as amounts of lipid lost during the production process were carefully monitored.

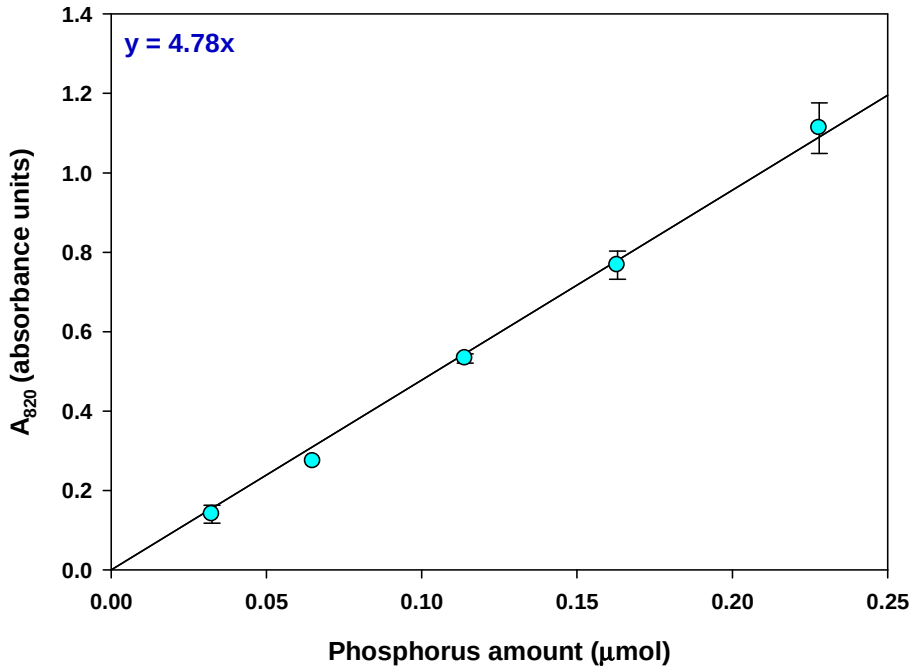

Figure 3.32. Phosphorus standard curve.

Total phosphorus assay for phospholipid concentration determination. Glassware was rigorously washed with phosphate-free detergent, and rinsed in distilled water, deionised water and methanol. Specific volumes of phosphorus standard solution were treated to acid hydrolysis with 8.9 N H_2SO_4 at 215 °C. Samples were oxidised with H_2O_2 with further heating, diluted, and then 2.5 % ammonium molybdate (VI) tetrahydrate followed by 10 % ascorbic acid were added with heating at 100 °C. Absorbance at 820 nm was recorded and linear regression analysis performed for calculation of phosphorus content of experimental samples. The above plot is the average of two phosphorus standard assays. $r^2 = 0.994$.

3.4.2.4. Entrapped volume calculation

The volume of aqueous buffer encapsulated inside extruded liposomes was calculated according to Equation 2-29 (Zuidam *et al.*, 2003). Phospholipid head group areas were taken as follows: PE = 0.57 x 10^{-18} m^2, PS = 0.65 nm^2 and cholesterol = 0.30 nm^2 (Zuidam *et al.*, 2003; Mathai *et al.*, 2008). This gives an entrapped volume 5.72 ℓ/mol for PE, 6.52 ℓ/mol for PS, and 3.01 ℓ/mol for cholesterol. If the concentration of liposomes in 1 mℓ is 45 mM (see Section 3.4.2.3.), using an average M_r of 740 for these lipids, there is 45 µmol lipid in the sample, 4 parts being PE, 1 part PS and 1 part cholesterol. This is 30 µmol PE, and 7.5 µmol each of PS and cholesterol. This gives 171.6 µℓ entrapped volume for PE, 48.9 µℓ entrapped volume for PS and 22.6 µℓ entrapped volume for cholesterol, for a total of 243.1 µℓ encapsulated by liposomes in a 1 mℓ preparation. This would be diluted approximately 10 times by passage through the size exclusion column, giving a final encapsulated volume within 1 mℓ liposome suspension of approximately 24 µℓ, which gives an estimated final MQAE concentration of about 240 µM.

Ideally, the encapsulated volume and concentration would have been determined experimentally; however, an attempt to record an absorbance spectrum of encapsulated MQAE by lysing the vesicles with Triton X-100 was unsuccessful due to scatter and apparently negligible concentration. The same sample, however, had a perfect emission profile.

3.4.4. MQAE characterisation

A functional assay for the detection and measurement of CLIC1-mediated chloride flux is proposed based on the methods of Verkman *et al*. (Illsley and Verkman, 1987; Verkman *et al.*, 1989; Verkman, 1990). The work here lays the foundation for such an assay should it be used, and characterises a halide-sensitive fluorescent dye and its encapsulation inside PE:PS:chol LUVETs.

3.4.4.1. MQAE concentration determination

Concentration of stock MQAE usually turned out to be approximately 12.4-13.8 mM as determined by linear regression using the Beer-Lambert law as described in Section 2.2.6.3. (Equation 2-1) (Figure 3.33). An absorbance spectrum was recorded between 250 nm and 450 nm, and an emission spectrum was recorded between 350 nm and 600 nm, with excitation at 350 nm (Figure 3.34). MQAE has an idiosyncratic absorbance spectrum, with a high peak at 319 nm and another at 352 nm. The emission spectrum peaks at 452 nm in 50 mM sodium phosphate containing 30 mM potassium nitrate, 1 mM DTT and 0.02 % NaN_3.

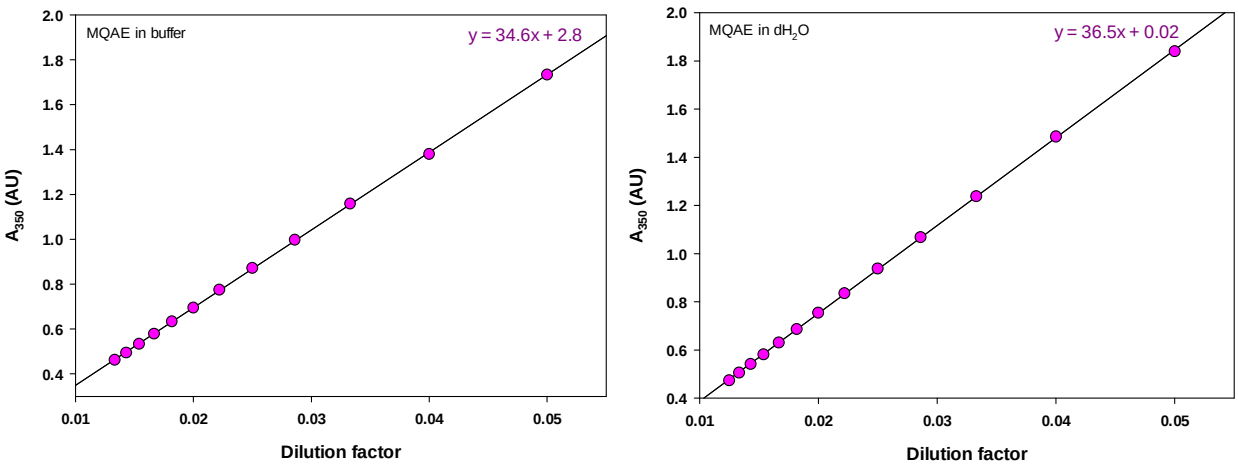

Figure 3.33. MQAE concentration determination.

Representative plots showing blank-corrected absorbance readings at 350 nm for 20x-100x dilutions of stock MQAE in 50 mM sodium phosphate buffer, 1 mM DTT, 0.02 % NaN_3 and 30 mM potassium nitrate, pH 7.0 (left), and in dH_2O (right), 20 °C. Stock concentrations were calculated from regression analysis as 12.4 mM (r^2 = 0.9999) (left) and 13 mM (r^2 = 0.9999) (right).

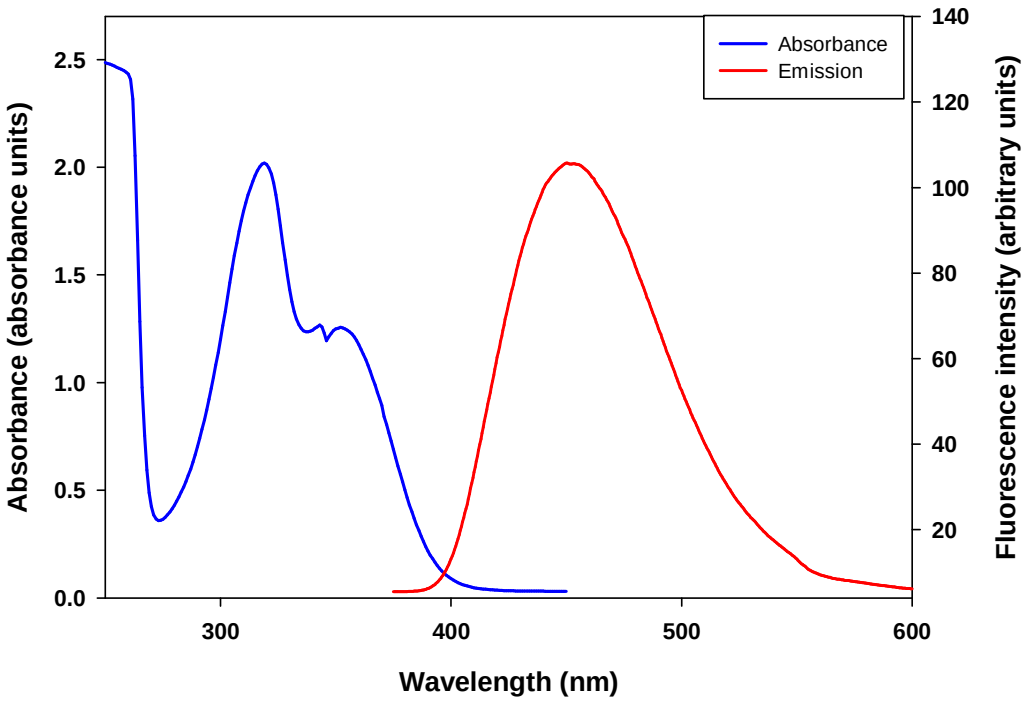

Figure 3.34. MQAE absorbance and emission spectra.

Absorbance (blue) and emission (red) spectra of MQAE in 50 mM sodium phosphate buffer, 1 mM DTT, 0.02 % NaN_3 and 30 mM KCl, pH 5.5, 20 °C. The absorbance spectrum peaks at 319 nm and 352 nm. The emission spectrum peaks at 452 nm. The absorbance spectrum was recorded on a Jasco V-550 UV/VIS spectrophotometer, and the emission spectrum on a Jasco FP6300 fluorometer.

3.4.4.2. MQAE Stern-Volmer constant determination

In order to determine the range of Cl^- concentrations best to use for Cl^- flux experiments, and the degree to which MQAE is quenched by specific concentrations of Cl^-, samples of 10 mM MQAE were titrated with 5 mM increments of KCl. Fluorescence emission intensity was monitored at 450 nm, buffer-corrected and plotted as a function of Cl^- concentration (Figure 3.35A). The data was converted to a Stern-Volmer plot by plotting F_0/F as a function of

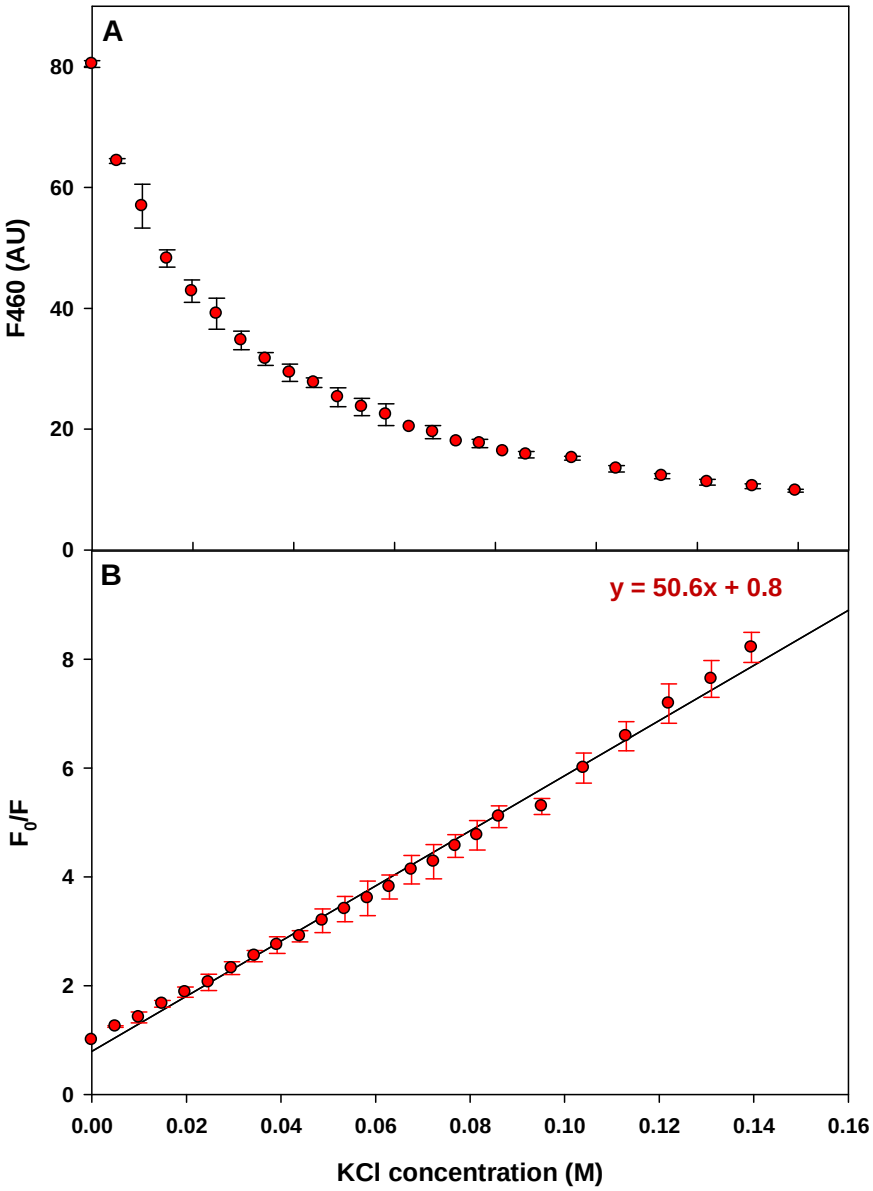

Figure 3.35. MQAE Stern-Volmer constant determination in buffer.

(**A**) Quenching of 10 mM MQAE in 50 mM sodium phosphate buffer, 1 mM DTT, 0.02 % NaN_3 and 50 mM potassium nitrate, pH 7.0, with ~5 mM aliquots of 2 M KCl at 20 °C. Fluorescence emission at 450 nm was buffer-corrected and plotted as a function of KCl concentration. (**B**) Stern-Volmer plot of data from (A). The slope of the fitted line gives the Stern-Volmer quenching constant. The Stern-Volmer constant determined from the equation of the line was 50.6 M^{-1} (r^2= 0.988). The data is the average of 2 data sets.

Cl^- concentration (see Equation 2-27) (Figure 3.35B). The plot is linear, indicating a collisional quenching mechanism (Lakowicz, 1999). The Stern-Volmer quenching constant determined from the slope of the fitted line was 50.6 M^{-1}, meaning that the Cl^- concentration at which half of the initial intensity is quenched is 19.7 mM, or $1/K_{SV}$. For comparison, the Stern-Volmer constant for 10 mM MQAE in distilled water was determined. Fluorescence emission monitoring at 460 nm indicated a higher initial emission intensity and a much steeper initial drop for MQAE in water (Figure 3.36A). The Stern-Volmer plot correspondingly gave a higher quenching constant (70 M^{-1}), indicating greater sensitivity of the dye to quenching when in water (Figure 3.36B). This discrepancy is unlikely to be concentration-related, since concentration determinations in buffer and in water were very accurate, as seen in the plots above (Figure 3.33). Verkman *et al*. (1989a) determined the Stern-Volmer constant for MQAE in 5 mM phosphate as 200 M^{-1}, or just 5 mM Cl^- required to quench half the emission intensity. There is no real explanation for this almost 3-fold discrepancy, except that Verkman *et al*. synthesised their own MQAE, and the compound used in this study was a commercial preparation (Sigma-Aldrich, USA). It was stored in the dark in a dark bottle covered with foil at 4 °C and only exposed to light briefly for weighing purposes. Fresh solutions were made up for each use, and these were protected from light at all times. Verkman *et al*. (1989a) also reported that MQAE is insensitive to phosphate and nitrate ions, but that would not seem to be the case here, where the K_{SV} for MQAE in phosphate and nitrate buffer is lower than that in water.

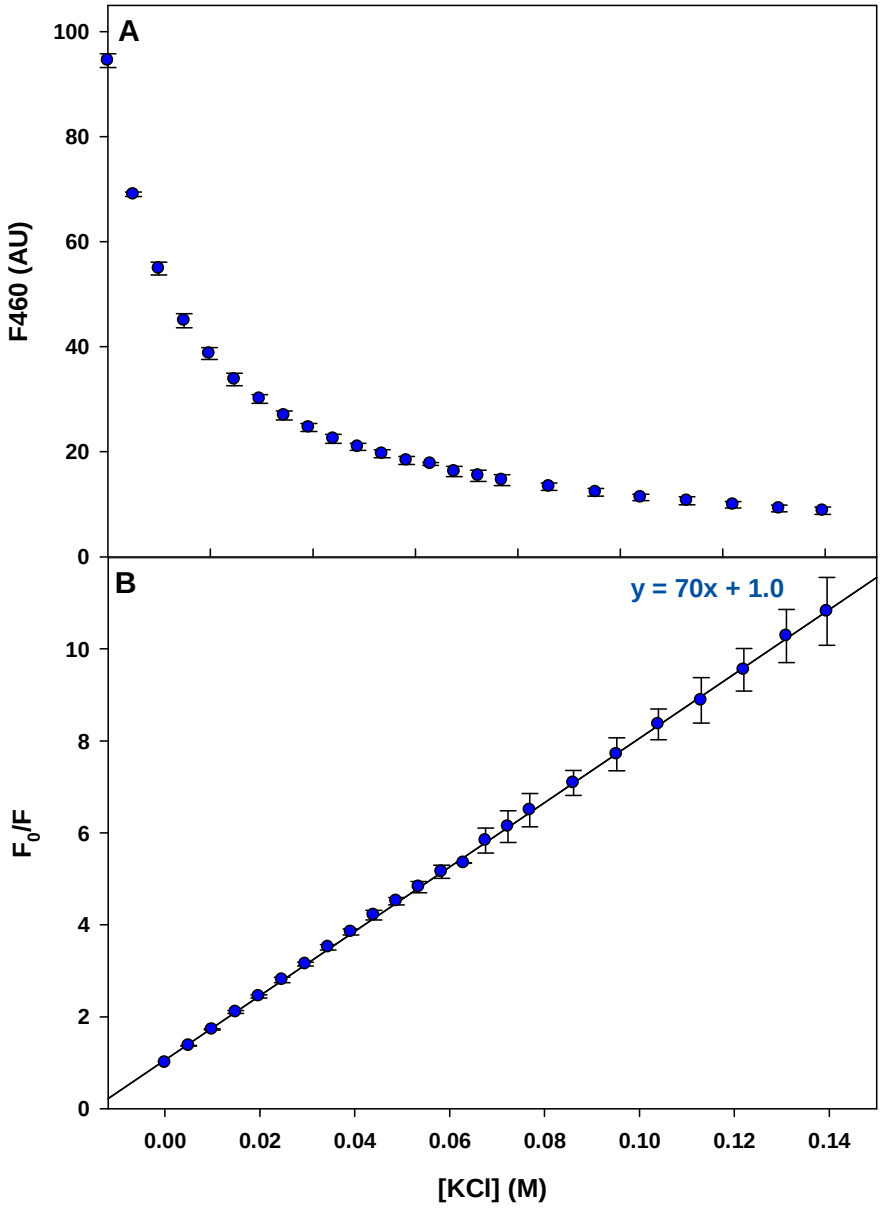

Figure 3.36. MQAE Stern-Volmer constant determination in dH_2O.

(**A**) Quenching of 10 mM MQAE in dH_2O with ~5 mM aliquots of 2 M KCl at 20 °C. Fluorescence emission at 450 nm was blank-corrected and plotted as a function of KCl concentration. (**B**) Stern-Volmer plot of data from (A). The slope of the fitted line gives the Stern-Volmer quenching constant. The Stern-Volmer constant determined from the equation of the fitted line was 70 M^{-1} (r^2= 0.994). The data is the average of 2 data sets.

3.4.4.3. Encapsulation of fluorescent dye, MQAE, in liposomes

MQAE was encapsulated in liposomes with the intention of providing a relatively simple means of indicating functional insertion of CLIC1 into the membrane. MQAE was encapsulated into liposomes by resuspending the vacuum-dried lipid mixture in MQAE-containing buffer as described in section 2.2.6.2. The liposomes were then prepared as usual by extrusion. Extravesicular MQAE was removed by size-exclusion chromatography as described in Section 2.2.6.5. and an emission spectrum of the liposome suspension recorded (Figure 3.37). An absorbance spectrum could not be recorded because the signal was obscured by light scatter by the liposomes, but an intense emission spectrum for the liposome fractions indicates the presence of MQAE. The spectrum peaks at 441 nm, a blue shift compared to MQAE in buffer. Absorbance and emission spectra of the extravesicular fractions also confirm that MQAE was, in fact, separated from the liposome fraction, since the spectra were exactly the same as those shown in Figure 3.34.

3.4.4.4. Removal of extravesicular MQAE

MQAE which was not encapsulated was removed from the medium surrounding the liposomes by size exclusion chromatography. An 85 mℓ Sephadex G25 column was initially used, and fluorescence emission at 450 nm was used to monitor the presence of MQAE. The resolution achieved with this column was not ideal – the two components were not completely separated. When test spectra of the liposomal suspension were recorded, the signal was enhanced with dilution, because the quenching of residual extravesicular MQAE by extravesicular KCl was reduced by dilution. An 82 mℓ Sepharose 300 High Resolution column that could be used on the ÄKTAprime purification system was then packed, and this column gave complete separation between MQAE-encapsulating liposomes and extravesicular MQAE (Figure 3.38B). The void volume of this column was determined as approximately 40 mℓ using 2 mℓ of 2 mg/mℓ Blue Dextran 2 000 000 (Figure 3.38A). It is clear from Figure 3.38 that the liposomes are eluted in the void volume of the column, which is to be expected, considering

their size. MQAE is eluted between 100 and 120 mℓ. Absorbance and emission spectra of fractions from this peak identify it as MQAE. The liposomes are mostly detected by scatter at 280 nm, and MQAE absorbs at 280 nm.

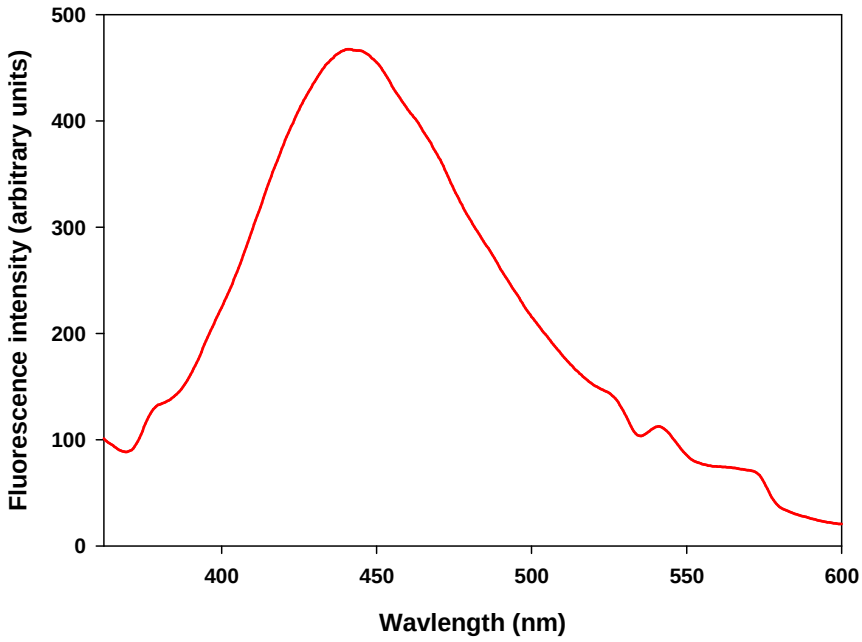

Figure 3.37. Liposome-encapsulated MQAE.

Emission spectrum of liposome-encapsulated MQAE in 50 mM sodium phosphate buffer, 1 mM DTT, 0.02 % NaN_3 containing 30 mM potassium nitrate (inside vesicles) or 30 mM KCl (outside vesicles). The spectrum peaks at 441 nm, a blue shift compared to MQAE in buffer.

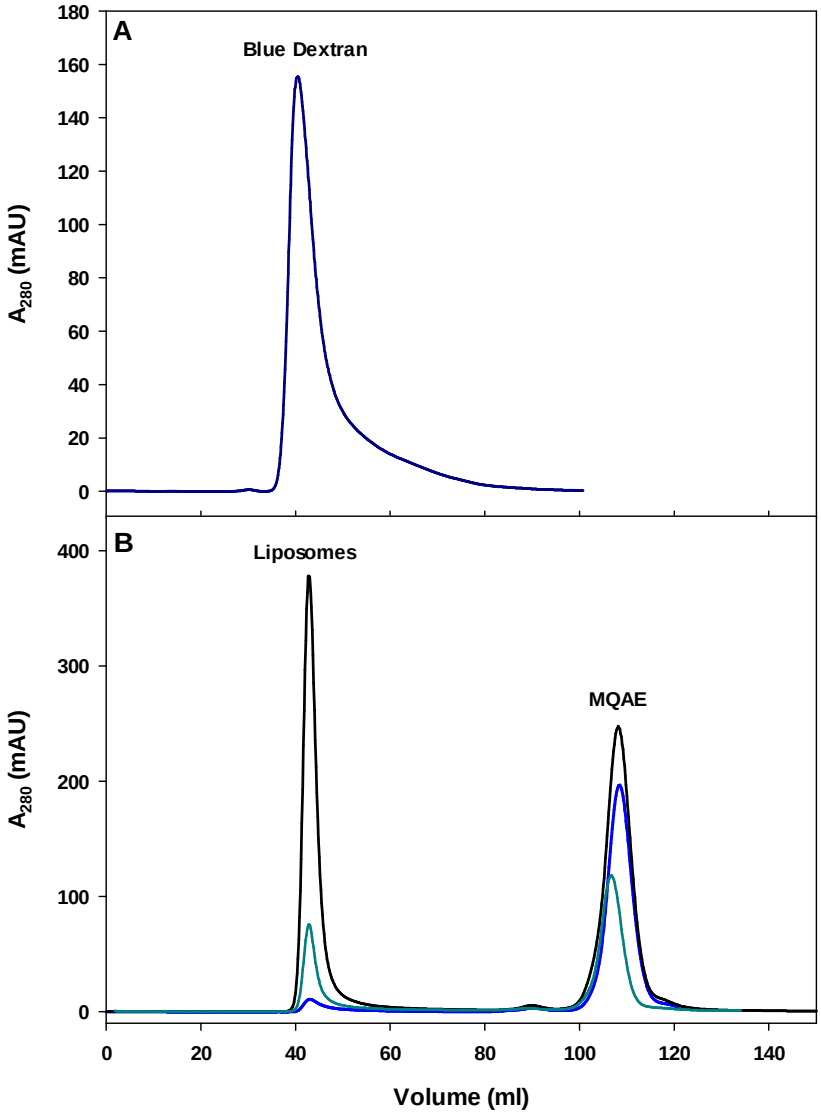

Figure 3.38. Separation of liposome-encapsulated MQAE from extravesicular MQAE on S300HR column.

Representative elution profiles for 2 mℓ of 2 mg/mℓ Blue Dextran 2 000 000 in dH_2O, indicating void volume of the S300HR size exclusion column (**A**), and liposomes and MQAE (**B**). The void volume peak occurs at 40 mℓ. Clean separation of liposome-encapsulated MQAE from extravesicular MQAE is achieved. MQAE was encapsulated in PE:PS:chol liposomes in 1-2 mℓ 50 mM sodium phosphate buffer, 1 mM DTT, 0.02 % NaN_3 and 30 mM potassium nitrate, pH 5.5, and then removed from the extravesicular medium using the S300HR column. The extravesicular MQAE is eluted between 100 and 120 mℓ. Flow rate was 2 mℓ/min. Detection was at 280 nm on an ÄKTAprime protein purification system (Amersham Biosciences).

3.4.4.5. Basal leakage of MQAE

Once extravesicular MQAE had been removed from the liposome dispersion, basal leakage rates were monitored to indicate for how long the liposomes could be used before the MQAE signal dropped too significantly. Some samples were maintained at 4 °C and others at room temperature (20 °C), protected from light. Quenching was monitored by fluorescence emission intensity at 440 nm. Figure 3.39 shows that basal leakage for liposomes kept at room temperature is far greater than that for liposomes maintained at 4 °C. Liposomes maintained in the cold lose little signal intensity for up to 7 days, whereas the signal for those kept at room temperature begins to drop within the first day, and by day 3 is almost 30 % quenched.

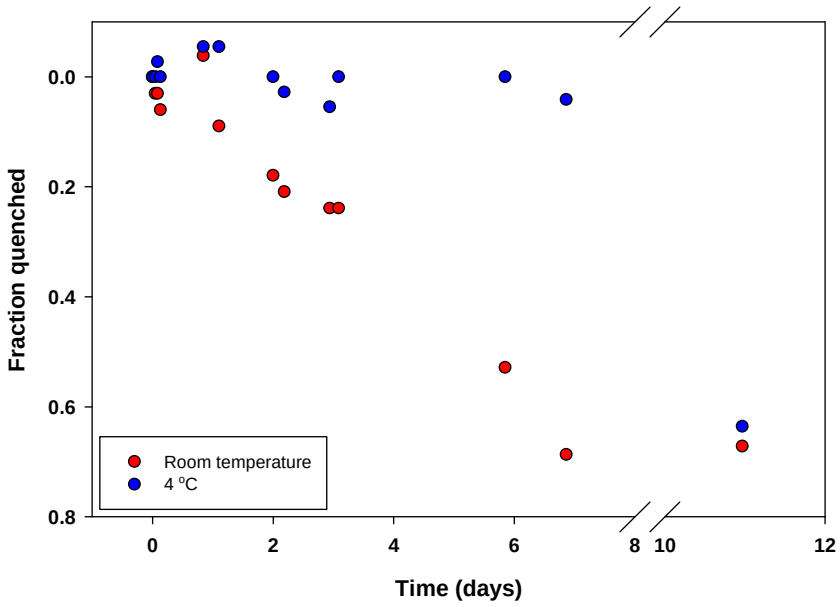

Figure 3.39. Basal leakage of PE:PS:chol liposomes at room temperature and 4 °C.

PE:PS:chol liposomes encapsulating 13.8 mM MQAE in 50 mM sodium phosphate buffer, 1 mM DTT, 0.02 % NaN_3 and 30 mM potassium nitrate, pH 5.5, with an external medium the same but with 30 mM KCl instead of potassium nitrate were stored at room temperature (red) or at 4 °C (blue). Emission signal intensity quenching was monitored at 440 nm on a Hitachi Model 650 fluorescence spectrophotometer. Liposomes stored at 4 °C maintained almost the same intensity signal for up to 7 days, whereas the signal dropped in the first day for liposomes at room temperature.

CHAPTER 4. DISCUSSION

CLIC1's most compelling feature is its dual soluble and membrane-bound nature. While the soluble structure and the functioning of the membrane-bound form have been fairly extensively characterised, little is known about the structure of the membrane-bound form. One of the primary aims of this project, in addition to a structural and stability characterisation of the soluble form of CLIC1, was to characterise a model membrane system that can be used in future studies to develop a deeper understanding of the structural properties of membrane-bound CLIC1. A basic requirement for any future study undertaken to investigate the structure of membrane-bound CLIC1 is confirmation that the protein is actually *inserted* into the membrane, and not simply bound to the surface. Therefore, this project also proposed a relatively user-friendly functional assay which could indicate whether CLIC1 is functioning as a channel or not.

4.1. Model membrane studies

4.1.1. Liposome characterisation

The phospholipids used in this study for liposome production were of two mixtures: the first, used initially to gain experience in the handling of lipids using a relatively inexpensive source of phospholipids, i.e. asolectin from soybean, was a rough mixture of various phospholipids, amounts of which may vary from batch to batch. Tulk *et al*. (2000) successfully used asolectin liposomes to characterise functionality of CLIC1 electrophysiologically. The second phospholipid mixture was a very specific 4:1:1 molar ratio of phosphatidylethanolamine, phosphatidylserine and cholesterol that was determined by Singh and Ashley (2006) to be the ideal lipid mixture for insertion of CLIC1. This mixture proved initially to be extremely difficult to work with during resuspension in aqueous buffer because of its tendency to form clumps and to stick to the glass tube, but experimentation with temperature solved this problem, along with the problem of lipid loss during resuspension and extrusion. Studies have shown that PE is most easily solubilised at high pH, where the molecule is negatively charged, and at

low ionic strength and that it aggregates at lower pH (Ellens *et al.*, 1986). This was certainly found to be the case here, where solubilisation at low pH proved more difficult than at pH 7.0, and attempted solubilisation at high KCl concentrations was totally unsuccessful.

Calculations of enclosed volume and consequently concentration of encapsulated MQAE could not be verified experimentally, but probably dilution in an organic solvent such as ethanol could solve the problem of light scatter that was experienced when attempting to measure encapsulated MQAE absorbance. Assuming the concentration of encapsulated MQAE is the same as that in the hydration solution, this would allow for direct measurement of encapsulated volume and a better understanding of encapsulation efficiencies under different conditions. A more accurate method of measuring encapsulated volume using a probe such as MQAE would be to separate the vesicles from the extravesicular volume by centrifugation with a spin column. The volume used to elute the vesicles is subtracted from the final volume, as is the calculated lipid volume (derived from the concentration, mass and density), to give the encapsulated volume. This method, or variations of it, have been used quite effectively using labelled isotopes for the entrapped solute (Szoka and Papahadjopoulos, 1978; Hope *et al.*, 1985; Perkins *et al.*, 1993).

The method used to calculate enclosed volume in this study (based on the volume of a sphere) is a very general estimate, since the exact areas of the relevant phospholipids in the membrane are not known, and are anyway affected by the type of fatty acid chains they are attached to, the composition of the rest of the membrane, the exact size of the liposome, the pH, the temperature and the ionic strength, among others (Mathai *et al.*, 2008). In addition, the *exact* concentration of the lipids in the dispersion is unknown. Nonetheless, as an estimate, it is useful, and a similar means was used as a comparative measure by Hope *et al.* (1985) to determine expected entrapped volumes. Their estimated and experimentally-derived values correlated reasonably well. MacDonald *et al.* (1991) and Perkins *et al.* (1993) both reported encapsulated volumes of between 1

and 2 µℓ/µmol lipid, although in the latter case this improved to up to 6 µℓ/µmol lipid when 5 freeze-thaw cycles were included. Applying these values to the lipid concentrations in the current study would give an encapsulation volume of between 9 µℓ and 27 µℓ in a 1 mℓ suspension. Thus, the calculated estimation used here (24 µℓ) was at the high side of experimentally determined values, but is perfectly in keeping with the values determined for the freeze-thaw method. Freeze-thaw-dependent increases in encapsulation volume had already been noted by Pick (1981). Pick (1981) furthermore confirmed that the addition of small amounts of lipids with net positive or negative charges increased the enclosed volume; thus, the inclusion of anionic lipids in this study may justify a slightly higher encapsulated volume estimation. Of course, a point already made in this study is that any change in the osmotic environment of the liposomes immediately changes the encapsulated volume due to the high permeability of bilayer membranes to water, thus the *caveat* here is to beware the dynamic size of the liposomes. Nonetheless, knowing the encapsulated volume is useful for estimating the concentration of encapsulated solute, assuming the osmotic environment is maintained, especially since encapsulated concentrations higher than that of the initial hydration solution have been reported as a feature of the freeze-thaw method (Chapman *et al.*, 1991).

The liposomes produced in this study were determined to be consistently homogeneously sized (although this size was dynamic depending on buffers) and, in later preparations, of fairly predictable concentrations. Encapsulation of MQAE and complete removal of the extravesicular MQAE proved to become fairly routine once the size exclusion parameters had been optimised. The liposomes were also relatively temperature-stable, and if required, could be used at 37 °C without fusion of contents or aggregation.

Although there is not full agreement on all factors, a number of studies have found the permeability properties of phospholipid bilayer membranes to be affected by the area occupied by the head groups of the phospholipids (Mathai *et al.*, 2008), the permeability coefficient of a given solute (Finkelstein, 1976; Walter and

Gutknecht, 1986), mechanical properties (Peters and Beck, 1983) bilayer surface density and chain ordering within the lipid bilayers (Xiang and Anderson, 1995), phospholipid chain length, cholesterol concentration, temperature and bilayer phase structure (Xiang and Anderson, 1997). The permeability coefficient of Cl^- ranges from 10^{-11} cm/s to 10^{-8} cm/s (Mimms *et al*., 1981; Paula *et al.,* 1998), so diffusion of this ion into liposomes probably only plays a small part in the time- and temperature-dependent quenching of MQAE seen in Figure 3.39. Verkman *et al.* (1989) reported a low octanol:water partition coefficient for MQAE which was related to the fact that it is a cationic salt, and thus has higher water solubility than otherwise. They also reported up to 30 % dye leakage from 90 % PC:10 % cholesterol liposomes after 24 hours at 4 °C, a much higher rate than that observed here. However, were leakage to be a problem during the duration of an experiment, it could simply be corrected for by running a "blank" sample and subtracting the signal from the experimental sample, as was done by Nishizawa *et al.* (2000).

It is known that the phospholipid types and fatty acyl chain lengths can significantly affect the function of membrane proteins, since these can alter the surface potential, protein-membrane interactions and packing of the membrane (Lee, 2005). For example, the activities of diacylglycerol kinase and Ca^{2+}-ATPase were significantly affected by changing the fatty acyl chain length of the bilayers they were in, and changing phospholipid head groups altered activity too. The optimal chain length was from C16-C20, which correlated well with the hydrophobic thickness of these proteins. Functional CLIC ion channel activity has been recorded in plasma and nuclear membranes of Chinese hamster ovary cells (Valenzuela *et al.*, 1997; Tonini *et al.*, 2000) and functional recombinant CLIC1 has been reconstituted in asolectin liposomes (Tulk *et al.*, 2000, 2002), a 7:3 mixture of PE:PS planar lipid bilayers (Tulk *et al.*, 2002), phosphatidylcholine monolayers (Harrop *et al.*, 2001); different mixtures of soybean phosphatidyl-choline, diphytanoylphosphatidylcholine, POPC, POPE, POPS and cholesterol (Singh and Ashley, 2006); a 9:1 (w/w) mixture of soybean PC: cholesterol liposomes (Warton *et al.*, 2002; Littler *et al.*, 2004), or in a 4:1:1 mixture of

POPE:POPS:cholesterol (mol/mol) in planar lipid bilayers (Singh *et al.*, 2007). This latter mixture proved to give the most reproducible ion channel activity of all the mixtures tested in that study. Where liposomes were used, the size ranged from 200-400 nm, and generally the potassium ionophore, valinomycin, was used to initiate voltage-driven flux (Tulk *et al.*, 2000; Littler *et al.*, 2004). In most cases asymmetric concentrations of KCl were used on either side of the membrane, but symmetric concentrations also produced channel activity. Thus, it is apparent that CLIC1 is able to insert functionally into a wide variety of monolayers and bilayers composed of numerous different lipid types, including crude and purified mixtures. This implies that the lipid mixture used in this study, despite fears that the use of a C18:2 fatty acid (linoleic acid) rather than a C18:1 fatty acid (oleic acid) may interfere with the required packing arrangement in the membrane, is likely to be perfectly adequate for reconstitution of functional activity.

The hydrophobic thickness (the distance between the glycerol backbones of phospholipids) of a C18:1 bilayer is estimated at about 27.2 Å (Lee, 2003), which would not change much with the added C16:0 fatty acyls used by Ashley's group (Singh and Ashley, 2006). For each additional double bond added the thickness decreases by up to 2.5 Å, giving a C18:2 bilayer a hydrophobic thickness of about 24.7 Å. The PTM region of CLIC1 runs for a predicted 21 residues, which would give a transmembrane region of 31.5 Å. However, an interesting fact about phosphatidylethanolamine is its unusual inverted cone-shape, which gives it a tendency to adopt non-bilayer phases such as the hexagonal H_{II} phase (Lee, 2005). In the presence of other lipids, which prefer bilayers, it will be forced to adopt the bilayer phase, leading to storage of curvature elastic stress (Lee, 2004). This elastic stress is proposed to allow distortions in the membrane to fill the free volume created when a protein inserts into the bilayer, and may also shift the conformational equilibrium of the protein to that which has the greatest hydrophobic thickness (Botelho *et al.*, 2002). Singh and Ashley (2007) suggested that the presence of PE and cholesterol, both associated with elastic stress, may promote the assembly of CLIC1 and CLIC4 in membranes in a manner similar to

the activation of protein kinase C. Furthermore, it has been shown that the bilayer is able to stretch or compress locally around the hydrophobic region of transmembrane segments of membrane proteins in order to avoid hydrophobic mismatch and the concomitant energetically unfavourable exposure of hydrophobic amino acid residues to water (Anderson and Koeppe, 2007). This means that the bilayer thickness close to the protein may differ from the unperturbed bulk bilayer thickness.

The presence of the anionic PS in the membranes is likely to be a more important factor than fatty acid type or hydrophobic thickness for the initial binding and ultimate stabilisation of CLIC1 in the membrane. The negative surface potential created at the membrane surface by PS has the potential to raise the pK_a values of some of the acidic residues in CLIC1, such that they are protonated, and thus able to bind the PS. This has been demonstrated, for example, with CTP:phosphocholine cytidylyltransferase, where key Glu residues dictated its selectivity for anionic membranes because of their altered pK_a values in the presence of anionic membranes (Johnson *et al.*, 2003). Also, the lowered pH at the surface of the membrane due to negatively charged lipids has been discussed in detail with regard to the pore-forming toxins, and how this results in the formation of a molten globule for many of the PFTs. CLIC1 has 23 Glu residues, 9 of them in the N-domain, and 12 Asp residues, 3 of them in the N-domain. The conserved KRR motif at residues 49-51, just after the PTM, most likely forms ion pairs with the acidic lipids. However, the fact that functional CLIC1 has been reconstituted in a range of lipids, with many of the mixtures containing no PS, indicates that anionic lipids are not an absolute requirement for insertion and channel activity *in vitro*, so long as the pH is controlled for maximal activity.

Analysis of the lipid mixture used in this study, along with the fact that highly homogeneous populations of relatively large unilamellar vesicles were achieved in high concentrations, indicates that the system characterised here should be absolutely sufficient for the demonstration of functional CLIC1-mediated ion channel activity. The fact that the lipid composition bears little real resemblance

to the actual composition of typical nuclear or plasma membranes (see Table 1) is not so important, since the activity of CLIC1 in cell cultures has been amply demonstrated, and the applications to which these liposomes are to be applied do not require an absolute determination of *in vivo* function, but a comparative demonstration of function between CLIC1 and CLIC1 mutants.

4.1.2. MQAE characterisation

The MQAE characterised in this study proved to be less sensitive to chloride quenching than published values would suggest (Verkman *et al.*, 1989), but is neverthetheless sensitive enough for the purposes of a functional assay involving CLIC1-mediated chloride flux. Singh and Ashley (2006) maintain that the existence of even a few functioning channels in the CLIC1-encapsulating liposomes (~200 nm) produced by Tulk *et al.* (2000) would empty the chloride contents (200 mM) of the vesicles within seconds. This suggests that functioning channels in MQAE-encapsulating liposomes would cause rapid and almost complete quenching. If the MQAE were found to be not sensitive enough, Br^- or I^- could be used, since MQAE is more sensitive to those ions, and CLIC1 also transports them (Singh and Ashley, 2006). An alternate option is Lucigenin, another chloride-sensitive dye which could be used in the same way as MQAE is proposed to be used here.

If increased leakage at higher temperatures became a problem, increasing the cholesterol content could decrease permeability, but may also interfere with insertion of CLIC1, since a certain amount of flexibility in the membrane is required for insertion. However, as mentioned, leakage rates can be controlled for. One issue that may be a problem with the use of MQAE (cationic) with anionic lipids is the possibility that it may bind the outside of the LUVETs, giving a false quenching signal upon addition of KCl. While the surface-bound amount of, say, a protein can be accounted for by using enzyme-linked immunosorbent assay (ELISA) on whole liposomes and liposomes destroyed by a detergent, where the difference in protein amount is the surface-bound amount (Manojlovic

et al., 2008), this is unfortunately not a viable option in the case of surface-bound MQAE. However, the best way to control for this potentially misleading factor is probably to exchange the liposomes into the KCl-containing buffer that is to be used for the assay at the same time that MQAE is removed, rather than add the KCl later. Any surface-bound MQAE will be quenched and any further quenching should be due only to CLIC1-mediated Cl^- flux.

The MQAE analogue, SPQ, was used to characterise parchorin chloride efflux function effectively (Nishizawa *et al.*, 2000), and has also been used to measure rates of chloride efflux from liposomes due to the insertion of α-toxin, one of the β-barrel PFTs (Vécsey-Semjén *et al.*, 1996). In the latter study, SPQ and KCl were encapsulated inside the liposomes, and the efflux was monitored by the increase in signal as Cl^- was transported out of the vesicles. These studies, as well as the seminal work by Verkman and colleagues (Illsley and Verkman, 1987; Verkman *et al*., 1989a; Verkman *et al.*, 1989b) illustrate that this is a viable assay for the detection and measurement of Cl^- transport from vesicles by CLIC1. The fact that CLIC1 is outwardly rectifying requires that the chloride has to be on the C-terminal domain side of the protein. This means that the chloride and CLIC1 would either have to be inside or outside the vesicles. Attempts to encapsulate 200 mM KCl in 4:1:1 PE:PS:chol LUVs were unsuccessful due to the low solubility of PE in relatively high salt concentrations, and attempts to encapsulate CLIC1 in liposomes were not particularly compatible with freeze-thaw and extrusion. Although proteins can be encapsulated in liposomes using this technique, a cryoprotectant is required (Sou *et al*., 2003). Detergent dialysis has been successfully applied to the encapsulation of CLIC1 in liposomes (Tulk *et al.*, 2000), but there is always the risk of interference with function or signal by residual detergent. Thus the most ideal way to set up the assay is to encapsulate the MQAE inside the vesicles, pass them through a size exclusion column equilibrated in buffer with the KCl concentration required, to separate the unencapsulated dye from the liposomes, and then add CLIC1 (and valinomycin) and measure the fluorescence across a time course. It is deeply regrettable that this assay could not be effectively tested during the duration of this project, since

it is a potentially powerful and relatively simple means to assess and compare the rates of chloride flux mediated by CLIC1 channel activity, as well as to determine the effects that redox conditions and molecules such as IAA-94 and NEM have on this activity.

4.2. Soluble CLIC1

The structural properties and conformational stability of CLIC1 were studied under conditions that it is most likely to encounter in the cellular environment, i.e. at pH 7.0, close to the physiological nucleoplasmic/cytoplasmic pH, and at pH 5.5, the pH at the surface of the membrane, due to H^+ ions being attracted to negatively charged phospholipid head groups of the bilayer (Menestrina *et al.*, 1989; van der Goot *et al.*, 1991; Bortoleto and Ward, 1999; Chenal *et al.*, 2002). Conditions within the cell are also highly reducing (Hwang *et al.*, 1992), and this was maintained throughout in all experiments.

4.2.1. Structural characterisation of soluble CLIC1

CLIC1 at pH 7.0 was found to be more structured than at pH 5.5. While Warton *et al*. (2002) found there to be no difference in the far-UV circular dichroism signals for CLIC1 at pH 7.0 and pH 6.0, distinct differences have been observed at pH 5.5 and below (Fanucchi *et al.*, 2008), and this study confirms the findings at pH 5.5. The 12 % loss of secondary structural content at pH 5.5 is less than that previously reported (Fanucchi *et al.*, 2008), but nonetheless does indicate changes in the asymmetry along the peptide backbone. An analysis of the spectral data with SELCON3 (Sreerama *et al.*, 2000) using the DICHROWEB interface (Whitmore and Wallace, 2004) and Reference Set 4, surprisingly, predicted a much lower helical structural content than evident in the crystal structure. The CLIC1 crystal structure is 47 % α-helical, 8 % β-strands and 45 % coils. The algorithm used predicted 33.2 % α-helices (14 % distorted), 14.6 % β-strands (7.5 % distorted), 20.8 % turns and 31.3 % unordered for CLIC1 at pH 7.0, and 29.8 %

α-helices (13 % distorted), 16.6 % β-strands (8 % distorted), 21.8 % turns and 31.2 % unordered for CLIC1 at pH 5.5. The CONTIN/LL algorithm (Provencher and Glöckner, 1981) did not give significantly different results. The results are curious, and unexpected. The server was simply used to check what aspects of secondary structure CLIC1 was losing at pH 5.5, but the apparently much lower than expected α-helical content exhibited for the spectra at both pH values points possibly to a greater plasticity in the structure than previously imagined. This may be related to the acidic loop region, which is a short helix in CLIC1 but disordered or simply a coil in CLIC2 and CLIC4; or to helix α2, which may have built-in plasticity as seen in the CLIC2 and CLIC4 structures. Disruption of the salt bridge formed between Arg29 on α1 and Glu81 on α2 at low pH could also lead to increased flexibility within the structure. Another candidate for lower helical content is helix α8 in the C-domain, which forms contacts with helix α1, itself a relatively flexible helix. It is not clear though, how this could account for a higher β-strand content. Nevertheless, according to these results CLIC1 at pH 5.5 has lower α-helical, higher β-strand content and basically equivalent unordered content compared to CLIC1 at pH 7.0. Thus the signal loss at pH 5.5 can be directly related to a small loss of α-helical content. This is particularly interesting in light of the fact that the crystal structure was determined at pH 5.0 (Harrop *et al*., 2001).

In terms of the fluorescence spectra, the small excitation wavelength-dependent shift in emission peak wavelength is probably not significant within the parameters of the instrument used, yet it is consistent for every spectrum collected, and is as much as 3 nm on a different instrument. While it is generally taken that the Ex.280 emission signal is dominated by Trp35 due to resonance energy transfer from Tyr residues to Trp, the emission maximum for Trp is often shifted back slightly to that of Tyr in the folded conformation (Schmid, 1997). The Ex.295 emission spectrum is of substantially lower intensity than that for Ex.280. This could generally be explained by the fact that Tyr residues are much more numerous than the lone Trp, despite their lower quantum yield, and probably pass on a good deal of their energy to Trp35, but if one considers Förster distances

(the distance at which resonance energy transfer is 50 % efficient (Lakowicz, 1999)) between aromatic residues in CLIC1, it can be seen that not all of the Tyr residues are likely to pass on energy to Trp35, since they are just too far away (Table 3). Typical Förster distances for energy transfer from Tyr to Trp residues range up to 16 Å (Lakowicz, 1999). Naturally, energy transfer and its efficiency would be dependent on the environments of the donors, which affect their quantum yield and emission spectrum. While it is feasible that much of the energy absorbed at 280 nm by Tyr93 and Tyr214 (cyan in Figure 4.1), and possibly Tyr69 and Tyr209 (pink in Figure 4.1) is passed on to Trp35, the other Tyr residues are probably too distant (~29 Å) for significant energy transfer. This most likely underlies the differences seen in the Ex.280 and Ex.295 spectra of CLIC1. It should be remembered, though, that a structure of CLIC1 crystallised at pH 7.0 may have closer Förster distances. The fluorescence maximum emission wavelength is anyway in keeping with the known crystal structure, where Trp35 is at least 26 % exposed to the aqueous solvent.

Table 3. Distances between Tyr and Trp35 residues in CLIC1.

Residue	Distance to Trp35 (Å)*	Domain
Tyr69	18.8	N
Tyr93	**14.5**	**N**
Tyr117	28.7	C
Tyr143	23.2	C
Tyr194	25.5	C
Tyr209	17.2	C
Tyr214	**12.5**	**C**
Tyr233	21.0	C

* Distances measured using Swiss PDB Viewer v. 4.01, and PDB 1k0m, A chain (Harrop *et al.*, 2001); residues in bold are within typical Förster distances for energy transfer from Tyr to Trp residues (Lakowicz, 1999).

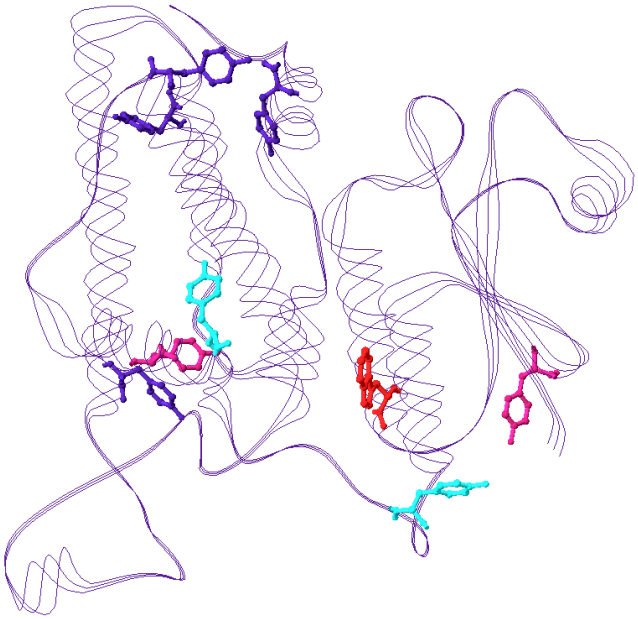

Figure 4.1. Location of Tyr residues in relation to Trp35 in CLIC1.

Ribbon structure of CLIC1 showing locations of Tyr residues. Tyr residues (blue, cyan and pink) are scattered around the entirety of the molecule, some of them quite distant from Trp35 (red). Tyr69 and Tyr209 (pink) are approximately 17 Å and 19 Å from Trp35, respectively, while Tyr93 and Tyr214 (cyan) are approximately 13 Å and 15 Å, respectively, from Trp35. PDB 1k0m was used (Harrop *et al*., 2001). Image generated using Swiss PDB Viewer v. 4.0.1. (Guex *et al.*, 1995).

The approximately 40 % drop in fluorescence emission intensity upon unfolding at pH 7.0 and pH 5.5 indicates that Tyr and Trp are relatively unquenched in the native environment of the protein. The red shift to 345-348 nm and the drop in fluorescence intensity upon unfolding indicate increased exposure of Trp35 to the polar solvent. *N*-acetyl-L-tryptophanamide (NATA) in water peaks at 350 nm on the instrument used for these measurements and has a much greater quantum yield in the presence of 8.0 M urea than in its absence. Thus there are definitely interactions occurring in the unfolded protein in the vicinity of Trp35 that are causing quenching, such as solvent quenching, or indeed, solvent quenching in addition to quenching by nearby charged residues such as arginine and lysine that are folded away from Trp in the native state. Lys37, for example, is folded to the other side of the helix, opposite Trp35 in the folded conformation, but would be

right next to it when unfolded. Regarding the lower peak wavelength for CLIC1 in 8.0 M urea than NATA (3-5 nm shorter), it is most likely that CLIC1 is not fully unfolded at 8.0 M urea in the sense of existing as a random coil. Numerous studies have shown that the denatured state ensemble is made up from conformations that not only include hydrophobic pockets and small secondary structural elements, but that long-range electrostatic interactions contribute to this ensemble too (Dill and Shortle, 1991; Shortle, 1996; Pace *et al.*, 2000; Whitten and García-Moreno, 2000; Baldwin, 2002; Cho *et al.*, 2008). Considering the high number of acidic residues in the CLIC1 sequence (~15 %), and the numerous basic residues (11 %), it would actually be more surprising if these did *not* contribute to the maintenance of residual structural elements in the denatured ensemble via electrostatic interactions.

Changes in fluorescence emission intensity are generally attributable to small changes in concentration, and so are not necessarily a good indicator of changes in tertiary structure. Nevertheless, the lower intensities recorded for CLIC1 at pH 5.5, particularly apparent in the Ex.280 spectra, could indicate shifts in relevant side-chains in relation to one another that allow more solvent accessibility or less energy transfer due to a slight "opening-up" or "loosening" of the structure. Similar decreases in the intensity of pH 5.5 emission spectra have been observed by a colleague in this laboratory (Fanucchi *et al.*, 2008). A loosening of the structure would allow solvent molecules that do not have access to the more buried parts of Trp35 at pH 7.0, access at pH 5.5. Or again, positively charged residues known to quench Trp fluorescence such as Arg, Lys and His may have additional access to Trp35 that they do not have at pH 7.0. Lys37 is again a candidate here, as is Arg216, which is situated on the loop just before helix α8 in close proximity to Trp35. In a more flexible conformation, it could conceivably contribute to Trp35 quenching, especially with changes at the domain interface. Additionally, a slightly more relaxed structure could result in lower energy transfer from Tyr residues to Trp35. When Harrop *et al*. (2001) resolved the crystal structure of CLIC1, they noted a degree of plasticity in the domain interface region that resulted in two conformers for helices α1 and α3, which

make up the N-domain side of the N- and C-domain interface. These conformers come about due to a highly Pro-rich region in the loop that joins helix α3 in the N-domain and helix α4a in the C-domain. Pro91 exists in either *cis* or *trans* conformations, the latter minor conformer of which displaces and tilts helices α1 and α3 with respect to the major conformer. Tyr93 is *right in the middle* of this Pro-rich region (Pro91, Pro92, Tyr93 and Pro94), and is also close enough to Trp35 for significant resonance energy transfer (Table 3), so in a flexible, looser structure this energy transfer would definitely be affected, leading to a slight loss of signal intensity, as is witnessed for the fluorescence spectrum at pH 5.5. However, the relatively low resolution of the probe means that the exact locations of any increased motion of relevant helices cannot be pinpointed. Hydrogen-deuterium exchange mass spectrometry (HDXMS) or NMR work could probably give much more specific information about relative changes around Trp35.

Contributions of the aromatic residues to the magnitude, sign and wavelength of near-UV CD data are still relatively inadequately understood, despite a number of mutational studies that have monitored the contributions of specific residues to protein spectra (Vuilleumier *et al*., 1993; Freskgård *et al*., 1994). Near-UV data show a more positive spectrum for CLIC1 at pH 5.5, particularly in the 260-290 nm region. While it is difficult without mutational studies to assign specific bands to specific residues, the negative bands at 280 nm and 287 nm and the less pronounced positive band at 295 nm can definitely be attributed to Trp35, since that is the only Trp residue in CLIC1, and the other aromatic residues, Tyr and Phe absorb in the lower wavelength regions. Bands at 266 nm have been attributed to Trp, whose contribution is generally positive in this region (Freskgård *et al*., 1994), but whether that is the case here is debatable. The decrease in intensity of the signal around 280-295 nm at pH 5.5 can almost certainly be attributed to a change in packing around Trp35, although there is no change in wavelength here. It is likely that dipole-dipole coupling between Trp35 and Phe residues clustered near Trp35 on β2 strand (Phe41) and α1 helix (Phe31) (Figure 4.2) contribute to the negative Trp35 bands at 280 nm and 287 nm in the near-UV CD spectrum of CLIC1. The near-UV CD of Trp side chains is

especially intense when other aromatic compounds are within 10 Å of the Trp, due to dipole-dipole coupling (Strickland, 1974). Phe31 is just 4.6 Å from Trp35, and Phe41 is 6.3 Å away. A loss of dipole-dipole coupling effects amongst these residues as a result of increased flexibility in α1 helix in relation to β2 strand would translate to a loss in signal in the Trp region of the spectrum. The 278 nm band in the pH 7.0 spectrum is slightly red-shifted to 279 nm in the pH 5.5 spectrum, generally indicating a move to a less polar environment (Freskgård *et al*., 1994). Again, the likely candidates for this shift are the aromatic cluster indicated in Figure 4.2. Movement away from each other in a more flexible conformation would lessen the dipole-dipole coupling effects contributing to the intensity of the signal.

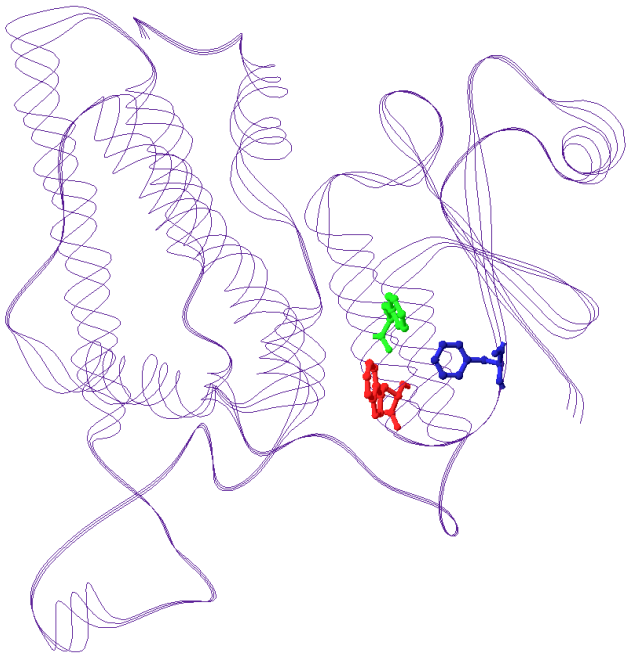

Figure 4.2. Clustered aromatic residues in the N-terminal domain of CLIC1. Ribbon structure of CLIC1 showing nearby aromatic residues that may contribute to the Trp35 near-UV CD intensity 275 nm and 295 nm. Phe31 (green) is 4.6 Å from Trp35 (red), and Phe41 (blue) is 6.3 Å away. PDB 1k0m, A chain was used (Harrop *et al.*, 2001). Image generated using Swiss PDB Viewer v. 4.0.1. (Guex *et al.*, 1995).

Incidentally, α1 forms part of the putative transmembrane region, so any increased flexibility here is likely to increase the capacity for the protein to transform from soluble to membrane-bound conformation. Certainly, CLIC1 has been shown to insert more readily into model membranes and function more efficiently at pH values in the range 5.0-5.5 than at pH 6.5-7.0 (Warton *et al*., 2002), and in the range pH 5.0-6.0 compared to pH 7.0 (Tulk *et al.,* 2002), which would mimic the situation *in vivo* where the pH at the membrane surface is lower than in bulk cytosol. Electrostatics probably play a role in the apparent loosening of the CLIC1 structure at lower pH. CLIC1 is an acidic protein with a low p*I*. By decreasing the pH, the number of H^+ ions in solution is increased, resulting in neutralising of negative charges on the surface of the protein and giving positive charges to basic residues on the surface, particularly His. The overall negative charge on CLIC1 drops from -7 at pH 7.0 to -3 at pH 5.5. Changing the charge on surface residues that form intramolecular contacts that help to maintain the stability of the protein could affect this stability, allowing greater overall flexibility in the molecule. This will be discussed in greater detail in the next section.

4.2.2. CLIC1 conformational stability is pH-dependent

Urea-induced equilibrium unfolding of CLIC1 at pH 7.0 shows a highly cooperative two-state transition from the native to the unfolded state. The free energy of unfolding is approximately 10 kcal/mol (Table 2), well within the range for monomeric proteins, although the *m*-value is 15 % lower than that predicted by a model correlating *m*-values with the number and area of residues becoming accessible to solvent (Myers *et al*., 1995). According to this model, the experimentally derived *m*-value suggests that up to 50 buried residues are already totally exposed to solvent before unfolding begins! It is entirely possible that the acidic loop in the C-terminal domain of the CLIC1 structure (Ser146-Thr174) is partially responsible for this discrepancy. This loop region is highly flexible, and probably very solvent-exposed, judging by the 1k0n and 1k0o crystal structures where this portion of CLIC1 was disordered, as it was in the CLIC4(ext) structure

(Harrop *et al*., 2001; Littler *et al*., 2005). In comparison to another monomer of the GST family, Grx2, the stability and cooperativity of unfolding of CLIC1 are lower. Grx2 is smaller (215 residues) but with a $\Delta G_{(H2O)}$ of 12 kcal/mol and an *m*-value of 2.7 kcal/mol M^{-1} urea has a higher free energy and cooperativity of unfolding (Gildenhuys *et al.*, 2008). These values are 15 % higher for a protein which is 10 % smaller than CLIC1, implying that the CLIC1 native structure is not only less stable, but less compact than that of Grx2. The major difference in the two structures is the acidic loop region present in the C-domain of CLIC1, but which is absent in Grx2. The native structure of CLIC1 may be even more flexible than its crystal structure implies, as was also evidenced by the unexpected results for the CD spectra from the DICHROWEB server. It would be fascinating to see an NMR structure of CLIC1, since the multiple conformers could give an idea of the degree of mobility within the structure.

The unfolding transitions for CLIC1 at pH 7.0 monitored by fluorescence (Ex.280 and Ex.295) and circular dichroism superimpose, and there is no detectable evidence of any stable intermediates along the entire transition. By all definitions, the transition is two-state, but with lower cooperativity than predicted. CLIC1 is stable in the native conformation until a critical concentration of urea of just under 4.0 M, at which point rapid unfolding takes place. At 7.0 M urea the protein is fully unfolded, barring residual structural content due to electrostatic and hydrophobic interactions making up the denatured state ensemble.

At pH 5.5, CLIC1 forms a highly populated stable unfolding intermediate with reduced secondary and tertiary structure and an exposed hydrophobic surface. A fascinating difference exists between the thermodynamic parameters derived from the fits to the Ex.280 and Ex.295 fluorescence data. The Ex.280 + E_{222} fit indicates a less stable structure that the pH 7.0 structure ($\Delta G_{(H2O)}$ = 8.0 kcal/mol *vs*. about 10 kcal/mol), and the same level of cooperativity for the N ↔ I transition at pH 5.5 as the N ↔ U transition at pH 7.0 (Table 2). The free energy of unfolding for the intermediate to the unfolded conformation is higher, near the top of the monomeric range. The *m*2-value, though, translates to an incredible

286 residues exposed upon unfolding, greater than the length of the protein. The thermodynamic parameters for the I ↔ U transition monitored by Ex.280 + CD are actually surprisingly close to those of a dimer of the GST family, rGSTM1-1, for the same transition (Thompson *et al.*, 2006). The Ex.295 parameters are even more remarkable. The $\Delta G_{(H2O)}$ values are well into the dimeric range, and *m*1 translates to an extraordinary 560 residues exposed upon unfolding, while the *m*2-value indicates 315 residues exposed! Clearly, for a monomer of size 241 residues, this is impossible.

So what is actually happening in the CLIC1 structure during unfolding at low pH? There is a dramatic difference between the thermodynamic parameters obtained for the fits to the Ex.280 + CD data and the Ex.295 data and their corresponding population plots, and it is apparent, simply by looking at the unfolding curves generated by excitation at 280 nm or 295, that the transitions monitored by the two probes must be detecting the same event from a more global and a more local perspective, respectively. The Ex.280 data averages changes over the whole structure across the urea concentration range used, and in so doing, partially masks the localised unfolding transitions occurring in the N-terminal domain as monitored by the localised probe near the domain interface, Trp35. Luque *et al.* (2002) point out that the Gibbs energy of stabilisation of a protein is not evenly distributed over the entire protein, and that local unfolding regions are scattered around the whole structure, giving rise to high- and low-stability constant areas. We already know from the crystal structure that the N-terminal domain of CLIC1 is more flexible than the C-terminal domain (Harrop *et al.*, 2001), and other CLIC structures exhibit flexibility in helix α2 (Littler *et al.*, 2005; Li *et al.*, 2006; Cromer *et al.*, 2007). Also it is apparent from the near-UV spectra at pH 7.0 and pH 5.5 that fairly significant differences in packing occur around Trp35 at pH 5.5. In addition, a study on wild type and mutant forms of rGSTM1-1 using HDXMS to probe the relative solvent accessibilities and therefore dynamics of the dimer interface found distinct differences in the fast exchange in the thioredoxin-like N-terminal domains of mutants *vs*. the wild type protein (Codreaunu *et al.*, 2005). Two of the mutants showed reduced stability at the dimer interface that shifted the

equilibrium of the intermediate to the monomeric state. While the wild type protein showed moderate fast exchange in the N-terminal domain, particularly in α1, β2 and α2, and rapid exchange in the C-terminal tail, α9, which correspond to the same structures in the CLICs, the destabilising mutants showed significantly enhanced exchange in the fast phase in large portions of the N-terminal domain, including α2, almost the entire β-sheet and parts of α1 and α3. A double mutant of this same protein which disrupted interdomain (salt bridge) and intersubunit (lock-and-key) interactions yielded only the monomeric form of rGSTM1-1 (Thompson *et al.*, 2006). Amide hydrogen/deuterium exchange of the entire N-terminal domain of this mutant was significantly enhanced relative to the wild type protein, indicating greater solvent accessibility and dynamics. These studies are significant in light of the highly conserved canonical thioredoxin-like fold within the N-domains of the GST superfamily. An intrinsic flexibility in this domain may serve various functions for specific family members, but it is the contention here that in CLIC1 it serves to aid the formation of a membrane-competent structure under certain conditions.

To date, little real attention has been paid to the Ex.295 data for CLIC1 at pH 5.5, on the assumption that the Ex.280 spectra are dominated by Trp35 anyway. It appears that this was an oversight. Clearly Ex.295 *is* acting as a much more localised probe than Ex.280. Is something happening in the N-terminal domain that is not apparent when probing the protein as a whole? Are parts of the N-terminal domain oligomerising with other intermediates in solution? The N-terminal domain contains the proposed membrane-insertion region of CLIC1, and thus would require a complete structural rearrangement in order to take up a membrane competent conformation. Does part of this structural rearrangement include oligomerisation of N-terminal domains just prior to insertion into the membrane? The slight blue shift in the λ_{max} for the intermediate, which has been reported to be up to 5 nm (Fanucchi *et al*, 2008), indicates a shift of Trp35 to a more hydrophobic environment – this would be consistent with a model where Trp35 becomes slightly more buried during unfolding and dimerisation or oligomerisation of the N-terminal domain. However, confoundingly, burial of

any residues would be inconsistent with the enormous *m*1-value. Complete unfolding of the N-terminal domain during structural rearrangement would account for 40 % loss in secondary structure of the whole protein, although this would in fact be slightly less because of the lower contribution of β-strand structures to the signal at 222 nm, all of which are in the N-terminal domain. The circular dichroism spectrum for the intermediate species indicates ~56 % loss. Could loss of secondary structure in the N-terminal domain account for the large majority of this loss? If the intermediate species at pH 5.5, which is also found at pH 7.0, 37 °C, is the pre-membrane-insertion conformation of CLIC1, which it is proposed to be (Fanucchi *et al.*, 2008), then the structural and stability data would appear to indicate that the N-terminal domain is completely, or almost completely unfolded, and that hydrophobic contacts between N-terminal domains are causing either dimerisation or oligomerisation just prior to rearrangement into the helical conformation which would be required for actual insertion. Is it possible that these hydrophobic contacts *aid* the formation of the insertion structure, protecting against collapse into an unstructured aggregate? Could the high *m*-values in fact be referring to exposure of the residues of a number of CLIC1 molecules coming together in solution? Unfortunately, concentration-dependent studies, which would indicate whether a dimeric or oligomeric species was present, were not performed. In theory, the exposure of 560 residues correlates to the total exposure of six N-terminal domains. Taking into account that the C-terminal domain, possibly beginning with α8 and α9, would also have reached a certain level of unfolding by the time the intermediate species is detected, theoretically, unfolding of four N-terminal domains and partial unfolding of the C-terminal domains of those four molecules could account for the high level of exposure indicated. Incidentally, the number of CLIC1 molecules proposed to make up the functional ion channel is four (Singh and Ashley, 2006).

Clearly, though, over-reliance on *m*-values for determinations of absolute numbers of residues exposed can only lead to frustration in a case like this. Anyway, it is probably not warranted, since the model upon which the dependence of the *m*-value on the amount of surface accessible area exposed is a purely two-state

model (Myers *et al.*, 1995). Staphylococcal nuclease, for example, of which probably hundreds of mutants have been generated, exhibits a broad range of *m*-values depending on the mutant (Shortle and Meeker, 1986; Shortle, 1995, 1996). The slope of the dependence of ΔG on denaturant concentration for these mutants can vary over a threefold range, implying that the solvent-exposed surface of the native state would have to shrink by as much as 25 % or expand by up to 50 %, depending on the mutant; an unlikely event indeed given the nature of the folded protein (Shortle, 1996). Thus, it was argued that the range of effects on thermodynamic parameters induced by different mutants actually reflect structural perturbations in the denatured state, since this is made up of an ensemble of microstates that would have a much higher capacity for perturbation than the native state could possibly encompass. Mutants which increase the *m*-value have larger, less structured denatured states. The denatured state of mutants which decrease the *m*-value is more compact, and has a greater amount of secondary structure. Whitten *et al*. (2001) expand this discussion by considering cases where the *m*-value increases or decreases upon a decrease in pH. Generally, where the *m*-value increases with a decrease in pH, it is correlated with an increase in the solvent accessible surface area (SASA) of the denatured state. Expansion of the denatured state is presumably driven by repulsive interactions brought about by a change in charge due to increased proton concentration. A decrease in the *m*-value with a decrease in pH is not interpreted in the same manner. Instead, it is correlated with the accumulation of an intermediate which is preferentially stabilised relative to the native state with a decrease in pH. The accumulation of the intermediate within the unfolding transition perturbs the two-state character of the transition, leading to a decreased *m*-value. While at first glance the *m*-values derived from the fits to the pH 5.5 data for CLIC1 appear to fit the former case, it should be borne in mind that the above discussion relates to the fitting of *two-state* model to the data. If one fits the pH 5.5 data to a two-state model, the *m*-value is, in fact, greatly depressed (1.2-1.6 kcal/mol M^{-1} urea), giving credence not only to the existence of the intermediate, but also negating the requirement for absolute correlation of the *m*-value with increase in SASA, especially since an ensemble of partially folded states, in accordance with folding

funnel theory, will have different amounts of exposed SASA at any one time. Nevertheless, the fact that the parameters derived for the fits to the Ex.295 data at pH 5.5 are well into the dimer range provide intriguing grist to the mill that the protein is forming some kind of oligomeric state that is localised to the N-terminal domain.

An essential aspect to consider in the reduced stability of CLIC1 at pH 5.5 relative to at pH 7.0 is the effect that an increased number of protons in solution will have on the structure and stability of the protein. At pH 7.0 the native protein is more stable, meaning that it requires greater energy to unfold. This presumably relates to a higher degree of interior packing and the stronger forces causing and/or resulting from this. In addition, surface residues engaged in salt-bridging are likely to contribute to the higher stability observed. Within the native, folded protein, local and long-range electrostatic interactions, the dielectric constant and the arrangement of charge may all result in the pK_a values of some titratable residues either being raised or lowered relative to model compounds in water. In general, it is found that at any given pH, the pK_a values of the carboxyl groups of the side chains of acidic residues (relevant to studies at low pH) can be quite significantly raised or depressed (Matthew *et al.*, 1979, Matthew, 1985). Additionally, and significant within the pH range studied, the pK_a value of the His imidazole group is subject to change dependent upon pH and electrostatic effects. In the presence of an increased concentration of hydrogen ions at lower pH, where the charge on CLIC1 drops from -7 at pH 7.0 to -3 at pH 5.5, charge-charge interactions are certain to be perturbed, due to protonation of acidic residues or due to protonation of His. In these cases, immediate repulsion will take place accompanied by small structural rearrangements and a modest expansion of the structure due to infiltration of water molecules into the new spaces as already witnessed in the small, but detectable pH-dependent changes apparent in the CD and fluorescence spectra of CLIC1. In theory, according to the model proposed by Linderstrøm-Lang (1924) and still held generally to be true, a protein should be most stable at its p*I*, because this is where most unfavourable electrostatic interactions are neutralised. However, the model assumes as its starting point that

the charges are uniformly smeared across the surface of the protein, which, for any real protein, is not necessarily true. In the case of CLIC1, whose p*I* is around 5, it is apparently not true, since the stability is lowered at pH 5.5 relative to pH 7.0. This can be accounted for by the non-uniform distribution of charge in CLIC1 (Figure 1.18), particularly in relation to the likely existence of buried nontitratable ionised groups, where buried generally refers to charges located a short distance within the interior of the protein in a region of low dielectric constant or in the dielectric boundary (Matthew and Gurd, 1986). The Born energy of these ionised groups is increased relative to those on the surface, with the result that their contribution to destabilisation becomes asymmetric and the maximum stability of the protein will not be at the isoelectric point (Stigter and Dill, 1990).

Figure 4.3 shows the distribution of ionisable residues on the surface of CLIC1. More than 25 % of the CLIC1 sequence consists of charged residues, and 9 % are in the N-domain. Most of the charged residues are on the surface or near the surface of the protein, but they are not evenly distributed. There are 12-15 acidic residues on the face of CLIC1 seen in Figure 4.3A, but only about eight on the surface in Figure 4.3B. There are nine basic residues on the face seen in Figure 4.3A, but at least 12 on the face seen in Figure 4.3B. Thus there is an asymmetric distribution of charge across the CLIC1. The face in Figure 4.3A has a more acidic character, while the opposite face has a more basic character. Many of these residues are involved in complete or incomplete salt bridge interactions with each other, but not all are, although it must be remembered that the default pH for the calculation of ion pair interactions is 7.0, and they are probably involved in hydrogen bonding interactions as well. There are two main “hotspots” of negative charge in the CLIC1 structure: the acidic loop region and helix α9 in the C-domain. There is also a region which contains no charged residues in Figure 4.3A. This region could be significant for binding of the protein to the membrane. If the cluster of acidic residues near the top of this patch were neutralised at the low pH at the membrane surface, the basic residues around the edge of the patch at the lower and upper left of it would easily be able to bind negative phospholipids

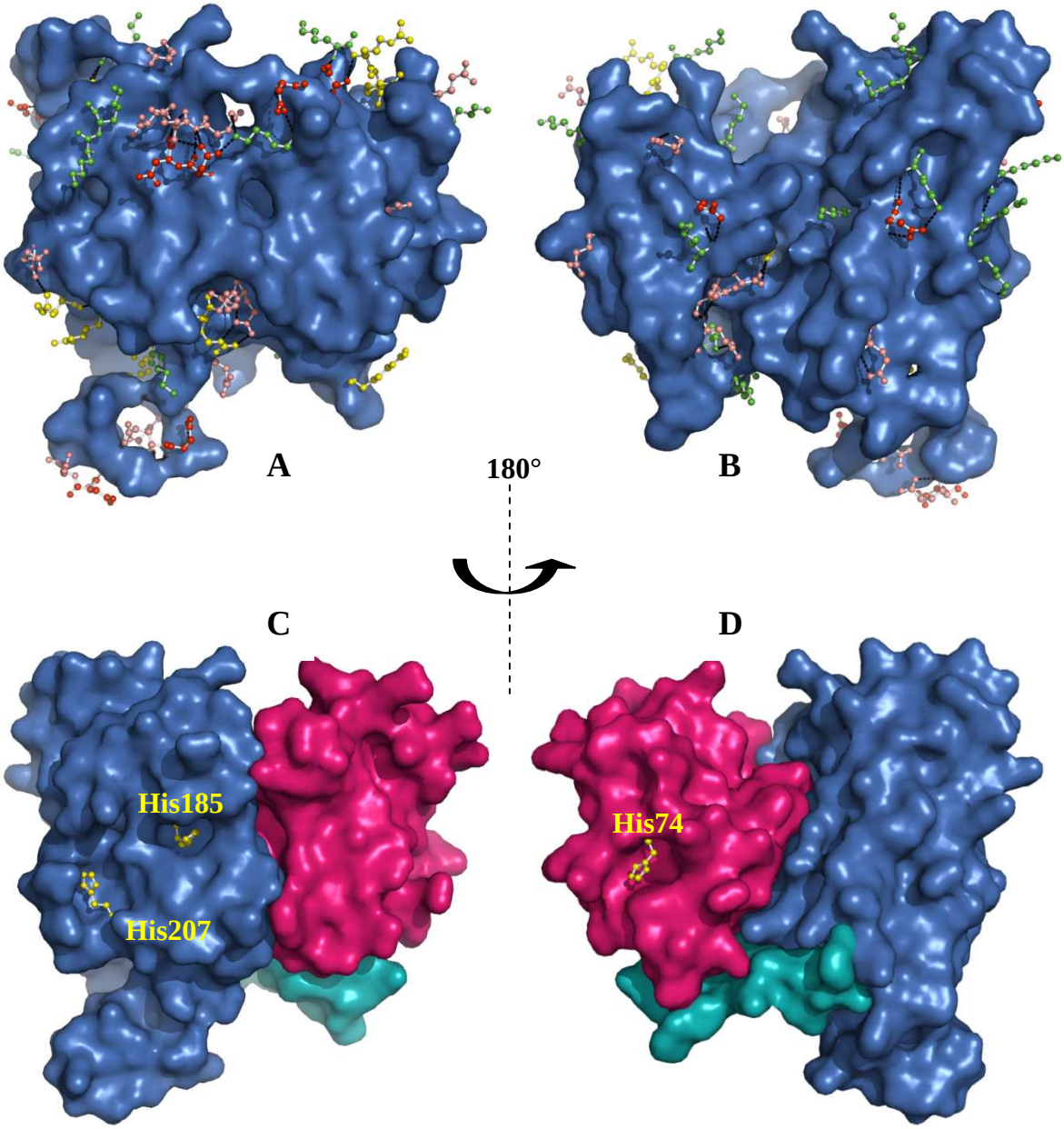

Figure 4.3. Distribution of ionisable residues in CLIC1.

(**A**) and (**B**) Distribution of basic and acidic residues on the surfaces of CLIC1. Asp is shown in red, Glu in pink, Lys in green and Arg in yellow. Salt bridges are shown with black dots. An uncharged patch is visible on the face shown in (A), but an equivalent patch does not exist on the other side of the molecule in (B). (**C**) and (**D**) Distribution of His residues on CLIC1 surface. The N-domain is pink, the C-domain is blue and the linker region is turquoise. PDB 1 k0m was used (Harrop *et al.*, 2001). Image rendered using PyMOL™ v. 0.99 (DeLano Scientific, 2006).

at the membrane surface and allow this uncharged region to lie flat against the membrane. On the other hand, the basic character of the opposite face could also easily allow for binding to negative membrane surfaces. The fact that CLIC1 inserts more readily into anionic lipid membranes (Tulk *et al.*, 2002; Singh and Ashley, 2006; Singh *et al.*, 2007) at low pH indicates that these scenarios are distinct possibilities.

CLIC1 has three His residues, His74 in the N-domain and His185 and His207 in the C-domain (Figure 4.3C and D). His74 and His207 are relatively solvent exposed. His74, on β4, is only about 15 % solvent exposed, potentially giving it a relatively large impact on stability when protonated at pH 5.5, especially since it is very close to α3. It is near to at least six acidic residues and only one basic residue, implying that its pK_a could be raised relative to model compounds (Matthew *et al.*, 1979). His185, on α6 is close to six acidic residues and three basic residues, possibly also giving it an increased effective pK_a. His207, on α7, is in the vicinity of only one acidic residue, and five basic residues, which may contribute to the depression of its pK_a. These His residues are in the unique position of being able to act as pH sensors. Above the typical pK_a value of 6.1 for imidazole, His will be neutral. Below that, it will be charged. Depending on the effect of the local electrostatic environments on the pK_a values of the His residues in CLIC1, they could either contribute significantly to stabilisation or destabilisation of CLIC1 due to perturbation of local and longer range electrostatic interactions. Judging by the lower stability of CLIC1 at pH 5.5, it is likely that they have a destabilising effect on the native state at this pH.

The capacity of a particular state of a protein, be it native, intermediate or denatured to bind protons will determine the stability of that state when the pH is lowered (Tanford, 1969; Matthew *et al.*, 1985; Tan *et al.*, 1995). The differences in affinity of various states for H^+ ions are a reflection of the differences in electrostatic contributions to their free energy because of the dependence of pK_a values of ionisable groups on electrostatic effects (Whitten and García-Moreno, 2000). The appearance of a stable intermediate species at low pH with a higher

free energy of unfolding relative to the unfolded state compared to the native state would tend to suggest that favourable electrostatic interactions contribute to the stabilisation of this species. This is significant in light of the proposed biological role of the intermediate as the pre-pore, insertion-competent conformation of CLIC1 (Fanucchi *et al.*, 2008), especially because of the low pH, high negative surface potential and low dielectric constant at the membrane surface.

4.2.3. The CLIC1 intermediate

As was discussed in Section 1.3.3., low pH-induced intermediate species populated under mild denaturing conditions are not unusual in the pore-forming toxins and other membrane-associated proteins, such as α-lactalbumin (Kuwajima, 1977; Dolgikh *et al.*, 1981; Griko *et al.*, 1994), equine lysozyme (van Dael *et al.*, 1993; Griko *et al.*, 1995), staphylococcal nuclease (Dill and Shortle, 1991; Shortle, 1993, 1995, 1996), Cry1Ab toxin (Rausell *et al.*, 2004), colicin A (van der Goot *et al.*, 1991; Muga *et al.*, 1993) and diphtheria toxin (Chenal *et al.*, 2002). Additionally, a molten globule-like intermediate of β-lactoglobulin was induced by lowering the dielectric constant of the solution (Uversky *et al.*, 1997), an interesting fact given the low dielectric constant near the membrane surface. Generally these intermediates have been characterised as molten globules, due to their compact nature, their retention of native-like secondary structure, lessening of orderly tertiary structure, and ability to bind ANS weakly (mM affinity) (Bailey *et al.*, 2001; Halskau *et al.*, 2005; Banerjee and Kishore, 2005; Prajapati *et al.*, 2007). The intermediate formed during the unfolding transition of CLIC1 at pH 5.5 is most highly populated around 3.8-4 M urea. Structural analysis of this species using far- and near-UV CD and fluorescence emission spectroscopy indicate that its secondary and tertiary structures are both affected to some degree. The loss of ~50 % secondary structure is inconsistent with a molten globule state, as is the relatively tight binding of ANS to hydrophobic patches exposed during formation of this intermediate species (K_d of 20 μM). The maximum emission wavelength of molten globule states is usually between that of the native and denatured states (Kuwajima *et al.*, 1996; Manceva *et al.*, 2004), but the λ_{max} of the

CLIC1 intermediate is actually blue-shifted relative to that of the native state. This would indicate relatively intact tertiary contacts and a shift of Trp35 and other exposed Tyr residues to a more hydrophobic environment. This is borne out by reduced accessibility of Trp35 to quenching by acrylamide (Fanucchi *et al.*, 2008). Not all molten globule intermediates have a higher maximum emission wavelength than the native state, though. For example, the λ_{max} of the molten globule state of Cry1Ab toxin is 3 nm blue-shifted relative to that of the native state, and it exhibits reduced acrylamide quenching (Rausell *et al.*, 2004). This is because the molten globule state is oligomeric, and the Trp residues are primarily located in the pore-forming domain. This is significant for the CLIC1 intermediate, whose unfolding data appear to indicate that it is at least dimeric if not oligomeric. Something interesting about some of the molten globules mentioned above is that the fluorescence intensity of the intermediate is higher than that of the native state, suggesting that their Trp residues have been removed from the vicinity of potentially quenching residues. The CLIC1 intermediate monitored by Ex.295 has a higher fluorescence intensity relative to the native state, compared with a slightly lower intensity for the intermediate excited at 280 nm. The near-UV CD spectrum of the CLIC1 intermediate appears to indicate a loss of tertiary packing with a rather drastic loss of signal around the Trp35 band at 287 nm. Whether this is due to a loss of specific contacts within a cluster or due to a global loss of tertiary packing is not entirely clear, but certainly there are some changes around Trp35. Whether contacts have simply been lost or new contacts formed with degenerate dipole-dipole coupling effects cannot be said. However, the fact that the intermediate species unfolds highly cooperatively would tend to suggest that significant tertiary interactions are present.

The population plots for the unfolding data for CLIC1 at pH 5.5 indicate that intermediate monitored by Ex.295 emission is more stable than when monitored with the more global probe of excitation at 280 nm. This would be consistent with the formation of an oligomer, where stabilising interactions would be more numerous. The data also indicate a greater proportion of intermediate species population than the Ex.280 data, which upholds the idea that the major structural

changes associated with the intermediate species are more locally located in the N-terminal domain. What is rather interesting about the unfolding transitions of CLIC1 at pH 5.5 monitored with CD and fluorescence is that the loss of secondary structure appears to occur at lower concentrations than the loss of tertiary structure (Figure 3.12). Overlaying of the Ex.295 data monitored by maximum emission intensity gives the same effect. This is very unusual and unexpected. Most of the molten globule states mentioned so far exhibit non-superimposable unfolding curves where the *tertiary* structure is lost at lower concentrations of denaturant. This is a puzzle, since generally all folding models account for formation of secondary structure prior to formation of tertiary interactions, and the loss of these interactions *first* during unfolding. In fact, rationally, it is very difficult to envision how this could possibly be occurring even in light of the proposal that the intermediate species is probably an oligomer whose contacts with other subunits are primarily in the N-terminal domain. Could significant tertiary-like interactions occur even in the relative absence of secondary structural elements? This is something only a higher resolution probe such as NMR or HDX could tell us, although it would be extremely interesting to see how near-UV CD-monitored unfolding curves of CLIC1 at pH 5.5 overlaid with far-UV CD data. It would also probably be enlightening to analyse unfolding curves of mutants where the lone Trp residue had been translocated to the C-domain, in terms of the significance of this residue as a local structural probe.

While the CLIC1 intermediate satisfies a number of the requirements for a molten globule state, there are several areas where it deviates from the norm, such as its loss of secondary structure, its blue-shifted maximum emission wavelength and its higher affinity for ANS than typical molten-globule states, and thus it cannot be definitively described as a molten globule. On the other hand, according to folding funnel theory, the intermediate state consists of an ensemble of non-equivalent states, and exists on a continuum of states between native and unfolded states, so, although the CLIC1intermediate does not precisely fit the definition of a molten globule, it could be described as molten-globule-like. It should be noted

at this point that the notion that the molten globule state as a universal, general intermediate state has been discredited somewhat with the characterisation of so-called pre-molten globule and highly ordered molten globule states (Ptitsyn, 1995a; Uversky and Ptitsyn, 1994, 1996). It has been proposed rather that partially folded intermediate states which exist under different conditions make up an ensemble of substates, each with regions of unique structure, and therefore exist as discrete intermediates of specific proteins (Fink *et al.*, 1997).

It is already established that the N-domain of at least one other member of the GST family is less stable than the C-domain (Codreaunu *et al.*, 2005; Thompson *et al.*, 2006), in addition to the known flexibility of some of the structural elements of the N-domain of the CLIC family. Of significance here too is the fact that a number of molten globule states already discussed, which in many cases are the membrane-competent forms of those proteins, exist as intermediates with one intrinsically less stable domain unfolded and the other domain still relatively native-like in its retention of secondary structure and a structured tertiary fold. In many of these cases the only requirement for formation of the membrane-competent conformation is the low pH at the surface of the membrane and the existence of a negative surface potential there due to the presence of anionic lipids. The conclusion that has to be drawn here, therefore, in light of these facts and the experimental evidence offered, is that the intermediate state of CLIC1 at pH 5.5 is a dimeric or oligomeric conformation whose subunits interact with other subunits via contacts in their N-terminal domains, which are unfolded relative to their C-terminal domains. The formation of this state is favoured by the looser structure and lower stability of the native state at pH 5.5 relative to that at pH 7.0, and the greater stability of the intermediate state at pH 5.5 relative to the native state. Given the reducing conditions under which all experiments were performed, this state is unlikely to resemble the CLIC1 dimer formed under oxidising conditions (Littler *et al*., 2004). The CLIC1 intermediate state is very likely to be, as has been proposed previously (Fanucchi *et al.*, 2008), the pre-form of the membrane-competent conformation.

4.2.4. A membrane insertion model for CLIC1

Although the experiments performed in this study were all done in the absence of membranes, the idea was to try to mimic some of the factors that would be present at the surface of a biological membrane *in vivo*. While it is obvious that a denaturant such as urea is not present at the membrane surface, the existence of an intermediate at pH 7.0, 37 °C, with basically the same properties as the intermediate characterised in this study, indicates that all that is really required for formation of the membrane-competent intermediate state is physiological temperature and the lower pH at the surface of the membrane. The physiological role of this intermediate state would be to lower the energy barrier for insertion into the membrane. Protonation of ionisable groups on the native state at pH 5.5 destabilise the native state relative to the intermediate state, which may have a favourable influence on the ability of the protein to interact with membranes. Tulk *et al*. (2002) and Warton *et al*. (2002) observed that CLIC1-mediated ion channel activity was highest at lower pH values, in other words, when the native conformation of CLIC1 was least stable.

Based on the assumption that the intermediate does represent the membrane-competent form of CLIC1, a series of steps whereby the protein moves from a soluble, cytosolic conformation to an integral membrane-bound conformation can be proposed.

First, it should be noted that the PTM region of CLIC1 has a high helical propensity as determined by AGADIR analysis (Muñoz and Serrano, 1994) (Figure 4.4). In addition, a helix formed by this region has a distinct amphipathic character with a hydrophobic dipole moment, except for Lys37, which would play a role in chloride ion transport through the pore. The hydrophobic dipole moment is defined as a measure of the amphiphilicity of a structure (Eisenberg *et al.*, 1982). The hydrophobic thickness of the PTM is approximately 31 Å. Asp47 (if protonated) and Thr48 could potentially exist within the membrane interface region, due to their hydrophilicity. Trp35 would be positioned right in the centre of the hydrophobic portion of the membrane (Figure 4.5), a somewhat unexpected

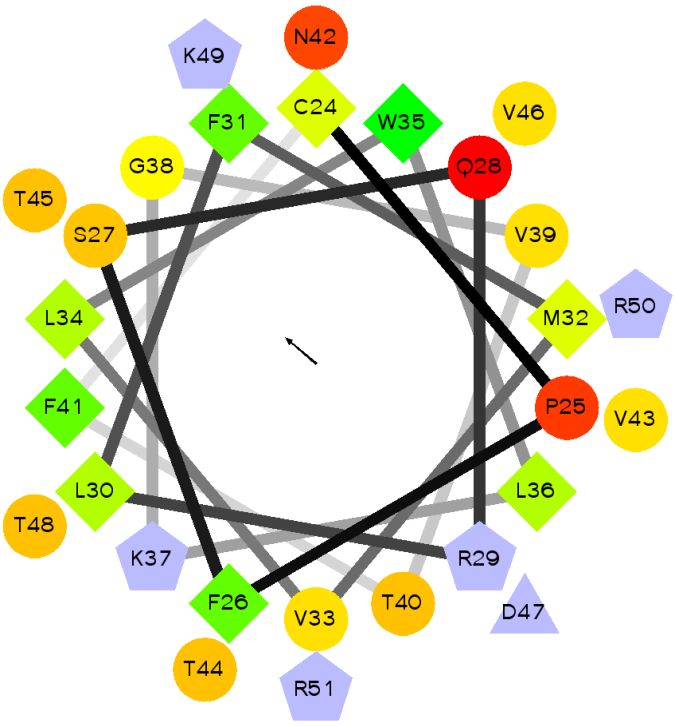

Figure 4.4. Helical wheel for the PTM region of CLIC1.

A helical wheel for residues 24-51 of CLIC1. Pro25 to Val46 are proposed to traverse the membrane, while the KRR motif from residues 49-51 act as a "plug" to anchor the helix in the membrane. Cys24 protrudes on the outside of the *trans* side of the membrane, where it is susceptible to redox regulation. The arrow indicates the hydrophobic moment. Hydrophilic residues are shown as circles, hydrophobic residues as diamonds, potentially negatively charged as triangles, and potentially positively charged as pentagons. Hydrophobicity is color coded: the most hydrophobic residue is green, and the amount of green decreases proportionally to the hydrophobicity, with zero hydrophobicity coded as yellow. Hydrophilic residues are coded red with pure red being the most hydrophilic (uncharged) residue, and the amount of red decreasing proportionally to the hydrophilicity. The potentially charged residues are light blue. Wheel created using the helical wheel programme available at http://www.rzlab.ucr.edu/scripts/wheel/wheel.pl.

location, given that Trp residues of membrane proteins are generally found just inside the interfacial region of the membrane surface, as discussed in Section 1.1.2. That is not to say, of course, that Trp residues are never found buried in the interior of the membrane. Cys24 would protrude into the interfacial region on the *trans* side of the membrane where it could play a role in redox regulation of channel function.

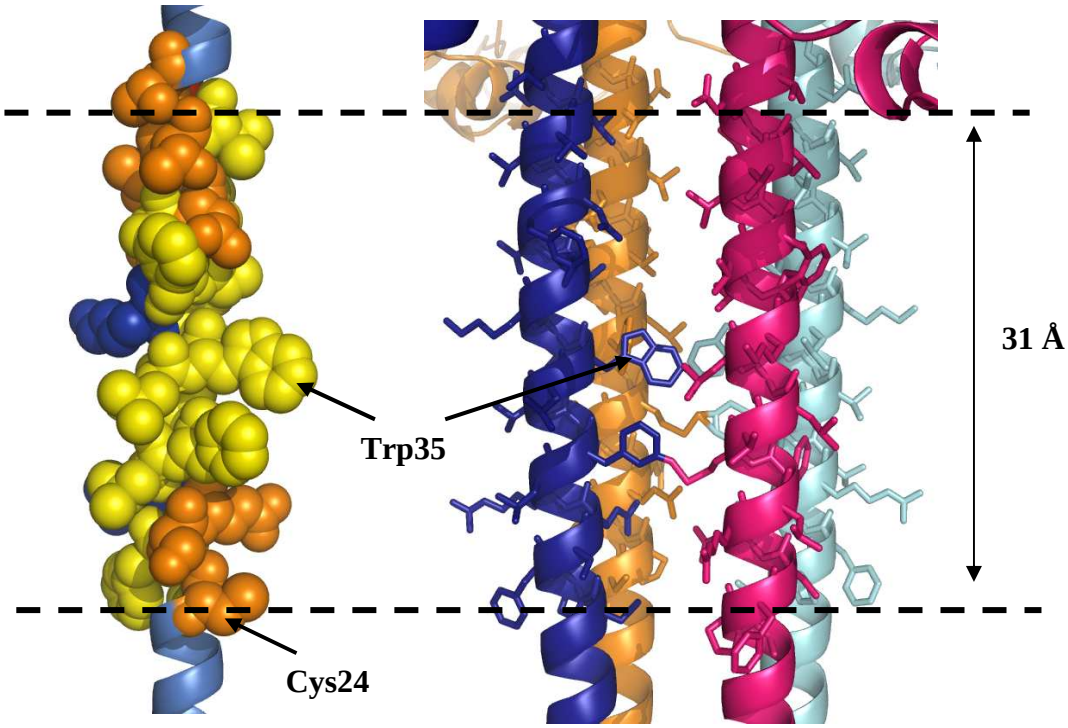

Figure 4.5. Possible orientation of CLIC1 PTM in membrane.

Schematic diagram of the PTM (residues Pro25 to Val46) including Cys24, Asp47 and Thr48, in a helical conformation, showing the possible orientation of this region within the membrane. **Left:** space-filling model of one helix with non-polar residues coloured yellow, uncharged polar residues coloured orange, basic residues blue and acidic residues (Asp47) shown in red. **Right:** proposed tetrameric conformation coloured by chain. In this conformation Trp35 would be buried facing inward toward the other helices. The dotted lines show the hydrophobic thickness of the membrane. Cys24, Asp47 and Thr48 would be in the interfacial region of the membrane.

The steps involved in insertion would probably follow the following outline (Figure 4.6): soluble, cytosolic or nucleoplasmic CLIC1 exists at physiological pH as a stable monomer with an asymmetrically distributed net negative charge giving it a distinct dipole moment. Salt bridges and hydrogen bonds on the surface act to stabilise the protein in a globular conformation.

Some signal, whether it be a change in pH or an oxidising signal due to changes in the cell cycle or some apoptotic response, cause the protein to relocate to the membrane surface, where it is subject to a strong net negative surface potential which brings with it a decrease in the local pH, and where the dielectric constant is lower than in bulk solution. An increase in net negative charge due to the lower pH at the membrane surface and protonation of ionisable residues on the surface of CLIC1 cause destabilisation of electrostatic interactions on the surface of the protein. The patch of uncharged surface area on one face of the protein helps to orient the protein relative to the membrane and as it comes closer to the interfacial region of the membrane, within reach of the multiple and complex electrostatic interactions in this region, CLIC1 loses a portion of its secondary and tertiary structure, mostly localised to the N-terminal domain, which is intrinsically less stable than the C-domain. The β1α1β2 supersecondary structure detaches from the surface of the N-domain and unfolds. Still bearing a net negative charge, but now with exposed hydrophobic surfaces, the N-domains of several monomers oligomerise to form a membrane-competent intermediate species which is stabilised by electrostatic interactions brought about by the low pH, and possibly also by hydrophobic interactions in the PTM region of the N-domain. This is the stable intermediate detected at low pH under mildly denaturing conditions in the absence of membranes during the urea-induced unfolding transition of the protein. Following this, the PTM takes on a helical conformation and inserts into the membrane to form the functional ion channel. The C-domain would probably be oriented with the α7-α8 face of the protein, with its hydrophobic patch, facing toward the membrane surface, and the opposite face, which has more basic residues, facing toward bulk solution, where its basic nature could help to concentrate Cl^- ions for passage through the channel.

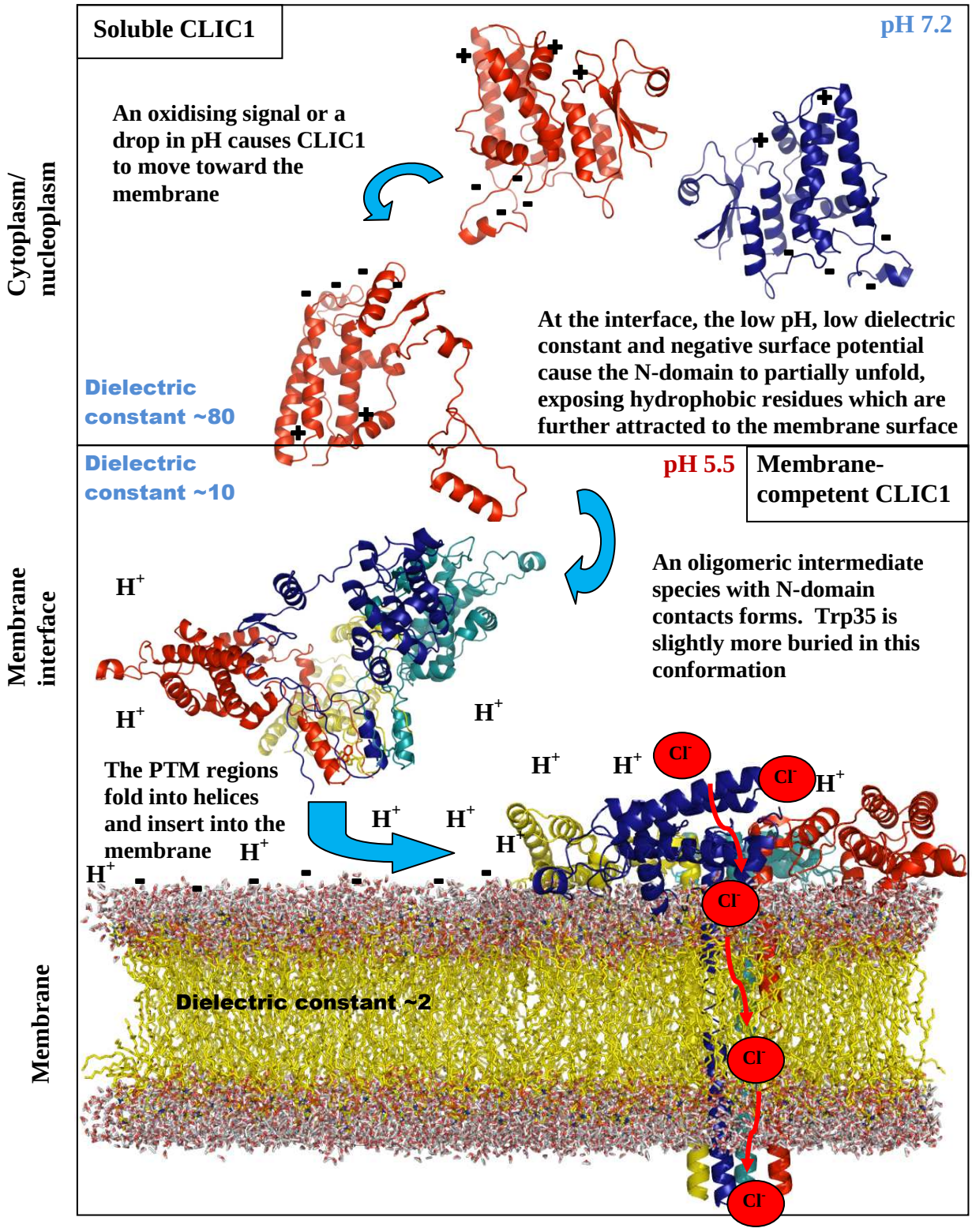

Figure 4.6. Proposed membrane insertion mechanism for CLIC1.

At physiological pH and temperature, CLIC1 is soluble and monomeric with a net negative charge and a dipole moment. An unknown signal, possibly a drop in pH or oxidising signal, causes the protein to move toward the membrane. The complex

electrostatic interactions in the membrane interface region, including a low pH and negative surface potential, interact with the charges on the surface of the protein, decreasing its stability and causing the intrinsically less stable N-terminal domain to partially unfold, exposing hydrophobic residues. The N-domains of different molecules interact with each other to form a stable dimeric or oligomeric pre-membrane insertion intermediate state possibly connected at the PTM regions. These regions then fold into helices and the protein inserts into the membrane to form a functional ion channel with a hydrophilic core. Membrane coordinates were taken from Heller *et al.*, 1993.

CHAPTER 5. REFERENCES

Adams, B., Burgess, R.J. and Pain, R.H. (1985) The folding and mutual interaction of the domains of yeast 3-phosphoglycerate kinase. *Eur. J. Biochem.* **152,** 715-720.

Adams, J. M., and Cory, S. (1998) The Bcl-2 protein family: Arbiters of cell survival, *Science* **281,** 1322-1326.

Adler, A.J., Greenfield, N.J. and Fasman, G.D. (1973) Circular dichroism and optical rotatory dispersion of proteins and polypeptides. *Methods Enzymol.* **27,** 675-735.

Al-Awqati, Q. (1995) Chloride channels of intracellular organelles. *Curr. Opin. Cell Biol.* **7,** 504–508.

Alberts, B., Johnson, A., Lewis, J., Raff, M., Roberts, K. and Walter, P. (2002) Molecular biology of the cell (4th Ed.), pp. 560-562, 615-618, 631-633, Garland Science, New York, USA.

Albi, E., Tomassoni, ML. and Viola-Magni, M. (1997) Effect of lipid composition on rat liver nuclear membrane fluidity. *Cell Biochem. Func.* **15,** 181-190.

Alhanaty, E., and Livne. A. (1974) Osmotic fragility of liposomes as affected by antihemolytic compounds. *Biochim. Biophys. Acta.* **339,** 146-155.

Allured, V.S., Collier, R.J., Carroll, S.F., McKay, D.B. (1986) Structure of exotoxin A of *Pseudomonas aeruginosa* at 3.0 Å resolution. *Proc. Natl. Acad. Sci. USA* **83,** 1310–1324.

Alouf, J.E. (2001) Pore-forming bacterial toxins: an overview. In: Pore-Forming Toxins (Ed.van der Goot, F.G.), pp. 1–14, Springer, Heidelberg, Germany.

Amann, E., Brosius, J., Ptashne, M. (1983) Vectors bearing a hybrid trp-lac promoter useful for regulated expression of cloned genes in *Escherichia coli*. *Gene* **25,** 167-178.

Andersen, O.S. and Koeppe, R.E. II (2007) Bilayer thickness and membrane protein function: An energetic perspective. *Annu. Rev. Biophys. Biomol. Struct*. **36,** 107–130.

Anfinsen, C.B. (1973) Principles that govern the folding of protein chains. *Science* **181,** 223-230.

Angelova, M.I. and Dimitrov, D.S. (1986) Liposome electroformation. *Faraday Discuss. Chem. Soc*. **81,** 303-311.

Antonsson, B., Montessuit, S., Lauper, S., Eskes, R. and Martinou, J.C. (2000) Bax oligomerization is required for channel-forming activity in liposomes and to trigger cytochrome *c* release from mitochondria. *Biochem. J.* **345,** 271–278.

Antonsson, B., Montessuit, S., Sanchez, B. and Martinou, J.C. (2001) Bax is present as a high molecular weight oligomer/complex in the mitochondrial membrane of apoptotic cells. *J. Biol. Chem*. **276,** 11615–11623.

Armstrong, R.N. (1997) Structure, catalytic mechanism and evolution of the glutathione transferases. *Chem. Res. Toxicol*. **10,** 2–18.

Aune, K.C., Salahuddin, A., Zarlengo, M.H. and Tanford, C. (1967) Evidence for residual structure in acid and heat denatured proteins. *J. Biol. Chem.* **242,** 4486-4489.

Aune, K. and Tanford, C. (1969) Thermodynamics of the denaturation of lysozyme by guanidine hydrochloride II. Dependence on denaturant concentration at 25 °C. *Biochemistry* **8,** 4586-4590.

Bailey, R.W., Dunker, A.K., Brown, C.J., Garner, E.C. and Griswold M.D. (2001) Clusterin, a binding protein with a molten globule-like region. *Biochemistry* **40,** 11828-11840.

Baker, E.N. and Hubbard, R E. (1984) Hydrogen bonding in globular proteins. *Prog. Biophys. Mol. Biol*. **44,** 97-179.

Balasubramanian, K. and Schroit, A.J. (2003) Aminophospholipid asymmetry: A matter of life and death. *Annu. Rev. Physiol*. **65,** 701-734.

Baldwin, R.L. and Roder, H. (1991) Characterizing protein folding intermediates. *Curr. Biol.* **1,** 218-220.

Baldwin, R.L. (2002) A new perspective on unfolded proteins. *Adv. Protein Chem*. **62,** 361–367.

Baldwin, R.L. (2003) In search of the energetic role of peptide hydrogen bonds. *J. Biol. Chem.* **278,** 17581-17588.

Ballard, J., Crabtree, J., Roe, B.A. and Tweten, R.K. (1995) The primary structure of *Clostridium septicum* alpha-toxin exhibits similarity with that of *Aeromonas hydrophila* aerolysin. *Infect. Immun*. **63,** 340**–**344.

Banerjee, T. and Kishore, N. (2005) 2,2,2-Trifluoroethanol-induced molten globule state of concanavalin A and energetics of 8-anilinonaphthalene sulfonate binding: Calorimetric and spectroscopic investigation. *J. Phys. Chem. B.* **109,** 22655-22662.

Bangham, A.D., De Gier, J., and Greville, G.D. (1967) Osmotic properties and water permeability of phospholipid liquid crystals. *Chem.Phys. Lipids*. **1,** 225-246.

Barlow, D.J. and Thornton, J.M. (1983) Ion-pairs in proteins. *J. Mol. Biol.* 168, 867-885.

Barrick, D. and Baldwin, R. L. (1993) The molten globule intermediate of apomyoglobin and the process of protein folding. *Protein Sci.* **2**, 869–876.

Bartlett, G.R. (1959) Phosphorus assay in column chromatography. *J. Biol. Chem.* **234,** 446-468.

Basanez, G., Zhang, J., Chau, B.N., Maksaev, G.I., Frolov, V.A., Brandt, T.A., Burch, J., Hardwick, J.M. and Zimmerberg, J. (2001) Pro-apoptotic cleavage products of Bcl-x_L form cytochrome *c*-conducting pores in pure lipid membranes. *J. Biol. Chem.* **276,** 31083**–**31091.

Baumrucker, C.R. and Keenan, T.W. (1973) Membranes of mammary gland. VIII. Isolation and composition of nuclei and nuclear membrane from bovine mammary gland. *J. Dair. Sci.* **57,** 24-31.

Becktel, W.J. and Schellman, J.A. (1987) Protein stability curves. *Biopolymers* **26,** 1859-1877.

Beecham, J. M. (1992) Global analysis of biochemical and biophysical data. *Methods Enzymol.* **210,** 37–54.

Belmonte, G., Pederzolli, C., MaWek, P. and Menestrina, G. (1993) Pore formation by the sea anemone cytolysin equinatoxin II in red blood cells and model lipid membranes. *J. Membr. Biol.* **131,** 11–22.

Bennett, M.J., Choe, S. and Eisenberg, D. (1994) Refined structure of dimeric diphtheria toxin at 2.0 Å resolution. *Protein Sci.* **3,** 1444–1463.

Bennion, B.J. and Daggett, V. (2003) The molecular basis for the chemical denaturation of proteins by urea. *Proc. Natl. Acad. Sci.* **100,** 5142-5147.

Berry, K.L., Bülow, H.E., Hall, D.H. and Hobert, O. (2003) A *C. elegans* CLIC-like protein required for intracellular tube formation and maintenance. *Science* **302,** 2134-2137.

Berry, K.L. and Hobert, O. (2006) Mapping functional domains of chloride intracellular channel (CLIC) proteins *in vivo*. *J. Mol. Biol.* **359,** 1316–1333.

Berryman, M. and Bretscher, A. (2000) Identification of a novel member of the chloride intracellular channel gene family (CLIC5) that associates with the actin cytoskeleton of placental microvilli. *Mol. Biol. Cell* **11,** 1509–1521.

Berryman, M.A. and Goldenring, J.R. (2003) CLIC4 is enriched at cell-cell junctions and colocalizes with AKAP350 at the centrosome and midbody of cultured mammalian cells. *Cell Motil. Cytoskeleton*. **56,** 159-172.

Berryman, M. A., Bruno, J., Price, J., and Edwards, J.C. (2004) CLIC-5A functions as a chloride channel *in vitro* and associates with the cortical actin cytoskeleton *in vitro* and *in vivo. J. Biol. Chem.* **279,** 34794-34801.

Betz, G., Aeppli, A., Menshutina, N. and Leuenberger, H. (2005) In vivo comparison of various liposome formulations for cosmetic application. *Int. J. Pharm*. **296,** 44-54.

Bilsel, O., Zitzewitz, J.A., Bowers, K.E. and Matthews, C.R. (1999) Folding mechanism of the α-subunit of tryptophan synthase, an α/β barrel protein: Global analysis highlights the interconversion of multiple native, intermediate, and unfolded forms through parallel channels. *Biochemistry* **38,** 1018-1029.

Birnboim, H.C. and Doly, J. (1979) A rapid alkaline extraction procedure for screening recombinant plasmid DNA. *Nucleic Acids Res.* **7,** 1513-1523.

Blok, M.C., van Deenen, L.L.M. and de Gier, J. (1976) Effect of the gel to liquid crystalline phase transition on the osmotic behaviour of phosphatidylcholine liposomes. *Biochim. Biophys. Acta.* **433,** 1-12.

Board, P.G., Coggan, M., Chelvanayagam, G., Easteal, S., Jermiin, L.S., Schulte, G.K., Danley, D.E., Hoth, L.R., Griffor, M.C., Kamath, A.V., Rosner, M.H., Chrunyk, B.A., Perregaux, D.E., Gabel, C.A., Geoghegan, K.F., and Pandit, J. (2000) Identification, characterization, and crystal structure of the omega class glutathione transferases. *J. Biol. Chem.* **275,** 24798–24806.

Board, P.G., Coggan, M., Watson, S., Gage, P.W. and Dulhunty, A.F. (2004) CLIC-2 modulates cardiac ryanodine receptor Ca^{2+} release channels. *Int. J. Biochem. Cell Biol.* **36,** 1599‑1612.

Born, M. (1920) Volume and heat of hydration of ions. *Z. Phys.* 1, 45-48.

Bortoleto, R.K. and Ward, R.J. (1999) A stability transition at mildly acidic pH in the alpha-hemolysin (alpha toxin) from *Staphylococcus aureus*. *FEBS Lett.* **459,** 438-442.

Bosshard, H.R., Marti, D.N. and Jelesarov, I. (2004) Protein stabilization by salt bridges: concepts, experimental approaches and clarification of some misunderstandings. *J. Mol. Recognit.* **17,** 1–16.

Botelho, A.V., Gibson, N.J., Thurmond, R.L., Wand Y. and Brown, M.F. (2002) Conformational energetics of rhodopsin modulated by nonlamellar-forming lipids. *Biochemistry* **41,** 6354-6368.

Brahms, S. and Brahms, J. (1980) Determination of protein secondary structure in solution by vacuum ultraviolet circular dichroism. *J. Mol. Biol.* **138,** 149.

Brand, L. and Witholt, B. (1967) Fluorescence measurements. *Methods Enzymol.* **11,** 776-856.

Brand, L. and Gohlke, J.R. (1972) Fluorescent probes for structure. *Annu. Rev. Biochem.* **41,** 843-868.

Bretscher, M.S. (1972) Asymmetric lipid bilayer structure for biological membranes. *Nature (New Biol.)* **236,** 11-12.

Brown, T.A. (1986) Gene cloning, an introduction. Pg. 30. Van Nostrand Reinhold, UK.

Carruthers, A., and Melchior, D.L. (1983) Studies of the relationship between bilayer water permeability and bilayer physical state. *Biochemistry* **22,** 5797–5807.

Chalvardjian, A. and Rudnicki, E. (1970) Determination of lipid phosphorus in the nanomolar range. *Anal. Biochem* **36,** 225-226.

Chan, H.S. and Dill, K A. (1990) The effects of internal constraints on the configurations of chain molecules. *J. Chem. Phys.* **92,** 3118-3135.

Chapman, C.J., Erdahl, W.E., Taylor, R.W. and Pfeiffer, D.R. (1991) Effects of solute concentration on the entrapment of solutes in phospholipid vesicles prepared by freeze-thaw extrusion. *Chem. Phys. Lipids* **60,** 201-208.

Chen, P.S., Jr., Toribara, T.Y. and Warner, H. (1956) Microdetermination of phosphorus. *Anal. Chem.* **28,** 1756-1758.

Chen, H.M., Leung, K.W., Thakur, N.N., Tan, A. and Jack, R.W. (2003) Distinguishing between different pathways of bilayer disruption by the related antimicrobial peptides, cecropins B, B1 and B3. *Eur. J. Biochem.* **270,** 911-920.

Chenal, A., Savarin, P., Nizard, P., Guillain, F., Gillet, D. and Forge, V. (2002) Membrane protein insertion regulated by bringing electrostatic and hydrophobic interactions into play: A case study with the translocation domain of the diphtheria toxin. *J. Biol. Chem.* **277,** 43425-43432.

Cho, J.-H., Sato, S., Horng, J.-C., Anil, B. and Raleigh, D.P. (2008) Electrostatic interactions in the denatured state ensemble: Their effect upon protein folding and protein stability. *Arch. Biochem. Biophys*. **469,** 20–28.

Choe, S., Bennett, M.J., Fujii, G., Curmi, P.M., Kantardjieff, K.A., Collier, R.J. and Eisenberg, D. (1992) The crystal structure of diphtheria toxin. *Nature 357*, 216-222.

Chung, C.T., Niemela, S.L. and Miller, R.H. (1989) One-step preparation of competent *Escherichia coli*: Transformation and storage of bacterial cells in the same solution. *Proc. Natl. Acad. Sci. USA* **86,** 2172-2175.

Chuang, J. Z., Milner, T. A., Zhu, M., and Sung, C. H. (1999) A 29 kDa intracellular chloride channel p64H1 is associated with large dense-core vesicles in rat hippocampal neurons. *J. Neurosci.* **19,** 2919–2928.

Chyan, C.L., Wormald, C., Dobson, C.M., Evans, P.A. and Baum, J. (1993) Structure and stability of the molten globule state of guinea pig α-lactalbumin: a hydrogen exchange study. *Biochemistry* **32,** 5681-5691.

Cocco, M.J., Kao, Y.H., Phillips, A.T. and Lecomte, J.T.J. (1992) Structural comparison of apomyoglobin and metaquomyoglobin: pH titration of histidines by NMR spectroscopy. *Biochemistry*, **31**, 6481–6491.

Codreanu, S.G., Thompson, L.C., Hachey, D.L., Dirr, H.W. and Armstrong, R.N. (2005) Influence of the dimer interface on Glutathione Transferase structure and dynamics revealed by amide H/D exchange mass spectrometry. *Biochemistry* **44,** 10605-10612.

Cordes, M.H.J., Davidsont, A.R. and Sauer, R.T. (1996) Sequence space, folding and protein design. *Curr. Opin. Struct. Biol*. **6,** 3-10.

Creighton, T.E. (1990) Protein folding. *Biochem. J.* **270,** 1-16.

Cromer, B.A., Morton, C.J., Board, P.G., and Parker, M.W. (2002) From glutathione transferase to pore in a CLIC. *Eur. Biophys. J.* **31,** 356-364.

Cromer, B.A., Gorman, M.A., Hansen, G., Adams, J.J., Coggan, M., Littler, D.R.,

Brown, L.J., Mazzanti, M., Breit, S.N., Curmi, P.M.G., Dulhunty, A.F., Board, P.G. and Parker, M.W. (2007) Structure of the Janus protein human CLIC2 *J. Mol. Biol.* **374,** 719–731.

De Gier, J. (1993) Osmotic behaviour and permeability properties of liposomes *Chem. Phys. Lipids* **64,** 187-196.

Desagher, S., Osen-Sand, A., Nichols, A., Eskes, R., Montessuit, S., Lauper, S., Maundrell, K., Antonsson, B., and Martinou, J.C. (1999) Bid-induced conformational change of Bax is responsible for mitochondrial cytochrome *c* release during apoptosis. *J. Cell. Biol.* **144,** 891-901.

Dill, K.A. (1990) Dominant forces in protein folding. *Biochemistry* **29,** 7133-7153.

Dill, K.A. and Shortle, D. (1991). Denatured states of proteins. *Annu. Rev. Biochem*. **60,** 795–825.

Dill, K.A. and Chan, H.S. (1997). From Levinthal to pathways to funnels. *Nature Struct. Biol.* **4,** 10-19.

Dill, K.A., Ozkan, S.B, Shell, M.S. and Weikl, T.R. (2008) The protein folding problem. *Annu. Rev. Biophys.* **37,** 289-316.

Dobson, C.M. and Karplus, M. (1999) The fundamentals of protein folding: Bringing together theory and experiment. *Curr. Opin. Struct. Biol*. **9,** 92-101.

Dolgikh, D.A., Gilmanshin, R.I., Brazhnikov, E.V., Bychkova, V.E., Semisotnov, G.V., Venyaminov, S.Y. and Ptitsyn, O.B. (1981) α-Lactalbumin compact state with fluctuating tertiary structure? *FEBS Lett.* **136,** 311–315.

Donovan, J.W. (1973) Spectrophotometric titration of the functional groups of proteins. *Methods Enzymol.* **27,** 525-548.

Doyle, D.A., Cabral, J.M., Pfuetzner, R.A., Kuo, A., Gulbis, J.M., Cohen, S.L., Chait, B.T. and Mackinnon, R. (1998) The structure of the potassium channel: molecular basis of K^+ conduction and selectivity. *Science* **280,** 69–77.

Draper, R.K. and Simon, M.I. (1980) The entry of diphtheria toxin into the mammalian cell cytoplasm: Evidence for lysosomal involvement. *J. Cell Biol*. **87,** 849–854.

Drews, J. (2000) Drug discovery: A historical perspective. *Science* **287,** 1960–1964.

Dulhunty, A., Gage, P., Curtis, S., Chelvanayagam, G., and Board, P. (2001) The glutathione transferase structural family includes a nuclear chloride channel and a ryanodine receptor calcium release channel modulator. *J. Biol. Chem.* **276,** 3319-3323.

Dulhunty, A.F., Pouliquin, P., Coggan, M., Gage, P.W. and Board, P.G. (2005) A recently identified member of the glutathione transferase structural family modifies cardiac RyR2 substate activity, coupled gating and activation by Ca^{2+} and ATP. *Biochem. J.* **390,** 333–343.

Duncan, R. R., Westwood, P. K., Boyd, A., and Ashley, R. H. (1997) Rat brain p64H1, expression of a new member of the p64 chloride channel protein family in endoplasmic reticulum. *J. Biol. Chem.* **272,** 23880–23886.

Dunker, A.K. and Rueckert, R.R. (1969) Observations on molecular weight determinations on polyacrylamide gel. *J. Biol. Chem.* **244**, 5074-5080.

Dutzler, R., Campbell, E.B., Cadene, M., Chait, B.T. and MacKinnon, R. (2002) X-ray structure of a ClC chloride channel at 3.0 Å reveals the molecular basis of anion selectivity. *Nature* **415,** 287-294.

Dutzler, R. (2006) The ClC family of chloride channels and transporters. *Curr. Opin. Struct. Biol.* **16,** 439-446.

Edwards, J.C. (1999) A novel p64-related Cl- channel: subcellular distribution and nephron segment-specific expression. *Am. J. Physiol.* **276,** F398–F408.

Edwards, J.C. (2006) The CLIC1 chloride channel is regulated by the cystic fibrosis transmembrane conductance regulator when expressed in Xenopus oocytes. *J. Membrane Biol.* 213, 39-46.

Eisenberg, D., Weiss, R.M., Terwilliger and Wilcox, W. (1982) Hydrophobic moments and protein structure. *Faraday Symp. Chem. Soc.* **17,** 109-120.

Ellens, H., Bentz, J. and Szoka, F.C. (1986) Destabilization of phosphatidylethanolamine liposomes at the hexagonal phase transition temperature. *Biochemistry* **25,** 285-294.

Epand, R.F., Martinou, J.-C., Montessuit, S. and Epand, R.M. (2002) Membrane perturbations induced by the apoptotic Bax protein. *Biochem. J.* **367,** 849-855.

Fanucchi, S., Adamson, R.J. and Dirr, H.W. (2008) Formation of an unfolding intermediate state of soluble chloride intracellular channel protein CLIC1 at acidic pH. *Biochemistry* **47,** 11674–11681.

Fernández-Salas, E., Sagar, M., Cheng, C., Yuspa, S. H., and Weinberg, W. C. (1999) p53 and tumor necrosis factor regulate the expression of a mitochondrial chloride channel protein. *J. Biol. Chem.* **274,** 36488–36497.

Fernández-Salas, E., Suh, K.S., Speransky, V.V., Bowers, W.L., Levy, J.M., Adams, T., Pathak, K.R., Edwards, L.E., Hayes, D.D., Cheng, C., Steven, A.C., Weinberg, W.C. and Yuspa, S.H. (2002) mtCLIC/CLIC4, an organellar chloride channel protein is increased by DNA damage and participates in the apoptotic response to p53. *Mol. Cell Biol.* **22,** 3610-3620.

Fersht, A.R. (1995) Optimisation of rates of protein folding - the nucleation-condensation mechanism and its implications. *Proc. Natl. Acad. Sci. USA* **92,** 10869**–**10873.

Fersht, A.R. (1997) Nucleation mechanisms in protein folding. *Curr. Opin. Struct. Biol.* **7,** 3-9.

Fink, A., Calciano, L., Goto, Y., Nishimura, M. and Swedberg, S. (1993) Characterization of the stable, acid-induced, molten globule-like state of staphylococcal nuclease. *Protein Sci.* **2,** 1155-1160.

Fink, A.L., Calciano, L.J., Goto, Y., Kurotsu, T. and Palleros D.R. (1994) Classification of acid denaturation of proteins: Intermediates and unfolded states. *Biochemistry* **33,** 12504-12511.

Fink, A.L., Oberg, K.A and Seshadri, S. (1997) Discrete intermediates versus molten globule models for protein folding: characterization of partially folded intermediates of apomyoglobin. *Fold. Des*. **3,** 19-25.

Finkelstein, A. (1976) Water and nonelectrolyte permeability of lipid bilayer membranes. *J. Gen. Physiol.* **68,** 127–135.

Fiske, C.H. and Subbarow, Y. (1925) The colorimetric determination of phosphorus. *J. Biol. Chem.* 66, 375-400.

Flewelling, R.F. and Hubbell, W.L. (1986) The membrane dipole potential in a total membrane potential model. Applications to hydrophobic ion interactions with membranes. *Biophys. J*. **49,** 541-552.

Freire, E., Murphy, K.P., Sanchez-Ruiz, J.M., Galisteo, M.L. and Privalov, P.L. (1992) The molecular basis of cooperativity in protein folding. Thermodynamic dissection of interdomain interactions in phosphoglycerate kinase. *Biochemistry* **31,** 250-256.

Freire, E. (1995) Thermodynamics of partly folded intermediates in proteins. *Annu. Rev. Biophys. Biomol. Struct.* **24**, 141-165.

Freskgård, P., Mårtensson, L., Jonasson, P., Jonsson, B. and Carlsson, U. (1994) Assignment of the contribution of the tryptophan residues to the circular dichroism spectrum of human carbonic anhydrase II. *Biochemistry* **33,** 14281-14288.

Friedli, M., Guipponi, M., Bertrand, S., Bertrand, D., Neerman-Arbez, M., Scott, H.S., Antonarakis, S.E. and Reymond, A. (2003) Identification of a novel member of the CLIC family, CLIC6, mapping to 21q22.12. *Gene* **320,** 31–40.

Garavito, R.M. and Ferguson-Miller, S. (2001) Detergents as tools in membrane biochemistry. *J. Biol. Chem.* **276,** 32403–32406.

Gasteiger, E., Hoogland, C., Gattiker, A., Duvaud, S., Wilkins, M.R., Appel, R.D. and Bairoch, A. (2005) Protein identification and analysis tools on the ExPASy server. In: The proteomics protocols handbook (Ed. Walker, J.M.), pp. 571-607. Humana Press, Totowna, NH, USA.

Gasymov, O.K. and Glasgow, B.J. (2007) ANS fluorescence: Potential to augment the identification of the external binding sites of proteins. *Biochim. Biophys. Acta* **1774**, 403–411.

Geiger, A., Rahman, A. and Stillinger, F.H. (1979) Molecular dynamics study of the hydration of Lennard-Jones solutes. *J. Chem. Phys*. **70,** 263-276.

Geny, B. and Popoff, M.R. (2006) Bacterial protein toxins and lipids: Pore formation or toxin entry into cells. *Biol. Cell* **98,** 667-678.

Gilbert, R.J.C. (2002) Pore-forming toxins. *Cell. Mol. Life Sci.* **59,** 832-844.

Gildenhuys, S., Wallace, L.A. and Dirr, H.W. (2008) Stability and unfolding of reduced *Escherichia coli* Glutaredoxin 2: A monomeric structural homologue of the Glutathione Transferase family. *Biochemistry* **47,** 10801-10808.

Goldberg, M.W., and Allen, T.D. (1995) Structural and functional organization of the nuclear envelope. *Curr. Opin. Cell Biol.* **7,** 301–309.

Gonen, T., Cheng, Y.F., Sliz, P., Hiroaki, Y., Fujiyoshi, Y., Harrison, S.C. and Walz, T. (2005) Lipid protein interactions in double-layered two dimensional AQP0 crystals. *Nature* **438,** 633-638.

Gouaux, E. (1997) Channel-forming toxins: tales of transformation. *Curr. Opin. Struct. Biol.* **7,** 566-573.

Gowri Shankar, B.A., Sarani, R., Michael, D., Mridula, P., Ranjani, C.V., Sowmiya, G., Vasundhar, B., Sudha, P., Jeyakanthan, J., Velmurugan, D. and Sekar, K. (2007) Ion pairs in non-redundant protein structures. *J. Biosci*. **32,** 693–704.

Greene, R.F. and Pace, C.N. (1974) Urea and guanidine hydrochloride denaturation of ribonuclease, lysozyme, α-chymotrypsin, and β-lactoglobulin. *J. Biol. Chem*. **249,** 5388-5393.

Greenhall, M.H., Yarwood, J., Brown, R. and Swart, R.M. (1998) Spectroscopic studies of model biological membranes in vesicles and Langmuir-Blodgett films. *Langmuir* **14,** 2619-2626.

Griffon, N., Jeanneteau, F., Prieur, F., Diaz, J. and Sokoloff, P. (2003) CLIC6, a member of the intracellular chloride channel family interacts with dopamine D(2)-like receptors. *Brain Res. Mol. Brain Res.* **117,** 47-57.

Griko, Y.V., Freire, E. and Privalov, P.L. (1994) Energetics of the α-lactalbumin states: a calorimetric and statistical thermodynamic study. *Biochemistry* **33,** 1889–1899.

Griko, Y.V., Freire, E., Privalov, G., Van Dael, H. and Privalov, P.L. (1995) The unfolding thermodynamics of *c*-type lysozymes. A calorimetric study of the heat denaturation of equine lysozyme. *J. Mol. Biol*. **252,** 447–459.

Grochulski, P., Masson, L., Borisova, S., Pusztai-Carey, M., Schwartz, J.-L., Brousseau, R. and Cygler, M. (1995) *Bacillus thuringiensis* CryIA(a) insecticidal toxin: crystal structure and channel formation. *J. Mol. Biol.* **254,** 447**–**464.

Gross, A., McDonnell, J. M., and Korsmeyer, S. J. (1999) BCL-2 family members and the mitochondria in apoptosis, *Genes Dev.* **13,** 1899-1911.

Guex, N., Peitsch, M., Schwede, T. and Diemand, A. (1995) Swiss-Model and the Swiss-PdbViewer: An environment for comparative protein modeling. *Electrophoresis* **18,** 2714-2723.

Gurtovenko, A.A. and Vattulainen, I. (2008) Membrane potential and electrostatics of phospholipid bilayers with asymmetric transmembrane distribution of anionic lipids. *J. Phys. Chem. B* **112,** 4629-4634.

Harpaz, Y., Gerstein, M. and Chothia, C. (1994) Volume changes on protein folding. *Structure* **2,** 641– 649.

Harrop, S.J., DeMaere, M.Z., Fairlie, W.D., Reztsova, T., Valenzuela, S.M., Mazzanti, M., Tonini, R., Qiu, M.R., Jankova, L., Warton, K., Bauskin, A.R., Wu, W.M., Pankhurst, S., Campbell, T.J., Breit, S.N., and Curmi, P.M.G. (2001) Crystal structure of a soluble form of the intracellular chloride ion channel CLIC1 (NCC27) at 1.4-Å resolution. *J. Biol. Chem.* **276,** 44993-45000.

Halskau, O., Underhaug, J., Frøystein, N.A. and Martínez, A. (2005) Conformational flexibility of *a*-lactalbumin related to its membrane binding capacity. *J. Mol. Biol.* **349,** 1072–1086.

Harding, S.E. (1997) Hydrodynamic properties of proteins. In: Protein structure – a practical approach (2nd ed.) (Ed. Creighton, T.E.), pp. 222-230. Oxford University Press, Oxford.

Haynie, D.T. and Freire, E. (1993) Structural energetics of the molten globule state. *Proteins Struct. Funct. Genet*. **16,** 115-140.

Hecht, M.H., Das, A., Go, A., Bradley, L.H. and Wei, Y. (2004) *De novo* proteins from designed combinatorial libraries. *Protein Sci.* **13,** 1711–23.

Heiss, N. S., and Poustka, A. (1997) Genomic structure of a novel chloride channel gene, CLIC2, in Xq28. *Genomics* **45,** 224–228.

Heller, H., Schaefer, M. and Schulten, K. (1993) Molecular dynamics simulation of a bilayer of 200 lipids in the gel and in the liquid crystal phase. *J. Phys. Chem.* **97,** 8343-8360.

Herskovits, T.T. (1967) Difference spectroscopy. *Methods Enzymol.* **11,** 748-775.

Honig, B., Ray, A. and Levinthal, C. (1976). Conformational flexibility and protein folding: rigid structural fragments connected by flexible joints in subtilisin BPN. *Proc. Natl Acad. Sci. USA* **73,** 1974-1978.

Honig, B.H., Hubbell, W.L. and Flewelling, R.F. (1986) Electrostatic interactions in membranes and proteins. *Annu. Rev. Biophys. Biophys. Chem.* **15,** 163-193.

Honig, B. (1999) Protein folding: From the Levinthal paradox to structure prediction. *J. Mol. Biol.* **293,** 283-293.

Hope, M.J., Bally, M.B., Webb, G., Cullis, P.R. (1985) Production of large unilamellar vesicles by a rapid extrusion procedure. Characterization of size distribution, trapped volume and ability to maintain a membrane potential. *Biochim. Biophys. Acta* **812,** 55-65.

Hunte, C. (2005) Specific protein-lipid interactions in membrane proteins. *Biochem. Soc. Trans*. **33,** 938-942.

Hunte, C. and Richers, S. (2008) Lipids and membrane protein structures. *Curr. Op. Str. Biol.* **18,** 406–411

Hsu, M.C. and Woody, R.W., (1971) The origin of the heme Cotton effects in myoglobin and hemoglobin. *J. Am. Chem.Soc.*, **93,** 3515.

Hwang, C., Sinskey, A.J. and Lodish, H.F. (1992) Oxidised redox state of glutathione in the endoplasmic reticulum. *Science* **257,** 1496-1502.

Illsley, N.P. and Verkman, A.S. (1987) Membrane chloride transport measured using a chloride-sensitive fluorescent probe. *Biochemistry* **26,** 1215-1219.

Inouye, M., Arnheim, N. and Sternglanz, R. (1973) Bacteriophage T7 lysozyme is an *N*-acetylmuramyl-L-alanine amidase. *J. Biol. Chem.* **248,** 7247-7252.

Ish-Horowicz, D. and Burke, J.F. (1981) Rapid and efficient cosmid cloning. *Nucleic Acids Res.* **9,** 2989.

Jalilian, C., Gallant, E.M., Board, P.G. and Dulhunty, A.F. (2008) Redox potential and the response of cardiac ryanodine receptors to CLIC-2, a member of the Glutathione *S*-Transferase structural family. *Antioxid. Redox Signal*. **10,** 1675–1686.

Janiak, F., Leber, B., and Andrews, D.W. (1994) Assembly of Bcl-2 into microsomal and outer mitochondrial membranes. *J. Biol. Chem.* **269,** 9842-9849.

Jayaraman, S., Verkman, A.S. (2000) Quenching mechanism of quinolinium-type chloride-sensitive fluorescent indicators. *Biophys. Chem*. 85, 49-57.

Jelinek, R. and Kolusheva, S. (2005) Membrane interactions of host-defense peptides studied in model systems. *Curr. Prot. Pep. Sci*. **6,** 103-114.

Jentsch, T.J., Stein, V., Weinreich, F. and Zdebik, A.A. (2002) Molecular structure and physiological function of chloride channels. *Physiol. Rev.* **82,** 503–568.

Jiang, J.X., and London, E. (1990) Involvement of denaturation-like changes in *Pseudomonas* exotoxin A hydrophobicity and membrane penetration determined by characterisation of pH and thermal transitions. Roles of two distinct conformationally altered states. *J. Biol. Chem.* **265,** 8636-8641.

Jiang, J.X., Abrams, F.S., and London, E. (1991) Folding changes in membrane inserted diphtheria toxin that play important roles in its translocation. *Biochemistry* **30,** 3857-3864.

Johnson, W.C., Jr. and Tinoco, I., Jr. (1972) Circular dichroism of polypeptide solutions in the vacuum ultraviolet. *J. Am. Chem. Soc.* **94,** 4389.

Johnson, J.E., Xie, M., Singh, L.M.R., Edge, R. and Cornell, R.B. (2003) Both acidic and basic amino acids in an amphitropic enzyme, CTP:phosphocholine cytidylyltransferase, dictate its selectivity for anionic membranes. *J. Biol. Chem.* **278,** 514–522.

Jones, M.N. (1995) The surface properties of phospholipid liposome systems and their characterisation. *Adv. Colloid Interface Sci.* 54, 93-128.

Kahya, N., Pecheur, E.I., de BoeiJ, W.P., Wiersma, D.A. and Hoekstra, D. (2001) Reconstitution of membrane proteins into giant unilamellar vesicles via peptide-induced fusion. *Biophys. J.* **81,** 1464-1474.

Kamtekar, S., Schiffer, J.M., Xiong, H., Babik, J.M. and Hecht, M.H. (1993) Protein design by binary patterning of polar and nonpolar amino acids. *Science* **262,** 1680–85.

Karmali, P.P. and Chaudhuri, A. (2007) Cationic liposomes as non-viral carriers of gene medicines: resolved issues, open questions, and future promises. *Med. Res. Rev.* **27,** 696-722.

Karplus, M. and Weaver, D. (1976) Protein-folding dynamics. *Nature* **260,** 404-406.

Kaufmann, T., Schlipf, S., Sanz, J., Neubert, K., Stein, R., and Borner, C. (2003) Characterization of the signal that directs $Bclx_L$, but not Bcl-2, to the mitochondrial outer membrane. *J. Cell. Biol.* **160,** 53-64.

Kaul, P., Silverman, J., Shen, W.H., Blanke, S.R., Huynh, P.D., Finkelstein, A. and Collier, R.J. (1996) Roles of Glu 349 and Asp 352 in membrane insertion and translocation by diphtheria toxin. *Protein Sci*. **5,** 687–692.

Kauzmann, W. (1959) Some factors in the interpretation of protein denaturation. *Adv. Protein Chem*. **14,** 1-63.

Kelly, J.W. (1998) The alternative conformations of amyloid proteins and their multi-step assembly pathways. *Curr. Opin. Struct. Biol*. **8,** 101-106.

Khandwala, A.S. and Kasper, C.B. (1971) The fatty acid composition of individual phospholipids from rat liver nuclear membrane and nuclei. *J. Biol. Chem.* **246,** 6242-6246.

Kim, D.E., Gu, H. and Baker, D. (1998) The sequences of small proteins are not extensively optimized for rapid folding by natural selection. *Proc. Natl. Acad. Sci. USA* **95,** 4982–86.

Kleinig, H. (1970) Nuclear membranes from mammalian liver: II. Lipid composition. *J. Biol. Chem*. **46**, 396-402.

Kleinig, H., Zentgraf, H., Comes, P. and Stadler, J. (1971) Nuclear membranes and plasma membranes from hen erythrocytes: II. Lipid composition. *J. Biol. Chem.* **246,** 2996-3000.

Kleinschmidt, J.H., and Tamm, L.K. (1996) Folding intermediates of a β-barrel membrane protein. Kinetic evidence for a multi-step membrane insertion mechanism. *Biochemistry* **35,** 12993-13000.

Koch, M.C., Steinmeyer, K., Lorenz, C., Ricker, K., Wolf, F., Otto, M., Zoll, B., Lehmann-Horn, F., Grzeschik, K.H. and Jentsch, T.J. (1992) The skeletal muscle chloride channel in dominant and recessive human myotonia. *Science* **257,** 797–800.

Kosower, E.M. (1986) Excited state electron and proton transfers. *Annu. Rev. Phys. Chem.* **37,** 127–156.

Kosower, E.M. and Kanety, H. (1983) Intramolecular donor–acceptor systems. 10. Multiple fluorescence from 8-(phenylamino)-1-naphthalenesulfonates. *J. Am. Chem. Soc.* **105,** 6236–6243.

Kraayenhof, R., Sterk, G.J. and Sang, H.W. (1993) Probing biomembrane interfacial potential and pH profiles with a new type of float-like fluorophores

positioned at varying distance from the membrane surface. *Biochemistry* **32,** 10057-10066.

Krishtalik, L.I. and Cramer W.A. (1995) On the physical basis for the *cis*-positive rule describing protein orientation in biological membranes. *FEBS Lett.* **369,** 140-143.

Krogh, A., Larsson, B., von Heijne, G., Sonnhammer, E.L.L. (2001) Predicting transmembrane protein topology with a hidden Markov model: application to complete genomes. *J. Mol. Biol.* **305,** 567-580.

Kumar, S. and Nussinov, R. (1999) Salt bridge stability in monomeric proteins. *J. Mol. Biol.* **293,** 1241-1255.

Kumar, S. and Nussinov, R. (2001) Fluctuations in ion pairs and their stabilities in proteins *Proteins: Struct. Func. Genet.* **43,** 433–454.

Kuwajima, K. (1977) A folding model of alpha-lactalbumin deduced from the three-state denaturation mechanism. *J Mol Biol.***114,** 241–258.

Kuwajima, K. (1989) The molten globule state as a clue for understanding the folding and cooperativity of globular-protein structure. *Proteins: Struct. Funct. Genet.* **6,** 87-103.

Kuwajima, K., Yamaya, H., and Sugai, S. (1996) The burst-phase intermediate in the refolding of β-lactoglobulin studied by stopped-flow circular dichroism and absorbance spectroscopy. *J. Mol. Biol.* **264,** 806-822.

Kyte, J. and Doolittle, R.F. (1982). A simple method for displaying the hydropathic character of a protein. *J. Mol. Biol.* **157,** 105–132.

Kyte, J. (1995) Structure in protein chemistry. Pp. 503-506. Garland Publishing, Inc., New York.

Laemmli, U.K. (1970) Cleavage of structural proteins during the assembly of the head of bacteriophage T4. *Nature* **227**, 680-685.

Lakey, J.H., Parker, M.W., González-Mañas, J.M., Duche, D., Vriend, G., Baty, D. and Pattus, F. (1994) The role of electrostatic charge in the membrane insertion of colicin A. Calculation and mutation. *Eur. J. Biochem.* **220,** 155**–**163.

Lakowicz, J. R. (1999) Principles of fluorescence spectroscopy. Pp 11-14, 188, 237-249, 447-449. Plenum Press, New York.

Lande, M.B., J.M. Donovan, and Zeidel, M.L. (1995) The relationship between membrane fluidity and permeabilities to water, solutes, ammonia, and protons. *J. Gen. Physiol.* **106,** 67–84.

Landry, D., Sullivan, S., Nicolaides, M., Redhead, C., Edelman, A., Field, M., al-Awqati, Q., and Edwards, J. (1993) Molecular cloning and characterization of p64, a chloride channel protein from kidney microsomes. *J. Biol. Chem.* **268,** 14948–14955.

Landolt-Marticorena, C., Williams, K.A., Deber, C.M. and Reithmeier, R.A.F. (1993) Non-random distribution of amino acids in the transmembrane segments of human type I single span membrane proteins. *J. Mol. Biol*. **229,** 602–608.

Lange, C., Nett, J.H., Trumpower, B.L. and Hunte, C. (2001) Specific roles of protein–phospholipid interactions in the yeast cytochrome bc_1 complex structure. *EMBO J.* **20,** 6591–6600.

Lasch, J., Weissig, V. and Brandl, M. (2003) Preparation of liposomes. In: Liposomes, 2nd Ed. (Ed. Torchilin, V.P. and Weissig, V.). Oxford University Press, Oxford, UK.

Lee, A.G. (2003) Lipid–protein interactions in biological membranes: a structural perspective. *Biochim. Biophys. Acta* **1612,** 1-40.

Lee, A.G. (2004) How lipids affect the activities of integral membrane proteins. *Biochim. Biophys. Acta* **1666,** 62-87.

Lee, A.G. (2005) How lipids and proteins interact in a membrane: a molecular approach. *Mol. BioSyst.* **1,** 203–212

Lehtovaara, P. (1978) Anomalous migration of leghaemoglobin on sodium dodecyl sulphate/polyacrylamide-gel electrophoresis. *Biochem. J.* **169,** 251-253.

Lesser, G.J. and Rose, G.D. (1990) Hydrophobicity of amino acid subgroups in proteins. *Proteins: Struct. Func. Genet*. **8,** 6-13.

Levinthal, C. (1968) Are there pathways for protein folding? *J. Chem. Phys*. **65,** 44–45.

Levinthal, F., Todd, A.P., Hubbel, W.L. and Levinthal, C. (1991) A single tryptic fragment of colicin E1 can form an ion channel: stoichiometry confirms kinetics. *Proteins* **11,** 254**–**262.

Leyland-Jones, B. (1993) Targeted drug delivery. *Semin. Oncol.* **20,** 12-17.

Li, J., Carrol, J. and Ellar, D.J. (1991) Crystal structure of insecticidal delta-endotoxin from *Bacillus thuringiensis* at 2.5 Å resolution. *Nature* **353,** 815-821.

Li, Y., Li, D., Zeng, Z. and Wang, D. (2006) Trimeric structure of the wild soluble chloride intracellular ion channel CLIC4 observed in crystals. *Biochem. Biophys. Res. Commun.* **343,** 1272–1278.

Li, S.D. and Huang, L. (2006) Gene therapy progress and prospects: Non-viral gene therapy by systemic delivery, *Gene Ther*. **13,** 1313–1319.

Liang, J. and Dill, K.A. (2001) Are proteins well-packed? *Biophys. J.* **81,** 751–766.

Linderstrøm-Lang, K. (1924) The ionisation of proteins. *Compt. Rend. Trav. Lab. Carlsberg* **15,** 1-29.

Lins, L. and Brasseur, R. (1995) The hydrophobic effect in protein folding. *FASEB J.* **9,** 535-540.

Littler, D.R., Harrop, S.J., Fairlie, W.D., Brown, L.J., Pankhurst, G.J., Pankhurst, S., DeMaere, M.Z., Campbell, T.J., Bauskin, A.R., Tonini, R., Mazzanti, M., Breit, S.N. and Curmi, P.M.G. (2004) The intracellular chloride ion channel protein CLIC1 undergoes a redox-controlled structural transition. *J. Biol. Chem.* **279**, 9298-9305.

Littler, D.R., Assaad, N.N., Harrop, S.J., Brown, L.J., Pankhurst, G.J., Luciani, P., Aguilar, M.I., Mazzanti, M., Berryman, M.A., Breit, S.N., Curmi, P.M. (2005) Crystal structure of the soluble form of the redox-regulated chloride ion channel protein CLIC4. *FEBS J.* **272,** 4996-5007.

Littler, D.R., Harrop, S.J., Brown, L.J., Pankhurst, G.J., Mynott, A.V., Luciani, P., Mandyam, R.A., Mazzanti, M., Tanda, S., Berryman, M.A., Breit, S.N. and Curmi, P.M.G. (2007) Comparison of vertebrate and invertebrate CLIC proteins: The crystal structures of *Caenorhabditis elegans* EXC-4 and *Drosophila melanogaster Dm*CLIC. *Proteins Struct. Func. Genet.* **71,** 364-378.

Liu, L., Yonetani, T. (1994) Preparation and characterization of liposome-encapsulated haemoglobin by a freeze-thaw method. *J. Microencaps.* **11,** 409-421.

Lloyd, S.E., Pearce, S.H., Fisher, S.E., Steinmeyer, K., Schwappach, B., Scheinman, S.J., Harding, B., Bolino, A., Devoto, M., Goodyer, P., Rigden, S.P., Wrong, O., Jentsch, T.J., Craig, I.W. and Thakker, R.V. (1996) A common molecular basis for three inherited kidney stone diseases. *Nature* **379,** 445**–**449.

Lomakin, A., Chung, D.S., Benedek, G.B., Kirscher, D.A. and Teplow, D.B. (1996) On the nucleation and growth of amyloid β-protein fibrils: Detection of nuclei and quantification of rate constraints. *Proc. Natl. Acad. Sci. USA* **93,** 1125-1129.

London, E. (1992) Diphtheria toxin: membrane interaction and membrane translocation. *Biochim. Biophys. Acta.* **1113,** 25-51.

London, E. (2002) Insights into lipid raft structure and formation from experiments in model membranes. *Curr. Opin. Struct. Biol.* **12,** 480-486.

Luque, I., Leavitt, S.A and Freire, E. (2002) The linkage between protein folding and functional cooperativity: Two sides of the same coin? *Ann. Rev. Biophys. Biomol. Str.* **31,** 235-256.

MacDonald, R.C., MacDonald, R.I., Menco, B.P.M., Takeshita, K., Subbarao N.K. and Hu, L. (1991) Small-volume extrusion apparatus for preparation of large, unilamellar vesicles. *Biochim. Biophys. Acta* **1061,** 297-303.

Maeda, K., Haraguchi, M., Kuramasu, A., Sato, T., Ariake, K., Sakagami, H., Kondo, H., Yanai, K., Fukunaga, K., Yanagisawa, T. and Sukegawa, J. (2008)

CLIC4 interacts with histamine H3 receptor and enhances the receptor cell surface expression. *Biochem. Biophys. Res. Comm.* **369,** 603–608.

Makowski, G.S. and Ramsby, M.L. (1997) Protein molecular weight determination by sodium dodecyl sulfate polyacrylamide gel electrophoresis. In Protein structure, a practical approach (2nd ed.) (Ed. Creighton, T.E.), pp. 3, 4. Oxford University Press, UK.

Manceva, S.D., Pusztai-Carey, M. and Butko, P. (2004) Effect of pH and ionic strength on the cytolytic toxin Cyt1A: a fluorescence spectroscopy study. *Biochim. Biophys. Acta* **1699,** 123-130.

Manojlovic, V., Winkler K., Bunjes, V., Neub, A., Schubert, R., Bugarski, B. and G. Leneweit (2008) Membrane interactions of ternary phospholipid/cholesterol bilayers and encapsulation efficiencies of a RIP II protein. *Colloids Surf. B: Biointerfaces* **64,** 284–296.

Mathai, J.C., Tristram-Nagle, S., Nagle, J.F. and Zeidel, M.L. (2008) Structural determinants of water permeability through the lipid membrane. *J. Gen. Physiol.* **131,** 69–76.

Matsuda, R., Kaneko, N. and Horikawa, Y. (1997) Presence and comparison of Ca^{2+} transport activity of annexins I, II, V, and VI in large unilamellar vesicles. *Biochem. Biophys. Res. Comm.* **237,** 499-503.

Matsuyama, S., Llopis, J., Deveraux, Q.L., Tsien, R.Y. and Reed, J.C. (2000) Changes in intramitochondrial and cytosolic pH: Early events that modulate caspase activation during apoptosis. *Nat. Cell Biol.* **2,** 318**–**325.

Matthew, J.B., Hanania, G.I.H. and Gurd, F.R.N. (1979) Coordination complexes and catalytic properties of proteins and related substances. 104. Electrostatic effects in hemoglobin: hydrogen ion equilibriums in human deoxy- and oxyhemoglobin A *Biochemistry* **18,** 1919-1928.

Matthew, J.B. (1985) Electrostatic effects in proteins. *Ann. Rev. Biophys. Biophys. Chem.* **14,** 387-417.

Matthew, J.B., Gurd, F.R.N., García-Moreno E.B., Flanagan, M.A., March, K.L. and Shire, S.J. (1985) pH dependent processes in proteins. *CRC Crit. Rev. Biochem*. **18,** 91-197.

Matthew, J.B. and Gurd, F.R.N. (1986) Calculation of electrostatic interactions in proteins. *Methods Enzymol*. **130,** 413-436.

Mayer, L.D., Hope, M.J., Cullis, P.R. and Janoff., A.S. (1985) Solute distributions and trapping efficiencies observed in freeze-thawed multilamellar vesicles. *Biochim. Biophys. Acta*. **817,** 193-196.

Mayhew, E., Lazo. R., Vail, W.J., King, J. and Green, A.M. (1984) Characterisation of liposomes prepared using a microemulsifier. *Biochim. Biophys. Acta.* **775,** 169-174.

McLaughlin, S. (1989) The electrostatic properties of membranes. *Annu. Rev. Biophys. Biophys. Chem.* **18,** 113-136.

Menestrina, G., Forti, S., and Gambale, F. (1989) Interaction of tetanus toxin with lipid vesicles. Effects of pH, surface charge, and transmembrane potential on the kinetics of channel formation. *Biophys J*. **55,** 393-405.

Menestrina, G., Pederzolli, C., Forti, S. and Gambale, F. (1991) Lipid interaction of *Pseudomonas eruginosa* exotoxin A. *Biophys. J.* **60,** 1388**–**1400.

Menestrina, G., Dalla Serra, M., Comai, M., Coraiola, M., Viero, G., Werner, S., Colin, D.A., Monteil, H. and Prévost G. (2003) Ion channels and bacterial infection: The case of β-barrel pore-forming protein toxins of *Staphylococcus aureus. FEBS Lett.* **552,** 54-60.

Mere, J., Morion-Guyot, J., Bonhoure, A., Chiche, L. and Beaumelle, B. (2005) Acid-triggered membrane insertion of Pseudomonas exotoxin A involves an original mechanism based on pH-regulated tryptophan exposure. *J. Biol. Chem*. **280,** 21194-21201.

Miller, M., Park, M. K., and Hanover, J. A. (1991) Nuclear pore complex: structure, function, and regulation. *Physiol. Rev.* **71,** 909–949.

Millsman, M.H.W., Schwendener, R.A. and Weder, H.G. (1978) The preparation of large single bilayer liposomes by a fast and controlled dialysis. *Biochim. Biophys. Acta.* **512,** 147-155.

Milton, R.H., Abeti, R., Averaimo, S., DeBiasi, S., Vitellaro, L., Jiang, L., Curmi, P.M.G., Breit, S.N., Duchen, M.R. and Mazzanti, M. (2008) CLIC1 function is required for β-amyloid-induced generation of reactive oxygen species by microglia. *J. Neurosci*. **28,** 11488–11499.

Mimms, L.T., Zampighi, G., Nozaki, Y., Tanford C. and Reynolds J.A. (1981) Phospholipid vesicle formation and transmembrane protein incorporation using octyl glucoside. *Biochemistry* **20,** 833-840.

Mirsky, A.E., and Pauling, L. (1936) On the structure of native, denatured, and coagulated proteins. *Proc. Natl. Acad. Sci. USA* **22,** 439-447.

Mitchell, D.J., Tiddy, G.J.T., Waring, L., Bostock T. and McDonald, M.P. (1983) Phase behavior of polyoxyethylene surfactants with water. Mesophase structures and partial miscibility (cloud points). *J. Chem. Soc. Faraday Trans.* **79,** 975–1000.

Miyamoto, S., T. Maeda, and S. Fujime. (1988) Change in membrane elastic modulus on activation of glucose transport system of brush border membrane vesicles studied by osmotic swelling and dynamic light scattering. *Biophys. J.* **53,** 505-512.

Miyashita, T. and Reed, J.C. (1995) Tumor suppressor p53 is a direct transcriptional activator of the human *bax* gene. *Cell* **80,** 293–299.

Moffat, B.A. and Studier, F.W. (1987) T7 lysozyme inhibits transcription by T7 RNA polymerase. *Cell* **49,** 221-227.

Morozova, L.A., Haynie, D.T., Arico-Muendel, C., Van Dael, H. and Dobson, C.M. (1995) Structural basis of the stability of a lysozyme molten globule. *Nature Struct. Biol*. **2,** 871–875.

Morris, C. (1990) Mechanosensitive ion channels. *J. Membr. Bio.* **113,** 93-107.

Mozafari, M.R. (2005) Liposomes: An overview of manufacturing techniques. *Cell. Mol. Biol. Lett.* **10,** 711-719.

Muchmore, S.W., Sattlen, M., Liang, H., Meadows, R.P., Harlan, J.E., Yoon, H.S., Nettesheim, D., Chang, B.S., Thompson, C.B., Wong, S.L., Ng, S.L., and Fesik, S.W. (1996) X-ray and NMR structure of human Bcl-x_L, an inhibitor of programmed cell death. *Nature* **381,** 335-341.

Muga, A., Gonzalez-Manas, J.M., Lakey, J.H., Pattus, F. and Surewicz, W.K. (1993) pH-dependent stability and membrane interaction of the pore-forming domain of colicin A. *J. Biol. Chem*. **268,** 1553-1557.

Mui, B.L.-S., Cullis, P.R., Evans, E.A. and Madden, T.D. (1993) Osmotic properties of large unilamellar vesicles prepared by extrusion. *Biophys. J.* **64,** 443-453.

Muñoz, V. and Serrano, L. (1994) Elucidating the folding problem of a-helical peptides using empirical parameters, II. Helix macrodipole effects and rational modification of the helical content of natural peptides. *J. Mol. Biol*. **245,** 275-296.

Murray, D., Arbuzova, A., Hangyas-Mihalyne, G., Gambhir, A., Ben-Tal, N., Honig, B. and McLaughlin, S. (1999) Electrostatic properties of membranes containing acidic lipids and adsorbed basic peptides: Theory and experiment. *Biophys. J.* **77,** 3176-3188.

Musse, A.A. and Merrill, A.R. (2003) The molecular basis for the pH-activation mechanism in the channel-forming bacterial colicin E1. *J. Biol. Chem*. 278, 24491-24499.

Myers, J.K., Pace, C.N. and Scholtz, J.M. (1995) Denaturant *m*-values and heat capacity changes: Relation to changes in accessible surface areas of protein unfolding. *Protein Sci.* **4,** 2138-2148.

Nasr, M., Mansour, S., Mortada, N.D. and El Shamy, A.A. (2008) Lipospheres as carriers for topical delivery of aceclofenac: preparation, characterization and *in vivo* evaluation. *AAPS PharmSciTech.* **9,** 154-62.

Neitcheva, T. and Peeva, D. (1995) Phospholipid composition, phospholipase A and sphingomylelinase activities in rat liver nuclear membrane and matrix. *Int. J. Biochem. Cell Biol.* **27,** 995-1001.

Nguyen, M., Millar, D.G., Yong, V.W., Korsmeyer, S.J., and Shore, G.C. (1993) Targeting of Bcl-2 to the mitochondrial outer membrane by a COOH-terminal signal anchor sequence. *J. Biol. Chem.* **268,** 25265-25268.

Nishizawa, T., Nagao, T., Iwatsubo, T., Forte, J. G., and Urushidani, T. (2000) Molecular cloning and characterization of a novel chloride intracellular channel-related protein, parchorin, expressed in water-secreting cells. *J. Biol. Chem.* **275,** 11164–11173.

Nolan, V., Perduca, M., Monaco, H.L. and Montich, G.G. (2005) Chicken liver bile acid-binding protein is in a compact partly folded state at acidic pH. Its relevance to the interaction with lipid membranes. *Biochemistry* **44,** 8486-8493.

Nölting, B. and Agard, D.A. (2008) How general is the nucleation–condensation mechanism? *Proteins: Struct. Func. Genet*. **73,** 754**–**764.

Novarino, G., Fabrizi, C., Tonini, R., Denti, M.A., Malchiodi-Albedi, F., Lauro, G.M., Sacchetti, B., Paradisi, S., Ferroni, A., Curmi, P.M., Breit, S.N., and Mazzanti, M. (2004) Involvement of the intracellular ion channel CLIC1 in microglia-mediated β-amyloid-induced neurotoxicity. *J. Neurosci.* **24,** 5322-5330.

Ohgushi, M. and Wada, A. (1983) Molten globule state: a compact form of protein with mobile side-chains. *FEBS Lett*. **164,** 21-24.

Olsen, F., Hunt, C.A., Szoka, F.C., Vail, W.J. and Papahadjopoulos, D. (1979) Preparation of liposomes of defined size distribution by extrusion through polycarbonate membranes. *Biochim. Biophys. Acta*. **557,** 9-23.

Pace, C.N. (1986) Determination and analysis of urea and guanidine hydrochloride denaturation curves. *Methods Enzymol.* **131,** 266-280.

Pace, C.N. (1990) Conformational stability of globular proteins. *Trends Biochem. Sci.* **15,** 14-17.

Pace, C.N., Laurents, D.V. and Thomson, J.A. (1990) pH dependence of the urea and guanidine hydrochloride denaturation of ribonuclease A and ribonuclease T1. *Biochemistry*, **29,** 2564-2572.

Pace, C.N., Vajdos, F., Fee, L., Grimsley, G. and Gray, T. (1995) How to measure and predict the molar absorption coefficient of a protein. *Protein Sci.* **11**, 2411-2423.

Pace, C.N., Shirley, B.A., McNutt, M., Gajiwala, K. (1996) Forces contributing to the conformational stability of proteins. *FASEB J.* **10,** 75-83.

Pace, C.N. and Scholtz, J.M. (1997) Measuring the conformational stability of a protein. In Protein structure, a practical approach (2nd ed.) (Ed. Creighton, T.E.), pp. 299. Oxford University Press, UK.

Pace, C.N., Alston R.W. and Shaw K.L. (2000) Charge-charge interactions influence the denatured state ensemble and contribute to protein stability. *Protein Sci*. **9,** 1395-1398.

Pain, R. (2004) Determining the CD spectrum of a protein. In: Current protocols in Protein Science, Vol. 1, 7.6.1-7.7.20. John Wiley and Sons, Inc., New York.

Papahadjopoulos, D. and Miller, N. (1967) Phospholipid model membranes. I. Structural characteristics of hydrated liquid crystals. *Biochim. Biophys. Acta* **135,** 624-638.

Papahadjopoulos, D. and Watkins, J.C. (1967) Phospholipid model membranes. II. Permeability properties of hydrated liquid crystals. *Biochim. Biophys. Acta.* **135,** 639-652.

Parker, M.W., Pattus, F., Tucker, A.D. and Tsernoglou, D. (1989) Structure of the membrane-pore-forming fragment of colicin A. *Nature* **337,** 93-96.

Parker, M.W., Tucker, A.D., Tsernoglou, D. and Pattus, F. (1990) Insights into membrane insertion based on studies of colicins. *Trends Biochem. Sci.* **15,** 126-129.

Parker, M.W., Postma, J.P.M., Pattus, F., Tucker, A.D. and Tsernoglou, P. (1992) Refined structure of the pore-forming domain of Colicin A at 2.4 Å resolution *J.Mol. Biol.* **224,** 639-657.

Parker, M.W., and Pattus, F. (1993) Rendering a membrane protein soluble in water: a common packing motif in bacterial protein toxins. *Trends Biochem. Sci.* **18,** 391-395.

Parker, M.W., Buckley, J.T., Postma, J.P., Tucker, A.D., Leonard, K., Pattus, F. and Tsernoglou, D. (1994) Structure of the *Aeromonas* toxin proaerolysin and the membrane-channel states. *Nature* **367,** 292**–**295.

Parker, M.W. and Feil, S.C. (2005) Pore-forming protein toxins: from structure to function. *Prog. Biophys. Mol. Biol.* **88,** 91**–**142.

Paula, S., Volkov, A.G. and Deamer D.W. (1998) Permeation of halide anions through phospholipid bilayers occurs by the solubility-diffusion mechanism. *Biophys. J.* **74,** 319–327.

Peng, Z.Y. and Kim, P.S. (1994) A protein dissection study of a molten globule. *Biochemistry* **33,** 2136-2141.

Perkins, S. J. (1986) Protein volumes and hydration effects. The calculations of partial specific volumes, neutron scattering matchpoints and 280-nm absorption coefficients for proteins and glycoproteins from amino acid sequences. *Eur. J. Biochem.* **157**, 169–180.

Perkins, W.R., Minchey, S.R., Ahl P.L. and Janoff A.S. (1993) The determination of liposome captured volume. *Chem. Phys. Lipids* **64,** 197-217.

Peters, R., and Beck, K. (1983) Translational diffusion in phospholipid monolayers measured by fluorescence microphotolysis. *Proc. Natl. Acad. Sci. USA.* **80,** 7183-7187.

Petosa, C., Collier, R.J., Klimpel, K.R., Leppla, S.H. and Liddington, R.C. (1997) Crystal structure of the anthrax toxin protective antigen. *Nature* **385,** 833**–**838.

Petros, A.M., Medek, A., Nettesheim, D.G., Kim, D.H., Yoon, H.S., Swift, K., Matayoshi, E.D., Oltersdorf, T. and Fesik, S.W. (2001) Solution structure of the antiapoptotic protein Bcl-2. *Proc. Natl. Acad. Sci. USA.* **98,** 3012–3017.

Petrova, D.T., Asif, A.R., Armstrong, V.W., Dimova, I., Toshev, T., Yaramov, N., Oellerich, M. and Toncheva, D. (2008) Expression of chloride intracellular channel protein 1 (CLIC1) and tumor protein D52 (TPD52) as potential biomarkers for colorectal cancer. *Clin. Biochem*. **41,** 1224–1236.

Phillips, N.C. (1992) Liposomal carriers for the treatment of acquired immune deficiency syndrome. *Bull. Inst. Pasteur* **90,** 205-230.

Pick, U. (1981) Liposomes with a large trapping capacity prepared by freezing and thawing of sonicated phospholipid mixtures. *Arch. Biochem. Biophys.* **212,** 186-194.

Pitt-Rivers, R. and Impiombato, F.S.A. (1968) The binding of sodium dodecyl sulphate to various proteins. *Biochem. J.* **109,** 825-830.

Plaxco, K.W. and Gross, M. (1997) The importance of being unfolded. *Nature* **386,** 657-659.

Prajapati, R.S., Indu, S. and Varadarajan, R. (2007) Identification and thermodynamic characterization of molten globule states of periplasmic binding proteins. *Biochemistry* **46,** 10339-10352.

Prats, M., Teissie, J. and Tocanne, J-F. (1986) Lateral proton conduction at lipid-water interfaces and its implications for the chemiosmotic hypothesis. *Nature* **322,** 756-758.

Privalov, P.L. and Gill, S.J. (1988) Stability of protein structure and hydrophobic interaction. *Adv. Protein Chem*. **39,** 191-234.

Privalov, P.L. (1996) Intermediate states in protein folding. *J. Mol. Biol*. **258,** 707-725.

Proutski, I., Karoulias, N., and Ashley, R.H. (2002) Overexpressed chloride intracellular channel protein CLIC4 (p64H1) is an essential molecular component

of novel plasma membrane anion channels. *Biochem. Biophys. Res. Comm.* **297,** 317-322.

Provencher, S. W., and Glöckner, J. (1981) Estimation of protein secondary structure from circular dichroism. *Biochemistry* **20,** 33-37.

Ptitsyn, O.B. (1973) Stage mechanism of the self-organization of protein molecules. *Dokl. Acad. Nauk.* **210,** 1213-1215.

Ptitsyn, O.B. (1987) Protein folding: Hypotheses and experiments. *J. Protein Chem*. **6,** 273-293.

Ptitsyn, O.B. and Uversky, V.N. (1994) The molten globule is a third thermodynamic state of protein molecules. *FEBS Lett.* **341,** 15-18.

Ptitsyn, O.B. (1995a) Molten globule and protein folding. *Adv. Prot. Chem*. **47,** 83–229.

Ptitsyn, O.B. (1995b) Structures of folding intermediates. *Curr. Opin. Str. Biol.* **5,** 74-78.

Puglia, C., Trombetta, D., Venuti, V., Saija, A. and Bonina, F. (2004) Evaluation of in-vivo topical anti-inflammatory activity of indometacin from liposomal vesicles. *J. Pharm. Pharmacol*. **56,** 1225-1232.

Puntheeranurak, T., Stroh, C., Zhu, R., Angsuthanasombat, C. and Hinterdorfer, P. (2005) Structure and distribution of the *Bacillus thuringiensis* Cry4Ba toxin in lipid membranes. *Ultramicros*. **105,** 115–124.

Qian, Z., Okuhara, D., Abe, M. K., and Rosner, M. R. (1999) Molecular cloning and characterization of a mitogen-activated protein kinase-associated intracellular chloride channel. *J. Biol. Chem.* **274,** 1621–1627.

Quinn, P.J. (1976) The molecular biology of cell membranes. Pp. 26-34. Macmillan Press, London, UK.

Ramsay, G., Montgomery, D., Berger, D. and Freire, E. (1989) Energetics of diphtheria toxin membrane insertion and translocation: Calorimetric characterization of the acid pH induced transition. *Biochemistry* **28,** 529–533.

Rausell, C., Pardo-Lopez, L., Sanchez, J., Munoz-Garay, C., Morera, C., Soberon, M. and Bravo, A. (2004) Unfolding events in the water-soluble monomeric Cry1Ab toxin during transition to oligomeric pre-pore and membrane-inserted pore channel. *J. Biol. Chem.* **279,** 55168-55175.

Re, F., Sesana, S., Barbiroli, A., Bonomi, F., Cazzaniga, E., Lonati, E., Bulbarelli, A and Masserini, M. (2008) Prion protein structure is affected by pH-dependent interaction with membranes: A study in a model system. *FEBS Lett.* **582,** 215–220.

Redhead, C., Sullivan, S. K., Koseki, C., Fujiwara, K., and Edwards, J. C. (1997) Subcellular distribution and targeting of the intracellular chloride channel p64. *Mol. Biol. Cell* **8,** 691–704.

Reed, R., Holmes, D., Weyers, J. and Jones, A. (2003) Practical skills in biomolecular sciences (2nd Ed.), pp 131. Pearson Education Ltd., UK.

Reynolds, J.A. and Tanford, C. (1970) Binding of dodecyl sulfate to proteins at high binding ratios. Possible implications for the state of proteins in biological membranes. *Proc. Natl. Acad. Sci.* **66,** 1002-1007.

Rice, P., Longden, I. and Bleasby, A. (2000) EMBOSS: The European Molecular Biology Open Software Suite. *Trends Gen.* **16,** 276-277.

Riordan, J.R., Rommens, J.M., Kerem, B., Alon, N., Rozmahel, R., Grzelczak, Z., Zielenski, J., Lok, S., Plavsic, N., Chou, J.L., Drumm, M.L., Iannuzzi, M.C., Collins, F.S. and Tsui, L.C. (1989) Identification of the cystic fibrosis gene: cloning and characterization of complementary DNA. *Science* **245,** 1066**–**1073.

Roder, H., and Colón, W. (1997) Kinetic role of early intermediates in protein folding. Kinetic role of early intermediates in protein folding. *Curr. Opin. Struct. Biol.* **7,** 15-28.

Rosconi, M.P. and London, E. (2002) Topography of helices 5–7 in membrane-inserted diphtheria toxin T domain. Identification and insertion boundaries of two hydrophobic sequences that do not form a stable transmembrane hairpin. *J. Biol. Chem.* **277,** 16517–16527.

Roseman, M.A. (1988) Hydrophobicity of the peptide C=O...HN hydrogen-bonded group. *J. Mol. Biol.* **201,** 621-623.

Rosen, C.G., and Weber, G. (1969) Dimer formation from 1-anilino-8-naphthalenesulfonate catalyzed by bovine serum albumin. Fluorescent molecule

with exceptional binding properties. *Biochemistry* **8,** 3915-3920

Royer, C.A. (1995) in Methods in Molecular Biology, Vol 40: Protein Stability and Folding: Theory and Practice (Shirley, B. A., ed) pp 65-89, Humana Press Inc., Totowa, NJ.

Saeki, K., Yasug, E., Okuma, E., Breit, S.N., Nakamura, M., Toda, T., Kaburagi, Y. and You, A. (2005) Proteomic analysis on insulin signalling in human hematopoietic cells: identification of CLIC1 and SRp20 as novel downstream effectors of insulin. *Am. J. Physiol. Endocrinol. Metab.* **289,** E419-E428.

Saito, M., Korsmeyer, S.J. and Schlesinger, P.H. (2000) BAX-dependent transport of cytochrome *c* reconstituted in pure liposomes. *Nat. Cell Biol*. **2,** 553-555.

Sambrook, J., Fritsch, E.F. and Maniatis, T. (1989) Molecular cloning: A laboratory manual (2^{nd} ed.), pp 1.25-1.28. Cold Spring Harbor Laboratory Press, Cold Spring Harbor, New York.

Sanders, C.R. and Prestegard, J.H. (1990) Magnetically orientable phospholipid bilayers containing small amounts of a bile salt analogue, CHAPSO. *Biophys. J.* **58,** 447-460.

Sanders, C.R. and Schwonek, J.P. (1992) Characterization of magnetically orientable bilayers in mixtures of dihexanoylphosphatidylcholine and dimyristoylphosphatidyl-choline by solid-state NMR. *Biochemistry* **31,** 8898-8905.

Sanders, C.R. and Landis, G.C. (1995) Reconstitution of membrane proteins into lipid-rich bilayered mixed micelles for NMR studies. *Biochemistry* **34,** 4030-4040.

Sanders, C.R. and Prosser, R.S. (1998) Bicelles: a model membrane system for all seasons? *Struct.* **6,** 1227–1234.

Sathish, H.A., Cusan, M., Aisenbrey, C. and Bechinger, B. (2002) Guanidine hydrochloride induced equilibrium unfolding studies of colicin B and its channel-forming fragment. *Biochemistry* **41,** 5340**–**5347.

Schellman, J. (1978) Solvent denaturation. *Biopolymers* **17,** 1305–1322.

Schendel S.L. and Cramer W.A. (1994) On the nature of the unfolded intermediate in the in vitro transition of the colicin E1 channel domain from the aqueous to the membrane phase. *Protein Sci*. **3,** 2272-2279.

Schendel, S.L., Montal, M. and Reed, J.C. (1998) Bcl-2 family proteins as ion channels. *Cell Death Differ.* **5,** 372–380.

Schiffer, M. and Edmundson, A.B. (1967) Use of helical wheels to represent the structures of proteins and to identify segments with helical potential. *Biophys. J.* **7,** 121-135.

Schlesinger, P.H., Blair, H.C., Teitelbaum, S.T., and Edwards, J.C. (1997) Characterisation of the osteoclast ruffled border chloride channel and its role on bone resorption. *J. Biol. Chem.* **272,** 18636-18643.

Schmid, F.X. (1997) Optical spectroscopy to characterise protein conformation. In Protein structure – a practical approach (2nd Ed.) (Ed. Creighton, T.E.), pp. 261-297. Oxford University Press, Oxford, UK.

Seddon, A.M., Curnow, P. and Booth, P.J. (2004) Membrane proteins, lipids and detergents: not just a soap opera. *Biochim. Biophys. Acta* **1666,** 105–117.

Segrest, J.P., De Loof, H., Dohlman, J.G., Brouillette, C.G. and Anantharamaiah, G.M. (1990) Amphipathic helix motif: classes and properties. *Proteins Struct. Funct. Genet.* **8,** 103–117.

Semisotnov, G.V., Rodionova, N.A., Razgulyaev, O.I., Uversky, Y.N., Gripas, A.F. and Gilmanshin, R.I. (1991) Study of the “molten globule” intermediate state in protein folding by a hydrophobic fluorescent probe. *Biopolymers* **31,** 119-128.

Simon, D.B., Bindra, R.S., Mansfield, T.A., Nelson-Williams, C., Mendonca, E., Stone, R., Schurman, S., Nayir, A., Alpay, H., Bakkaloglu, A., Rodriguez-Soriano, J., Morales, J.M., Sanjad, S.A., Taylor, C.M., Pilz, D., Brem, A.,

Trachtman, H., Griswold, W., Richard, G.A., John, E. and Lifton, R.P. (1997) Mutations in the chloride channel gene, *CLCNKB*, cause Bartter's syndrome type III. *Nat. Genet*. **17,** 171**–**178.

Singer, S.J. and Nicolson, G.L. (1972) The fluid mosaic model of the structure of cell membranes. *Science* **175,** 720-731.

Singh, H. and Ashley, R.H. (2006) Redox regulation of CLIC1 by cysteine residues associated with the putative channel pore. *Biophys. J.* **90**, 1628-1638.

Singh, H., Cousin, M.A. and Ashley, R.H. (2007) Functional reconstitution of mammalian 'chloride intracellular channels' CLIC1, CLIC4 and CLIC5 reveals differential regulation by cytoskeletal actin. *FEBS J.* **274,** 6306–6316.

Shatsky, M., Nussinov, R. and Wolfson, H.J. (2004) A method for simultaneous alignment of multiple protein structures. *Proteins: Struct. Func. Bioinf.* **56,** 143-156.

Shimizu, S., Narita, M. and Tsujimoto, Y. (1999) Bcl-2 family proteins regulate the release of apoptogenic cytochrome *c* by the mitochondrial channel VDAC. *Nature* **399,** 483–487.

Shimizu, S., Konishi, A., Kodama, T. and Tsujimoto, Y. (2000) BH4 domain of antiapoptotic Bcl-2 family members closes voltage-dependent anion channel and inhibits apoptotic mitochondrial changes and cell death. *Proc. Natl. Acad. Sci. USA.* **97,** 3100–3105.

Shortle, D. and Meeker, A.K. (1986) Mutant forms of staphylococcal nuclease with altered patterns of guanidine hydrochloride and urea denaturation. *Proteins Struct. Func. Genet*. **1,** 81-89.

Shortle, D. (1993) Denatured states of proteins and their roles in folding and stability. *Curr. Opin. Struct. Biol.* **3**, 66–74.

Shortle, D. (1995) Staphylococcal nuclease: a showcase of *m*-value effects. *Adv. Protein Chem.* **46,** 217–278.

Shortle, D. (1996) The denatured state (the other half of the folding equation) and its role in protein stability. *FASEB J.* **10**, 27-34.

Škalko, N., Čajkova M. and Jalšenjak, I. (1992) Liposomes with clindamycin hydrochloride in the therapy of acne vulgaris. *Int. J. Pharm.* **85,** 97-101.

Smith, D.B. and Johnson, K.S. (1988) Single-step purification of polypeptides expressed in *Escherichia coli* as fusions with glutathione S-transferase. *Gene* **67,** 31-40.

Song, L., Hobaugh, M.R., Shustak, C., Cheley, S., Bayley, H. and Gouaux, J.E. (1996) Structure of staphylococcal α-hemolysin, a heptameric transmembrane pore. *Science* **274,** 1859**–**1866.

Sou, K., Naito, Y., Endo, T., Takeoka, S. and Tsuchida, E. (2003) Effective encapsulation of proteins into size-controlled phospholipid vesicles using freeze-thawing and extrusion. *Biotechnol. Prog*. **19,** 1547-1552.

Soulages, J.L. (1998) Chemical denaturation: Potential impact of undetected intermediates in the free energy of unfolding and *m*-values obtained from a two-state assumption. *Biophys. J.* **75,** 484–492.

Sreerama, N., Venyaminov, S.Y. and Woody, R.W. (2000) Estimation of protein secondary structure from CD spectra: inclusion of denatured proteins with native protein in the analysis. *Anal. Biochem*. **287,** 243**–**251.

Stark, G.R. (1965) Reactions of cyanate with functional groups of proteins. III. Reactions with amino and carboxyl groups. *Biochemistry* **4,** 1030-1036.

Stern, O. (1924) Zur theorie der elektrolytischen doppelschicht. *Z. Elektrochem* **30,** 508-516.

Stewart, J.C.M. (1980) Colorimetric determination of phospholipids with ammonium ferrothiocyanate. *Anal. Biochem.* **104,** 10-14.

Stickle, D.F., Presta, L.G., Dill, K.A., and Rose, G.D. (1992) Hydrogen bonding in globular proteins. *J. Mol. Biol.* **226,** 1143-1159.

Stigter, D. and Dill, K.A. (1990) Charge effects on folded and unfolded proteins. *Biochemistry* **29,** 1262-1271.

Stillinger, F.H. (1980) Water revisited. *Science* **209,** 451-457.

Stochaj, U., and Silver, P. (1992) Nucleocytoplasmic traffic of proteins. *Eur. J. Cell Biol.* **59,** 1–11.

Strickland, E.H. (1974) Aromatic contributions to circular dichroism spectra of proteins. *Crit. Rev. Biochem.* **2,** 113-175.

Studier, F.W., Rosenberg, A.H., Dunn, J.D. and Dubendorff, J.W. (1990) Use of T7 RNA polymerase to direct expression of cloned genes. *Methods Enzymol.* **185,** 60-89.

Suh, K.S., Mutoh, M., Nagashima, K., Fernandez-Salas, E., Edwards, L.E., Hayes, D.D., Crutchley, J.M., Marin, K.G., Dumont, R.A., Levy, J.M., Cheng, C., Garfield, S. and Yuspa, S.H. (2004) The organellar chloride channel protein CLIC4/mtCLIC translocates to the nucleus in response to cellular stress and accelerates apoptosis. *J. Biol. Chem.* **279,** 4632–4641.

Suh, K.S., Mutoh, M., Nagashima, K., Fernandez-Salas, E., Edwards, L.E. and Hayed, D.D. (2005) Antisense suppression of the chloride intracellular family induces apoptosis, enhances tumour necrosis factor α-induced apoptosis, and inhibits tumour growth. *Cancer Res.* **65,** 562-571.

Suzuki, M., Youle, R.J., and Tjandra, N. (2000) Structure of Bax. Co-regulation of dimer formation and intracellular localization. *Cell* **103,** 645-654.

Svensson-Ek, M., Abramson, J., Larsson, G., Tornroth, S., Brzezinski, P. and Iwata, S. (2002) The x-ray crystal structures of wild-type and EQ(I-286) mutant cytochrome *c* oxidases from *Rhodobacter sphaeroides*. *J. Mol. Biol.* **321,** 329–339.

Szoka, Jr., F. and Papahadjopoulos, D. (1978) Procedure for preparation of liposomes with large internal aqueous space and high capture by reverse-phase evaporation. *Proc. Natl. Acad. Sci. USA* **75,** 4194-4198.

Talmon, Y., Burns, J.L., Chestnut, M.H. and Siegel, D.P. (1990) Time resolved cryotransmission electron microscopy. *J. Electron Microsc. Tech.* **14,** 6-12.

Tan, Y.J., Oliveberg, M., Davis, B. and Fersht, A.R. (1995) Perturbed pK_a-values of the denatured states of proteins. *J. Mol. Biol.* **254,** 980-992.

Tanford, C., Kawahara, K. and Lapanje, S. (1967) Proteins as random coils. I. Intrinsic viscosities and sedimentation coefficients in concentrated guanidine hydrochloride. *J. Am. Chem. Soc*. **89,** 729-736.

Tanford, C. (1968) Protein denaturation. *Adv. Protein Chem*. **23,** 121-282.

Tanford, C. (1970) Protein denaturation part C: Theoretical models for the mechanism of denaturation. *Adv. Protein Chem.* **24,** 1-95.

Tanford, C. (1980) The hydrophobic effect: Formation of micelles and biological membranes (2nd Ed.). Pp. 1-3, 109. John Wiley and Sons, Inc., Canada.

Tejuca, M., Dalla Serra, M., Ferreras, M., Lanio, M.E. and Menestrina, G. (1996) Mechanism of membrane permeabilization by sticholysin I, a cytolysin isolated from the venom of the sea anemone *Stichodactyla helianthus*. *Biochemistry* **35,** 14947**–**14957.

Terstappen, G.C. and Reggiani, A. (2001) *In silico* research in drug discovery. *Trends Pharmacol. Sci.* **22,** 23–26.

Thompson, L.C., Walters, J., Burke, J., Parsons, J.F., Armstrong, R.N. and Dirr, H.W. (2006) Double mutation at the subunit interface of glutathione transferase rGSTM1-1 results in a stable, folded monomer. *Biochemistry* **45,** 2267-2273.

Thuduppathy, G.R. and Hill, R.B (2005) Acid destabilization of the solution conformation of Bcl-x_L does not drive its pH-dependent insertion into membranes *Protein Sci.* **15,** 248-257.

Thuduppathy, G.R., Craig, J.W., Kholodenko, V., Schon, A. and Hill, B. (2006) Evidence that membrane insertion of the cytosolic domain of Bcl-xL is governed by an electrostatic mechanism. *J. Mol. Biol.* **359,** 1045-1058.

Tilley, S.J. and Saibil, H. R. (2006) The mechanism of pore formation by bacterial toxins. *Curr. Opin. Struct. Biol.* **16,** 230-236.

Tonini, R., Ferroni, A., Valenzuela, S.M., Warton, K., Campbell, T.J., Breit, S.N. and Mazzanti, M. (2000) Functional characterization of the NCC27 nuclear protein in stable transfected CHO-K1 cells. *FASEB J.* **14,** 1171–1178.

Tory, M.C. and Merrill, A.R. (1999) Adventures in membrane protein topology. A study of the membrane bound state of colicin E1. *J. Biol. Chem*. **274,** 24539**–** 24549.

Träuble, H. and Eibl, H. (1974) Electrostatic effects on lipid phase transitions: membrane structure and ionic environment. *Proc. Nat. Acad. Sci. USA* **71,** 214-219.

Tulk, B.M., and Edwards, J.C. (1998) NCC27, a homologue of intracellular chloride channel p64, is expressed in brush border of renal proximal tubule. *Am. J. Physiol.* **274,** F1140-F1149.

Tulk, B.M., Schlesinger, P.H., Kapadia, S.A. and Edwards, J.C. (2000) CLIC1 functions as a chloride channel when expressed and purified from bacteria. *J. Biol. Chem.* **275,** 26986- 26993.

Tulk, B.M., Kapadia, S. and Edwards, J.C. (2002) CLIC1 inserts from the aqueous phase into phospholipid membranes, where it functions as an anion channel. *Am. J. Physiol. Cell Physiol.* 282, C1103-C1112.

Tweten, R.K., Parker, M.W. and Johnson, A.E. (2001) The cholesterol-dependent cytolysins. In: Pore-Forming Toxins (Ed. van der Goot, F.G.), pp. 1**–**14. Springer, Heidelberg, Germany.

Ulmasov, B., Bruno, J., Woost, P.G. and Edwards, J.C. (2007) Tissue and subcellular distribution of CLIC1. *BMC Cell Biol.* **8,** 8-26.

Ulmschneider, M.D. and Sansom, M.S.P. (2001) Amino acid distributions in integral membrane protein structures. *Biochim. Biophys. Acta* **1512,** 1–14.

Ulrih, N.P., Anderluh, G., Maček, P. and Chalikian, T.V. (2004) Salt-induced oligomerisation of partially folded intermediates of equinatoxin II. *Biochemistry* **43,** 9536-9545.

Uversky V.N. and Ptitsyn O.B. (1994) 'Partly folded' state, a new equilibrium state of protein molecules: four-state guanidinium chlorideinduced unfolding of beta-lactamase at low temperature. *Biochemistry* **33,** 2782-2791.

Uversky V.N. and Ptitsyn O.B. (1996) Further evidence on the equilibrium 'pre-molten globule state': four-state guanidinium chlorideinduced unfolding of carbonic anhydrase B at low temperature. *J. Mol. Biol*. **255,** 215-228.

Uversky, V.N., Narizhneva, N.V., Kirschstein, S.O., Winter, S. and Löber, G. (1997) Conformational transitions provoked by organic solvents in β-lactoglobulin: can a molten globule like intermediate be induced by the decrease in dielectric constant? *Fold. Des.* **2,** 163-172.

Uversky, V.N., Talapatra, A., Gillespie, J.R. and Fink, A.L. (1999a) Protein deposits as the molecular basis of amyloidosis: part I. Systemic amyloidosis. *Med. Sci. Monitor* **5,** 1001-1012.

Uversky, V.N., Talapatra, A., Gillespie, J.R. and Fink, A.L. (1999b) Protein deposits as the molecular basis of amyloidosis: Part II. Localized amyloidosis and neurodegenerative disorders. *Med. Sci. Monitor* **5,** 1238-1254.

Valenzuela, S.M., Martin, D.K., Por, S.B., Robbins, J.M., Warton, K., Bootcov, M.R., Schofield, P.R., Campbell, T.J., and Breit, S.N. (1997) Molecular cloning and expression of a chloride ion channel of cell nuclei. *J. Biol. Chem.* **272,** 12575-12582.

Valenzuela, S.M., Mazzanti, M., Tonini, R., Qiu, M.R., Warton, K., Musgrove, E.A., Campbell, T.J., and Breit, S.N. (2000) The nuclear chloride ion channel NCC27 is involved in regulation of the cell cycle. *J. Physiol.* **529,** 541-552.

Vance, J.E. and Steenbergen, R. (2005) Metabolism and functions of phosphatidylserine. *Prog. Lipid Res*. 44, 207-234.

Van Dael, H., Haezebrouck, P., Morozova, L., Arico-Muandel, C. and Dobson, C.M. (1993). Partially folded states of equine lysozyme. Structural characterization and significance for protein folding. *Biochemistry* **32,** 1186–1194.

Van der Goot, F.G., González-Manãs, J.M., Lakey, J.H., and Pattus, F. (1991) A 'molten-globule' membrane-insertion intermediate of the pore-forming domain of colicin A. *Nature* **354,** 408-410.

Van Holde, K.E., Johnson, W.C and Ho, P.S. (1998) Principles of physical biochemistry. Pp. 452-456. Prentice Hall, Inc., New Jersey, USA.

Vaz, W.L., Nisksch, A. and Jahnig, F. (1978) Electrostatic interactions at charged lipid membranes. Measurement of surface pH with fluorescence lipoid pH indicators. *Eur. J. Biochem.* **83,** 299-305.

Vécsey-Semjén, B., Mollby, R. and Van der Goot, F.G. (1996) Partial C-terminal unfolding is required for channel formation by Staphylococcal α-toxin. *J. Biol. Chem.* **271,** 8655-8660.

Venyaminov, S.Y. and Yang, J.T. (1996) Determination of protein secondary structure. In: Circular dichroism and the conformational analysis of biomolecules. (Ed. Fasman, G.D.) Plenum Press, New York.

Verkman, A.S., Sellers, M.C., Chao, A.C., Leung, T. and Ketcham, R. (1989a) Synthesis and characterization of improved chloride-sensitive fluorescent indicators for biological applications. *Anal. Biochem.* **178,** 355-361.

Verkman, A.S., Takla, R., Sefton, B., Basbaum, C. and Widdicombe J. H. (1989b) Quantitative fluorescence measurement of chloride transport mechanisms in phospholipid vesicles. *Biochemistry,* **28,** 4240-4244.

Verkman, A.S. (1990) Development and biological applications of chloride-sensitive fluorescent indicators. *Am. J. Physiol.* **259** (Cell Physiol. 28), C375-C388.

Voet, D. and Voet J.G. (2004) Biochemistry (3rd Ed.) pp. 259. John Wiley and Sons, Inc., New York.

Von Heijne, G. (1986) Mitochondrial targeting sequences may form amphiphilic helices. *EMBO J.* **5,** 1335–1342.

Vreuls, C., Filée, P., Van Melckebeke, H., Aerts, T., De Deyn, P., Llabrès, G., Matagne, A., Simorre, J.-P., Frère, J.-M. and Joris, B. (2004) Guanidinium chloride denaturation of the dimeric *Bacillus licheniformis* BlaI repressor highlights an independent domain unfolding pathway. *Biochem. J.* **384,** 179–190.

Vuilleumier, S., Sancho, J., Loewentha1, R. and Fersht, A.R. (1993) Circular dichroism studies of barnase and its mutants: Characterization of the contribution of aromatic side chains. *Biochemistry* **32,** 10303-10313.

Wallin, E. and von Heijne, G. (1998) Genome-wide analysis of integral membrane proteins from eubacterial, archaean and eukaryotic organisms. *Protein Sci.* **7,** 1029–1038.

Warton, K., Tonini, R., Fairlie, W.D., Matthews, J.M., Valenzuela, S.M., Qiu, M.R., Wu, W.M., Pankhurst, S., Bauskin, A.R., Harrop, S.J., Campbell, T.J., Curmi, P.M., Breit, S.N., and Mazzanti, M. (2002) Recombinant CLIC1 (NCC27) assembles in lipid bilayers via a pH-dependent two-state process to form chloride ion channels with identical characteristics to those observed in Chinese hamster ovary cells expressing CLIC1. *J. Biol. Chem.* **277,** 26003-26011.

Weber, K. and Osborn, M. (1969) The reliability of molecular weight estimations by dodecyl sulfate-polyacrylamide gel electrophoresis. *J. Biol. Chem.* **244,** 4406-4412.

Weber, G. and Young, L.B. (1964) Fragmentation of bovine serum albumin by pepsin. I. The origin of the acid expansion of the albumin molecule. *J. Biol. Chem.* **239,** 1415-1423.

Wedekind, J.E., Trame, C.B., Dorywalska, M., Koehl, P., Raschke, T.M., Mckee, M., Fitzgerald, D., Collier, R.J., and Mckay, D.B. (2001) Refined crystallographic structure of *Pseudomonas aeruginosa* exotoxin A and its implications for the molecular mechanism of toxicity. *J. Mol. Biol.* **314,** 823-829.

Wennerström, H. and Lindman, B. (1979) Micelles. Physical chemistry of surfactant association. *Phys. Reports* **52,** 1-86.

White, S.H. (2004) The progress of membrane protein structure determination. *Protein Sci.* **13,** 1948-1949.

White, S.H. and Wimley, W. C. (1999) Membrane protein folding and stability: physical principles. *Annu. Rev. Biophys. Biomol. Struct.* **28,** 319-365.

Whitten, S.T. and García-Moreno, B.E. (2000) pH dependence of stability of staphylococcal nuclease: evidence of substantial electrostatic interactions in the denatured state. *Biochemistry* **39,** 14292-14304.

Whitten, S.T., Wooll, J.O., Razeghifard, R., García-Moreno, E. and Hilser, V.J. (2001) The origin of pH-dependent changes in m-values for the denaturant-induced unfolding of proteins. *J. Mol. Biol*. **309,** 1165-1175.

Whitmore, L. and Wallace, B.A. (2004) DICHROWEB, an online server for protein secondary structure analyses from circular dichroism spectroscopic data. *Nucleic Acids Res*. **32,** W668**–**W673.

Wilce, M.C., and Parker, M.W. (1994) Structure and function of glutathione *S*-transferases. *Biochim. Biophys. Acta* **1205,** 1–18.

Wilson, K and Walker, J. (2005) Principles and techniques of biochemistry and molecular biology (6^{th} ed.). Pp 451, 524, 526, 535, 571, 579, 581-582. Cambridge University Press, Cambridge.

Winterhalter, M. (2000) Black lipid membranes. *Curr. Opin. Coll. Interf. Sci.* **5,** 250-255.

Wolter, K.G., Hsu, Y.T., Smith, C.L., Nechushtan, A., Xi, X.G., and Youle, R.J. (1997) Movement of Bax from the cytosol to mitochondria during apoptosis. *J. Cell. Biol.* **139,** 1281-1292.

Woody, R.W. (1995) Circular dichroism. *Methods Enzymol.* **246,** 34-71.

Woody, R.W. (1996) Theory of circular dichroism of proteins. In: Circular dichroism and the conformational analysis of proteins. (Ed. G.D. Fasman) Plenum Press, New York.

Woody, R.W. and Dunker, A.K. (1996) Aromatic and cystine side-chain CD in proteins. In: Circular dichroism and the conformational analysis of biomolecules. (Ed. Fasman, G.D.) Plenum Press, New York.

Wolynes, P.G., Onuchic, J.N. and Thirumalai, D. (1995). Navigating the folding routes. *Science* **267,** 1619-1620.

Wüthrich, K., Wagner, G., Richart, R. and Braun, W. (1980) Correlations between internal mobility and stability of globular proteins. *Biophys. J.* 32, 549-558.

Xiang, T.-X., and Anderson, B.D. (1995) Phospholipid surface density determines the partitioning and permeability of acetic acid in DMPC: cholesterol bilayers. *J. Membr. Biol.* **148,** 157-167.

Xiang, T.-X. and Anderson, B.D. (1997) Permeability of acetic acid across gel and liquid-crystalline lipid bilayers conforms to free-surface-area theory. *Biophys. J.* **72,** 223-237.

Yan, J.X., Wait, R., Berkelman, T., Harry, R.A., Westbrook, J.A., Wheeler, C.H. and Dunn, M.J. (2000) A modified silver staining protocol for visualisation of proteins compatible with matrix-assisted laser desorption/ionisation and electrospray ionisation-mass spectrometry. *Electrophoresis* **21,** 3666-3672.

Zachowski, A. (1993) Phospholipids in animal eukaryotic membranes: transverse asymmetry and movement. *Biochem. J.*, **294,** 1-14.

Zitzewitz, J.A., Bilsel, O., Luo, J., Jones, B.E. and Matthews, C.R. (1995) Probing the folding mechanism of a leucine zipper peptide by stopped-flow circular dichroism spectroscopy. *Biochemistry*, **34,** 12812-12819.

Zhou, Y., Morals-Cabral, J.H., Kaufman, A. and Mackinnon, R. (2001) Chemistry of ion coordination and hydration revealed by a K^+ channel-Fab complex at 2.0 Å resolution. *Nature* **414,** 43-48.

Zuidam, N.J., de Vrueh, R. and Crommelin, D.J.A. (2003) Characterisation of liposomes. In: Liposomes, 2nd Ed. (Ed. Torchilin, V.P. and Weissig, V.). Oxford University Press, Oxford, UK.